

# Effects of rare recurrent copy number variations on brain structure



Dissertation for the degree of Philosophiae Doctor (Ph.D)

Rune Bøen

Faculty of Medicine

University of Oslo

2023

© Rune Bøen, 2024

*Series of dissertations submitted to the  
Faculty of Medicine, University of Oslo*

ISBN 978-82-348-0381-9

All rights reserved. No part of this publication may be reproduced or transmitted, in any form or by any means, without permission.

Cover: UiO.

Print production: Graphic center, University of Oslo.

## Acknowledgments

This thesis would not have been possible without the participants who generously volunteered to take part in this research. I extend my heartfelt thanks to each and every one of you.

I would like to thank my main supervisor, Ida E. Sønderby, and my co-supervisors Kaja K. Selmer and Dag Alnæs, for their unwavering support and guidance throughout these years. Thank you, Ida, for introducing me to the world of CNVs and for your exceptional generosity, kindness, and wealth of knowledge. You have been extremely generous with your time over the years, constantly providing me with helpful comments and edits to my many drafts. Thank you, Kaja, for your insight and supportiveness, and for leaving me with uplifted spirit and renewed passion after our meetings. Thank you, Dag, for your help with statistics, and for teaching me something new in every meeting.

I would also like to thank Srdjan Djurovic, Lars T. Westlye, and Ole A. Andreassen, for creating inspiring and creative research environments, and all my colleagues at AMG and NORMENT, for making every single day inspirational, educational, and enjoyable. A special thanks goes to my colleagues, Rikka Kjelkenes, Irene Voldsbekk, Dennis van der Meer, Nadine Parker, Ibrahim Akkouh, and Guy Hindley. Rikka and Irene, for being wonderful companions during the SOBP conference and for always taking the time for a chat during my daily walks across the hallway in building 48. Dennis, Nadine, and Ibrahim, for your insight and helpful comments on my drafts. Guy, for being an impeccable office mate and most importantly, sharing my passion for football.

The research work carried out in this thesis was made possible by extensive international and national collaborations. Thus, I would like to thank the researchers and funders of the UK Biobank and our collaborators from the ENIGMA-CNV working group. I would also like to acknowledge South-Eastern Norway Regional Health Authority for funding

my PhD position and my research stay abroad. I would like to thank Paul Thompson and Carrie Bearden and their wonderful lab members, who hosted me and made my stay in L.A. a true pleasure.

Thank you to all my friends, who make my life a true joy, and for not abandoning me when Liverpool is doing exceptionally well. A special thanks to my friend, Sigurd L. Alnes, who always takes the time to talk about life and science, and for calling me in the middle of the night to discuss his research.

Finally, I would like to thank my family for their boundless love and encouragement. I am endlessly grateful for you all. Thank you.



## Table of contents

1	GENERAL SUMMARY .....	5
2	LIST OF STUDIES .....	13
3	ABBREVIATIONS .....	14
4	INTRODUCTION.....	15
4.1	Genetics and phenotypic variation .....	18
4.1.1	Quantitative genetics and phenotypic variation .....	18
4.1.2	Molecular genetics and phenotypic variation.....	20
4.1.3	CNVs and phenotypic variation .....	22
4.2	Brain architecture .....	25
4.2.1	Macrostructural and microstructural characteristics of the brain.....	25
4.2.2	Phylogenetic and ontogenetic perspectives on the brain.....	26
4.2.3	CNV-related gene expression and the brain .....	29
4.3	Magnetic Resonance Imaging (MRI).....	31
4.3.1	Physics of MRI.....	31
4.3.2	T1-weighted imaging .....	33
4.3.3	T1-weighted MRI-derived measures.....	34
4.3.4	Diffusion weighted imaging.....	36
4.3.5	Diffusion MRI-derived measures.....	36
4.3.6	MRI-derived measures and cognition .....	38
4.3.7	MRI-derived measures and age-related differences.....	38
4.4	Characteristics of 1q21.1 distal, 15q11.2 BP1-BP2, and 22q11.2 CNVs.....	41
4.4.1	1q21.1 distal deletion and duplication.....	42
4.4.2	15q11.2 BP1-BP2 deletion and duplication .....	42
4.4.3	22q11.2 deletion .....	43
4.4.4	Implications of CNV brain profiling.....	44
4.5	Summary .....	46
5	THESIS AIMS.....	47
5.1	Study I .....	47
5.2	Study II.....	47
5.3	Study III.....	47
6	METHODOLOGY .....	49
6.1	Samples .....	49

6.1.1	The UK Biobank. ....	51
6.1.2	The ENIGMA-CNV working group .....	51
6.1.3	The 22q11.2 deletion sample.....	52
6.2	MRI acquisition, quality control and preprocessing .....	52
6.3	Statistical analyses.....	54
6.4	Ethical considerations .....	57
7	SUMMARY OF STUDIES .....	61
7.1	Study I.....	61
7.2	Study II.....	63
7.3	Study III.....	64
8	DISCUSSION .....	66
8.1	Main findings .....	66
8.2	Discussion of the results.....	66
8.3	Methodological considerations .....	77
8.3.1	Samples .....	77
8.3.2	Sample size and effect size.....	78
8.3.3	Intraindividual variability measures.....	80
8.3.4	Brain age gap estimations .....	80
8.3.5	Gene expression and brain profile.....	82
9	CONCLUDING REMARKS AND PERSPECTIVES .....	84
10	REFERENCES.....	86
11	Studies I-III .....	114

# 1 GENERAL SUMMARY

## English summary

Twin studies have shown high heritability estimates for brain structure. However, common genetic variants only account for a minor proportion of this heritability, where the individual common genetic variants show minor associations to brain structure. In recent years, emerging evidence suggests that certain rare recurrent copy number variants (CNVs) have substantial impact on brain structure in addition to putting people at higher risk for somatic, psychiatric, and neurodevelopmental disorders. CNVs are deletions or duplications of a large segment of the genome that may occur during meiosis or be inherited from the parents to the offspring. CNVs can alter transcription levels, including affecting spatiotemporal gene expression levels during neurodevelopment, potentially resulting in atypical brain structure. Thus, establishing the brain profile of CNV carriers may provide a window into early neurodevelopmental mechanisms and thus inform our understanding of brain development.

The current thesis aims to provide novel insight into the brain structural differences in the relatively frequent 1q21.1 distal, 15q11.2 BP1-BP2 and 22q11.2 CNVs, by examining differences in magnetic resonance imaging (MRI)-derived measures. We did this through investigating different aspects of the influence of the CNVs on brain structure.

Carriers of the 1q21.1 distal deletion or the 15q11.2 BP1-BP deletion have shown global differences in brain structure compared to non-carriers. Specifically, they exhibit a lower cortical surface area (both 1q21.1 distal deletion carriers and 15q11.2 BP1-BP2 deletion carriers) and a thicker cortex (15q11.2 BP1-BP2 deletion carriers) compared to non-carriers. Still, some of the regional estimates do not appear to follow the overall global pattern: Some brain regions show structural characteristics that resemble those of non-carriers, while other brain regions diverge more than the global difference. This indicates variation within the brain

of 1q21.1 distal deletion carriers and 15q11.2 BP1-BP2 deletion carriers. In study I, we shed light on brain structural variability by applying a novel method, i.e., regional intra-deviation scores, to estimate regional divergence from the global effect on the brain on carriers of the 15q11.2 BP1-BP2 and 1q21.1 distal CNVs. We found that certain brain regions differed more than the overall global effect on the brain, whereas other brain regions differed less than the overall global effect. The regions that differed more than the global effect were mostly areas associated with higher-order level processing (i.e., association cortices). In contrast, regions that differed less than the global effect were, for the majority, areas associated with sensorimotor processing (i.e., sensorimotor cortices). 15q11.2 BP1-BP2 duplication carriers also showed evidence for a thinner cortex compared to non-carriers, but they do not exhibit differences in regional intra-deviation scores. The results indicate that 1q21.1 distal deletion and 15q11.2 BP1-BP2 deletion may yield differential effect on regional brain structure, possibly reflecting regional specific disruptions during neurodevelopment.

The atypical brain structure in 15q11.2 BP1-BP2 deletion carriers is thought to reflect disruptions to neurodevelopmental processes. However, middle-to-old aged 15q11.2 BP1-BP2 deletion carriers also show alterations in physical traits that typically deteriorates with age, possibly indicating altered ageing. However, it is unclear if the differences in brain structure and performance in physical traits that declines with age indicate neurodegenerative effects. In study II, we examined this by estimating brain age gap through machine learning models in older individuals carrying the 15q11.2 BP1-B2 deletion or duplication, and non-carriers. Brain age gap is defined as the discrepancy between the estimated age from the machine learning model and the chronological age. We found small to moderate differences in brain structure between 15q11.2 BP1-BP2 deletion carriers and non-carriers, which were characterized by thicker cortex, lower cortical surface area and lower subcortical volume in 15q11.2 BP1-BP2 deletion carriers. Nevertheless, we did not find evidence for a group difference in brain age. In

accordance with the lack of differences in brain age gap, the ageing trajectories of measures of motor, heart, and lung function in 15q11.2 BP1-BP2 CNVs were comparable to the age trajectories of non-carriers. The results indicate that 15q11.2 BP1-BP2 deletion and duplication carriers display typical age-related differences in brain structure, and a relatively typical age trajectory in motor, heart, and lung function. Thus, they do not show clear signs of neurodegenerative effects.

Previous studies have shown that MRI can yield measures that are sensitive for detecting brain structural differences between CNV carriers and non-carriers. However, the neurobiology that contributes to the group-level differences is poorly understood. This is partly because MRI provides relatively nonspecific measures of the underlying biological tissue. In study III, we investigated the neurobiological underpinnings of the white and grey matter differences in 22q11.2 deletion carriers. We applied advanced diffusion MRI techniques that are sensitized to displacement of water molecules, yielding measures of axonal density and dispersion of white matter microstructure in 22q11.2 deletion carriers compared to controls. Further, we established neurobiological correlates of the interregional group differences in cortical grey matter (i.e., brain profile) of 22q11.2 deletion carriers vs controls, by examining the spatial convergence of cell-type gene expression levels and the brain profile of 22q11.2 deletion carriers. Finally, we examined gene expression data obtained from cortical spheroids, to identify potential disrupted gene networks in 22q11.2 deletion carriers compared to controls. We found evidence for higher axonal density in white matter microstructure, spatial convergence between the cortical brain profile of 22q11.2 deletion carriers and gene expression of cell-type markers and disrupted gene networks in 22q11.2 deletion carriers. The results indicate widespread alterations to axonal density in white matter and regional-specific effects of cell-types and disrupted gene networks in cortical grey matter in 22q11.2 deletion carriers.

To conclude, the 1q21.1 distal deletion and the 15q11.2 BP1-BP2 deletion may impact brain structure, but the effect on brain structure is not equal for all brain regions – some regions appear to be more affected by the deletion than others. The effect of 15q11.2 BP1-BP2 CNVs on brain structure does not seem to include atypical brain age but may be established by early biological processes. The 22q11.2 deletion may result in higher axonal density in white matter microstructure, alterations to cell-specific properties of the brain, and disruption of early gene networks, possibly contributing to the observed differences in MRI-derived measures. The results from the thesis provide novel insight into the impact of CNVs on brain structure, enhancing our understanding of the genetic underpinnings of brain architecture.

## Norsk sammendrag

Tvillingstudier har vist høye arvbarhetsestimater for hjernestruktur. Derimot, så har studier fra molekylær genetikk vist at vanlige genetiske variasjoner kun forklarer en mindre del av arvbarhetsestimaterne fra tvillingstudier. I tillegg til dette, så har vanlige genetiske varianter, individuelt sett, vist kun små statiske assosiasjoner til hjernestruktur. Nyere forskning viser derimot at sjeldne kopitallsvarianter kan ha store effekter på hjernestruktur. Kopitallsvarianter er delesjoner eller duplikasjoner av en større del av arvematerialet som kan forekomme spontant under meiose eller være nedarvet fra foreldre. Kopitallsvarianter kan endre transkripsjonsnivåer, som kan påvirke spatiotemporale genuttrykk under hjerneutvikling. Dermed kan kopitallsvarianter påvirke typisk hjerneutvikling, som kan resultere i en atypisk hjernestruktur hos bærere av visse typer kopitallsvarianter. En karakterisering av hjerneprofilen til bærere av kopitallsvarianter kan dermed gi oss et innblikk inn i de tidlige biologiske mekanismene som er viktig for hjerneutvikling. En slik karakterisering kan også bidra til å øke vår forståelse av psykiatriske og nevroutviklingsforstyrrelser som er antatt å være påvirket av forstyrrelser under hjerneutvikling.

Denne avhandlingen tar sikte på å gi ny innsikt i hjernestruktur hos de relativt frekvente 1q21.1 distal, 15q11.2 BP1-BP2 og 22q11.2 kopitallsvariantene, med varierende grad av klinisk penetrans, ved å undersøke forskjeller i deriverte mål fra magnetresonanstomografi (MR). Vi gjorde dette ved å undersøke forskjellige aspekter ved atypisk hjernestruktur hos bærere av en patogen kopitallsvariant.

Både bærere av en 1q21.1 distal delesjon eller en 15q11.2 BP1-BP2 delesjon har tidligere vist globale forskjeller i hjernestruktur sammenlignet med ikke-bærere. Det vil si at de, generelt sett, har en mindre kortikal overflate (observert hos både 1q21.1 distal delesjon og 15q11.2 BP1-BP2 delesjon), og en tykkere korteks (observert hos 15q11.2 BP1-BP2

delesjon) enn ikke-bærere. Likevel, så ser det ut til at noen hjerneområder ikke følger dette globale mønsteret, hvor noen hjerneområder har strukturelle karakteristikk som ligner på de observert hos ikke-bærere, mens andre hjerneområder ser ut til å avvike mer enn den globale forskjellen. Dette tyder på at det også er variasjon innad i hjernen til 1q21.1 distal delesjonsbærere og 15q11.2 BP1-BP2 delesjonsbærere. I studie I kaster vi nytt lys over den regionale variasjon i hjernestruktur ved å ta i bruk en ny metode, i.e., regional intraavviksskåre, for å estimere regionalt avvik fra den globale effekten på hjernen hos bærere av en 1q21.1 distal eller 15q11.2 BP1-BP2 kopitallsvariant. Her fant vi at visse hjerneregioner avviker mer enn den globale effekten på hjernen, mens andre hjerneregioner avviker mindre enn den globale effekten på hjernen hos 1q21.1 distal delesjonsbærere og 15q11.2 BP1-BP2 delesjonsbærere. Hjerneregionene som avviket mer enn den globale effekten, var stort sett hjerneområder som er assosiert med høyere-ordens kognitiv prosessering (i.e., assosiasjonsområder). Hjerneregionene som avviker mindre enn den globale effekten var stort sett hjerneområder som er assosiert med sensomotorisk prosessering (i.e., sensomotoriske områder). Vi fant også at 15q11.2 BP1-BP2 duplikasjonsbærere har en tynnere korteks sammenlignet med ikke-bærere, men de viser ingen statistiske forskjeller i de regionale intraavviksskårene. Resultatene tyder på at 1q21.1 distal delesjonsbærere og 15q11.2 BP1-BP2 delesjonsbærere kan ha ulik påvirkning på regionale hjernemål, noe som muligens reflekter regional spesifikke forstyrrelser under hjerneutvikling.

Den atypiske hjernestrukturen hos bærere av en 15q11.2 BP1-BP2 kopitallsvariant er antatt å reflektere forstyrrelser under hjerneutvikling. Det er derimot uklart hvorvidt de atypiske trekkene i hjernestruktur hos eldre individer også kan reflektere nevrodegenerative effekter. I studie II undersøkte vi dette ved å estimere hjernealder ved bruk av maskinlæringsmodeller hos eldre individer som var bærere av en 15q11.2 BP1-BP2 delesjon eller duplikasjon og ikke-bærere. Hjernealder defineres som diskrepansen mellom predikert



alder fra maskinlæringsmodellen og kronologisk alder. Her fant vi små til moderate forskjeller i hjernestruktur mellom 15q11.2 BP1-BP2 delesjoner og ikke-bærere, karakterisert av en tykkere korteks, mindre kortikal overflate og mindre subkortikalt volum. Det var derimot ingen statistiske signifikante forskjeller i hjernealder. I tråd med dette, fant vi heller ingen statistiske forskjeller i aldringsrelaterte endringer i motorisk, hjerte-, og lunge-funksjon hos bærere av en 15q11.2 BP1-BP2 kopitallsvariant sammenlignet med ikke-bærere. Resultatene tyder på at 15q11.2 BP1-BP2 delesjons og duplikasjonsbærere har et mer eller mindre typisk aldringsforløp i hjernestruktur og motorisk, hjerte- og lunge-funksjon.

Tidligere studier har vist at MR kan gi sensitive mål for å oppdage forskjeller i hjernestruktur mellom kopitallsbærere og ikke-bærere. Likevel har vi en manglende forståelse av den underliggende nevrobiologien som bidrar til disse gruppeforskjellene. Dette skyldes at MR gir et relativt uspesifikt mål på spesifikke karakteristikk av hjernevev, inkludert celle komposisjon og morfologi. I studie III undersøkte vi de nevrobiologiske korrelatene til gruppe forskjellene i hvit og grå hjernematerie hos 22q11.2 delesjonsbærere. Vi tok i bruk avanserte hjerneavbildningsteknikker for å estimere tettheten og spredningen av aksoner i hvit materie hos 22q11.2 delesjoner sammenlignet med kontroller. Videre etablerte vi nevrobiologiske korrelater mellom grå materie hjerneprofil (i.e., variasjonen i regionale grupper forskjeller på tvers av korteks) hos 22q11.2 delesjonsbærere, ved å analysere den spatiale konvergensen mellom genuttrykks data fra gener som er assosiert med spesifikke celletyper og hjerneprofilen til 22q11.2 delesjonsbærere. Til slutt undersøkte vi genekspressjonsdata fra kortikale sfæroider (differensiert fra humane induerte pluripotente stamceller) for å identifisere mulige forstyrrelser i gen nettverkene (i.e., gener som har et genuttrykk som viser høyt topologisk overlapp med hverandre) hos 22q11.2 delesjonsbærere. Her fant vi at gener som er en del av et forstyrret gen nettverk under tidlig utvikling hos

22q11.2 delesjonsbærere, har et genuttrykk som spatialt konvergerer med hjerneprofilen for kortikal tykkelse hos 22q11.2 delesjonsbærere.

For å konkludere, så kan både 1q21.1 distal delesjon og 15q11.2 BP1-BP2 delesjon påvirke hjernestruktur, men effekten på hjernen er ikke lik for alle hjerneregioner, og noen hjerneregioner ser ut til å være mer avvikende enn andre. Effekten av 15q11.2 BP1-BP2 kopitallsvarianter på hjernestruktur kan reflektere forstyrrelser av tidlige biologiske prosesser under utvikling, men det ser ikke ut til at de reflekterer atypisk hjernealdring. 22q11.2 delesjonen kan føre til høyere aksontetthet i hvit hjernematerie, endringer i celle-spesifikke karakteristikk i hjernen og forstyrrelser av tidlige nevrobiologiske prosesser, som alle er biologiske karakteristikk som kan bidra til de observerte forskjellene i deriverte MR mål. Resultatene fra avhandlingen gir ny kunnskap om hvordan kopitallsvarianter påvirker hjernestruktur, og øker vår forståelse av de genetiske mekanismene som er involvert i hjerneutvikling.

## 2 LIST OF STUDIES

### Study I:

**Beyond the global brain differences: intra-individual variability differences in 1q21.1 distal and 15q11.2 BP1-BP2 deletion carriers**

Boen R., Kaufmann, T., van der Meer, D., Frei, O., Agartz, I., Ames, D., ... & Søndery, I. E.

*Published online ahead of print in Biological Psychiatry September 2023*

*DOI: 10.1016/j.biopsych.2023.08.018.*

### Study II:

**No signs of neurodegenerative effects in 15q11. 2 BP1-BP2 copy number variant carriers in the UK Biobank.**

Boen, R., Kaufmann, T., Frei, O., van der Meer, D., Djurovic, S., Andreassen, O. A., ... & Søndery, I. E.

*Translational Psychiatry (2023), 13(1), 61.*

*DOI: 10.1038/s41398-023-02358-w.*

### Study III:

**Characterizing the neurobiological correlates of brain structural alterations in 22q11.2 deletion syndrome**

Boen, R., Villalón-Reina, J.E., Forsyth, J.K., Parker, N., Akkouch, I.A., Alnæs. D., ... & Søndery I.E, Bearden C.E.

*Manuscript*

### 3 ABBREVIATIONS

AD	Axial Diffusivity
ADC	Apparent Diffusion Coefficient
bp	base pairs
BP1-BP2	Breakpoint 1 to Breakpoint 2
CNV	Copy Number Variant
DTI	Diffusion Tensor Imaging
DWI	Diffusion Weighted Imaging
ENIGMA-CNV	Enhancing Neuro Imaging Genetics through Meta Analysis – CNV
ECVF	Extracellular Volume Fraction
FA	Fractional Anisotropy
GWAS	Genome-Wide Association Studies
ICVF	Intracellular Volume Fraction
iPSC	induced Pluripotent Stem Cells
iSD	intraindividual Standard Deviation
ISO	Isotropic Volume Fraction
MD	Mean Diffusivity
MRI	Magnetic Resonance Imaging
NODDI	Neurite Orientation Dispersion and Density Imaging
ODI	Orientation Dispersion Index
RD	Radial diffusivity
RID	Regional Intra-Deviation
ROI	Region of Interest
SNP	Single Nucleotide Polymorphism
TE	Echo Time
TR	Repetition Time

## 4 INTRODUCTION

In the current thesis, we take a genetic-first approach to increase our understanding of brain structural variations between individuals. We focus on brain structural group differences between individuals that are carriers of a copy number variant (CNV), i.e., deletion or a duplication of longer stretches of genetic material and compare to individuals without a corresponding deletion or duplication

(Figure 1). The 15q11.2 breakpoint 1 to breakpoint 2 (BP1-BP2) and 1q21.1 distal CNVs and the 22q11.2 deletion will be described in more detail, since these are the specific CNVs examined in the three thesis studies.

Depending on the field of interest, the use of the term CNV may refer to different biological origins of the CNV.

Thus, it is important to establish clear definitions of the terminology used in this thesis. CNVs occur during cell division,

either during meiosis or mitosis, and can be transmitted from the parents to the offspring (inherited). If the CNV occurs during meiosis, it is referred to as being *de novo*. The inherited or *de novo* CNVs are then referred to as germline CNVs. If the CNV occurs during mitosis, it is referred to as a somatic CNV. Several CNVs are recurrent, which means that they reoccur spontaneously in the population at the same genomic loci. The recurrent CNVs are typically flanked by low copy repeats, which makes them susceptible to misalignment during recombination. This is also known as non-allelic homologous recombination<sup>1</sup>. In this thesis,

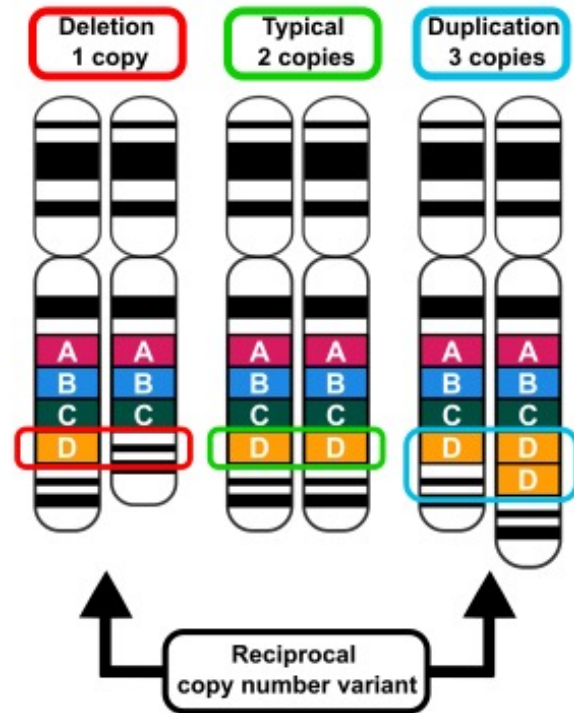


**Figure 1. Copy number variants.** Copy number variant carriers may have a deletion (left, one copy of D) or a duplication (right, three copies of D) compared to non-carriers (middle, two copies of D).

CNVs that are associated with a clinical phenotype will be referred to as pathogenic CNVs, and the proportion of CNV carriers that exhibit clinical phenotypes indicate the clinical penetrance of the CNV. This is often measured with odds ratio or Cohen's D that are measures of effect size. Here, the odds ratio of 1.68, 3.47 and 6.71 will be used to indicate small, medium and large effect sizes, respectively, which are equivalent to Cohen's D of 0.2 (small effect size), 0.5 (medium effect size) and 0.8 (large effect size)<sup>2,3</sup>. The current thesis will focus on rare recurrent germline CNVs whose copy number differ between individuals in the human population. Henceforward, these will be referred to as simply CNVs unless stated otherwise. Likewise, individuals without a known pathogenic CNV will be referred to as non-carriers, unless it is uncertain if the controls carry a pathogenic CNV, then they will be referred to as controls.

By focusing on CNVs, we restrict the genetic link to differences in brain structure to structural variation of a smaller fragment of the DNA (i.e., CNV-harboring region), where studying the differences in gene dosage (i.e., having one, two or three copies of certain genes) has the potential to yield a mechanistic understanding of the links between genes and brain structural phenotypes. This is predicated on the idea that alterations in gene dosage can disrupt neurobiological processes that are important for brain ontogeny. Thus, studying the impact of CNVs on brain structure may provide a window into mechanisms that are involved in early neurodevelopment. Further, certain CNVs confer a higher risk of developing neuropsychiatric disorders. Thus, it has the potential to aid our understanding of neurodevelopmental psychiatric disorders, which are thought to be due to disruptions to neurodevelopmental processes<sup>4,5</sup>.

In the following sections, I will provide an overview of some of the key discoveries and concepts that underlies the rationale behind this thesis. First, I describe why genetics are thought to influence variation in brain structure. Second, I will address what constitutes

typical brain structure to understand what constitutes atypical brain structure, and how we can use CNVs to inform our understanding of atypical brain structure. Finally, a description of the neuroimaging techniques and their applications in elucidating the brain structural characteristics between individuals will be provided.

## 4.1 Genetics and phenotypic variation

*[Children] resemble their parents more than remoter ancestors, and resemble those ancestors more than any chance individual.*

Aristotle<sup>6</sup> (p.126)

As illustrated by the quote from Aristotle, it has long been thought that individuals resemble their family. Founded on this idea, several scientific questions have arisen. One of which is how much of this familial resemblance can be attributed to nurture (i.e., shared environment) and nature (i.e., genetics). Even today, there are ongoing scientific discussions about how much of the variation in complex phenotypic traits that can be attributed to genetics and environmental factors. Still, results from quantitative genetics have yielded important findings that aid our understanding of the genetic influence on phenotypic variation, including brain structure.

### 4.1.1 Quantitative genetics and phenotypic variation

Over the last century, substantial efforts have been put into examining how genetic variation between individuals is associated with individual differences in phenotypic traits, including behavioral and psychological traits. Although Francis Galton suggested that “intellectual capacity” is transmitted by descent more than 150 years ago<sup>7</sup>, it was not until the 1920s that quantitative genetic research emerged (e.g., Freeman et al., 1928<sup>8</sup> Lauterbach, 1925<sup>9</sup>; Merriman, 1924<sup>10</sup>). The early 1900s was also a period that was heavily influenced by environmentalism, where individuals were thought to be born as a “blank slate”, neglecting the importance of genetic influence on behavioral and psychological traits<sup>11</sup>. Still, efforts to examine the genetic influence on behavioral and psychological traits were growing. Over the following years, researchers took advantage of the genetic similarity between individuals



within the same family to examine the heritability of a range of different phenotypes, including cognitive ability<sup>12,13</sup> and psychopathology<sup>14</sup>.

To estimate heritability of a phenotype, one calculates how much genetic differences among individuals statistically account for the variation in a phenotype. Historically, heritability estimates were based on three main types of studies: adoption, family, and twin studies. Twin studies became the golden standard for estimating heritability due to the high genetic similarity between twins, and since age, environmental and familial factors are more even compared to family and adoption studies. Twin studies are based on dizygotic twins (i.e., siblings that, on average, share 50% of their genes) and/or monozygotic twins (i.e., siblings that share approximately 100% of their genes). Twins that are reared together share much of the same environmental influences. Thus, if the phenotypic correlation between monozygotic twins is higher than that of dizygotic twins, this can be attributed to genetic influences. Heritability estimates are calculated by subtracting the concordance rate of dizygotic twins from the concordance rate of monozygotic twins and multiply the product by two<sup>15</sup>.

Twin and family studies have found high heritability estimates for both global and regional brain structures<sup>16-22</sup>. Global features (i.e., brain volume, total cortical surface area, mean cortical thickness) all show high heritability estimates: ~70%, whereas brain regional heritability estimates are more variable: From ~10% to ~70%<sup>22</sup>. Moreover, the genetic correlation between cortical thickness and cortical surface area is weak, indicating that there are distinct genetic factors that influence the two global measures<sup>23</sup>. In addition, when accounting for global cortical thickness, others have identified specific genetic influence on regional cortical thickness<sup>24</sup>. However, it is important to note that regional heritability estimates may differ across datasets and that environmental factors are also important contributors to the variation in brain structure, despite the lack of evidence for strong effects of shared environmental factors on brain structure<sup>25</sup>

Taken together, the results indicate substantial, but also regional-specific, genetic influences on brain structure. However, the genetic variants that underlie the high heritability estimates are still under extensive investigation.

#### **4.1.2 Molecular genetics and phenotypic variation**

The discovery of the double helix structure of DNA is arguably one of the most important scientific findings in human history. Accompanied by the sequencing of the human genome in 2003<sup>26</sup>, it has allowed us to examine genetic variation at a molecular level, which has revolutionized our investigation of diseases and disorders. Genetic variation refers to the differences in genetic material within and between individuals of a population. The genetic variation between individuals has been extensively used to examine the relationship between variations in the DNA and phenotypic variation, which has the potential to provide a molecular understanding of heritable traits. Today, an impressive amount of research has yielded novel insight into the association between genetic variation and brain structure. Much of this research has focused on the association to common genetic variants, with a particular focus on single nucleotide polymorphisms (SNPs) present in at least 1% of the population. SNPs refer to variation in a single base position, whereas other genetic variants can include longer stretches of base pairs (bp).

The definition of the other types of genetic variants are somewhat arbitrarily defined with regards to the number of bp. Indels can refer to an insertion or deletion of 1-49 bp<sup>27</sup>, whereas translocations and inversions may refer to structural variations that are at least >50 bp long<sup>28</sup>. Translocations and inversions refer to instances where a piece of genetic material from one chromosome attaches to another chromosome or at the same chromosome but in the reverse orientation, respectively. Finally, CNVs are deletions or duplications of a larger segment of DNA, often defined as a structural variant spanning >1000 bp<sup>28-30</sup>.

In genome-wide association studies (GWAS), thousands of SNPs can be studied at once. Results from GWAS of different phenotypes are an alternative and a relatively new approach to estimating heritability, the so-called SNP-based heritability. SNP-based heritability estimates are lower than the twin-based heritability estimates, and thus cannot fully account for the epidemiological heritability estimates from e.g. twin studies, a numerical gap that has been termed “missing heritability”<sup>31</sup>. For instance, GWAS have identified hundreds of significant SNPs associated with brain structure, but the total explained variance of the common variants explains only ~1/3 of the heritability estimates derived from twin studies<sup>32</sup>. Moreover, the association between common genetic variants and brain structure vary across the cortex, indicating that genetic variants have regional-specific effects on the brain<sup>33</sup>. However, individual SNPs explain only a minor proportion of the variance in brain structure, and even the strongest regionally associated SNP accounts only for a minor proportion of the variance (i.e., 1.03%)<sup>32</sup>.

In parallel, twin studies have also reported high heritability estimates for autism spectrum disorder and schizophrenia (i.e., > 60%)<sup>34-36</sup>, whereas the SNP-based heritability is estimated to explain only ~12%<sup>37</sup> and ~24% of the variance, respectively. Same as for brain structures, individual SNPs typically only show minor effects on the risk for neurodevelopmental psychiatric disorders, exemplified by the significant SNPs in schizophrenia for which the highest reported odds ratio was 1.23 and the median odds ratio reported to be < 1.05<sup>38,39</sup>. Interestingly, emerging evidence indicates that variation in brain structure and neurodevelopmental psychiatric disorders are related, as indicated by their shared genetic architecture<sup>40-43</sup>. Still, the genetic architecture of brain structure appears to be less polygenic than brain-related disorders, such as schizophrenia<sup>42</sup>, indicating that there are overlapping but also distinct genetic influences on brain structure and brain-related disorders.

The numerical gap between SNP-based heritability and twin-based heritability indicate that the genetic determinants of brain structure and brain-related disorders are not fully characterized. There are several plausible reasons for the missing heritability, one of which may be due to unidentified SNPs of small effect size or rare genetic variants that are not included in GWAS, such as CNVs<sup>44</sup>.

### 4.1.3 CNVs and phenotypic variation

In recent years, individuals carrying a CNV have gained considerable interest due to their elevated risk of neurodevelopmental psychiatric disorders<sup>38,45-47</sup> and somatic disorders<sup>48</sup>. In parallel, some display altered anthropometrics (physical traits) with variable effect size estimates<sup>49</sup> and small to large effects on brain structure compared to non-carriers<sup>50,51</sup>. CNVs have also been used to investigate phenotypic variation across species and are important contributors to evolutionary changes. Indeed, gene duplication is considered to be a primary force for evolutionary changes by creating new genes<sup>52</sup> while preserving the function of the original gene copy<sup>53</sup>. For instance, duplication of the *opsin* genes have been linked to the development of trichromatic vision in Old World monkeys and apes<sup>54</sup>, and duplication of *NOTCH2* gene followed by modification to the *NOTCH2NL* gene have been linked to the expansion of the human brain<sup>55,56</sup>. Efforts to examine the impact of CNVs on current human phenotypic traits are ongoing, including the effects on brain structure and brain-related disorders.

Previous large-scale studies have typically examined up to 93 CNVs of interest<sup>48,49,57</sup>, which are individual CNVs present in less than 0.5% of the population<sup>45,58-61</sup>. In the UK Biobank, which is a large-scale biomedical database of over 500,000 middle-to-old aged individuals, the majority of these 93 CNVs have a prevalence of less than 0.01%<sup>57</sup>. However, the UK Biobank has been found to have a participation bias<sup>62</sup>, and generally yields lower

prevalence estimates of pathogenic CNVs compared to unbiased population estimates<sup>45,60</sup>. Despite CNVs being individually rare in the population, it is estimated that they are present in ~10-15% of neurodevelopmental disorder cases<sup>58,63-65</sup>. Indeed, previous studies have found that ~9% of individuals diagnosed with an autism spectrum disorder and ~2.5% of individuals diagnosed with schizophrenia are carriers of a known pathogenic CNV<sup>66,67</sup>. The higher risk for being diagnosed with a neurodevelopmental psychiatric disorder when carrying a CNV is also illustrated by odds ratio estimates that range from ~2 to >60 depending on the CNV of interest<sup>38,46</sup>. In accordance, chromosomal microarray is considered a first-tier clinical diagnostic test for patients with neurodevelopmental disorders, such as intellectual disability or autism<sup>64</sup>, with a potential to be used in psychiatric clinics<sup>1</sup>, emphasizing the clinical relevance of studying CNVs.

In patients referred for chromosomal microarray analyses, the most commonly observed inherited or *de novo* CNVs include 1p36 deletion, 1q21.1 deletion, 2q13 deletion and duplication, 7q11.23 deletion (Williams-Beuren syndrome), 9q34 deletion, 15q11.2 BP1-BP2 deletion, 15q13.3 deletion and duplications, 16p11.2 deletion, 22q11.21 deletions (22q11.2 deletion/DiGeorge/Velocardiofacial syndrome), and *SHANK3* deletion (Phelan-McDermid syndrome) with variable degree of clinical penetrance for neurodevelopmental disorders<sup>68,69</sup>. For instance, the clinical penetrance for neurodevelopmental disorders is considered to be lower for the 15q11.2 BP1-BP2 deletion compared to other pathogenic CNVs and it has been suggested to be a pathogenic CNV of mild effect size<sup>70</sup>. In contrast, the clinical penetrance of the 22q11.2 deletion syndrome is associated with a broad spectrum of clinical phenotypes, including variable penetrance of immune deficiencies, palatal anomalies, congenital heart defects, hypocalcemia<sup>71</sup>, as well as neurodevelopmental psychiatric disorders<sup>38,60,72-74</sup>.

It is important to note that studies that report the clinical phenotype of CNV carriers are largely based on clinical studies, which invariably gives an ascertainment bias, i.e., the included participants had a clinical phenotypic profile that initiated genetic investigations. However, as indicated by the prevalence estimates and phenotypic profile from the population studies, a substantial proportion of individuals in the population carry a “genetically undetected” CNV. Thus, the phenotypic profile of the whole population of CNV carriers is rarely fully characterized, including their phenotypic brain profile.

Due to the low prevalence of CNV carriers, studies examining brain structural differences between CNV carriers and non-carriers are scarce. However, studies have investigated brain structural differences in a subset, primarily those with a higher frequency, including the 1q21.1 distal<sup>75</sup> CNV, 7q11.13 deletion<sup>76,77</sup>, 15q11.2 BP1-BP2<sup>78–81</sup>, 16p11.2 proximal<sup>82–84</sup> and 16p11.2 distal<sup>85</sup>, and 22q11.2 CNVs<sup>86,87</sup>. For these, the effect sizes on brain structure range from small/moderate (Cohen’s  $D = \sim .3$ ) to large (Cohen’s  $D > 1.0$ ) depending on the CNV. The results from the abovementioned studies indicate that CNVs may play an important role in understanding the genetic architecture that is associated with variation in brain structure.

To summarize, both common and rare genetic variants contribute to the genetic architecture of the brain. Some of the “missing heritability” – the numerical gap between SNP-based and twin-based heritability, can be accounted for by rare genetic variants, including CNVs. Certain individual CNVs are enriched in individuals diagnosed with brain-related disorders and show small to large effects on brain structure. However, the characterization of the phenotypic profile of each CNV has been difficult to research due to the low prevalence of CNVs. Thus, most CNVs still remain to be investigated in detail. Establishing the brain profile of CNVs may provide a window into alterations in early neurodevelopmental processes that contributed to the atypical brain structure, with the

potential to provide a molecular link between gene variants and the development of the brain. However, a prerequisite to understanding what constitutes atypical brain architecture and neurodevelopment is to establish what constitutes typical brain architecture and neurodevelopment.

## **4.2 Brain architecture**

Brain architecture refers to the complex structural organization of the brain, including the macrostructural and microstructural components of cortical brain areas. The spatial organization of the brain is hierarchically organized according to their functions, connectivity, cell type composition and properties, gene expression, and ontogenetic and phylogenetic development<sup>88-90</sup>. Understanding the typical organization and development of the brain is of importance to understand the disruptions and mechanisms that may underlie atypical brain structure, with a further potential to inform the etiology of brain-related disorders.

### **4.2.1 Macrostructural and microstructural characteristics of the brain**

At the macrostructural level, the organization of the human brain corresponds to a sensorimotor to transmodal gradient, where the sensorimotor areas (i.e., primary visual, auditory, somatosensory cortex) are thought to be unimodal and involved in lower-order cognitive processing, such as visual, auditory and somatosensory processing. Transmodal areas (i.e., areas in the temporal, parietal and prefrontal cortex) are thought to be primarily multimodal and involved in higher-order cognitive processing<sup>88</sup>, also known as the association cortex<sup>90</sup>.

At the microstructural level, the human brain is made up by different cell types, including neuronal and non-neuronal cells. Non-neuronal cells include glial cells (oligodendrocytes, microglia, astrocytes) and endothelial cells. In the adult human brain, there are ~86 billion neurons and ~85 billion non-neuronal cells. The neuronal and non-neuronal

cell numbers differ between different parts of the brain, where ~80% of the neurons are found in the cerebellum and ~19% and ~1% of the neurons are found in the cerebral cortex and the rest of the brain (i.e., diencephalon, mesencephalon, basal ganglia and pons), respectively. The non-neuronal cells are mostly found in the cerebral cortex, which occupy ~72% of all non-neuronal cells, whereas the cerebellum and the rest of the brain consist of ~19% and ~9% of all the non-neuronal cells, respectively<sup>91</sup>. The neurons are connected through synapses, allowing them to be functionally connected by transmitting information across the brain, but the neuronal composition also varies across the cortical grey matter. For instance, the number of neurons change along the posterior to anterior axis (i.e., higher number of neurons in the posterior regions and lower numbers in the anterior regions)<sup>92</sup> and, in the macaque brain, areas with lower neuronal density have been found to be associated with larger number of structural connections to other areas<sup>93</sup>. Further, lower neuronal density has been suggested to be associated with larger neuronal size, including dendritic and axonal branching and soma<sup>94</sup>, and likewise, there is considerable variation in the dendritic architecture across the human brain. For instance, there is a higher dendritic spine density, length and number of spines in regions within the association cortex compared to regions in the somatosensory cortex<sup>95</sup>. Furthermore, histological studies have shown that the organization of the brain has deep roots in humans' phylogenetic and ontogenetic history.

#### **4.2.2 Phylogenetic and ontogenetic perspectives on the brain**

The human brain has been suggested to reflect a scaled-up primate brain and is accordingly the largest brain among primates with more neurons compared to other non-human primates. However, when accounting for brain size, the scaled cellular composition of the brain is relatively similar to that of other non-human primates<sup>96,97</sup>. Still, humans show a longer period of development with a gestation time of 268 days<sup>98</sup> compared to other primates



(gestation period ranging from 133 to 238 days)<sup>99</sup>, pointing towards a complex and protracted ontogenetic development of the human brain.

The human brain changes across the lifespan, but most of the brain development occurs during the prenatal period. According to the radial unit hypothesis, radial glial cells (also referred to as stem cells) create a scaffold of the brain during gestation, and the radial fibers span from the embryonic ventricular zone (inner layer of the brain) up to pial surface of the brain (outer layer

of the brain, Figure 2).

During development, neurons migrate along the radial fibers forming ontogenetic columns, which make up the cortex<sup>100</sup>. In

later gestation periods in humans, this has been shown to be a physically discontinuous

process<sup>101</sup>. Radial glial cells can also produce daughter cells that migrate along the parental fiber into the subventricular zone. These daughter cells also reproduce (referred to as intermediate progenitor cells) and can generate both neurons and glial cells, including astrocytes and oligodendrocytes<sup>102,103</sup>. In the outer subventricular zone, radial glia cells without contact to the ventricular surface, referred to as outer radial glia cells, also undergo self-renewing divisions<sup>104</sup>. Outer glial cells are highly enriched in the human brain and have

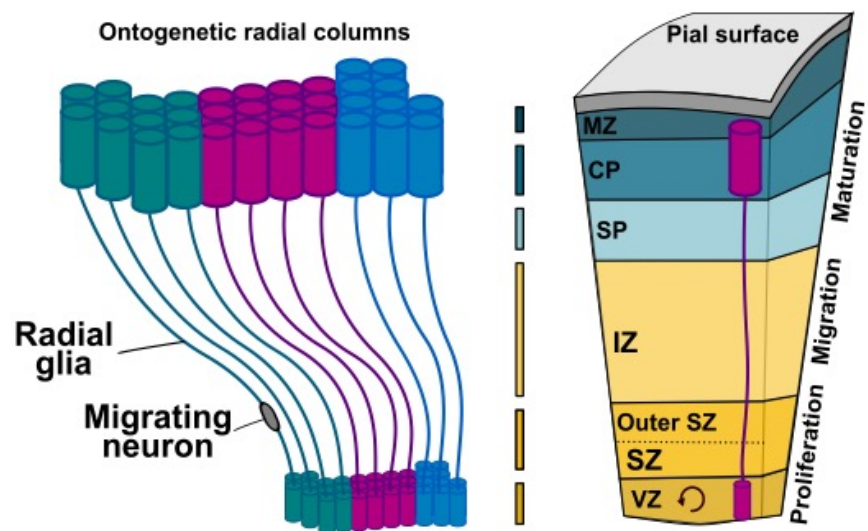


**Figure 2.** Simplified illustration of the radial unit hypothesis. Radial glia cells in the ventricular zone (VZ) proliferate and migrate towards the pial surface of the brain, through the subventricular zone (SZ), intermediate zone (IZ), subplate (SP), cerebral plate (CP) to its end point in the marginal zone (MZ), creating ontogenetic radial columns in the outer layer of the brain. Neurons migrate along these fibers, contributing to the complex cellular architecture of the brain. In humans, the creation of the scaffold of the brain has been found to be a discontinuous process in the outer subventricular zone. Inspired by Rakic (1988).

been suggested to be important for the evolutionary expansion of the human cortex<sup>104,105</sup>. The evolutionary conserved NOTCH signaling pathway plays a key role in this process by regulating cell fate<sup>106,107</sup> and influencing dendritic morphology<sup>108</sup>.

The formation of new neurons (i.e., neurogenesis) and synapses (i.e., synaptogenesis) play key roles in the organization of the brain. For instance, it has been suggested that the developmental processes during the prenatal period can be divided into two phases and that disruption to one of the two phases may result in different cortical phenotypes: A disruption before neurogenesis influences cortical surface area due to altered number of radial units, which can result in microcephaly (small surface area of the brain) and/or lissencephaly (smooth cortex), whereas a disruption after neurogenesis influences cortical thickness due to alterations in the ontogenetic column formation, which can result in a thinner cortex<sup>109</sup>.

Synaptogenesis show rapid development into postnatal stages, with continuous pruning well beyond childhood<sup>110,111</sup>. The number of synapses reaches its peak earlier in the visual and auditory cortex compared to the prefrontal cortex<sup>112</sup>. In the prefrontal cortex, the dendritic spine density peaks during childhood and shows subsequent synaptic pruning into young adulthood<sup>113,114</sup>. In addition, the gene expression levels of gene markers for synaptic density in the human prefrontal cortex peak in childhood, four years later than what is observed in the chimpanzees and macaques<sup>115</sup>. In the corpus callosum, the number of oligodendrocytes, which is important for myelination of the brain, seems to reach a plateau before the age of 5 years. Still, the myelination of the brain continues well into young adulthood<sup>116</sup>, where the myelination appears to develop in areas within the sensory cortices before areas within association cortices<sup>117</sup>.

The size of the brain shows rapid expansion during early development, and reaches 90% of an adult size brain around 5 years of age<sup>118,119</sup>. There is an increase in areal expansion of the cortex across ontogenetic development, where areas in the association cortices show

greater expansion relative to limbic and sensorimotor areas<sup>120</sup>. Interestingly, the brain areas that show greater evolutionary cortical expansion in humans reflect the regions that show the greatest postnatal brain development<sup>121</sup>.

Aging affects the brain in various ways: It has been characterized by brain volume and weight loss<sup>122,123</sup>, loss of myelination<sup>124</sup> and synapses<sup>125</sup>, lower dendritic spine density<sup>126</sup>, and neuronal shrinkage<sup>127</sup>. However, the actual number of cortical neurons does not appear to show a strong decrease with age<sup>128,129</sup> and programmed cell death is thought to be absent in old age<sup>130</sup>.

To conclude, the organization of the billions of neuronal and non-neuronal cells of the human brain is complex. The spatial variability of cellular composition in the human brain is not random but is deeply rooted in humans' ontogenetic and phylogenetic development. Sensorimotor regions appear to be evolutionary conserved, exhibit higher neuronal density, and develop faster compared to association cortices. Thus, it becomes apparent that disruptions to the spatiotemporal neurogenesis can have dramatic consequences for brain development, potentially affecting both global and regional-specific brain features. Disruptions to the spatiotemporal neurogenesis could be caused by altered gene expression, for instance through the effects of a CNV.

#### **4.2.3 CNV-related gene expression and the brain**

The complex ontogenetic development of the human brain is dependent on spatiotemporal gene expression<sup>131,132</sup>, and altered gene expression during development has been suggested to contribute to the development of neurodevelopmental psychiatric disorders<sup>133,134</sup>. The study of CNVs offers an opportunity to examine the impact of altered gene expression levels on cellular morphology and function, providing novel insight into the structural and functional consequences of altered gene expression levels.

CNVs are likely to have a direct influence on gene expression, as haploinsufficiency and triplosensitivity most often alter transcription levels<sup>135</sup>. For instance, the 22q11.2 deletion has been shown to reduce the protein-coding gene expression levels of the haploinsufficient genes by ~50% in cortical spheroids<sup>136</sup>. Such altered gene expression may also have important consequences for cell composition, morphology and function. As an example, cortical spheroid-derived neurons from 22q11.2 deletion carriers showed altered neuronal excitability and calcium signaling compared to controls<sup>136</sup>. Likewise, heterozygous deletion of the cytoplasmic FMRP interacting protein 1 (*CYFIP1*), present in the 15q11.2 BP1-BP2 genomic region in humans, reduced the number of oligodendrocytes and lower myelin thickness in the corpus callosum in rats<sup>137</sup>. In addition, expression of the human-specific *NOTCH2NL* gene (humans have three to four copies, whereas non-human primates have only one copy), located within the 1q21.1 distal genomic region, has been shown to increase NOTCH signaling. The human-specific *NOTCH2NL* gene delays neuronal progenitors and prolong neurogenesis, which ultimately leads to a higher number of cortical neurons<sup>55,56</sup>. Thus, the human-specific *NOTCH2NL* gene is a likely contributing factor to the smaller head size (i.e., microcephaly) in 1q21.1 distal deletion carriers and the larger head size (i.e., macrocephaly) in 1q21.1 distal duplication carriers<sup>138</sup>. This supports a role of the *NOTCH2NL* genes and NOTCH signaling in the phylogenetically and ontogenetically related brain expansion and is in line with radial unit hypothesis.

CNVs can also affect gene expression levels of genes outside the deleted or duplicated loci, presumably by influencing regulatory elements or disrupting the organization of the chromosomes<sup>139,140</sup>. For instance, compared to controls, individuals with a 22q11.2 deletion show different gene expression levels within and outside the 22q11.2 locus in blood: Individuals with a 22q11.2 deletion show downregulation of 23 genes within the 22q11.2

locus, and 2 downregulated genes and 1 upregulated gene outside the 22q11.2 locus after adjusting for medication and cell type composition<sup>141</sup>.

Studying CNVs may yield important insight into the phylogenetic and ontogenetic expansion of the human brain, as well as cellular phenotypes. CNVs change the microstructural and macrostructural properties of the brain likely through alterations of gene expression. However, the cellular composition of the brain varies across brain regions, and less is known about how CNVs impact specific brain regions at the microstructural level. Moreover, much of the abovementioned research on the cellular complexity and development of the brain is based on post-mortem *ex vivo* examinations. Such studies require slicing of brain tissue to examine the microstructural properties of the brain and an extensive effort to map different brain regions. Other methods are required to study the human brain *in vivo*, such as magnetic resonance imaging.

### **4.3 Magnetic Resonance Imaging (MRI)**

Using MRI scanners, we can obtain 3D images of the whole brain *in vivo*. Today, images from MR are widely used in research to examine brain structural changes within individuals and differences between individuals. To understand MRI findings, there is a need to characterize what a MR image reflects. A comprehensive description of the MRI sequence and physics is beyond the scope of the current thesis, but a brief overview of what an MRI image represents is presented due to the emphasis on MRI findings in the current thesis.

#### **4.3.1 Physics of MRI**

MRI takes advantage of the abundance of water in humans. A water molecule consists of two hydrogen atoms (H<sub>2</sub>) and one oxygen atom (O). The hydrogen atom consists of an electron and a proton. In a magnetic field, such as in an MRI scanner, the protons will line up with the magnetic field in either a parallel (low energy state) or antiparallel (high energy state)

fashion. Here, the protons will move in a circular “cone-like” fashion along the Z-direction of the magnet, called precession. The precession rate is given by the Larmor equation that is dependent on the strength of the magnetic field, which is measured in Tesla (T), formulated as follows:

$$\omega_0 = \gamma B_0,$$

where  $\omega_0$  is the precession frequency determined by the gyromagnetic ratio  $\gamma$  times the magnetic field  $B_0$ .

For protons, the  $\gamma$  equals  $\sim 42.5$  MHz and the magnetic field  $B_0$  in an MRI is typically either 1.5T or 3.0T. For a 3T MRI, the precession frequency  $\omega_0$  will be  $42.5 \times 3 = 127.5$ . This produces a net magnetic vector along the direction of the magnet (i.e., Z-direction). The MRI also contains gradient coils in the x-y-z directions, which are used to alter the magnetic field. This is done to alter the Larmor frequency rate of the atoms in a linear fashion (i.e., faster with higher magnetic field), which is crucial for slice localization of the brain (or any other tissue of interest). Subsequently, the gradients can be turned on and off to generate a phase shift of the proton spins (spinning at different rates), which is important for localization within the slice of interest.

A radiofrequency coil transmits radio frequency pulses at the Larmor frequency into the body where the energy is picked up by the precessing protons with the same Larmor frequency, a phenomenon referred to as resonance. This tilts the alignment of the nuclei, where some protons in the low energy state go into a high energy state. The protons start to synchronize and precess in phase, producing a magnetic vector in the transverse direction. When the radiofrequency pulse is turned off, the atoms go back into their original state. During this process, the absorbed energy from the radiofrequency pulse is released and is picked up by the surrounding radiofrequency coils. The coils receive signals at different radiofrequency waves (with different amplitudes, frequencies and phases). This signal is

digitalized and make up a data matrix, which is referred to as  $k$ -space and contains information about the spatial frequencies and phases of the signal. To obtain the image of the brain, an inverse Fourier transformation is performed on the  $k$ -space data matrix.

#### 4.3.2 T1-weighted imaging

Different MRI sequences (e.g. T1 and T2) are used to obtain different information. The parameters adjusted to achieve different sequences are: Repetition time (TR) - represents the time between each radiofrequency pulse is sent to the same slice. The echo time (TE) - refers to the period when the signal is received. Flip angle - represents how much the magnetic vector is tilted or flipped and will be influenced by the magnitude of the radiofrequency pulse.

A T1 sequence is characterized by a short TR and TE, whereas a T2 sequence is characterized by a longer TR and TE. For a T1-weighted image, the coils are picking up the radiofrequency signal that is emitted by the protons when they return to their original state (i.e., in the low energy state). The time period where the protons return to their original state varies as a function of the surrounding tissue. In the ventricles, where the protons are in the cerebrospinal fluid, the protons hold on to the energy for a longer period compared to other tissue types that release the energy faster. Hence, depending on the surrounding tissue, the protons return faster to their original state compared to the protons in the ventricles. With the short TR and TE in T1, the transverse magnetization will be different across tissues. Protons in fluids are not given sufficient time to go out of phase and return to their original state, whereas protons in other tissues are further into that process. Thus, the additional radiofrequency signals tilt more of the protons in fluid faster into a high energy state, yielding small transverse magnetization. However, protons in brain tissue will produce a greater transverse magnetization. Thus, the radiofrequency coils receive a low amount of energy from the protons in fluid and higher amount of energy from other tissue types. Still, different tissue types will also yield slightly different amount of energy. By convention, the areas that have

been releasing low amount of energy will appear black (low intensity values) and the areas that have been releasing higher amount of energy will appear grey/whiter (high intensity values) on the T1-weighted MR image.

A T1-weighted MR image is made up by voxels that are typically 1x1x1 mm, where the voxels consist of different intensity values that form the image of the brain. There are two important limitations to the output of the T1-weighted image. First, the intensity values in an MR image are based on the released energy from water molecules, and do not directly measure specific cell types, cell density or myelinated axons. Still, the intensity values are influenced by the surrounding tissue, which contribute to the spatial map of the brain. Second, the intensity values may be influenced by a complex composition of different cell types. Since there are over ~86 billion neurons and ~85 billion non-neuronal cells in the human brain<sup>91</sup> and the cellular composition varies across the brain<sup>92,95</sup>, it becomes apparent that the intensity value of a single voxel is influenced by many and also different cell types. For instance, by extrapolating numbers from a rat, with the caveat that we do not know the exact scaling between rats and humans, it has been estimated that that a 2 mm isotropic voxel in humans may contain as much as ~0.5 to >5 million axons or 52,000 oligodendrocyte precursor cells and 76,000 microglia or ~700,000 oligodendrocytes and 180,000 astrocytes<sup>142</sup>. The accuracy of the estimate is unknown, but this uncertainty warrants caution in our interpretation of what an MR image reflects. Still, MRI can provide insight into larger anatomical structures of the brain, suitable to detect variation in global brain measures, as well as regional macrostructural variations.

### **4.3.3 T1-weighted MRI-derived measures**

Over the last couple of decades, powerful tools have been developed to analyze the T1-weighted MR images of the brain. One of the most popular tool for analyzing brain structural imaging data is FreeSurfer<sup>143</sup>, which can be used to parcellate the brain into distinct



brain regions using brain atlases and to extract global and regional specific brain measures. The most common brain measures extracted include cortical surface area, cortical thickness, and subcortical volume. The cortical surface area is reconstructed to get an estimate of the pial surface of the brain<sup>144</sup>. Cortical thickness is estimated by the shortest distance between the grey/white matter boundary and the pial surface<sup>145</sup>. Subcortical volume is estimated by labeling voxels in the subcortical structures and calculating the volume of the structures<sup>146</sup>. Cortical regional-specific brain measures can be obtained by labeling different regions using a brain atlas, such as the Desikan-Killiany atlas that includes 34 gyral based regions of interest (ROI)<sup>147</sup>. A visualization of the derivation of MRI-derived measures is shown in Figure 3.

The MRI-derived measures of cortical thickness, surface area, and subcortical volume show overlapping, but primarily distinct genetic architecture<sup>32,33</sup>, which indicates different genetic influences on the MRI-derived measures. Global and regional-specific MRI-derived measures have been extensively used to examine group level differences between neurodevelopmental psychiatric disorders, and in recent years differences between CNV-carriers and non-carriers (see section 4.4 for a detailed description).

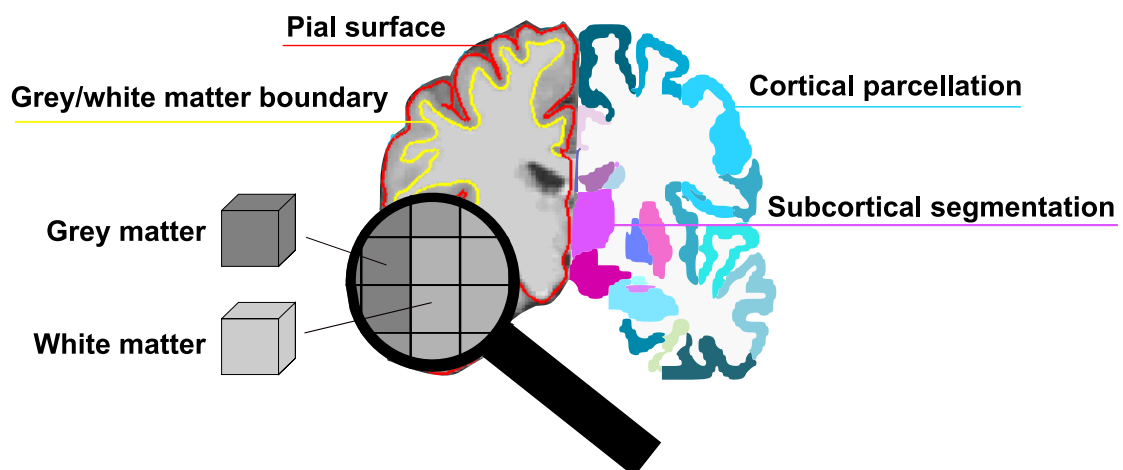


**Figure 3. Parcellation and segmentation of brain structures.** A brain atlas is overlaid on the T1-weighted image that makes up the regions of interest. Cortical parcellation is based on the outer layers of the brain, whereas subcortical segmentation is based on subcortical structures. Grey matter and white matter may yield different voxel intensity values that appear darker and lighter on the T1-weighted image, respectively.

#### 4.3.4 Diffusion weighted imaging

Diffusion weighted imaging (DWI) is an MRI sequence that is sensitized to the motion of water molecules *in vivo*. In a free environment, water molecules will exhibit Brownian motion and will follow a Gaussian distribution in a 3-dimensional space over a given time interval. This random motion of molecules in a specific space and time is described as diffusion (see Beaulieu, 2002<sup>148</sup>; Le Bihan, 2003<sup>149</sup> for reviews). To obtain DW images, a dephasing gradient pulse will vary along the gradient and a second rephasing pulse will be applied in the opposite direction. The dephasing of the precession of protons will rephase to its initial state after the second pulse if the molecules have not changed their position. In contrast, the molecules that have moved will not have protons in phase after the second pulse, which will result in a loss of signal. The signal loss can be used to estimate an apparent diffusion coefficient (ADC) indicating the diffusion of water molecules in each voxel<sup>148</sup>. Without any barriers, such as in the cerebrospinal fluid, water molecules will flow freely in space and time and the diffusion displacement across time will be isotropic reflected by a high ADC value<sup>150</sup>. However, in biological tissue this is rarely the case, as biological barriers such as myelin, cell membranes and microtubules would hinder or restrict the movement of water molecules<sup>148</sup>. For instance, myelin surrounding axons will restrict the diffusion perpendicular to the axonal direction of a neuron and at the same time allow water molecules to flow relatively freely along the direction of the axon, reflected by a low ADC value<sup>148,149</sup>.

#### 4.3.5 Diffusion MRI-derived measures

Diffusion MRI-derived measures can be used to gain insight into white matter microstructure. From diffusion MRI, we can obtain ADC maps that are sensitive to diffusivity along the applied magnetic gradient. However, a single ADC image is insufficient to describe overall displacement of water molecules in three dimensions, as required for

diffusion tensor imaging (DTI). In DTI, at least six different gradient directions and a non-weighted image are required to create a tensor<sup>151</sup>. A tensor represents a three-dimensional ellipsoid and can be calculated in each voxel with DTI. Here, 3 parameters define the length (eigenvalues:  $\lambda_1, \lambda_2, \lambda_3$ ) and 3 parameters define the orientation (eigenvectors:  $\epsilon_1, \epsilon_2, \epsilon_3$ ) of a tensor. The eigenvalues and eigenvector are used to calculate fractional anisotropy (FA), mean diffusivity (MD), radial diffusivity (RD), and axial diffusivity (AD) of white matter fiber tracts. DTI is a tensor-based approach, meaning that the MRI-derived signal is used to fit a tensor and the derived measures are used to describe the properties of the tensors. Thus, it is relatively nonspecific to the underlying biology.

In contrast, neurite orientation dispersion and density imaging (NODDI) is a multicompartment-based approach and can be used to estimate specific biological properties of the underlying cellular architecture<sup>152</sup>. In NODDI, predefined geometrical representations are used to predict microstructural properties from the MR signal. By setting a priori model parameters of microstructural properties, NODDI generates normalized signals that represent extracellular, intracellular, and cerebrospinal fluid compartments. This can be used to obtain measures that are useful for characterizing white matter microstructure, including the extracellular volume fraction (ECVF), intracellular volume fraction (ICVF), isotropic volume fraction (ISO) and orientation dispersion index (ODI). In white matter, the ECVF represents the extra-axonal space, ICVF represents the volume of intra-axonal space, ISO represents the isotropic Gaussian diffusion (i.e., diffusion in free water), whereas ODI represent the dispersion of axons<sup>152</sup>. It is important to note that both DTI and NODDI measures are only indirect measures of white matter microstructure. Nevertheless, it can be used to get insight into some of the microstructural properties of white matter of the brain.

#### 4.3.6 MRI-derived measures and cognition

The MRI-derived estimate of total brain volume is considered to be the best and most replicated neuroimaging predictor of cognitive performance, where higher estimates of brain volume is linked to better cognitive performance<sup>153–155</sup>. It is important to note, however, that the association between brain volume and cognitive performance is likely not driven by brain volume per se. For instance, there are substantial differences in total brain volume between males and females (Cohen's  $d = 1.41$ )<sup>156</sup>, but no to negligible sex differences in general cognitive ability<sup>157,158</sup>. In accordance with this, the association between total brain size and general cognitive ability do not vary by sex, indicating that the association still holds within sexes<sup>155</sup>. Thus, this points towards a more complex relationship between brain size and cognitive ability, likely reflecting an important role of the cellular architecture and function of the brain.

Regional measures of grey and white matter have also been associated with cognitive performance, with variable regional effect size estimates. For instance, the strongest associations between regional volume and cognitive ability are found in the prefrontal cortex<sup>155</sup>. For white matter microstructure, the strongest associations between FA and general cognitive ability are found in thalamic pathways, association fibers and forceps minor<sup>155</sup>. In general, brain-cognition associations are characterized by small effect sizes, and large sample sizes are required to reliably detect such associations<sup>159,160</sup>. Still, the results point toward an association between brain structure and cognitive functioning, indicating that alterations to brain structure have functional consequences.

#### 4.3.7 MRI-derived measures and age-related differences

MRI-derived measures can be used to gain insight into age-related differences *in vivo*. For instance, cortical grey matter in sensorimotor regions have a slower growth rate compared

to association cortices in the first two years after birth using longitudinal data<sup>161</sup>. Structural covariance analyses (i.e., grouping brain regions based on high inter-regional correlations) have shown that the gray matter networks in sensorimotor cortex are well established in early childhood, whereas gray matter networks in the association cortex show a continuous expansion through adolescence<sup>162</sup>. In line with this, MRI-derived cortical regions in the sensorimotor areas appear to mature faster than association areas, supported by their differential trajectories in cortical volumes<sup>163</sup>, cortical surface area<sup>121</sup> and cortical thickness<sup>164</sup>. Both the numerical estimates of cortical thickness and cortical surface area show a steep increase during the first two years of life<sup>165</sup>, where cortical thickness peaks in early childhood and cortical surface area in late childhood<sup>166</sup>. This is followed by a subsequent decline in cortical thickness from childhood and a slight decline in cortical surface area during adolescence<sup>166–168</sup>. The MRI-derived measures continue to show age-related changes across the lifespan<sup>169–172</sup>. Some of the late maturing areas in the association cortices are regions that are susceptible for atrophy in older age<sup>163</sup>. The association between MRI-derived measures and age, indicate that MRI-derived measures carry age-related information about an individual, which has the potential to be used as a marker for biological age.

### **Brain age prediction**

Since the brain changes across the lifespan, MRI-derived measures can be used to train models to predict an individual's age. The accuracy is quite high but still, some variation between the predicted age and chronological age will exist: Some individuals get a predicted age that is lower than their chronological age, while others get a higher predicted age than their chronological age. Such differences have been termed brain age gap and has been suggested to be a biomarker for brain ageing, where a higher brain age gap could indicate accelerated or accentuated (i.e., a sudden change or “hit” in the ageing trajectory) but

otherwise stable ageing<sup>173</sup>. Higher brain age gap has been associated with a number of markers of older age, including increased mortality risk, worse motor and lung function<sup>174</sup>, increase in measures of cardiometabolic and cardiovascular risk factors<sup>175,176</sup>, lower performance on cognitive tasks<sup>177,178</sup>, and older looking facial appearance<sup>177</sup>. In addition, brain age gap is heritable and is higher in individuals diagnosed with certain brain-related disorders compared to controls<sup>179</sup>.

Brain age may be of interest for CNV research as certain CNV carriers associate with brain disorders and show group differences in brain structure. Interestingly, carriers of certain pathogenic CNVs show poorer physical health and increased mortality risk in middle-to-old age<sup>48,49</sup>, potentially indicating atypical ageing. If the haploinsufficient genes in CNV carriers influence brain structure, this may also affect age-related brain structural changes, either through accelerated or accentuated brain ageing. This can be tested through brain age gap calculations. Still, the interpretation of differences in brain age is limited to the input of MRI-derived measures, and the cellular architecture underlying MRI-derived measures are largely unknown. However, such interpretations can be aided by recent advances in imaging transcriptomics.

### **Spatial convergence between MRI-derived phenotypes and gene expression**

The emerging field of imaging transcriptomics can provide novel insights into the spatial convergence between *ex-vivo* gene expression levels and *in-vivo* MRI-derived measures<sup>180,181</sup>. A widely used database to obtain *ex vivo* gene expression levels comes from the Allen Human Brain Atlas derived from post-mortem brain tissues<sup>182</sup>. Despite low number of specimens (i.e., 6 post-mortem brains), it includes gene expression data that span the macrostructural regions across the cortex, which can be used to obtain regional gene expression levels that can be spatially overlapped with MRI-derived measures extracted from

a brain atlas, such as the Desikan-Killiany atlas<sup>180</sup>. This approach is founded on the idea that gene expression levels can be exploited to provide insights into the cellular and molecular underpinnings of MRI-derived measures. As such, since gene expression levels vary across brain regions<sup>183</sup>, there is a potential to identify genes that have an expression pattern that spatially converge with regional variation in MRI measures. Further, by establishing regional overlap between gene expression levels and variation in the MRI-derived phenotypes, we can potentially infer biological processes and cellular phenotypes that are associated with the MRI-derived phenotypes through functional and cell-type enrichment analyses<sup>184,185</sup>.

Another similar approach, known as virtual histology, can be used to link cell-type gene expression and MRI-derived phenotypes by focusing on genes that are enriched in different cell types<sup>4,186–188</sup>. For instance, cortical regions that experience less cortical thinning during childhood through early adulthood also exhibit higher gene expression of astrocytes and microglia gene markers<sup>186</sup>, whereas higher expression of genes involved in myelination are associated with greater cortical thinning in childhood and adolescence<sup>188</sup>. The imaging transcriptomics approach has also been fruitful in identifying neurobiological correlates of the regional variation in group differences in various brain disorders<sup>4,187</sup>. For instance, higher expression levels of genes specific to astrocyte, CA1 pyramidal and microglia cells have been associated with greater case vs control differences in cortical thickness for schizophrenia and autism spectrum disorder<sup>187</sup>. Such studies can be useful for establishing neurobiological correlates of group differences in case-control studies, including those observed in CNV carriers.

#### **4.4 Characteristics of 1q21.1 distal, 15q11.2 BP1-BP2, and 22q11.2 CNVs**

Studying CNVs offer a powerful, yet relatively unexplored, approach to examine associations between genetic variants and phenotypic variability. By establishing their brain

profile, we may get insights into the consequences of the early formative years of brain organization, which may be useful to disentangle neurodevelopmental events that contribute to the global and regional brain structural characteristics of CNV carriers. Previous studies of the phenotypic profile, including the brain profile, of the 1q21.1 distal, 15q11.2 BP1-BP2, and 22q11.2 CNVs have provided some intriguing findings.

#### **4.4.1 1q21.1 distal deletion and duplication**

The 1q21.1 distal deletion has a prevalence of approximately 1 in 4800 and the reciprocal duplication approximately 1 in 1030<sup>45</sup>. The 1q21.1 distal CNVs are both associated with schizophrenia<sup>73,189</sup>, autism spectrum disorder<sup>45</sup>, attention deficit/hyperactivity disorder<sup>45,190</sup> and major depression disorder<sup>45,191</sup>. The 1q21.1 distal deletion carriers show worse cognitive and motor functioning, as well as speech problems and hypotonia compared to controls<sup>192</sup>.

Both 1q21.1 CNVs display small to large effects on the brain. Group differences on intracranial volume to non-carriers are present for 1q21.1 distal deletion and duplication carriers, respectively, with a Cohen's *d* of -1.84 and 0.9, respectively. This mirrors previous findings of microcephaly in deletion carriers and macrocephaly in duplication carriers<sup>138,192</sup>. Microstructurally, the 1q21.1 distal deletion carriers show evidence for a lower total cortical surface area compared to non-carriers including effects on several individual regional cortical surface areas<sup>75</sup>. In turn, the 1q21.1 distal duplication carriers show lower volume of the caudate and hippocampus in addition to higher cortical surface area of the pars opercularis<sup>75</sup>.

#### **4.4.2 15q11.2 BP1-BP2 deletion and duplication**

The 15q11.2 BP1-BP2 deletion and duplication prevalence is estimated at approximately 1 in 230 and 1 in 204 individuals<sup>45</sup>. The 15q11.2 BP1-BP2 deletion confers a higher odds ratio for schizophrenia<sup>46,73,189</sup> and is associated with dyslexia and dyscalculia<sup>79</sup>.



Likewise, deletion carriers show worse performance in cognitive tasks of small to moderate effect sizes compared to non-carriers<sup>57,78,81</sup>. Deletion carriers also exhibit lower height, worse lung functioning, and increased body mass index, fat, blood pressure, heel bone density and waist-to-hip ratio of small effect size in middle-to-old aged individuals<sup>49</sup>. The 15q11.2 BP1-BP2 duplication have not been convincingly associated with any specific neuropsychiatric disorder<sup>45</sup> although they display higher body mass index and higher fat percentage in addition to lower hand grip strength compared to non-carriers<sup>49</sup>.

Both 15q11.2 CNV carriers display small to moderate effects on the brain. The 15q11.2 BP1-BP deletion carriers show an overall thicker cortex, lower total cortical surface area, as well as smaller nucleus accumbens compared to non-carriers. The higher cortical thickness and lower cortical surface were primarily found in frontal regions. The 15q11.2 BP1-BP2 duplication carriers show a higher cortical thickness in postcentral gyri, insular cortex, and pars opercularis compared to non-carriers<sup>81</sup>.

#### **4.4.3 22q11.2 deletion**

The 22q11.2 deletion occurs in approximately 1 in 3700 individuals<sup>60</sup>. The 22q11.2 deletion syndrome is caused by the 22q11.2 deletion and is a multisystem disorder characterized by psychiatric disorders, congenital malformations, immune deficiencies, heart defects, and palatal and facial anomalies<sup>193,194</sup>. In addition, it represents one of the largest known genetic risk factor for schizophrenia to date (estimated odds ratio up to  $> 67$ )<sup>38,73</sup>, and yields a significant risk for other neurodevelopmental disorders such as attention deficit/hyperactivity disorder and autism spectrum disorder<sup>72,74,195</sup>. The 22q11.2 deletion show moderate to large effects on brain structure, including a higher cortical thickness and lower cortical surface area with variable effect size estimates for regional specific estimates of cortical thickness and cortical surface area. In contrast to the wide-spread lower cortical surface area and higher cortical thickness, the 22q11.2 deletion carriers specifically show a

higher cortical surface area in the precentral gyri and insula and thinner cortex in the parahippocampal and superior temporal gyri and left caudal anterior cingulate compared to controls<sup>87</sup>. For subcortical structures, the 22q11.2 deletion carriers show lower volume for the hippocampus, thalamus, amygdala, and putamen, and higher volumes for the lateral ventricle, caudate and nucleus accumbens compared to controls<sup>86</sup>. Further, 22q11.2 deletion carriers with psychosis show overall thinner cortex and lower volumes of the thalamus, hippocampus, and amygdala compared to 22q11.2 deletion carriers without psychosis, where the interregional effect sizes for cortical thickness and subcortical volume resemble those observed in idiopathic schizophrenia<sup>86,87</sup>.

#### **4.4.4 Implications of CNV brain profiling.**

The group differences in CNV carriers may provide clues about possible neurodevelopmental processes that results in atypical brain structure. For instance, the differences in intracranial volume and cortical surface area in 1q21.1 distal CNV carriers has been hypothesized to be a consequence of the altered copy numbers of the *NOTCH2NL* gene (mentioned above), which influence neurogenesis<sup>55,56</sup>. Likewise, the higher cortical thickness in 15q11.2 BP1-BP2 deletion carriers may be due to alterations in myelin thickness<sup>137</sup>, as increased myelin is linked to cortical thinning as measured with MRI<sup>196</sup>. The 15q11.2 BP1-BP2 CNVs also show group differences in diffusion MRI-derived measures compared to controls<sup>78,197</sup>, which includes measures that are influenced by myelination.

Differences in diffusion MRI-derived measures are also found in 22q11.2 deletion carriers. The deletion carriers display lower MD, RD, and AD of moderate to large effect sizes on cortical white matter tracts, but also regionally varying directional effects (i.e., higher and lower) for FA on the white matter tracts<sup>198</sup>. Just as MRI-derived measures, DTI-derived measures are also challenging to interpret as they are inherently nonspecific to the underlying microstructural characteristics<sup>199</sup>. Through imaging transcriptomics, the gene expression

levels of the protein-coding genes within the 22q11.2 loci were correlated to the 22q11.2 deletion brain profile. The gene expression levels of the *P2RX6* gene were found to be associated with the cortical thickness brain profile, whereas the gene expression levels of the *AIFM3* and *DGCR8* genes were associated with the cortical surface area brain profile of 22q11.2 deletion carriers<sup>200</sup>. It should be noted, that the 1q21.1 distal, 15q11.2 BP1-BP2 and 22q11.2 CNVs harbor many genes. Thus, even if specific genes are implicated through imaging transcriptomics, a direct link between any genes and MRI-derived measures are speculative at this point and must be supported by complementary evidence.

Establishing the brain profile of CNV carriers may in itself aid in future stratification of brain-related disorders. Despite robust mean group differences in neuroimaging studies, brain-related disorders are characterized by substantial brain heterogeneity. For instance, individuals with schizophrenia show increased inter-individual differences in MRI-derived measures compared to healthy controls<sup>201</sup>. The effect sizes in MRI-derived measures observed in CNV research yield two-to-four times larger effects sizes (Cohen's D from ~0.3 to > 1.0) compared to those observed in case-control studies of neurodevelopmental and psychiatric disorders (Cohen's D from ~0.1 to ~0.5)<sup>202</sup>.

Interestingly, some of the effect sizes in CNV carriers go in the opposite direction of what is observed in case-control studies of schizophrenia, even for CNVs associated with schizophrenia. For instance, the higher cortical thickness in 15q11.2 BP1-BP2 deletion and 22q11.2 deletion contrasts with lower mean cortical thickness observed in schizophrenia<sup>203</sup>. This could indicate distinct subprofiles of individuals with brain-related disorders, potentially useful for stratification.

A recent paper established the CNV-specific brain profile of 8 different CNV carriers based on clinical samples<sup>204</sup>. This was used to identify individuals in the UK biobank with brain profiles that resembled the CNV-specific brain profiles and then the brain profile was

correlated to ~1,000 lifestyle indicators through the UK Biobank resource. Although the CNV-specific brain profiles are distinct from each other, their associations to phenotypical traits converged, including convergence to various bodily systems. This illustrates how brain profiling of CNV carriers can be used to detect meaningful associations to clinical phenotypes.

## **4.5 Summary**

The high heritability of brain structure combined with the relatively lower SNP-based heritability estimates (compared to twin-derived estimates) indicate that something beyond common genetic variants contributes to the genetic architecture of the brain. Some CNVs show substantial effects on brain structure as measured with MRI, implicating CNVs as contributors. Macro- and microstructural characteristics of the brain are determined by complex biological processes during neurodevelopment. In certain CNV-carriers biological processes are likely disrupted by the haploinsufficiency or triplosensitivity of the CNV-harboring region. The 1q21.1 distal, 15q11.2 BP1-BP2 and 22q11.2 CNVs all harbor genes that can potentially alter cellular characteristics of the brain, which may contribute to the observed differences in MRI-derived measures of brain structure. Thus, MRI studies of CNV carriers may provide a window into the mechanisms that are important for neurodevelopment. Taken together, studying CNVs provides a ‘genetic-first’ approach that has the potential increase our understanding of brain structural variations between individuals.

## 5 THESIS AIMS

The primary objective of the current thesis is to gain novel insight into how rare recurrent copy number variants impact brain structure. To address this objective, we examined how the brain architecture of the 1q21.1 distal (study I), the 15q11.2 BP1-BP2 (study I & study II), and the 22q11.2 (study III) CNV carriers differ from non-carriers. The secondary objectives were to advance our understanding of what the brain structural differences reflect in terms of age-related differences and the underlying neurobiology.

### 5.1 Study I

In study I, we aimed to dissect the regional and global differences of the brain in the 1q21.1 distal and 15q11.2 BP1-BP2 CNV carriers. We hypothesized that anterior regions within the association cortices were more affected, whereas posterior regions within the primary sensorimotor cortices were less affected in carriers of the 1q21.1 distal and 15q11.2 BP1-BP2 CNVs.

### 5.2 Study II

In study II, we aimed to examine the apparent brain ageing and ageing trajectories of motor, heart and lung functioning in a sample of older adults with either a 15q11.2 BP1-BP2 deletion or duplication. We hypothesized that the 15q11.2 BP1-BP2 CNV carriers will exhibit group differences in the estimated brain age gap.

### 5.3 Study III

In study III, we aimed to characterize 1) differences in axonal density between 22q11.2 deletion and controls using NODDI measures, 2) the spatial convergence between gene expression levels of cell types and 22q11.2-specific gene networks and the cortical brain

profiles of 22q11.2 deletion carriers using imaging transcriptomics. We hypothesized that the 22q11.2 deletion carriers will show evidence for higher axonal density compared to controls and aimed to establish novel neurobiological correlates of the cortical brain profiles of the 22q11.2 deletion carriers.

## 6 METHODOLOGY

Research on rare CNVs – including the 1q21.1 distal, 15q11.2 BP1-BP2 and 22q11.2 CNVs - require extensive national and international collaboration between researchers and participants to obtain sufficient sample sizes and thus power to test the hypotheses statistically. Consequently, large collections of data are of fundamental importance for CNV research. The current thesis contains data from several cohorts across the world, as well as data available from open access databases. The statistical analyses applied are based on case-control designs and the data is primarily cross-sectional data. This section provides an overview of the material and methods used in the studies of the thesis.

### 6.1 Samples

The three studies included in the thesis are based on samples from a variety of data sources.

For study I, the samples were derived from the UK Biobank and the Enhancing Neuro Imaging Genetics Through Meta Analysis-Copy Number Variant (ENIGMA-CNV) working group core dataset. An overview of the sample characteristics for study I is shown in Table 1.

For study II, the sample was derived from the UK Biobank only. An overview of the sample characteristics for study II is shown in Table 2.

For study III, the samples were derived from data collected at Stanford University and University of California, Los Angeles (UCLA), as well as gene expression data obtained from cortical spheroids, the Allen Human Brain Atlas, and the Gene Expression Omnibus database. An overview of the sample characteristics of the diffusion MRI dataset used in study III is shown in Table 3. Note that this overview describes the sample characteristics after exclusion of participants with insufficient MRI data quality (see below for details).

Cortical spheroids are three-dimensional brain cultures derived from human induced pluripotent stem cells (iPSCs), which is found to yield high reliability of neural differentiation across cell lines<sup>205</sup> and to recapitulate the transcriptional architecture of fetal brain tissue<sup>206,207</sup>. Here, the gene expression data from cortical spheroids were derived from 17 22q11.2 deletion samples and 25 control samples. Gene expression data were derived from day 25, 50, 75 and 100 of differentiation. Post-mortem gene expression data from the Allen Human Brain Atlas were derived from 6 adults without a diagnosed psychiatric or neurological disorder (mean age = 42.50 years, age range = 24-57 years, 1 female).

**Table 1:** Sample characteristics for the participants included in study I.

	<b>1q21.1 distal deletion</b>	<b>1q21.1 distal deletion comparison group</b>	<b>1q21.1 distal duplication</b>	<b>1q21.1 distal duplication comparison group</b>
<b>N</b>	30	150	27	135
<b>Mean Age</b>	41.6	44.6	56.4	53.7
<b>Age range</b>	7.7-68.7	9.2-76.2	18.7-73.1	9.5-77.2
<b>Females (%)</b>	14 (46.7%)	73 (48.7%)	15 (55.6%)	77 (57.0%)
	<b>15q11.2 BP1-BP2 deletion</b>	<b>15q11.2 BP1-BP2 deletion comparison group</b>	<b>15q11.2 BP1-BP2 duplication</b>	<b>15q11.2 BP1-BP2 duplication comparison group</b>
<b>N</b>	170	850	243	1,215
<b>Mean Age</b>	55.9	55.9	55.8	55.9
<b>Age Range</b>	7.1-77.7	6.8-90.0	7.83-88.5	3.75-89.8
<b>Females (%)</b>	90 (52.9%)	428 (50.4%)	127 (52.3%)	608 (50.0%)



**Table 2:** Sample characteristics for the participants included in study II.

	<b>15q11.2 BP1-BP2 deletion</b>	<b>15q11.2 BP1-BP2 deletion comparison group</b>	<b>15q11.2 BP1-BP2 duplication</b>	<b>15q11.2 BP1-BP2 duplication comparison group</b>
<b>N</b>	124	496	142	568
<b>Mean Age</b>	64.7	64.9	63.9	63.6
<b>Age Range</b>	49.3-77.5	47.2-80.5	46.7-81.3	48.3-80.2
<b>Females (%)</b>	62 (50.0%)	248 (50.0%)	75 (52.8%)	300 (52.8%)

**Table 3:** Sample characteristics for the participants with diffusion MRI included in study III.

	<b>22q11.2 deletion</b>	<b>22q11.2 deletion comparison group</b>
<b>N</b>	50	35
<b>N scans</b>	69	46
<b>Mean Age</b>	21.0	20.4
<b>Age Range</b>	7.40-51.1	7.81-45.3
<b>Female (%)</b>	46 (66.7%)	27 (58.7%)

Note. Age and sex are based on the full sample, across all observations.

### 6.1.1 The UK Biobank.

The UK Biobank is a large biomedical database, including >500,000 middle to older aged participants across the United Kingdom. The biobank contains a variety of genetic and health-related information and measures from the participants included in the study. At the time of the analysis for study I and II, genome-wide genetic data were available for ~490,000 participants and MRI data of the brain were available for ~40,000 participants. To determine the presence of CNVs, we utilized the returned dataset (Return 1701, <https://biobank.ndph.ox.ac.uk/ukb/dset.cgi?id=1701>) as described elsewhere<sup>48,57</sup>.

### 6.1.2 The ENIGMA-CNV working group

The ENIGMA-CNV is a working group under the Enhancing Neuroimaging Genetics through Meta-Analysis (ENIGMA) consortium. ENIGMA is an international collaboration

between researchers across the world aiming to understand brain architecture and function based mainly on MRI-derived measures – often in combination with other types of data including genetics. At the time of analysis for study I, MRI-derived data from 1q21.1 distal and 15q11.2 BP1-BP2 CNV carriers were available from a total of 61 scanner sites (including three scanner sites from the UK Biobank). CNV calling and MRI preprocessing were performed independently by each cohort following standardized protocols (<https://github.com/ENIGMA-git/ENIGMA-CNV>).

### **6.1.3 The 22q11.2 deletion sample**

The 22q11.2 deletion sample contains MRI data from individuals scanned at Stanford University and UCLA. A minor subset of the individuals with MRI data also had cortical spheroids derived - 22q11.2 deletion carriers and a control group (i.e., five participants: 4 22q11.2 deletion carriers and 1 control).

For the cortical spheroids, gene expression data were obtained from four time points: Days 25, 50, 75 and 100, as described elsewhere<sup>136</sup>. In brief, fibroblasts were derived from carriers of the 22q11 deletion (n = 12; 7 females) and controls (n = 11; 6 females) to generate human iPSCs. Note that several lines of iPSCs were derived from the same individual, resulting in a total of 17 gene expression arrays derived from 22q11.2 deletion carriers and 25 gene expression arrays derived from the control group. Regional microarray gene expression data from the Allen Human Brain Atlas were obtained from 6 post-mortem brains<sup>208</sup> and spatiotemporal gene expression data were obtained from the Gene Expression Omnibus database series GSE25219<sup>131</sup>.

## **6.2 MRI acquisition, quality control and preprocessing**

UK biobank: The MRI data derived from the UK Biobank were acquired across three different scanner sites using a 3T Siemens Skyra scanner. Full documentation of the image

acquisition protocol can be found on the UK Biobank website ([https://biobank.ctsu.ox.ac.uk/crystal/crystal/docs/brain\\_mri.pdf](https://biobank.ctsu.ox.ac.uk/crystal/crystal/docs/brain_mri.pdf)). Briefly, the 3D T1-weighted magnetization prepared rapid gradient echo images were acquired with the following parameters: TI = 880ms, TE = 2.01ms, TR= 2000ms, flip angle = 8°, resolution = 1x1x1 mm. The preprocessing steps, including quality control, of the T1-weighted MR images are described elsewhere<sup>209</sup>. Images that were severely affected by artifacts or incomplete were not made available by the UK Biobank team. In addition, we removed participants that were flagged as outliers according to their standardized Euler number, which is used as an index of image quality<sup>210</sup>.

ENIGMA-CNV: For the ENIGMA-CNV working group core dataset, all participating cohorts were asked to preprocess and quality control the MRI data. The quality control and preprocessing were conducted according to the ENIGMA protocols (<https://enigma.ini.usc.edu/protocols/>). An overview of the MRI acquisition for each scanner site and FreeSurfer version for each individual site can be found in appendix 1 in study I. As the data were obtained from multiple scanner sites, we harmonized the data before downstream analysis using ComBat, which is an instrument for data harmonization that has been found to improve statistical power for mega-analyses<sup>211</sup>.

Both UK biobank and ENIGMA-CNV: The MRI-derived measures used in study I and II were extracted/obtained using FreeSurfer using the Desikan-Killany atlas and include measures of cortical surface area, cortical thickness, and subcortical volumes.

The 22q11.2 sample: The multi-shell diffusion MRI data from the 22q11.2 deletion sample were acquired at two different scanner sites using a 3T Siemens Prisma scanner. The diffusion MRI data were acquired with the following parameters: TE = 89.2ms, TR = 3230ms, flip angle = 78°, resolution = 1.5x1.5x1.5mm. The images were acquired with both anterior to posterior and posterior to anterior phase encoding directions, resulting in a total of 216

volumes and 14 b0 images. For quality control, the images were visually inspected to exclude individuals with excessive artifacts, primarily due to excessive head motion. Here, 18 individuals had one or more MRI scans that were deemed to be of insufficient quality and were discarded from further analyses, yielding a total sample of 85 individuals with one or more MRI scans for analyses. For preprocessing, diffusion data underwent denoising, and correction for Gibbs ringing artifacts, susceptibility induced distortions, head movement and eddy currents using DIPY and FSL<sup>212-215</sup>. The DTI and NODDI derived scalar maps were registered to the ENIGMA-DTI template<sup>216</sup>. Average ROI-based measures were calculated for each DTI and NODDI measure based on the Johns Hopkins University White Matter atlas<sup>217</sup>

### 6.3 Statistical analyses

All statistical analyses were performed in R v.4.0.0 (study I and II) and v.4.2.0 (study III).

**Study I:** We used the FreeSurfer-derived regional values from 68 cortical regions (34 regions per hemisphere) and 16 subcortical regions (8 regions per hemisphere). All values were harmonized across scanner site using ComBat (see above) and subsequently adjusted for age, age<sup>2</sup>, sex and intracranial volume. We calculated the regional Z-score (standard deviation from the control group mean) for each ROI across measures of cortical surface area, cortical thickness, and subcortical volume. Further, we estimated the mean Z-score (global index) and the intraindividual standard deviation (iSD) per MRI-derived feature (i.e., cortical surface area, cortical thickness, and subcortical volume) as an individualized measure of the regional deviation across the MRI-derived measures. In addition, we calculated the intra-regional deviation (RID) score that takes into account the standardized difference from the global index for each individual. Thus, the RID score will represent to what extent the regional ROI deviates from the individualized global index, thus accounting for each individual's overall difference in cortical surface area, cortical thickness, and subcortical volume. A group

difference in RID scores for a given ROI indicates that the regional differences are more pronounced or less pronounced than the overall global difference of the MRI-derived measure. To test for group differences in the global index, iSD and RID, we used a linear regression model with carrier status (carrier or non-carrier) as the independent factor variable and the global index, iSD and RID scores as the continuous dependent variables. To account for multiple comparisons, we adjusted the p-values using the False Discovery Rate (FDR) correction.

**Study II:** We used machine learning (ML) to create four different models to predict age, based on MRI-derived features. The models were based on a training set of 36,013 individuals with a ten-fold cross validation. We utilized a total of 1,145 MRI-derived measures to predict age, referred to as the “full ML model”. Three separate ML models that included either measures of (i) cortical thickness (360 MRI-derived measures), (ii) surface area (360 MRI-derived measures or (iii) subcortical volume measures (16 MRI-derived measures) were also created and referred to as “cortical thickness ML model”, “surface area ML model” and “subcortical volume ML model”, respectively.

All the models were applied to the independent groups of 15q11.2 BP1-BP2 CNV carriers and matched non-carrier groups. The difference between the estimated age and chronological age is referred to as the brain age gap. A brain age gap will indicate if an individual has a brain profile that resembles a younger looking brain (a numerically negative value) or an older looking brain (a numerically positive value), which is used to index brain ageing.

In addition, we estimated the cross-sectional, age-related differences of the cortical thickness, cortical surface area, and subcortical volume, and the age-related trajectories of reaction time, grip strength (motor function), forced expiratory volume (lung function),

systolic and diastolic blood pressure (heart function) using mixed cross-sectional and longitudinal data.

Group differences in brain age gap were tested using a two-sided t-test and reported with Cohen's *d* as a measure of effect size. For the age-related trajectories, we used linear regression models to test for differential age-related changes in mean cortical thickness, total cortical surface area and total subcortical volume by examining the interaction term between age and carrier status. To adjust for multiple comparisons, the p-value thresholds were determined by dividing 0.05 with the number of comparisons.

For the motor, lung and heart function age-related trajectories, linear mixed effects models were fitted with a random effect of participant on intercepts and with sex and affection status (i.e., having an F or G-diagnosis based on the International Classification of Diseases) included as covariates (+ body mass index for the blood pressure measures). To obtain the model that best fitted the data, we compared models with either: (a) only covariates, (b) age and covariates, or (c) age, age<sup>2</sup> and covariates. Then, we tested the model that best fitted the data against the same model but including carrier status as either (d) main effect or (e) interaction effect. We used the Akaike information criterion (AIC) as model criterion, where the more complex model was chosen if the AIC dropped by 2 with a p-value < 0.05.

***Study III:*** The diffusion MRI-derived measures were analyzed using mixed effects linear models. The diffusion MRI-derived measures were included as the dependent variable, and group status (22q11.2 deletion vs control) as the independent factor variable. We included age, age<sup>2</sup>, sex, scanner site and the average root mean square voxel displacement as covariates. Participant IDs were fitted as a random intercept to account for repeated measures.

Confirmation of the 22q11 deletion was obtained through analysis of single nucleotide polymorphism arrays. For the gene expression data derived from cortical spheroids, gene expression levels were collected at four time points (days 25, 50, 75, and 100) and consisted

of expression levels for 17,043 genes after quality control across 42 cell lines on day 100 of differentiation. Gene expression data were obtained through bulk RNA-seq and corrected for sex, batch, the first 2 principal components for genetic ancestry, and the first 20 principal components for sequencing, and were used to detect gene networks using the weighted correlation network analysis package in R<sup>218</sup>. The gene expression data from day 100 of differentiation were used to create clusters of highly correlated genes, defined as modules or gene networks. Further, the eigengene (i.e., first principal component) for each module was calculated and is used as a measure of the gene expression network. The eigengenes for all modules were compared between the 22q11.2 deletion carriers and control group using linear mixed models. Here, individual ID as a random intercept in the model was used to account for the dependency in the data (i.e., samples derived from the same individual). For the imaging transcriptomics analyses, we obtained four sources of cell-type gene sets, including two sources of gene sets derived from the fetal brain, one source of gene sets derived from the adult brain and one source of gene sets derived from the mouse brain<sup>219–221</sup>, as well as one gene set representing disrupted gene networks in 22q11.2 deletion carriers identified from cortical spheroid data (as mentioned above). The gene expression resampling approach (i.e., imaging transcriptomics) was conducted using gene expression data from the Allen Human Brain Atlas, preprocessed with the abagen toolbox<sup>180,182,208</sup>, resulting in gene expression data from a total of 15,633 genes. P-values were adjusted for multiple comparisons using FDR correction.

## **6.4 Ethical considerations**

Due to the sensitive nature of the data used in this thesis, including brain imaging, genetics and disease information, appropriate ethical approvals and considerations are of importance. The research presented in the thesis was carried out in full accordance with the

Helsinki declaration and implemented based on the Responsible Research and Innovation standards.

The Thematically Organised Psychosis Research Study (TOP)/Norwegian Centre for Mental Disorders Research (NORMENT) projects were approved by Regional Committees for Medical and Health Research Ethics (REK), South East division in Norway (Ref: REK 2009/2485 & 2016/1226) and the Norwegian Data Protection Authority (Ref: 03/02051-16/HPG) to collect and store sensitive information until 2050, including neuroimaging data.

Data collection of the 22q11.2 deletion sample was approved by for the Institutional Review Board (IRB) for the UCLA sample (Ref: 10-001071) and the Stanford sample (Ref: eProtocol, 41517).

For study I and II, the research on UK Biobank data was conducted using the UK Biobank resource under Application Number 27412. Participants who withdrew from the UK Biobank were removed from the analyses and were not included in the studies. For study I, all ENIGMA sites involved obtained ethical approvals and all participants gave written informed consent. If required by the participating ENIGMA cohorts, necessary Data Transfer Agreements (DTA) were obtained and signed.

All data from study I and II were stored and analyzed on services for sensitive data (TSD), University of Oslo, Norway, with resources provided by UNINETT Sigma2 - the National Infrastructure for High Performance Computing and Data Storage in Norway, in line with the General Data Protection Regulation (GDPR). For study III, samples were deidentified and stored at a secure high-performance cluster (The Hoffman2 Cluster, Institute for Digital Research and Education Cluster Hosting Program).

Some ethical considerations regarding the research conducted need to be mentioned. In the context of this study, we identify CNVs that are potentially pathogenic in the individuals who, for the majority of cases, are unlikely to have knowledge of their genetic



condition. This information is not reported back to the participants, and, to our knowledge, the majority of studies do not provide the opportunity to return such information to the participants. To underline how CNVs are often unknown to the individual, in a clinical context where CNV carriers were identified only 5.8 % already had a genetic diagnosis<sup>222</sup>. These individuals overall had high rates of CNV-related clinical symptoms. Returning such information could introduce the opportunity for early intervention treatment both for neurodevelopmental and somatic disease. Nevertheless, despite the higher risk of developing neurodevelopmental, psychiatric and somatic disorders, the vast majority do not develop such disorders<sup>45,48,60,223</sup>. Thus, a potential practice of providing genetic information back to the individuals must be weighted up against the harm of receiving such information, including the knowledge and potential discrimination of being at a higher risk of developing such disorders. The ethical questions related to returning genetic information need more attention and more neuroethics research.

Overall, when disseminating and communicating, it is crucial to emphasize that many individuals with a pathogenic CNV live their lives without any psychological or somatic diagnoses.

Genetic testing for CNVs is part of today's clinical practice, aiding medical care and genetic counselling<sup>1,64</sup>. Nevertheless, only a fraction of the ~15% of neurodevelopmental disorder cases that is estimated to be explained by *de novo* and inherited CNVs are identified<sup>224</sup>. This high rate of CNV carriers among neurodevelopmental cases shows that the health care system has met and will meet many patients with a pathogenic CNV regardless of whether the genetic diagnosis is known or not. Despite the high clinical relevance of CNVs, research on CNV carriers is scarce and is hampered by their overall low prevalence in the population. A better understanding of CNV carriers can inform on CNV-specific profiles and additional insight into the general disease mechanisms of neurodevelopmental disorders can

be gained which may improve health care, prediction, and early interventions for CNV carriers.

To summarize, certain CNVs may yield an increased risk of developing neurodevelopmental, psychiatric, and somatic disorders, however, the utility of providing genetic information back to the individuals may be limited. The ethical considerations of providing genetic information need to be considered with regards to the benefits, privacy, and integrity of the individuals.

## 7 SUMMARY OF STUDIES

### 7.1 Study I

**Title:** Beyond the Global Brain Differences: Intra-individual Variability Differences in 1q21.1 Distal and 15q11.2 BP1-BP2 Deletion Carriers

**Background:** The 1q21.1 distal deletion and the 15q11.2 BP1-BP2 deletion carriers exhibit brain structural differences compared to non-carriers using MRI-derived measures, characterized by global differences and wide-spread regional differences. However, it is unclear to what extent the regional effects vary across brain regions within deletion carriers and if the regional MRI-derived measures show a more pronounced or less pronounced difference relative to the overall global effect. Here, we define more affected brain regions as regions that differ more than the global mean difference, and less affected brain regions as regions that differ less than the global mean difference.

**Methods:** MRI data were used to obtain regional brain values for 1q21.1 distal and 15q11.2 BP1-BP2 deletion CNV carriers and matched non-carriers. A global index, which is the mean Z-score across all ROIs for an MRI-derived feature (i.e., either cortical surface area, cortical thickness, or subcortical volume) was estimated for each individual. An intraindividual standard deviation (iSD) measure was calculated based on the standard deviation of the global index. The global index and the iSD were used to test for group differences between CNV carriers and non-carriers. Regional intra-deviation (RID) scores i.e., the standardized difference between an individual's regional difference and global difference, were used to test for regional differences that diverge from their global difference in CNV carriers and non-carriers.

**Results:** The 1q21.1 distal deletion and the 15q11.2 BP-BP2 deletion carriers showed a lower global index for surface area, whereas the 15q11.2 BP1-BP2 deletion and duplication carriers showed a higher global index for cortical thickness and a lower global index for surface area compared to non-carriers. The iSD for cortical surface area was higher for the 1q21.1 distal duplication, whereas the iSDs for cortical thickness and cortical surface area were higher for the 15q11.2 BP1-BP2 deletion carriers compared to non-carriers. For the 1q21.1 distal deletion carriers, cortical surface area for regions in the medial visual cortex, posterior cingulate and temporal pole differed less, and regions in the prefrontal and superior temporal cortex differed more than the global difference in cortical surface area. For the 15q11.2 BP1-BP2 deletion carriers, cortical thickness in regions in the medial visual cortex, auditory cortex and temporal pole differed less, and regions in the prefrontal and somatosensory cortex differed more than the global difference in cortical thickness.

**Conclusion:** We find evidence for a global effect on brain structure of 1q21.1 distal deletion and 15q11.2 BP1-BP2 deletion and duplication carriers. The iSD measure indicates that the 1q21.1 distal duplication and the 15q11.2 BP1-BP2 deletion show a more heterogeneous regional neuroanatomic profile compared to non-carriers. Differences in the RID scores in the 1q21.1 distal deletion and 15q11.2 BP1-BP2 deletion carriers indicate that some brain regions are differentially affected by the genetic deletion, potentially underlying differences in the ontogenetic development of the sensorimotor and association cortices. The results provide new insight into the neuroanatomic profile of the 1q21.1 distal deletion and the 15q11.2 BP1-BP2 deletion.

## 7.2 Study II

**Title:** No signs of neurodegenerative effects in 15q11.2 BP1-BP2 copy number variant carriers in the UK Biobank

**Background:** The 15q11.2 BP1-BP2 CNV carriers show group differences in MRI-derived measures (i.e., cortical thickness, cortical surface area, and subcortical volume) and physical traits (i.e., reaction time, hand grip strength, lung function and blood pressure) that are associated with age-related changes in older age. The differences in brain morphology and performance on physical measures may indicate altered ageing in 15q11.2 BP1-BP2 CNV carriers.

**Method:** MRI-derived measures in 15q11.2 BP1-BP2 deletion and duplication carriers and matched controls were obtained from the UK Biobank study to examine the association with MRI-derived brain measures and estimates of brain ageing. Machine learning algorithms were trained on MRI-derived measures on an independent group of non-carriers to create models that predict brain age in a sample of 15q11.2 BP1-BP2 CNV carriers and matched controls. We tested for group differences in measures of brain age gap and age-related changes in MRI-derived measures using cross-sectional data. We also tested for group differences in the ageing trajectories of measures of motor, lung, and heart function (reaction time, hand grip strength, lung function, and blood pressure) in 15q11.2 BP1-BP2 CNV carriers compared to non-carriers using mixed cross-sectional and longitudinal data.

**Results:** In this ageing population, the results recapitulated previously identified group differences in brain structure, with deletion carriers displaying thicker cortex and lower subcortical volume compared to the deletion-controls and duplication carriers, and lower surface area compared to the deletion-controls. However, the estimated brain age gaps

did not differ between the 15q11.2 BP1-BP2 CNV carriers and non-carriers, and the 15q11.2 BP1-BP2 CNV carriers did not significantly deviate from non-carriers on any of the brain and physical age-affected measures.

**Conclusion:** Middle-to-old aged 15q11.2 BP1-BP2 deletion carriers show moderate effects on cortical thickness, cortical surface area and subcortical volume. However, we did not find any clear signs of altered apparent brain age, nor in motor, heart, or lung function. The results do not indicate neurodegenerative effects in 15q11.2 BP1-BP2 CNV carriers, suggesting that factors unrelated to ageing influence the atypical brain structure observed in the 15q11.2 BP1-BP2 CNV carriers.

### 7.3 Study III

**Title:** Characterizing the neurobiological correlates of brain structural alterations in 22q11.2 deletion syndrome

**Background:** The 22q11.2 deletion carriers show large differences on MRI-derived measures compared to controls, including wide-spread differences in white matter tracts, cortical thickness, and cortical surface area. However, the underlying neurobiology that contributes to the group-level differences is poorly understood. Here, the word “brain profile” will refer to variation in interregional differences across the regional measures of cortical thickness and cortical surface area using the Desikan-Killiany atlas.

**Method:** Measures of diffusion MRI were obtained from a sample of 22q11.2 deletion carriers and controls. To complement the differences in DTI-derived measures, we used measures from NODDI to examine differences in the ICVF, ECVF and ISO and ODI between 22q11.2 deletion carriers and controls. A resampling approach were used to associate gene expression, related to the disrupted gene networks in 22q11.2 deletion carriers and cell-

specific markers, and the brain profiles of cortical thickness and surface area in 22q11.2 deletion carriers.

**Results:** In line with previous results, the 22q11.2 deletion carriers showed higher mean FA, lower mean MD, RD, and AD in white matter tracts compared to controls. In addition, they showed lower overall ECVF, and higher overall ICVF compared to controls. 22q11.2 deletion carriers showed group differences in 4 gene expression networks, in addition to a group of genes that were not placed into a distinct gene network, compared to the control group. Gene expression levels of genes that are found to be altered in the gene networks were also associated with the brain profile of cortical thickness of 22q11.2 deletion carriers. In addition, both neuronal and non-neuronal cell-specific gene expression markers were associated with the brain profiles of cortical thickness and cortical surface area of the 22q11.2 deletion carriers.

**Conclusion:** The widespread lower ECVF and higher ICVF in 22q11.2 deletion carriers compared controls, indicate a higher density of axons in white matter microstructure in 22q11.2 deletion carriers. Gene expression levels of gene networks, containing genes within and outside the 22q11.2 genomic region, are altered in 22q11.2 deletion carriers and correlates with their brain profile of cortical thickness, possibly indicating that specific disruptions to gene networks contribute to regional variation in cortical thickness among 22q11.2 deletion carriers. The cortical thickness and cortical surface area brain profiles of the 22q11.2 deletion carriers are correlated with cell-specific gene expression levels, possibly indicating regional-specific glial involvement for thicker regions and regional specific number of cortical columns in regions with greater cortical surface area.

## 8 DISCUSSION

The primary objective of the current thesis is to gain novel insight into how rare recurrent copy number variants impact brain structure. To reach this aim, we used several different methods to examine the effect of the 1q21.1 distal 15q11.2 BP1-BP2 and 22q11.2 CNVs on brain structure.

### 8.1 Main findings

We advanced the field by doing the largest mega-analysis on brain structure in the 1q21.1 distal and 15q11.2 BP1-BP2 CNVs (study I), the first study on brain ageing of CNV carriers (study II) in a sample of middle-to-old aged 15q11.2 BP1-BP2 CNV carriers, and the first study on NODDI measures in 22q11.2 deletion carriers (study III). In the process, we adapted a new methodological approach to the field of neuroimaging, i.e., intraindividual variability measures of brain structure (study I), utilized state-of-the-art neuroimaging techniques including machine learning algorithms (study II) and advanced diffusion MRI (study III).

The three studies provide novel insight into intraindividual variability of brain structure in 1q21.1 distal and 15q11.2 BP1-BP2 CNVs, brain age in 15q11.2 BP1-BP2 CNVs and neurobiological correlates of the brain profile in 22q11.2 deletion carriers.

### 8.2 Discussion of the results

At the set-up of this thesis, group-wise brain structural differences had already been identified for both the 1q21.1 distal and 15q11.2 BP1-BP2 CNV carriers<sup>75,81</sup>. Thus, further pursuit of classical case-control comparisons of brain structural differences could potentially add power and depth. Nevertheless, not being in possession of that much larger samples, we chose a different approach to extend our understanding of these CNVs, namely by adapting a novel method - intraindividual variability measures of structural differences across the brain.



Inspired by the research in cognitive neuropsychology<sup>225-227</sup>, where intraindividual variability refers to the variation in a measure or across measures within an individual, we adapted a similar method to the profile of interregional differences of cortical and subcortical measures in CNV carriers to identify regional-specific differences in brain structure (i.e., RID) and individual measures of structural variation (i.e., iSD). Besides being a novel methodological contribution to neuroimaging research, it is also a methodological approach that confronts one major challenge in CNV research, i.e., disentangling the regional effects from the substantial global effect on the brain, by identifying regions that are less affected or more affected relative to the global CNV effect on the brain.

In study I, we hypothesized that that anterior regions within the association cortices were more affected, whereas posterior regions within the primary sensorimotor cortices were less affected in carriers of the 1q21.1 distal and 15q11.2 BP1-BP2 CNVs. Our findings of lower RID scores for cortical surface area in regions within the association cortices and lower RID scores for cortical surface area in sensorimotor regions in 1q21.1 distal deletion, and higher RID scores for cortical thickness in association cortices and lower RID scores for cortical thickness in sensorimotor regions provide partial support for our hypothesis. However, we also find that some regions deviate from the interpretation of a less affected sensorimotor cortex and a more affected association cortex exemplified by a more affected cortical thickness of the postcentral gyri, a primary somatosensory region, in the 15q11.2 BP1-BP2 deletion carriers.

For the 1q21.1 distal deletion carriers, the lower cortical surface area in the 1q21.1 distal deletion carrier would be in line with a disruption to the cell cycle processes in the ventricular zone before the onset of neurogenesis<sup>109</sup>, possibly due to haploinsufficiency of the *NOTCH2NL* gene, present in the 1q21.1 distal region, which can affect Notch signaling, neuronal differentiation, and progenitor self-renewal<sup>55,56</sup>. This would trigger premature

neurogenesis, possibly resulting in a disruption to progenitor self-renewal<sup>56</sup> and early differentiation of neuronal progenitor cells into cortical neurons<sup>55</sup>. Self-renewal in the outer subventricular zone has also been suggested to be important for the evolutionary expansion of the human cortex<sup>104,105</sup>, where association cortices appear to have expanded more relative to the sensorimotor regions – which mirrors the cortical expansion during ontogenetic development<sup>121</sup>. This could indicate that progenitor self-renewal continues for a longer period in association cortices compared to sensorimotor regions. Thus, the 1q21.1 distal deletion may disrupt the progenitor self-renewal process, which may have a more prolonged effect on the cortical expansion of the association cortices compared to sensorimotor regions, possibly underlying the observed higher RID score for association cortices in study I.

In line with previous results<sup>81</sup>, we found evidence for a lower cortical thickness for the 15q11.2 BP1-BP2 deletion. In addition, we identified regional specific effects on cortical thickness. Previous studies have shown that different brain regions are differentially influenced by genetic variants<sup>33</sup>, and that the regional differences in cortical thickness underlie specific genetic influence after accounting for global cortical thickness<sup>24</sup>. Intracortical myelination is thought to contribute to the grey/white matter boundary in MRI-derived estimates, influencing MRI-derived estimates of cortical thickness<sup>196</sup>. A heterozygous deletion *CYFIP1* (present as one of four genes in the 15q11.2 BP1-BP2 region) has been found to reduce the number of oligodendrocytes and lower myelin thickness in the corpus callosum in rats, where the larger axons appear exhibit a more pronounced decrease in myelin thickness<sup>137</sup>. Thus, to speculate, the 15q11.2 genomic region may be involved in the genetic architecture that underlies regional-specific characteristics of the brain, such as myelination. Gene expression of genes implicated in in myelination are associated with greater cortical thinning in children and adolescents<sup>188</sup>, and myelination appears to develop in areas within the sensory cortices before areas within association cortices<sup>117</sup>. Thus, it seems plausible that some

of our findings of a higher RID scores in cortical thickness in 15q11.2 BP1-BP2 deletion carriers may reflect disruptions to the prolonged myelination processes, such as in the association cortices. Anterior brain regions are characterized by lower number of neurons compared to posterior regions<sup>92</sup> and lower neuronal density has been suggested to be associated with larger neuronal size, including dendritic and axonal branching and soma<sup>94</sup>. To speculate, if the more pronounced effect of *CYFIP1* on myelination thickness of larger axons<sup>137</sup> can be extrapolated to neurons in anterior regions in 15q11.2 BP1-BP2 deletion carriers, it may be that that a reduced myelin thickness in larger neurons cause a less clear grey/white matter boundary in the MRI-derived estimates of anterior regions, ultimately yielding higher RID scores for anterior regions compared to posterior regions in 15q11.2 BP1-BP2 deletion carriers.

The differences in RID scores were not affected by affection status, nor did we observe any significant interaction effects between CNV status and affection status, indicating that the RID score differences are relatively specific to the corresponding genetic deletion. These results provide complementary insight into classical case-control differences, where some significant regional differences may be driven by a global effect on the brain, and do not necessarily provide insight into which brain regions that are more affected (or less affected) by the genetic deletion.

By going beyond global brain differences, novel insight can be made into the regional convergence and divergence with psychiatric disorders. For instance, the 15q11.2 BP1-BP2 deletion is characterized by overall thicker cortex compared to non-carriers (study I), whereas schizophrenia is characterized by overall thinner cortex<sup>203</sup>. After adjustment, for the global mean differences in cortical thickness, both 15q11.2 BP1-BP2 deletion and individuals with schizophrenia show evidence of a thicker right precentral gyrus (study I, van Erp et al., 2018<sup>203</sup>). Likewise, both 1q21.1 distal deletion and individuals diagnosed with schizophrenia

are characterized by overall lower cortical surface area. However, after adjustment for global differences in cortical surface area, the cortical size of the left paracentral gyrus is lower for 1q21.1 distal deletion carriers (study I) and higher for individuals diagnosed with schizophrenia<sup>203</sup>. Such converging and diverging patterns may have gone unnoticed without going beyond the global differences.

There are some key conceptual differences between the RID approach and the classical covariation approach (as used in e.g., van Erp et al., 2018<sup>203</sup>). Of note, the classical covariation approach utilizes the linear relationship between a global metric (e.g., total cortical surface area, mean cortical thickness, total subcortical volume) and the values derived from an ROI, which is used to regress out the linear relationship between the global metric and the ROI values. Thus, the variability in the adjusted regional values is based on the residuals from the linear slope. It seems plausible that the residuals also contain noise, possibly due to an inaccurate estimation of the linear relationship or a more complex relationship between the global metric and regional measures. For instance, subgroups within the sample may exhibit different relationships between global and regional measures. Thus, the linear slope may not be an accurate way of extracting out the effect of the global measure on regional measures for each individual included in the study. In contrast, the RID score for a given ROI, depends on the mean and distribution of the MRI-derived feature for a particular individual. As shown in study I, the classical covariation and RID score approach yield somewhat similar, but also different results, where the RID scores yield a numerically higher number of significant ROIs compared to the classical covariation approach. This may indicate that the RID scores are more sensitive to detect regional-specific differences in brain structure compared to the classical covariation approach that predominates today. This may be useful for studies in molecular genetics that have sought to identify the genetic determinants and heritability estimates of regional estimates of brain structure<sup>25,33</sup>. Thus, the RID approach may

provide novel insight into the genetic determinants of brain architecture if applied in GWAS and twin studies.

Further, the results may be useful for stratification of cases in clinical neuroimaging studies, as schizophrenia is characterized by higher heterogeneity in measures of cortical thickness and cortical surface area compared to healthy controls<sup>201</sup>. It remains an open question if evidence for a higher heterogeneity in schizophrenia will remain in RID scores. If there is none, the RID approach has the potential to reduce heterogeneity in clinical groups, possibly increasing the sensitivity of meaningful biological signals that are related to the disorder. In contrast, if the higher heterogeneity persists, both the conventional case-control and the RID score approach may be useful for future stratification of CNV carriers in clinical groups. For instance, a classification model showed that the most informative brain structures to differentiate 22q11.2 deletion from controls were the cortical surface area in the left caudal anterior cingulate, precentral gyrus, and bilateral cuneus and cortical thickness in the left insula<sup>87</sup>. These are regions that, at face value, appear to deviate from the overall global effect on brain structure among 22q11.2 deletion carriers vs controls. Although the RID scores for 22q11.2 deletion carriers are unknown, it seems plausible that the main contributors to the classification model mentioned above are regions that will show a different RID scores in 22q11.2 deletion carriers compared to controls.

The RID score approach utilizes the distribution across several brain measures. This relates to another major challenge in neuroimaging research, which is to incorporate high-dimensional neuroimaging data and relate them to meaningful clinical biomarkers, such as disease risk or brain ageing. In recent years, machine learning algorithms have been used to incorporate high dimensional MRI data to predict a phenotype. In study II, we used machine learning algorithms to create models that predict age based on MRI-derived features. The difference between the predicted age and chronological age (i.e., brain age gap) has been

suggested to be an ageing biomarker<sup>173,174</sup>, where a higher brain age gap could indicate early genetic or environmental factors that alter the ageing trajectory, accelerated ageing or accentuated (i.e., a sudden change or “hit” in the ageing trajectory) but otherwise stable ageing<sup>173</sup>. Thus, CNV carriers are of interest, as they may confer a genetic risk of altered ageing trajectory. Thus, if the 15q11.2 BP1-BP2 CNVs cause altered neurodevelopment this may also alter their brain-ageing trajectories. If true, it could be hypothesized that the 15q11.2 BP1-BP2 will show altered brain age gap estimations. This could also complement their somatic profile. For instance, the phenotypic profile of middle-to-old age 15q11.2 BP1-BP2 CNV carriers are characterized by alterations to physical traits<sup>49</sup>, which are also measures that associate with brain age gap<sup>174–176</sup>.

Since 15q11.2 BP1-BP2 deletion carriers exhibit a higher cortical thickness, and lower cortical surface area and subcortical volume (study I), it seems reasonable that this reflects an altered neurodevelopmental trajectory caused by the genetic deletion. In study II, we hypothesized that 15q11.2 BP1-BP2 CNV carriers will show group differences in brain age gap compared to non-carriers. We validated our brain age models in a sample of individuals diagnosed with multiple sclerosis, which yielded moderate to large group differences compared to healthy controls. Thus, the models were sufficient to detect brain age gap differences in individuals that are diagnosed with a neurodegenerative disorder compared to healthy controls. We also found an association between brain age gap and lung function in a sample of 15q11.2 BP1-BP2 duplication and non-carriers, which indicate that the brain age gap captures meaningful biological associations beyond measurement error. However, contrary to our expectations, we did not find evidence for differences in brain age gap in any of the brain age models, nor did we find support for alterations in the age trajectories of motor, heart, and lung function in 15q11.2 BP1-BP2 CNV carriers compared to non-carriers. The lack of brain age gap differences, including the comparable age trajectories in physical

and somatic traits, do not support neurodegenerative effects of the 15q11.2 BP1-BP2 CNVs in the UK Biobank.

In addition, whilst caution is warranted given the lack of results to support such hypothesis, this may suggest that the brain alterations identified in 15q11.2 BP1-BP2 CNV carriers are more likely explained by an early offset in brain structure caused by atypical neurodevelopment rather than alterations in neurodegeneration. It may also indicate that brain age models capture patterns in brain structure that are important for the prediction of age, but do not capture differential brain age trajectories caused by altered early neurodevelopment. If the latter is true, this has important implications for our understanding of brain age estimates. For instance, this may indicate that the differences in brain age in brain related disorders<sup>179</sup> do not necessarily reflect a sudden “hit” or acceleration of their brain age trajectories during early neurodevelopment but rather changes in brain structure later in life.

We also find that alterations to physical measures in CNV carriers vs non-carriers are not necessarily reflective of neurodegenerative processes. For instance, we found that although 15q11.2 BP1-BP2 CNV carriers may exhibit a group difference in physical traits that typically deteriorate with age, the age trajectories of these measures were relatively comparable to the non-carriers. The results emphasize the importance of examining longitudinal trajectories to get a deeper insight into age trajectories including those of CNV carriers. Still, there is a scarcity of longitudinal data overall, also for CNV carriers, and more research is highly needed.

Overall, the results from studies I and II indicate that MRI-derived measures are sensitive to detect differences between CNV carriers and non-carriers. However, MRI-derived measures are relatively nonspecific to the underlying biological tissue, and other methods are required to gain insight into their neurobiological correlates.

Structural alterations in white matter microstructure and cortical and subcortical grey matter of the brain have been well characterized for the 22q11.2 deletion carriers compared to controls<sup>86,87,198,228</sup>. However, the neurobiological mechanisms driving the group-level differences remain poorly understood. To further advance the field, we characterized the neurobiological correlates of the brain structural differences in 22q11.2 deletion carriers compared to controls, by using advanced diffusion MRI and imaging transcriptomics. Regarding white matter microstructure, it has been postulated that the DTI results in 22q11.2 deletion carriers relate to larger cellular membrane circumference<sup>198</sup>, possibly caused by a higher density of axons in conjunction with a smaller axonal diameter<sup>198,228</sup>.

In study III, we found evidence for widespread higher ICVF and lower ECVF in 22q11.2 deletion carriers compared to controls, indicating a higher density of axons in white matter in 22q11.2 deletion carriers. In addition, our results provide novel information about the structural dispersion of the three major white matter tracts in 22q11.2 deletion carriers: The ROIs with a higher component of association fibers (i.e., tracts connecting regions within the same hemisphere), such as the superior longitudinal fasciculus and superior fronto-occipital fasciculus, appear to be more dispersed, whereas some of the ROIs with a higher component of projection fibers (i.e., tracts connecting cortical regions to subcortical regions), such as the internal capsule and posterior thalamic radiation, appear to be less dispersed in 22q11.2 deletion carriers compared to controls. We also found that the posterior limb of the internal capsule showed a higher AD in 22q11.2 deletion carriers compared to controls. The higher AD may indicate larger axonal diameter in 22q11.2 deletion carriers compared to controls for the posterior internal capsule. The motor axons travel through the posterior limb of the internal capsule from the precentral gyrus, which is one of few regions that is larger in 22q11.2 deletion carriers compared to controls<sup>87</sup>. Thus, our results indicate that a larger



number of neurons contribute to the greater expansion of the precentral gyrus in 22q11.2 deletion carriers.

Using imaging transcriptomics, we provided novel neurobiological correlates of the cortical brain profiles of the 22q11.2 deletion carriers to the gene expression levels of cell-type markers from the fetal, adult and mice brain<sup>219–221,229</sup>. The use of four dataset sources is an improvement from previous studies that have used only one source of cell-type genes from mice to examine the neurobiological correlates of MRI-derived brain profiles<sup>187,230,231</sup>. In study III, we found that thicker regions among 22q11.2 deletion carriers were associated with higher gene expression of neuronal cell-types and lower gene expression of non-neuronal cell-types. Higher cortical surface area among 22q11.2 deletion carriers was associated with higher gene expression of neuronal and nonneuronal-specific cell types. The association between the brain profile of cortical thickness in 22q11.2 deletion carriers and non-neuronal cell types, may point towards a role of biological processes such as synaptic pruning and axonal myelination during neurodevelopment<sup>5,112,196,232</sup>. For instance, synaptic pruning is thought to be driven by glial cells, including astrocyte and microglia<sup>232</sup>, whereas myelin related genes have been associated with an MRI-marker of myelination<sup>233</sup> and are associated with greater cortical thinning in children and adolescents<sup>188</sup>. These are biological processes that have been postulated to be involved in the atypical cortical thinning of 22q11.2 deletion carriers during development<sup>234</sup>. Moreover, the neurobiological correlates of the brain profile of cortical surface area in 22q11.2 deletion carriers, may indicate a higher density of neuronal and non-neuronal cells in larger areas among 22q11.2 deletion carriers. To speculate, this may be related to alterations to cortical columns and tangential cell migration to the developing cortex, where the amount of cortical columns are directly related to the degree of symmetric cell division among the radial glial population<sup>100,109</sup>.

A previous study has established neurobiological correlates of the brain profiles of cortical thickness and cortical surface area in 22q11.2 deletion carriers by using gene expression profiles of 22q11.2 protein coding genes<sup>200</sup>. However, functional genomics analysis of the 22q11.2 locus suggests that many of the genes within the locus are part of gene networks that target similar biological processes<sup>235</sup> and is likely part of gene networks that include genes outside the 22q11.2 locus<sup>141</sup>. Thus, to further advance the field, we sought to further characterize the transcriptional architecture during early neurodevelopment and to establish a link between genes implicated in the disrupted gene networks in 22q11.2 deletion carriers to the cortical brain profiles of 22q11.2 deletion carriers.

The study of cortical spheroids has emerged as a powerful tool to examine early neurodevelopment as these models have been shown to recapitulate the transcriptional architecture of fetal brain tissue<sup>206,207</sup>. By using gene expression data from cortical spheroids derived from 22q11.2 deletion carriers and controls, we identified three gene expression modules that showed significant case-control differences and a significant association with the brain profile of cortical thickness, implicating disruptions to cell adhesion, subcellular compartments, and protein degradation and synthesis (i.e., deubiquitinase activity) and modification of ribosomal RNA in 22q11.2 deletion carriers. When comparing the results to cell-type gene expression analyses as described above, we find further support for a role of synaptic alterations in 22q11.2 deletion carriers. For instance, cadherin binding is important for spine pruning and maturation<sup>236</sup>, whereas deubiquitination has been suggested to play a role in synapse size and morphology<sup>237</sup>.

Taken together, the results from study III support the hypothesis of higher density of axons in 22q11.2 deletion carriers as indicated by the NODDI results. In addition, we establish novel neurobiological correlates of the cortical brain profiles in 22q11.2 deletion carriers, which may be useful for targeting specific cell types in cortical spheroid research.

Finally, we take a novel approach in imaging transcriptomics research, by utilizing gene expression from cortical spheroids to identify disrupted gene networks in 22q11.2 deletion carriers. This can be used to establish gene sets of altered CNV-specific gene networks to associate with their cortical brain profiles.

### **8.3 Methodological considerations**

The results of the present thesis are based on state-of-the-art neuroscientific and imaging transcriptomics methods, and novel applications of standard methodological approaches. The results need to be considered with regards to the limitations and methodological frameworks in each of three studies, including sample characteristics, effect size, and operationalization of the dependent variables.

#### **8.3.1 Samples**

The CNVs studied in this thesis are all rare CNVs found in less than 1% of the population. Thus, large or targeted recruitment datasets are of fundamental importance to examine individuals with CNVs, and even more important in neuroimaging research where MRI data is limited. This thesis has some key strengths and limitations with the datasets used. The UK Biobank neuroimaging dataset is the largest existing sample on neuroimaging in existence and all individuals were imaged at only three sites limiting scanner variation. However, the sample is restricted to older adults and is limited to a smaller proportion of the UK population. Samples derived from volunteers are also subject to a “healthy volunteer bias”, meaning that the individuals that take part in research may be healthier than the rest of the population. For instance, individuals in the UK Biobank have a lower rate of cancer and obesity, and smoke and drink less, compared to the general population<sup>62</sup>. Such healthy volunteer bias seems even more prominent in neuroimaging samples. For instance, individuals

that participate in neuroimaging research have been found to show lower levels of anxiety compared to individuals included in behavioral studies<sup>238</sup>.

Some of this healthy volunteer bias may be partially compensated by individuals included from the ENIGMA-CNV core working group dataset in study I, as this dataset also includes clinical cohorts. Still, many of the cohorts included in the ENIGMA-CNV dataset are also likely to involve a healthy volunteer bias.

For MRI, excessive MRI artifacts (e.g., due to head motion) do not yield sufficient data quality and are discarded from further analyses. This is evident in the 22q11.2 deletion sample in study III, where a significant proportion of the MRI data was discarded due to insufficient data quality (i.e., 18 individuals). In contrast to the samples in studies I and II, the 22q11.2 deletion sample is a clinical sample consisting of individuals with 22q11.2 deletion syndrome with associated behavioral issues, which may yield a higher proportion of discarded MRI data in clinical samples compared to volunteer-based studies.

It is remarkable that, despite the phenotypic variability, the CNVs can yield group differences of small to large effect sizes. Nevertheless, neuroimaging studies have a history of replication failure due to low statistical power<sup>239</sup>, warranting caution in interpretation of results. One important consideration in this regard is sample and effect size.

### **8.3.2 Sample size and effect size**

Over the last couple of decades, a substantial part of research in both genetics and neuroimaging has failed to replicate. One important reason for the replication failures has been due to low statistical power, resulting in false positive results<sup>239,240</sup>. Effect sizes of SNPs on MRI-derived brain measures are small<sup>32</sup> and brain-cognition associations are found to be of negligible to small effect sizes<sup>159,160</sup>, indicating that large sample sizes are required to detect such associations. In study I, we find small effect sizes for associations between structural MRI-derived measures and a measure of cognitive ability using ~40k individuals

from the UK Biobank. Thus, given the low frequency of CNVs (most are <0.5%) and thus small sample size, examining the associations between brain structure and cognition in CNV carriers will probably remain exploratory for some years.

Brain structural group differences in neurodevelopmental and psychiatric disorders compared to controls have yielded higher effect sizes compared to brain-cognition associations, including small to moderate effect sizes for attention deficit/hyperactivity disorder, autism spectrum disorder<sup>241</sup> and schizophrenia<sup>203,242</sup> based on samples of thousands of cases and controls. Brain structural group differences in CNV research yield two to four times larger effect sizes than those reported in case-control studies of neurodevelopmental and psychiatric disorders<sup>50,51,202</sup>. Thus, despite the low number of CNV carriers compared to those included in psychiatric research, reliable case-control differences can be detected in CNV research due to the high effect sizes in some MRI-derived estimates.

For study I and II, we detected moderate to large group differences, which is expected based on previous studies<sup>75,81</sup> and the power sensitivity analysis reported in study II. However, the results do not exclude the possibility of group differences in MRI-derived measures of negligible to small effect sizes. Non-significant group differences in brain structure may represent regional variability that falls within the typical variation of individuals but can also consist of important biological signals that are not detected using conventional mass-univariate approaches. Thus, larger sample sizes are needed in CNV research, as well as other complementary approaches to the conventional mass-univariate approach. One such complementary approach includes the use of intraindividual variability measures (as mentioned above), which can be used to characterize the heterogeneity of regional variation within individuals.

### **8.3.3 Intraindividual variability measures**

The intraindividual variability measures provide a new methodological approach to examine the non-uniformity of brain structural differences. While the interpretation of these measures is still in its infancy, the insights gleaned from study I could be of interest to a wider audience in neuroimaging research. However, some methodological considerations need to be addressed.

The RID approach considers the distribution of the regional-specific effects across the MRI-derived feature, thus substantial anatomical disruptions, indicating deviations from a typical organization of the brain, may have a significant impact on the RID scores. Therefore, a significant RID score may indicate group differences that are more pronounced or less pronounced than the global index, but it can also indicate substantial alterations in the anatomical relationship between regions. Thus, it is of importance to use complementary approaches, as examining the regional Z-score differences for each ROI across the brain, iSD and the classical global covariation approach to get a deeper overview of the brain profile of the group of interest.

The differences in RID scores and iSD indicate that new insight into the neuroanatomical brain structure of CNV carriers can be made by examining brain structural variations within individuals. Thus, CNV carriers show group differences that cannot be accounted for by a global effect alone, emphasizing the importance of studying both regional-specific and global brain measures, as well as the relation between the regional and global measures. This also shows that it may be useful to evaluate regional differences between individuals, but also regional variation within an individual.

### **8.3.4 Brain age gap estimations**

Brain age gap has been suggested to be an ageing biomarker<sup>173,174</sup>, and has been found to be associated with measures that are relevant for ageing, including mortality risk, motor

and lung function<sup>174</sup>, cardiometabolic and cardiovascular risk factors<sup>175,176</sup>, cognitive performance<sup>177,178</sup>, and physical appearance<sup>177</sup>, emphasizing its potential as a clinical relevant biomarker for ageing. Still, there are some inherent limitations with the approach used in study II. The predicted age is still based on cross-sectional data, both in the training group and in the test group. Thus, brain age gap estimations are still limited to a static view of the included participants and do not contain information about within-individual brain age gap changes over time, i.e., age trajectories, which would require longitudinal data. Indeed, others have raised concerns about the interpretation of the brain age gap, indicating that the variations in cross-sectional brain age gap estimations are not associated with within-individual changes in longitudinal measures of brain age gap estimations, but are rather associated with early life factors<sup>243</sup>. The results from study II also indicate that brain age estimations are not necessarily sensitive to detect alterations in brain structure during neurodevelopment, as indicated by the lack of brain age gap differences in 15q11.2 BP1-BP2 CNV carriers.

The high data dimensionality that are fed into the machine learning model, makes it somewhat difficult to understand the mechanisms that are involved in producing the output (i.e., predicted age). It is clear that the MRI-derived measures contain information that can predict age, as demonstrated by the high correlation between predicted age and chronological age. However, this may also indicate that the algorithm simply recapitulates interregional differences in brain structure. Simply put, if the volume estimates of subcortical structures are lower as a consequence of having a generally lower total subcortical volume than what is typically observed in population, this may yield a lower brain age prediction that is unrelated to ageing. However, individuals with a 15q11.2 BP1-BP2 deletion that show group differences in mean cortical thickness, total cortical surface area and total subcortical volume (study I) did not show brain age gap differences in any of the brain age models (study II). This

is surprising because the models are likely to focus on the information from regions that are susceptible for atrophy in older age. Frontal regions are more susceptible for atrophy in older age compared to posterior regions<sup>163</sup>, and frontal regions are also those that diverge more than the global effect in 15q11.2 BP1-BP2 deletion carriers as shown in study I. Thus, our results indicate that case-control differences in brain structures, even in regions often considered to be specifically affected by old age, are not sufficient to yield case-control differences in brain age gap.

### **8.3.5 Gene expression and brain profile**

In imaging transcriptomics, genes selected for gene expression correlations should be associated with the phenotype of the group of interest. In study III, we selected gene sets that were shown to be altered in 22q11.2 deletion carriers (i.e. disrupted gene networks), as well as genes that were identified as cell-specific based on previous results<sup>219–221,229</sup>. The use of a resampling approach, as used in virtual histology<sup>186,187,230,231</sup>, provides an overview of gene expression sets that are significantly associated with the cortical brain profiles of the 22q11.2 deletion carriers compared to a random distribution of gene sets correlations. Importantly, the gene expression data used for correlations between network-specific and cell-type specific genes are derived from post-mortem data of adults, providing correlations between gene expression levels and MRI-derived phenotypes across space. However, it does not provide any information about the association between regional gene expression levels and regional MRI-derived estimates of the same individuals, which would be an ideal method to study the link between gene expression levels and brain phenotypes.

We also utilized weighted correlation network analysis to detect group differences in gene networks, where the gene networks are interpreted as genes that are co-expressed based on topological overlap of gene expression correlations<sup>218</sup>. However, in case-control designs where group differences exist, the correlations may also be driven by group differences in



gene expression levels and cannot be solely attributed to co-expression. Such occurrence is demonstrated in one of the modules presented in study III, where 34 out of 119 genes are in the 22q11.2 genomic region. Thus, the constructed gene networks need to be considered as gene networks consisting of co-expressed genes but are also likely to be influenced by gene expression differences between groups.

For the imaging transcriptomics analyses, using cell-specific markers, we included one gene list that are based on cell-specific genes derived from single-cell RNA sequencing from the mouse cortex and hippocampus<sup>229</sup>. Although, the cellular architecture between mice and humans is well conserved between the species, there are some differences that may not have been accounted for using this cell-specific gene list<sup>244</sup>. To account for this, we also included several gene lists that were derived from the human fetal and adult brain<sup>219-221</sup>, which replicated the associations detected using the cell-specific gene list derived from the mice.

## 9 CONCLUDING REMARKS AND PERSPECTIVES

The present thesis aimed to examine the effects of copy number variants on brain structure. It complements and extends on previous findings by showing 1) regional-specific effects of the 1q21.1 distal deletion and 15q11.2 BP1-BP2 deletion beyond the global effect on the brain, partially reflective of the sensorimotor to association axis, 2) that the structural group differences in the 15q11.2 BP1-BP2 deletion do not signal clear patterns of neurodegenerative effects in middle to late adulthood, 3) that the brain architecture of the 22q11.2 deletion carriers are characterized by widespread lower neurite density in white matter, whereas the cortical brain profiles spatially overlap with typical gene expression levels of cell-type markers and disrupted gene networks in 22q11.2 deletion carriers.

In study I, we showed that new insight into CNV brain profiles can be made by going beyond global differences in brain structure by applying the novel method, intra-individual variability approach. Such approaches may be useful to disentangle the genetic effect of global and regional group differences, providing a window into early neurodevelopmental mechanisms. In addition, brain profiling of CNV carriers have the potential to be used for future stratification of brain-related disorders, such as schizophrenia – which are characterized by higher inter-individual differences in MRI-derived measures compared to healthy controls<sup>201</sup>. Moreover, CNV-associated brain profiles have shown to be useful to detect meaningful associations to clinical phenotypes in individuals with similar brain profiles<sup>204</sup> and RID score profiles could potentially be used for the same type of analysis. Thus, the intraindividual variability measures in brain structure has the potential to be used by the neuroimaging community for various purposes, providing a novel tool to examine non-uniformity of brain structural differences.

In study II, we showed that 15q11.2 BP1-BP2 CNV carriers do not display differences in brain age gap, nor in the ageing trajectories of motor, heart and lung function compared to

non-carriers. Our results suggest that brain age models do not necessarily capture altered neurodevelopment in CNV carriers. It would be of interest to compare these results to brain age estimates in other CNV carriers that do show evidence for longitudinal neurodegenerative effects in physical traits.

In study III, we showed that advanced diffusion MRI and imaging transcriptomics methods can yield novel insight into the white matter and grey matter brain structure of 22q11.2 deletion carriers. The results demonstrate the usefulness of utilizing complementary methods to get a deeper understanding of the MRI-derived measures of CNV carriers. The use of NODDI measures has the potential yield novel insight into the underlying white matter microstructure in CNV carriers. In addition, the use of gene expression data from cortical spheroids can be used to establish gene sets of disrupted gene networks in CNV carriers, moving beyond the association between the CNV-harboring region and the CNV brain profile.

Taken together, the results from the thesis have expanded our knowledge on the brain structure of 1q21.1 distal, 15q11.2 BP1-BP2, 22q11.2 CNVs, as well as providing novel methodological approaches to study CNVs. The results can provide a window into the neurodevelopmental mechanisms in the formative years of brain organization and has the potential to be used for stratification of brain-related disorders and to detect meaningful associations to clinical phenotypes of individuals with CNV-associated brain profiles.

## 10 REFERENCES

1. Kirov, G., Rees, E. & Walters, J. What a psychiatrist needs to know about copy number variants. *BJPsych Adv.* **21**, 157–163 (2015).
2. Chen, H., Cohen, P. & Chen, S. How Big is a Big Odds Ratio? Interpreting the Magnitudes of Odds Ratios in Epidemiological Studies. *Commun. Stat. - Simul. Comput.* **39**, 860–864 (2010).
3. Cohen, J. *Statistical Power Analysis for the Behavioral Sciences*. (Routledge, 1988). doi:10.4324/9780203771587.
4. Patel, Y. *et al.* Virtual Ontogeny of Cortical Growth Preceding Mental Illness. *Biol. Psychiatry* **92**, 299–313 (2022).
5. Paus, T., Keshavan, M. & Giedd, J. N. Why do many psychiatric disorders emerge during adolescence? *Nat. Rev. Neurosci.* **9**, 947–957 (2008).
6. Aristotle. On the Generation of Animals: Book IV. The Electronic Scholarly Publishing Project. <http://www.esp.org/books/aristotle/generation-of-animals/contents/book4.pdf> [Accessed September 2023] (Original work published 350 B.C.E)
7. Galton, F. Hereditary talent and character. *Macmillans Mag.* **12**, 318–327 (1865).
8. Freeman, F. N., Holzinger, K. J., Mitchell, B. C., Bobo, H. B. & Lorenzen, C. H. The Influence of Environment on the Intelligence, School Achievement, and Conduct of Foster Children. *Teach. Coll. Rec.* **29**, 103–217 (1928).
9. Lauterbach, C. E. Studies in Twin Resemblance. *Genetics* **10**, 525–568 (1925).
10. Merriman, C. The intellectual resemblance of twins. *Psychol. Monogr.* **33**, i–57 (1924).

11. Pinker, S. *The blank slate: The modern denial of human nature*. xvi, 509 (Viking, 2002).
12. Bouchard, T. J. & McGue, M. Familial Studies of Intelligence: A Review. *Science* **212**, 1055–1059 (1981).
13. Plomin, R. & Loehlin, J. C. Direct and indirect IQ heritability estimates: A puzzle. *Behav. Genet.* **19**, 331–342 (1989).
14. Kallmann, F. J. & Baroff, G. S. Abnormalities of behavior (in the light of psychogenetic studies). *Annu. Rev. Psychol.* **6**, 297–326 (1955).
15. Susser, E., Schwartz, S., Morabia, A. & Bromet, E. J. Twin Studies of Heritability. in *Psychiatric Epidemiology: Searching for the Causes of Mental Disorders* (eds. Susser, E., Schwartz, S., Morabia, A. & Bromet, E.) 375–388 (Oxford University Press, 2006). doi:10.1093/acprof:oso/9780195101812.003.31.
16. Bartley, A. J., Jones, D. W. & Weinberger, D. R. Genetic variability of human brain size and cortical gyral patterns. *Brain* **120**, 257–269 (1997).
17. Biondi, A. *et al.* Are the brains of monozygotic twins similar? A three-dimensional MR study. *Am. J. Neuroradiol.* **19**, 1361–1367 (1998).
18. Oppenheim, J. S., Skerry, J. E. & Gazzaniga, M. S. Magnetic resonance imaging morphology of the corpus callosum in monozygotic twins. *Ann. Neurol.* **26**, 100–104 (1989).
19. Pfefferbaum, A., Sullivan, E. V., Swan, G. E. & Carmelli, D. Brain structure in men remains highly heritable in the seventh and eighth decades of life☆. *Neurobiol. Aging* **21**, 63–74 (2000).

20. Thompson, P. M. *et al.* Genetic influences on brain structure. *Nat. Neurosci.* **4**, 1253–1258 (2001).
21. Tramo, M. J. *et al.* Brain size, head size, and intelligence quotient in monozygotic twins. *Neurology* **50**, 1246–1252 (1998).
22. Winkler, A. M. *et al.* Cortical thickness or grey matter volume? The importance of selecting the phenotype for imaging genetics studies. *NeuroImage* **53**, 1135–1146 (2010).
23. Panizzon, M. S. *et al.* Distinct Genetic Influences on Cortical Surface Area and Cortical Thickness. *Cereb. Cortex* **19**, 2728–2735 (2009).
24. Schmitt, J. E. *et al.* Identification of Genetically Mediated Cortical Networks: A Multivariate Study of Pediatric Twins and Siblings. *Cereb. Cortex* **18**, 1737–1747 (2008).
25. Strike, L. T. *et al.* Genetic Complexity of Cortical Structure: Differences in Genetic and Environmental Factors Influencing Cortical Surface Area and Thickness. *Cereb. Cortex N. Y. NY* **29**, 952–962 (2019).
26. International Human Genome Sequencing Consortium. Finishing the euchromatic sequence of the human genome. *Nature* **431**, 931–945 (2004).
27. Ebert, P. *et al.* Haplotype-resolved diverse human genomes and integrated analysis of structural variation. *Science* **372**, eabf7117 (2021).
28. Eichler, E. E. Genetic Variation, Comparative Genomics, and the Diagnosis of Disease. *N. Engl. J. Med.* **381**, 64–74 (2019).

29. Feuk, L., Carson, A. R. & Scherer, S. W. Structural variation in the human genome. *Nat. Rev. Genet.* **7**, 85–97 (2006).
30. Redon, R. *et al.* Global variation in copy number in the human genome. *Nature* **444**, 444–454 (2006).
31. Manolio, T. A. *et al.* Finding the missing heritability of complex diseases. *Nature* **461**, 747–753 (2009).
32. Grasby, K. L. *et al.* The genetic architecture of the human cerebral cortex. *Science* **367**, (2020).
33. van der Meer, D. *et al.* Understanding the genetic determinants of the brain with MOSTest. *Nat. Commun.* **11**, 3512 (2020).
34. Hilker, R. *et al.* Heritability of Schizophrenia and Schizophrenia Spectrum Based on the Nationwide Danish Twin Register. *Biol. Psychiatry* **83**, 492–498 (2018).
35. Sandin, S. *et al.* The Heritability of Autism Spectrum Disorder. *JAMA* **318**, 1182–1184 (2017).
36. Tick, B., Bolton, P., Happé, F., Rutter, M. & Rijdsdijk, F. Heritability of autism spectrum disorders: a meta-analysis of twin studies. *J. Child Psychol. Psychiatry* **57**, 585–595 (2016).
37. Grove, J. *et al.* Identification of common genetic risk variants for autism spectrum disorder. *Nat. Genet.* **51**, 431–444 (2019).
38. Singh, T. *et al.* Rare coding variants in ten genes confer substantial risk for schizophrenia. *Nature* **604**, 509–516 (2022).

39. Trubetskoy, V. *et al.* Mapping genomic loci implicates genes and synaptic biology in schizophrenia. *Nature* **604**, 502–508 (2022).
40. Lee, P. H. *et al.* Partitioning heritability analysis reveals a shared genetic basis of brain anatomy and schizophrenia. *Mol. Psychiatry* **21**, 1680–1689 (2016).
41. van der Meer, D. *et al.* Boosting Schizophrenia Genetics by Utilizing Genetic Overlap With Brain Morphology. *Biol. Psychiatry* **92**, 291–298 (2022).
42. Cheng, W. *et al.* Genetic Association Between Schizophrenia and Cortical Brain Surface Area and Thickness. *JAMA Psychiatry* **78**, 1020–1030 (2021).
43. Elvsåshagen, T. *et al.* The genetic architecture of the human thalamus and its overlap with ten common brain disorders. *Nat. Commun.* **12**, 2909 (2021).
44. Owen, M. J. & Williams, N. M. Explaining the missing heritability of psychiatric disorders. *World Psychiatry* **20**, 294–295 (2021).
45. Calle Sánchez, X. *et al.* Comparing Copy Number Variations in a Danish Case Cohort of Individuals With Psychiatric Disorders. *JAMA Psychiatry* **79**, 59–69 (2022).
46. Kirov, G. CNVs in neuropsychiatric disorders. *Hum. Mol. Genet.* **24**, R45–R49 (2015).
47. Mollon, J., Almasy, L., Jacquemont, S. & Glahn, D. C. The contribution of copy number variants to psychiatric symptoms and cognitive ability. *Mol. Psychiatry* 1–14 (2023)  
doi:10.1038/s41380-023-01978-4.
48. Crawford, K. *et al.* Medical consequences of pathogenic CNVs in adults: analysis of the UK Biobank. *J. Med. Genet.* **56**, 131–138 (2019).



49. Owen, D. *et al.* Effects of pathogenic CNVs on physical traits in participants of the UK Biobank. *BMC Genomics* **19**, (2018).
50. Moderato, C. *et al.* Lessons Learned From Neuroimaging Studies of Copy Number Variants: A Systematic Review. *Biol. Psychiatry* **90**, 596–610 (2021).
51. Sønderby, I. E. *et al.* Effects of copy number variations on brain structure and risk for psychiatric illness: Large-scale studies from the ENIGMA working groups on CNVs. *Hum. Brain Mapp.* **43**, 300–328 (2022).
52. Bailey, J. A. & Eichler, E. E. Primate segmental duplications: crucibles of evolution, diversity and disease. *Nat. Rev. Genet.* **7**, 552–564 (2006).
53. Innan, H. & Kondrashov, F. The evolution of gene duplications: classifying and distinguishing between models. *Nat. Rev. Genet.* **11**, 97–108 (2010).
54. Gilad, Y., Wiebe, V., Przeworski, M., Lancet, D. & Pääbo, S. Loss of Olfactory Receptor Genes Coincides with the Acquisition of Full Trichromatic Vision in Primates. *PLOS Biol.* **2**, e5 (2004).
55. Fiddes, I. T. *et al.* Human-Specific NOTCH2NL Genes Affect Notch Signaling and Cortical Neurogenesis. *Cell* **173**, 1356-1369.e22 (2018).
56. Suzuki, I. K. *et al.* Human-Specific NOTCH2NL Genes Expand Cortical Neurogenesis through Delta/Notch Regulation. *Cell* **173**, 1370-1384.e16 (2018).
57. Kendall, K. M. *et al.* Cognitive Performance Among Carriers of Pathogenic Copy Number Variants: Analysis of 152,000 UK Biobank Subjects. *Biol. Psychiatry* **82**, 103–110 (2017).

58. Coe, B. P. *et al.* Refining analyses of copy number variation identifies specific genes associated with developmental delay. *Nat. Genet.* **46**, 1063–1071 (2014).
59. Gillentine, M. A., Lupo, P. J., Stankiewicz, P. & Schaaf, C. P. An estimation of the prevalence of genomic disorders using chromosomal microarray data. *J. Hum. Genet.* **63**, 795–801 (2018).
60. Olsen, L. *et al.* Prevalence of rearrangements in the 22q11.2 region and population-based risk of neuropsychiatric and developmental disorders in a Danish population: a case-cohort study. *Lancet Psychiatry* **5**, 573–580 (2018).
61. Smajlagić, D. *et al.* Population prevalence and inheritance pattern of recurrent CNVs associated with neurodevelopmental disorders in 12,252 newborns and their parents. *Eur. J. Hum. Genet.* **29**, 205–215 (2021).
62. Fry, A. *et al.* Comparison of Sociodemographic and Health-Related Characteristics of UK Biobank Participants With Those of the General Population. *Am. J. Epidemiol.* **186**, 1026–1034 (2017).
63. Kaminsky, E. B. *et al.* An evidence-based approach to establish the functional and clinical significance of copy number variants in intellectual and developmental disabilities. *Genet. Med.* **13**, 777–784 (2011).
64. Miller, D. T. *et al.* Consensus Statement: Chromosomal Microarray Is a First-Tier Clinical Diagnostic Test for Individuals with Developmental Disabilities or Congenital Anomalies. *Am. J. Hum. Genet.* **86**, 749–764 (2010).

65. Tammimies, K. *et al.* Molecular Diagnostic Yield of Chromosomal Microarray Analysis and Whole-Exome Sequencing in Children With Autism Spectrum Disorder. *JAMA* **314**, 895–903 (2015).
66. Munnich, A. *et al.* Impact of on-site clinical genetics consultations on diagnostic rate in children and young adults with autism spectrum disorder. *Mol. Autism* **10**, 33 (2019).
67. Rees, E. *et al.* Analysis of copy number variations at 15 schizophrenia-associated loci. *Br. J. Psychiatry* **204**, 108–114 (2014).
68. Dittwald, P. *et al.* NAHR-mediated copy-number variants in a clinical population: Mechanistic insights into both genomic disorders and Mendelizing traits. *Genome Res.* **23**, 1395–1409 (2013).
69. Cooper, G. M. *et al.* A copy number variation morbidity map of developmental delay. *Nat. Genet.* **43**, 838–846 (2011).
70. Jønch, A. E. *et al.* Estimating the effect size of the 15Q11.2 BP1–BP2 deletion and its contribution to neurodevelopmental symptoms: recommendations for practice. *J. Med. Genet.* **56**, 701–710 (2019).
71. Morrow, B. E., McDonald-McGinn, D. M., Emanuel, B. S., Vermeesch, J. R. & Scambler, P. J. Molecular genetics of 22q11.2 deletion syndrome. *Am. J. Med. Genet. A.* **176**, 2070–2081 (2018).
72. Jonas, R. K., Montojo, C. A. & Bearden, C. E. The 22q11.2 Deletion Syndrome as a Window into Complex Neuropsychiatric Disorders Over the Lifespan. *Biol. Psychiatry* **75**, 351–360 (2014).

73. Marshall, C. R. *et al.* Contribution of copy number variants to schizophrenia from a genome-wide study of 41,321 subjects. *Nat. Genet.* **49**, 27–35 (2017).
74. Schneider, M. *et al.* Psychiatric Disorders From Childhood to Adulthood in 22q11.2 Deletion Syndrome: Results From the International Consortium on Brain and Behavior in 22q11.2 Deletion Syndrome. *Am. J. Psychiatry* **171**, 627–639 (2014).
75. Sønderby, I. E. *et al.* 1q21.1 distal copy number variants are associated with cerebral and cognitive alterations in humans. *Transl. Psychiatry* **11**, 1–16 (2021).
76. Fan, C. C. *et al.* Williams syndrome-specific neuroanatomical profile and its associations with behavioral features. *NeuroImage Clin.* **15**, 343–347 (2017).
77. Meda, S. A., Pryweller, J. R. & Thornton-Wells, T. A. Regional Brain Differences in Cortical Thickness, Surface Area and Subcortical Volume in Individuals with Williams Syndrome. *PLOS ONE* **7**, e31913 (2012).
78. Silva, A. I. *et al.* Analysis of Diffusion Tensor Imaging Data From the UK Biobank Confirms Dosage Effect of 15q11.2 Copy Number Variation on White Matter and Shows Association With Cognition. *Biol. Psychiatry* **90**, 307–316 (2021).
79. Stefansson, H. *et al.* CNVs conferring risk of autism or schizophrenia affect cognition in controls. *Nature* **505**, 361–366 (2014).
80. Ulfarsson, M. O. *et al.* 15q11.2 CNV affects cognitive, structural and functional correlates of dyslexia and dyscalculia. *Transl. Psychiatry* **7**, e1109–e1109 (2017).

81. Writing Committee for the ENIGMA-CNV Working Group *et al.* Association of Copy Number Variation of the 15q11.2 BP1-BP2 Region With Cortical and Subcortical Morphology and Cognition. *JAMA Psychiatry* **77**, 420–430 (2020).
82. Maillard, A. M. *et al.* The 16p11.2 locus modulates brain structures common to autism, schizophrenia and obesity. *Mol. Psychiatry* **20**, 140–147 (2015).
83. Martin-Brevet, S. *et al.* Quantifying the Effects of 16p11.2 Copy Number Variants on Brain Structure: A Multisite Genetic-First Study. *Biol. Psychiatry* **84**, 253–264 (2018).
84. Qureshi, A. Y. *et al.* Opposing Brain Differences in 16p11.2 Deletion and Duplication Carriers. *J. Neurosci.* **34**, 11199–11211 (2014).
85. Sønderby, I. E. *et al.* Dose response of the 16p11.2 distal copy number variant on intracranial volume and basal ganglia. *Mol. Psychiatry* **25**, 584–602 (2020).
86. Ching, C. R. K. *et al.* Mapping Subcortical Brain Alterations in 22q11.2 Deletion Syndrome: Effects of Deletion Size and Convergence With Idiopathic Neuropsychiatric Illness. *Am. J. Psychiatry* **177**, 589–600 (2020).
87. Sun, D. *et al.* Large-scale mapping of cortical alterations in 22q11.2 deletion syndrome: Convergence with idiopathic psychosis and effects of deletion size. *Mol. Psychiatry* **25**, 1822–1834 (2020).
88. Huntenburg, J. M., Bazin, P.-L. & Margulies, D. S. Large-Scale Gradients in Human Cortical Organization. *Trends Cogn. Sci.* **22**, 21–31 (2018).
89. Keller, A. S. *et al.* Hierarchical functional system development supports executive function. *Trends Cogn. Sci.* **27**, 160–174 (2023).

90. Sydnor, V. J. *et al.* Neurodevelopment of the association cortices: Patterns, mechanisms, and implications for psychopathology. *Neuron* **109**, 2820–2846 (2021).
91. Azevedo, F. A. C. *et al.* Equal numbers of neuronal and nonneuronal cells make the human brain an isometrically scaled-up primate brain. *J. Comp. Neurol.* **513**, 532–541 (2009).
92. Ribeiro, P. *et al.* The human cerebral cortex is neither one nor many: neuronal distribution reveals two quantitatively different zones in the gray matter, three in the white matter, and explains local variations in cortical folding. *Front. Neuroanat.* **7**, (2013).
93. Beul, S. F., Barbas, H. & Hilgetag, C. C. A Predictive Structural Model of the Primate Connectome. *Sci. Rep.* **7**, 43176 (2017).
94. Herculano-Houzel, S. The glia/neuron ratio: How it varies uniformly across brain structures and species and what that means for brain physiology and evolution. *Glia* **62**, 1377–1391 (2014).
95. Jacobs, B. *et al.* Regional Dendritic and Spine Variation in Human Cerebral Cortex: a Quantitative Golgi Study. *Cereb. Cortex* **11**, 558–571 (2001).
96. Herculano-Houzel, S. The human brain in numbers: a linearly scaled-up primate brain. *Front. Hum. Neurosci.* **3**, (2009).
97. Herculano-Houzel, S. The remarkable, yet not extraordinary, human brain as a scaled-up primate brain and its associated cost. *Proc. Natl. Acad. Sci.* **109**, 10661–10668 (2012).

98. Jukic, A. M., Baird, D. D., Weinberg, C. R., McConnaughey, D. R. & Wilcox, A. J. Length of human pregnancy and contributors to its natural variation. *Hum. Reprod.* **28**, 2848–2855 (2013).
99. Tardif, S., Carville, A., Elmore, D., Williams, L. E. & Rice, K. Reproduction and Breeding of Nonhuman Primates. *Nonhum. Primates Biomed. Res.* 197–249 (2012) doi:10.1016/B978-0-12-381365-7.00008-X.
100. Rakic, P. Specification of Cerebral Cortical Areas. *Science* **241**, 170–176 (1988).
101. Nowakowski, T. J., Pollen, A. A., Sandoval-Espinosa, C. & Kriegstein, A. R. Transformation of the Radial Glia Scaffold Demarcates Two Stages of Human Cerebral Cortex Development. *Neuron* **91**, 1219–1227 (2016).
102. Kriegstein, A. & Alvarez-Buylla, A. The glial nature of embryonic and adult neural stem cells. *Annu. Rev. Neurosci.* **32**, 149–184 (2009).
103. Noctor, S. C., Flint, A. C., Weissman, T. A., Dammerman, R. S. & Kriegstein, A. R. Neurons derived from radial glial cells establish radial units in neocortex. *Nature* **409**, 714–720 (2001).
104. Hansen, D. V., Lui, J. H., Parker, P. R. L. & Kriegstein, A. R. Neurogenic radial glia in the outer subventricular zone of human neocortex. *Nature* **464**, 554–561 (2010).
105. Lui, J. H., Hansen, D. V. & Kriegstein, A. R. Development and Evolution of the Human Neocortex. *Cell* **146**, 18–36 (2011).
106. Artavanis-Tsakonas, S., Rand, M. D. & Lake, R. J. Notch Signaling: Cell Fate Control and Signal Integration in Development. *Science* **284**, 770–776 (1999).

107. Gaiano, N. & Fishell, G. The role of notch in promoting glial and neural stem cell fates. *Annu. Rev. Neurosci.* **25**, 471–490 (2002).
108. Redmond, L., Oh, S.-R., Hicks, C., Weinmaster, G. & Ghosh, A. Nuclear Notch1 signaling and the regulation of dendritic development. *Nat. Neurosci.* **3**, 30–40 (2000).
109. Geschwind, D. H. & Rakic, P. Cortical Evolution: Judge the Brain by Its Cover. *Neuron* **80**, 633–647 (2013).
110. Huttenlocher, P. R., de Courten, C., Garey, L. J. & Van der Loos, H. Synaptogenesis in human visual cortex — evidence for synapse elimination during normal development. *Neurosci. Lett.* **33**, 247–252 (1982).
111. Peter R., H. Synaptic density in human frontal cortex — Developmental changes and effects of aging. *Brain Res.* **163**, 195–205 (1979).
112. Huttenlocher, P. R. & Dabholkar, A. S. Regional differences in synaptogenesis in human cerebral cortex. *J. Comp. Neurol.* **387**, 167–178 (1997).
113. Glantz, L. A., Gilmore, J. H., Hamer, R. M., Lieberman, J. A. & Jarskog, L. F. Synaptophysin and postsynaptic density protein 95 in the human prefrontal cortex from mid-gestation into early adulthood. *Neuroscience* **149**, 582–591 (2007).
114. Petanjek, Z. *et al.* Extraordinary neoteny of synaptic spines in the human prefrontal cortex. *Proc. Natl. Acad. Sci.* **108**, 13281–13286 (2011).
115. Liu, X. *et al.* Extension of cortical synaptic development distinguishes humans from chimpanzees and macaques. *Genome Res.* **22**, 611–622 (2012).



116. Yeung, M. S. Y. *et al.* Dynamics of Oligodendrocyte Generation and Myelination in the Human Brain. *Cell* **159**, 766–774 (2014).
117. Miller, D. J. *et al.* Prolonged myelination in human neocortical evolution. *Proc. Natl. Acad. Sci.* **109**, 16480–16485 (2012).
118. Dekaban, A. S. Tables of cranial and orbital measurements, cranial volume, and derived indexes in males and females from 7 days to 20 years of age. *Ann. Neurol.* **2**, 485–491 (1977).
119. Dekaban, A. S. Changes in brain weights during the span of human life: relation of brain weights to body heights and body weights. *Ann. Neurol.* **4**, 345–356 (1978).
120. Reardon, P. K. *et al.* Normative brain size variation and brain shape diversity in humans. *Science* **360**, 1222–1227 (2018).
121. Hill, J. *et al.* Similar patterns of cortical expansion during human development and evolution. *Proc. Natl. Acad. Sci.* **107**, 13135–13140 (2010).
122. Scahill, R. I. *et al.* A longitudinal study of brain volume changes in normal aging using serial registered magnetic resonance imaging. *Arch. Neurol.* **60**, 989–994 (2003).
123. Svennerholm, L., Boström, K. & Jungbjer, B. Changes in weight and compositions of major membrane components of human brain during the span of adult human life of Swedes. *Acta Neuropathol. (Berl.)* **94**, 345–352 (1997).
124. Marnier, L., Nyengaard, J. R., Tang, Y. & Pakkenberg, B. Marked loss of myelinated nerve fibers in the human brain with age. *J. Comp. Neurol.* **462**, 144–152 (2003).

125. Masliah, E., Mallory, M., Hansen, L., DeTeresa, R. & Terry, R. D. Quantitative synaptic alterations in the human neocortex during normal aging. *Neurology* **43**, 192–192 (1993).
126. Jacobs, B., Driscoll, L. & Schall, M. Life-span dendritic and spine changes in areas 10 and 18 of human cortex: A quantitative golgi study. *J. Comp. Neurol.* **386**, 661–680 (1997).
127. Terry, R. D., DeTeresa, R. & Hansen, L. A. Neocortical cell counts in normal human adult aging. *Ann. Neurol.* **21**, 530–539 (1987).
128. Fabricius, K., Jacobsen, J. S. & Pakkenberg, B. Effect of age on neocortical brain cells in 90+ year old human females—a cell counting study. *Neurobiol. Aging* **34**, 91–99 (2013).
129. von Bartheld, C. S. Myths and truths about the cellular composition of the human brain: A review of influential concepts. *J. Chem. Neuroanat.* **93**, 2–15 (2018).
130. Kirkwood, T. B. L. & Melov, S. On the Programmed/Non-Programmed Nature of Ageing within the Life History. *Curr. Biol.* **21**, R701–R707 (2011).
131. Kang, H. J. *et al.* Spatiotemporal transcriptome of the human brain. *Nature* **478**, 483–489 (2011).
132. Nowakowski, T. J. *et al.* Spatiotemporal gene expression trajectories reveal developmental hierarchies of the human cortex. *Science* **358**, 1318–1323 (2017).
133. Harris, L. W. *et al.* Gene expression in the prefrontal cortex during adolescence: implications for the onset of schizophrenia. *BMC Med. Genomics* **2**, 1–14 (2009).

134. Tebbenkamp, A. T. N., Willsey, A. J., State, M. W. & Šestan, N. The Developmental Transcriptome of the Human Brain: Implications for Neurodevelopmental Disorders. *Curr. Opin. Neurol.* **27**, 149–156 (2014).
135. Hastings, P. J., Lupski, J. R., Rosenberg, S. M. & Ira, G. Mechanisms of change in gene copy number. *Nat. Rev. Genet.* **10**, 551–564 (2009).
136. Khan, T. A. *et al.* Neuronal defects in a human cellular model of 22q11.2 deletion syndrome. *Nat. Med.* **26**, 1888–1898 (2020).
137. Silva, A. I. *et al.* Cyfip1 haploinsufficient rats show white matter changes, myelin thinning, abnormal oligodendrocytes and behavioural inflexibility. *Nat. Commun.* **10**, 3455 (2019).
138. Brunetti-Pierri, N. *et al.* Recurrent reciprocal 1q21.1 deletions and duplications associated with microcephaly or macrocephaly and developmental and behavioral abnormalities. *Nat. Genet.* **40**, 1466–1471 (2008).
139. Spielmann, M., Lupiáñez, D. G. & Mundlos, S. Structural variation in the 3D genome. *Nat. Rev. Genet.* **19**, 453–467 (2018).
140. Loviglio, M. N. *et al.* Chromosomal contacts connect loci associated with autism, BMI and head circumference phenotypes. *Mol. Psychiatry* **22**, 836–849 (2017).
141. Lin, A. *et al.* Transcriptomic profiling of whole blood in 22q11.2 reciprocal copy number variants reveals that cell proportion highly impacts gene expression. *Brain Behav. Immun. - Health* **18**, 100386 (2021).

142. Walhovd, K. B., Johansen-Berg, H. & Káradóttir, R. T. Unraveling the secrets of white matter – Bridging the gap between cellular, animal and human imaging studies. *Neuroscience* **276**, 2–13 (2014).
143. Fischl, B. FreeSurfer. *NeuroImage* **62**, 774–781 (2012).
144. Dale, A. M., Fischl, B. & Sereno, M. I. Cortical Surface-Based Analysis: I. Segmentation and Surface Reconstruction. *NeuroImage* **9**, 179–194 (1999).
145. Fischl, B. & Dale, A. M. Measuring the thickness of the human cerebral cortex from magnetic resonance images. *Proc. Natl. Acad. Sci.* **97**, 11050–11055 (2000).
146. Fischl, B. *et al.* Whole Brain Segmentation: Automated Labeling of Neuroanatomical Structures in the Human Brain. *Neuron* **33**, 341–355 (2002).
147. Desikan, R. S. *et al.* An automated labeling system for subdividing the human cerebral cortex on MRI scans into gyral based regions of interest. *NeuroImage* **31**, 968–980 (2006).
148. Beaulieu, C. The basis of anisotropic water diffusion in the nervous system - a technical review. *NMR Biomed.* **15**, 435–455 (2002).
149. Le Bihan, D. Looking into the functional architecture of the brain with diffusion MRI. *Nat. Rev. Neurosci.* **4**, 469–480 (2003).
150. Mori, S. & Zhang, J. Principles of Diffusion Tensor Imaging and Its Applications to Basic Neuroscience Research. *Neuron* **51**, 527–539 (2006).
151. Basser, P. J., Mattiello, J. & LeBihan, D. MR diffusion tensor spectroscopy and imaging. *Biophys. J.* **66**, 259–267 (1994).

152. Zhang, H., Schneider, T., Wheeler-Kingshott, C. A. & Alexander, D. C. NODDI: Practical in vivo neurite orientation dispersion and density imaging of the human brain. *NeuroImage* **61**, 1000–1016 (2012).
153. Pietschnig, J., Penke, L., Wicherts, J. M., Zeiler, M. & Voracek, M. Meta-analysis of associations between human brain volume and intelligence differences: How strong are they and what do they mean? *Neurosci. Biobehav. Rev.* **57**, 411–432 (2015).
154. Gignac, G. E. & Bates, T. C. Brain volume and intelligence: The moderating role of intelligence measurement quality. *Intelligence* **64**, 18–29 (2017).
155. Cox, S. R., Ritchie, S. J., Fawns-Ritchie, C., Tucker-Drob, E. M. & Deary, I. J. Structural brain imaging correlates of general intelligence in UK Biobank. *Intelligence* **76**, 101376 (2019).
156. Ritchie, S. J. *et al.* Sex Differences in the Adult Human Brain: Evidence from 5216 UK Biobank Participants. *Cereb. Cortex* **28**, 2959–2975 (2018).
157. Deary, I. J., Irwing, P., Der, G. & Bates, T. C. Brother–sister differences in the g factor in intelligence: Analysis of full, opposite-sex siblings from the NLSY1979. *Intelligence* **35**, 451–456 (2007).
158. Johnson, W., Carothers, A. & Deary, I. J. Sex Differences in Variability in General Intelligence: A New Look at the Old Question. *Perspect. Psychol. Sci. J. Assoc. Psychol. Sci.* **3**, 518–531 (2008).
159. Marek, S. *et al.* Reproducible brain-wide association studies require thousands of individuals. *Nature* **603**, 654–660 (2022).

160. Liu, S., Abdellaoui, A., Verweij, K. J. H. & van Wingen, G. A. Replicable brain–phenotype associations require large-scale neuroimaging data. *Nat. Hum. Behav.* **7**, 1344–1356 (2023).
161. Gilmore, J. H. *et al.* Longitudinal Development of Cortical and Subcortical Gray Matter from Birth to 2 Years. *Cereb. Cortex N. Y. NY* **22**, 2478–2485 (2012).
162. Zielinski, B. A., Gennatas, E. D., Zhou, J. & Seeley, W. W. Network-level structural covariance in the developing brain. *Proc. Natl. Acad. Sci.* **107**, 18191–18196 (2010).
163. Tamnes, C. K. *et al.* Brain development and aging: Overlapping and unique patterns of change. *NeuroImage* **68**, 63–74 (2013).
164. Shaw, P. *et al.* Neurodevelopmental Trajectories of the Human Cerebral Cortex. *J. Neurosci.* **28**, 3586–3594 (2008).
165. Lyall, A. E. *et al.* Dynamic Development of Regional Cortical Thickness and Surface Area in Early Childhood. *Cereb. Cortex* **25**, 2204–2212 (2015).
166. Bethlehem, R. a. I. *et al.* Brain charts for the human lifespan. *Nature* **604**, 525–533 (2022).
167. Tamnes, C. K. *et al.* Development of the Cerebral Cortex across Adolescence: A Multisample Study of Inter-Related Longitudinal Changes in Cortical Volume, Surface Area, and Thickness. *J. Neurosci.* **37**, 3402–3412 (2017).
168. Wierenga, L. M., Langen, M., Oranje, B. & Durston, S. Unique developmental trajectories of cortical thickness and surface area. *NeuroImage* **87**, 120–126 (2014).

169. Fjell, A. M. *et al.* High Consistency of Regional Cortical Thinning in Aging across Multiple Samples. *Cereb. Cortex* **19**, 2001–2012 (2009).
170. Fjell, A. M., McEvoy, L., Holland, D., Dale, A. M. & Walhovd, K. B. What is normal in normal aging? Effects of aging, amyloid and Alzheimer’s disease on the cerebral cortex and the hippocampus. *Prog. Neurobiol.* **117**, 20–40 (2014).
171. Fjell, A. M. & Walhovd, K. B. Structural brain changes in aging: courses, causes and cognitive consequences. *Rev. Neurosci.* **21**, 187–221 (2010).
172. Frangou, S. *et al.* Cortical thickness across the lifespan: Data from 17,075 healthy individuals aged 3–90 years. *Hum. Brain Mapp.* **n/a**, (2021).
173. Cole, J. H., Marioni, R. E., Harris, S. E. & Deary, I. J. Brain age and other bodily ‘ages’: implications for neuropsychiatry. *Mol. Psychiatry* **24**, 266–281 (2019).
174. Cole, J. H. *et al.* Brain age predicts mortality. *Mol. Psychiatry* **23**, 1385–1392 (2018).
175. Beck, D. *et al.* Cardiometabolic risk factors associated with brain age and accelerate brain ageing. *Hum. Brain Mapp.* **43**, 700–720 (2022).
176. de Lange, A.-M. G. *et al.* Multimodal brain-age prediction and cardiovascular risk: The Whitehall II MRI sub-study. *NeuroImage* **222**, 117292 (2020).
177. Elliott, M. L. *et al.* Brain-age in midlife is associated with accelerated biological aging and cognitive decline in a longitudinal birth cohort. *Mol. Psychiatry* **26**, 3829–3838 (2021).

178. Richard, G. *et al.* Assessing distinct patterns of cognitive aging using tissue-specific brain age prediction based on diffusion tensor imaging and brain morphometry. *PeerJ* **6**, e5908 (2018).
179. Kaufmann, T. *et al.* Common brain disorders are associated with heritable patterns of apparent aging of the brain. *Nat. Neurosci.* **22**, 1617–1623 (2019).
180. Arnatkevičiūtė, A., Fulcher, B. D. & Fornito, A. A practical guide to linking brain-wide gene expression and neuroimaging data. *NeuroImage* **189**, 353–367 (2019).
181. Fornito, A., Arnatkevičiūtė, A. & Fulcher, B. D. Bridging the Gap between Connectome and Transcriptome. *Trends Cogn. Sci.* **23**, 34–50 (2019).
182. Hawrylycz, M. J. *et al.* An anatomically comprehensive atlas of the adult human brain transcriptome. *Nature* **489**, 391–399 (2012).
183. Hawrylycz, M. *et al.* Canonical genetic signatures of the adult human brain. *Nat. Neurosci.* **18**, 1832–1844 (2015).
184. Dai, Y. *et al.* WebCSEA: web-based cell-type-specific enrichment analysis of genes. *Nucleic Acids Res.* **50**, W782–W790 (2022).
185. Kolberg, L., Raudvere, U., Kuzmin, I., Vilo, J. & Peterson, H. gprofiler2 -- an R package for gene list functional enrichment analysis and namespace conversion toolset g:Profiler. Preprint at <https://doi.org/10.12688/f1000research.24956.2> (2020).
186. Vidal-Pineiro, D. *et al.* Cellular correlates of cortical thinning throughout the lifespan. *Sci. Rep.* **10**, 21803 (2020).



187. Writing Committee for the Attention-Deficit/Hyperactivity Disorder *et al.* Virtual Histology of Cortical Thickness and Shared Neurobiology in 6 Psychiatric Disorders. *JAMA Psychiatry* **78**, 47–63 (2021).
188. Parker, N. *et al.* Assessment of Neurobiological Mechanisms of Cortical Thinning During Childhood and Adolescence and Their Implications for Psychiatric Disorders. *JAMA Psychiatry* **77**, 1127–1136 (2020).
189. Stefansson, H. *et al.* Large recurrent microdeletions associated with schizophrenia. *Nature* **455**, 232–236 (2008).
190. Gudmundsson, O. O. *et al.* Attention-deficit hyperactivity disorder shares copy number variant risk with schizophrenia and autism spectrum disorder. *Transl. Psychiatry* **9**, 1–9 (2019).
191. Kendall, K. M. *et al.* Association of Rare Copy Number Variants With Risk of Depression. *JAMA Psychiatry* **76**, 818–825 (2019).
192. Bernier, R. *et al.* Clinical phenotype of the recurrent 1q21.1 copy-number variant. *Genet. Med. Off. J. Am. Coll. Med. Genet.* **18**, 341–349 (2016).
193. Delio, M. *et al.* Enhanced Maternal Origin of the 22q11.2 Deletion in Velocardiofacial and DiGeorge Syndromes. *Am. J. Hum. Genet.* **92**, 439–447 (2013).
194. Kates, W. R., Tang, K. L., Antshel, K. M. & Fremont, W. P. Behavioral and Psychiatric Phenotypes in 22q11.2 Deletion Syndrome. *J. Dev. Behav. Pediatr. JDBP* **36**, 639–650 (2015).

195. Fiksinski, A. M., Hoftman, G. D., Vorstman, J. A. S. & Bearden, C. E. A genetics-first approach to understanding autism and schizophrenia spectrum disorders: the 22q11.2 deletion syndrome. *Mol. Psychiatry* **28**, 341–353 (2023).
196. Natu, V. S. *et al.* Apparent thinning of human visual cortex during childhood is associated with myelination. *Proc. Natl. Acad. Sci.* 201904931 (2019)  
doi:10.1073/pnas.1904931116.
197. Silva, A. I. *et al.* Reciprocal White Matter Changes Associated With Copy Number Variation at 15q11.2 BP1-BP2: A Diffusion Tensor Imaging Study. *Biol. Psychiatry* **85**, 563–572 (2019).
198. Villalón-Reina, J. E. *et al.* Altered white matter microstructure in 22q11.2 deletion syndrome: a multisite diffusion tensor imaging study. *Mol. Psychiatry* **25**, 2818–2831 (2020).
199. Pierpaoli, C., Jezzard, P., Basser, P. J., Barnett, A. & Di Chiro, G. Diffusion tensor MR imaging of the human brain. *Radiology* **201**, 637–648 (1996).
200. Forsyth, J. K. *et al.* Prioritizing Genetic Contributors to Cortical Alterations in 22q11.2 Deletion Syndrome Using Imaging Transcriptomics. *Cereb. Cortex N. Y. NY* **31**, 3285–3298 (2021).
201. Alnæs, D. *et al.* Brain Heterogeneity in Schizophrenia and Its Association With Polygenic Risk. *JAMA Psychiatry* **76**, 739–748 (2019).
202. Moreau, C. A., Ching, C. R., Kumar, K., Jacquemont, S. & Bearden, C. E. Structural and functional brain alterations revealed by neuroimaging in CNV carriers. *Curr. Opin. Genet. Dev.* **68**, 88–98 (2021).

203. van Erp, T. G. M. *et al.* Cortical Brain Abnormalities in 4474 Individuals With Schizophrenia and 5098 Control Subjects via the Enhancing Neuro Imaging Genetics Through Meta Analysis (ENIGMA) Consortium. *Biol. Psychiatry* **84**, 644–654 (2018).
204. Kopal, J. *et al.* Rare CNVs and phenome-wide profiling highlight brain structural divergence and phenotypical convergence. *Nat. Hum. Behav.* **7**, 1001–1017 (2023).
205. Yoon, S.-J. *et al.* Reliability of human cortical organoid generation. *Nat. Methods* **16**, 75–78 (2019).
206. Akkouh, I. A. *et al.* Longitudinal transcriptomic analysis of human cortical spheroids identifies axonal dysregulation in the prenatal brain as a mediator of genetic risk for schizophrenia. *Biol. Psychiatry* **0**, (2023).
207. Gordon, A. *et al.* Long-term maturation of human cortical organoids matches key early postnatal transitions. *Nat. Neurosci.* **24**, 331–342 (2021).
208. Markello, R. D. *et al.* Standardizing workflows in imaging transcriptomics with the abagen toolbox. *eLife* **10**, e72129 (2021).
209. Alfaro-Almagro, F. *et al.* Image processing and Quality Control for the first 10,000 brain imaging datasets from UK Biobank. *NeuroImage* **166**, 400–424 (2018).
210. Monereo-Sánchez, J. *et al.* Quality control strategies for brain MRI segmentation and parcellation: Practical approaches and recommendations - insights from the Maastricht study. *NeuroImage* **237**, 118174 (2021).
211. Radua, J. *et al.* Increased power by harmonizing structural MRI site differences with the ComBat batch adjustment method in ENIGMA. *NeuroImage* **218**, 116956 (2020).

212. Andersson, J. L. R., Skare, S. & Ashburner, J. How to correct susceptibility distortions in spin-echo echo-planar images: application to diffusion tensor imaging. *NeuroImage* **20**, 870–888 (2003).
213. Andersson, J. L. R. & Sotiropoulos, S. N. An integrated approach to correction for off-resonance effects and subject movement in diffusion MR imaging. *NeuroImage* **125**, 1063–1078 (2016).
214. Garyfallidis, E. *et al.* Dipy, a library for the analysis of diffusion MRI data. *Front. Neuroinformatics* **8**, (2014).
215. Manjón, J. V. *et al.* Diffusion Weighted Image Denoising Using Overcomplete Local PCA. *PLOS ONE* **8**, e73021 (2013).
216. Jahanshad, N. *et al.* Multi-site genetic analysis of diffusion images and voxelwise heritability analysis: A pilot project of the ENIGMA–DTI working group. *NeuroImage* **81**, 455–469 (2013).
217. Mori, S. *et al.* Stereotaxic white matter atlas based on diffusion tensor imaging in an ICBM template. *NeuroImage* **40**, 570–582 (2008).
218. Langfelder, P. & Horvath, S. WGCNA: an R package for weighted correlation network analysis. *BMC Bioinformatics* **9**, 559 (2008).
219. Bhaduri, A. *et al.* An atlas of cortical arealization identifies dynamic molecular signatures. *Nature* **598**, 200–204 (2021).
220. Wang, D. *et al.* Comprehensive functional genomic resource and integrative model for the human brain. *Science* **362**, eaat8464 (2018).

221. Zhong, S. *et al.* A single-cell RNA-seq survey of the developmental landscape of the human prefrontal cortex. *Nature* **555**, 524–528 (2018).
222. Martin, C. L. *et al.* Identification of Neuropsychiatric Copy Number Variants in a Health Care System Population. *JAMA Psychiatry* **77**, 1276–1285 (2020).
223. Hoeffding, L. K. *et al.* Risk of Psychiatric Disorders Among Individuals With the 22q11.2 Deletion or Duplication: A Danish Nationwide, Register-Based Study. *JAMA Psychiatry* **74**, 282–290 (2017).
224. Wilfert, A. B., Sulovari, A., Turner, T. N., Coe, B. P. & Eichler, E. E. Recurrent de novo mutations in neurodevelopmental disorders: properties and clinical implications. *Genome Med.* **9**, 101 (2017).
225. Dykiert, D., Der, G., Starr, J. M. & Deary, I. J. Sex differences in reaction time mean and intraindividual variability across the life span. *Dev. Psychol.* **48**, 1262–1276 (2012).
226. Hilborn, J. V., Strauss, E., Hultsch, D. F. & Hunter, M. A. Intraindividual variability across cognitive domains: Investigation of dispersion levels and performance profiles in older adults. *J. Clin. Exp. Neuropsychol.* **31**, 412–424 (2009).
227. Schretlen, D. J., Munro, C. A., Anthony, J. C. & Pearlson, G. D. Examining the range of normal intraindividual variability in neuropsychological test performance. *J. Int. Neuropsychol. Soc.* **9**, 864–870 (2003).
228. Raven, E. P. *et al.* In vivo evidence of microstructural hypo-connectivity of brain white matter in 22q11.2 deletion syndrome. *Mol. Psychiatry* 1–11 (2023) doi:10.1038/s41380-023-02178-w.

229. Zeisel, A. *et al.* Brain structure. Cell types in the mouse cortex and hippocampus revealed by single-cell RNA-seq. *Science* **347**, 1138–1142 (2015).
230. Patel, Y. *et al.* Virtual histology of multi-modal magnetic resonance imaging of cerebral cortex in young men. *NeuroImage* **218**, 116968 (2020).
231. Shin, J. *et al.* Cell-Specific Gene-Expression Profiles and Cortical Thickness in the Human Brain. *Cereb. Cortex* **28**, 3267–3277 (2018).
232. Neniskyte, U. & Gross, C. T. Errant gardeners: glial-cell-dependent synaptic pruning and neurodevelopmental disorders. *Nat. Rev. Neurosci.* **18**, 658–670 (2017).
233. Whitaker, K. J. *et al.* Adolescence is associated with genomically patterned consolidation of the hubs of the human brain connectome. *Proc. Natl. Acad. Sci.* **113**, 9105–9110 (2016).
234. Jalbrzikowski, M. *et al.* Longitudinal trajectories of cortical development in 22q11.2 copy number variants and typically developing controls. *Mol. Psychiatry* **27**, 4181–4190 (2022).
235. Motahari, Z., Moody, S. A., Maynard, T. M. & LaMantia, A.-S. In the line-up: deleted genes associated with DiGeorge/22q11.2 deletion syndrome: are they all suspects? *J. Neurodev. Disord.* **11**, 1–28 (2019).
236. Bian, W.-J., Miao, W.-Y., He, S.-J., Qiu, Z. & Yu, X. Coordinated Spine Pruning and Maturation Mediated by Inter-Spine Competition for Cadherin/Catenin Complexes. *Cell* **162**, 808–822 (2015).

237. Mabb, A. M. & Ehlers, M. D. Ubiquitination in Postsynaptic Function and Plasticity. *Annu. Rev. Cell Dev. Biol.* **26**, 179–210 (2010).
238. Charpentier, C. J. *et al.* How representative are neuroimaging samples? Large-scale evidence for trait anxiety differences between fMRI and behaviour-only research participants. *Soc. Cogn. Affect. Neurosci.* **16**, 1057–1070 (2021).
239. Button, K. S. *et al.* Power failure: why small sample size undermines the reliability of neuroscience. *Nat. Rev. Neurosci.* **14**, 365–376 (2013).
240. Border, R. *et al.* No Support for Historical Candidate Gene or Candidate Gene-by-Interaction Hypotheses for Major Depression Across Multiple Large Samples. *Am. J. Psychiatry* **176**, 376–387 (2019).
241. Boedhoe, P. S. W. *et al.* Subcortical Brain Volume, Regional Cortical Thickness, and Cortical Surface Area Across Disorders: Findings From the ENIGMA ADHD, ASD, and OCD Working Groups. *Am. J. Psychiatry* **177**, 834–843 (2020).
242. van Erp, T. G. M. *et al.* Subcortical brain volume abnormalities in 2028 individuals with schizophrenia and 2540 healthy controls via the ENIGMA consortium. *Mol. Psychiatry* **21**, 547–553 (2016).
243. Vidal-Pineiro, D. *et al.* Individual variations in ‘brain age’ relate to early-life factors more than to longitudinal brain change. *eLife* **10**, e69995 (2021).
244. Hodge, R. D. *et al.* Conserved cell types with divergent features in human versus mouse cortex. *Nature* **573**, 61–68 (2019).

## **11 Studies I-III**



I

I

**Beyond the Global Brain Differences: Intra-individual Variability Differences in 1q21.1  
Distal and 15q11.2 BP1-BP2 Deletion Carriers**

Rune Boen<sup>1,2\*</sup>, Tobias Kaufmann<sup>2,3</sup>, Dennis van der Meer<sup>2,4</sup>, Oleksandr Frei<sup>2,5</sup>, Ingrid Agartz<sup>6,7,8</sup>, David Ames<sup>9,10</sup>, Micael Andersson<sup>11,12</sup>, Nicola J. Armstrong<sup>13</sup>, Eric Artiges<sup>14,15</sup>, Joshua R. Atkins<sup>16,17,18</sup>, Jochen Bauer<sup>19</sup>, Francesco Benedetti<sup>20,21</sup>, Dorret I. Boomsma<sup>22</sup>, Henry Brodaty<sup>23</sup>, Katharina Brosch<sup>24</sup>, Randy L. Buckner<sup>25,26</sup>, Murray J. Cairns<sup>16,27</sup>, Vince Calhoun<sup>28</sup>, Svenja Caspers<sup>29,30</sup>, Sven Cichon<sup>29,31,32</sup>, Aiden P. Corvin<sup>33</sup>, Benedicto Crespo-Facorro<sup>34,35,36</sup>, Udo Dannlowski<sup>37</sup>, Friederike S. David<sup>38</sup>, Eco J.C. de Geus<sup>22</sup>, Greig I. de Zubicaray<sup>39</sup>, Sylvane Desrivieres<sup>40</sup>, Joanne L. Doherty<sup>41,42</sup>, Gary Donohoe<sup>43</sup>, Stefan Ehrlich<sup>44</sup>, Else Eising<sup>45</sup>, Thomas Espeseth<sup>46,47</sup>, Simon E. Fisher<sup>45,48</sup>, Andreas J. Forstner<sup>38,29</sup>, Lidia Fortaner-Uyà<sup>20,21</sup>, Vincent Frouin<sup>49</sup>, Masaki Fukunaga<sup>50</sup>, Tian Ge<sup>51,52</sup>, David C. Glahn<sup>53,54</sup>, Janik Goltermann<sup>37</sup>, Hans J. Grabe<sup>55</sup>, Melissa J. Green<sup>56,57</sup>, Nynke A. Groenewold<sup>58</sup>, Dominik Grotegerd<sup>37</sup>, Gøril Rolfseng Grøntvedt<sup>65,109</sup>, Tim Hahn<sup>37</sup>, Ryota Hashimoto<sup>59</sup>, Jayne Y. Hehir-Kwa<sup>60</sup>, Frans A. Henskens<sup>61,62</sup>, Avram J. Holmes<sup>63,64</sup>, Asta K. Håberg<sup>65,66</sup>, Jan Haavik<sup>67,68</sup>, Sebastien Jacquemont<sup>69,70</sup>, Andreas Jansen<sup>71,72</sup>, Christiane Jockwitz<sup>29,30</sup>, Erik G. Jönsson<sup>6,73</sup>, Masataka Kikuchi<sup>74,75</sup>, Tilo Kircher<sup>24</sup>, Kuldeep Kumar<sup>76</sup>, Stephanie Le Hellard<sup>77,78</sup>, Costin Leu<sup>79,80</sup>, David E. Linden<sup>81,82</sup>, Jingyu Liu<sup>83,84</sup>, Robert Loughnan<sup>85,86</sup>, Karen A. Mather<sup>23</sup>, Katie L. McMahon<sup>87</sup>, Allan F. McRae<sup>88</sup>, Sarah E. Medland<sup>89,90,91</sup>, Susanne Meinert<sup>37,140</sup>, Clara A. Moreau<sup>92</sup>, Derek W. Morris<sup>93</sup>, Bryan J. Mowry<sup>94,95</sup>, Thomas W. Mühlisen<sup>29,30,96</sup>, Igor Nenadić<sup>24</sup>, Markus M. Nöthen<sup>38</sup>, Lars Nyberg<sup>97</sup>, Roel A. Ophoff<sup>103,137</sup>, Michael J. Owen<sup>41,98</sup>, Christos Pantelis<sup>106,128</sup>, Marco Paolini<sup>20,21</sup>, Tomas Paus<sup>99,100</sup>, Zdenka Pausova<sup>101,102</sup>, Karin Persson<sup>104, 114</sup>, Yann Quidé<sup>57,105</sup>, Tiago Reis Marques<sup>107</sup>, Perminder S. Sachdev<sup>23,108</sup>, Sigrid B. Sando<sup>65,109</sup>, Ulrich Schall<sup>110</sup>, Rodney J. Scott<sup>111,112,113</sup>, Geir Selbæk<sup>114,115,104</sup>, Elena Shumskaya<sup>48,116</sup>, Ana I. Silva<sup>81</sup>, Sanjay M. Sisodiya<sup>79,117</sup>, Frederike Stein<sup>24</sup>, Dan J. Stein<sup>118</sup>, Benjamin Straube<sup>24</sup>, Fabian Streit<sup>119</sup>, Lachlan T. Strike<sup>89,120</sup>, Alexander Teumer<sup>121,55,122</sup>, Lea Teutenberg<sup>24</sup>, Anbupalam Thalamuthu<sup>23</sup>, Paul A Tooney<sup>16,123</sup>, Diana Tordesillas-Gutierrez<sup>124,125</sup>, Julian N Trollor<sup>126,127</sup>, Dennis van 't Ent<sup>22</sup>, Marianne B.M. van den Bree<sup>129,130,140</sup>, Neeltje E.M. van Haren<sup>131,132</sup>, Javier Vázquez-Bourgon<sup>133,134,35</sup>, Henry Völzke<sup>135,122</sup>, Wei Wen<sup>23</sup>, Katharina Wittfeld<sup>55</sup>, Christopher R.K. Ching<sup>92</sup>, Lars T. Westlye<sup>2,46,136</sup>, Paul M. Thompson<sup>92</sup>, Carrie E. Bearden<sup>137</sup>, Kaja K. Selmer<sup>138</sup>, Dag Alnæs<sup>2,139</sup>, Ole A. Andreassen<sup>2,6,136</sup>, Ida E. Sønderyb<sup>1,2,136</sup>

- 2 NORMENT, Division of Mental Health and Addiction, Oslo University Hospital and Institute of Clinical Medicine, University of Oslo, Oslo, Norway
- 3 Department of Psychiatry and Psychotherapy, Tübingen Center for Mental Health, University of Tübingen, Germany
- 4 School of Mental Health and Neuroscience, Faculty of Health, Medicine and Life Sciences, Maastricht University, Maastricht, Netherlands
- 5 Centre for Bioinformatics, Department of Informatics, University of Oslo, Oslo, Norway
- 6 NORMENT, Institute of Clinical Medicine, University of Oslo, Oslo, Norway
- 7 Department of Clinical Research, Diakonhjemmet Hospital, Oslo, Norway
- 8 Centre for Psychiatry Research, Department of Clinical Neuroscience, Karolinska Institutet & Stockholm Health Care Services, Stockholm, Sweden
- 9 University of Melbourne Academic Unit for Psychiatry of Old Age, St George's Hospital, Kew, VIC, Australia
- 10 National Ageing Research Institute, Parkville, VIC, Australia
- 11 Department of Integrative Medical Biology (IMB), Umeå University, Umeå, Sweden
- 12 Umeå Center for Functional Brain Imaging, Umeå University, Umeå, Sweden
- 13 Mathematics & Statistics, Curtin University, Perth, WA, Australia
- 14 INSERM U1299, ENS Paris Saclay, Université Paris Saclay, Gif-sur-Yvette, France
- 15 EPS Barthelemy Durand, Etampes, France
- 16 School of Biomedical Sciences and Pharmacy, University of Newcastle, Callaghan, NSW, Australia
- 17 Precision Medicine Research Program, Hunter Medical Research Institute, Newcastle, NSW, Australia
- 18 The Cancer Epidemiology Unit, Nuffield Department of Population Health, University of Oxford, Oxford, UK
- 19 University Clinic for Radiology, University of Münster, Muenster, Germany
- 20 Vita-Salute San Raffaele University, Milan, Italy
- 21 Division of Neuroscience, Psychiatry and clinical psychobiology Unit, IRCCS San Raffaele Scientific Institute, Milan, Italy.
- 22 Department of Biological Psychology, Vrije Universiteit Amsterdam, Amsterdam, NH, Netherlands
- 23 Centre for Healthy Brain Ageing, School of Clinical Medicine, University of New South Wales, Sydney, NSW, Australia

- 24 Department of Psychiatry and Psychotherapy, Philipps-University Marburg, Marburg, Germany
- 25 Psychology and Center for Brain Science. Harvard University, Cambridge, MA, USA
- 26 Psychiatry, Massachusetts General Hospital, Boston, MA, USA
- 27 Precision Medicine Research Program, Hunter Medical Research Institute, New Lambton Heights, NSW, Australia
- 28 Tri-institutional Center for Translational Research in Neuroimaging and Data Science (TReNDS), Georgia State, Georgia Tech, Emory, Atlanta, GA 30303, USA
- 29 Institute of Neuroscience and Medicine (INM-1), Research Centre Jülich, Jülich, Germany
- 30 Institute for Anatomy I, Medical Faculty & University Hospital Düsseldorf, Heinrich Heine University Düsseldorf, Düsseldorf, Germany
- 31 University of Basel, Basel, Switzerland
- 32 University Hospital Basel, Basel, Switzerland
- 33 Department of Psychiatry, Trinity College Dublin, Dublin, Ireland
- 34 Hospital Universitario Virgen del Rocío/ IBIS/ CSIC, Sevilla, Spain
- 35 Centro de Investigación Biomedica en Red Salud Mental (CIBERSAM), Sevilla, Spain
- 36 Department of Psychiatry, University of Sevilla, Sevilla, Spain
- 37 Institute for Translational Psychiatry, University of Münster, Münster, Germany
- 38 Institute of Human Genetics, University of Bonn, School of Medicine & University Hospital Bonn, Bonn, Germany
- 39 School of Psychology and Counselling, Queensland University of Technology, Brisbane, QLD, Australia
- 40 Social Genetic and Developmental Psychiatry Centre, Institute of Psychiatry, Psychology & Neuroscience, King's College London, London, UK
- 41 Centre for Neuropsychiatric Genetics and Genomics, Cardiff University, Cardiff, UK
- 42 Cardiff University's Brain Research Imaging Centre, School of Psychology, Cardiff University, Cardiff, UK
- 43 School of Psychology & Center for Neuroimaging, Cognition and Genomics, University of Galway, Galway, Ireland
- 44 Translational Developmental Neuroscience Section, Division of Psychological and Social Medicine and Developmental Neurosciences, Faculty of Medicine, TU Dresden, Germany

- 45 Language and Genetics Department, Max Planck Institute for Psycholinguistics,  
Nijmegen, Netherlands
- 46 Department of Psychology, University of Oslo, Oslo, Norway
- 47 Department of Psychology, Oslo New University College, Oslo, Norway
- 48 Donders Institute for Brain, Cognition and Behaviour, Radboud University, Nijmegen,  
Netherlands
- 49 Université Paris-Saclay, Neurospin, CEA, Gif sur Yvette, France
- 50 Section of Brain Function Information, National Institute for Physiological Sciences,  
Okazaki, Japan
- 51 Psychiatric and Neurodevelopmental Genetics Unit, Center for Genomic Medicine,  
Massachusetts General Hospital, Boston, MA, USA
- 52 Department of Psychiatry, Massachusetts General Hospital, Harvard Medical School,  
Boston, MA, USA
- 53 Department of Psychiatry and Behavioral Sciences, Boston Children's Hospital,  
Boston, MA, USA
- 54 Department of Psychiatry, Harvard Medical School, Boston, MA, USA
- 55 Department of Psychiatry and Psychotherapy, University Medicine Greifswald,  
Greifswald, Germany
- 56 Discipline of Psychiatry and Mental Health, School of Clinical Medicine, University  
of New South Wales, Sydney, NSW, Australia
- 57 Neuroscience Research Australia, Sydney, NSW, Australia
- 58 Department of Psychiatry & Mental Health, Neuroscience Institute, University of  
Cape Town, Cape Town, South Africa
- 59 Department of Pathology of Mental Diseases, National Institute of Mental Health,  
National Center of Neurology and Psychiatry, Kodaira, Tokyo, Japan
- 60 Princess Máxima Center for Pediatric Oncology, Utrecht, Netherlands
- 61 School of Medicine and Public Health, University of Newcastle, Newcastle, NSW,  
Australia
- 62 PRC for Health Behaviour, University of Newcastle, Newcastle, NSW, Australia
- 63 Psychiatry, Rutgers University, New Brunswick, NJ, USA
- 64 Brain Health Institute, Rutgers University, Piscataway, NJ, USA
- 65 Department of Neuromedicine and Movement Science (INB), Faculty of Medicine and  
Health Sciences, NTNU, Trondheim, Norway
- 66 Department of Radiology and Nuclear Medicine, St. Olav's Hospital, Trondheim,

Norway

- 67 Department of Biomedicine, University of Bergen, Bergen, Norway
- 68 Division of Psychiatry, Haukeland University Hospital, Bergen, Norway
- 69 Sainte Justine Hospital Research Center, Montreal, QC, Canada
- 70 Department of Pediatrics, University of Montreal, QC, Canada
- 71 Core-Facility Brainimaging, Marburg, Germany
- 72 Department of Psychiatry, Marburg, Germany
- 73 Centre for Psychiatry Research, Department of Clinical Neuroscience, Karolinska  
Institutet & Stockholm Health Care Services, Stockholm Region, Stockholm, Sweden
- 74 Department of Genome Informatics, Graduate School of Medicine, Osaka University,  
Osaka, Japan
- 75 Department of Computational Biology and Medical Sciences, Graduate School of  
Frontier Science, The University of Tokyo, Chiba, Japan
- 76 Centre de recherche CHU Sainte-Justine and University of Montréal, Montréal, QC,  
Canada
- 77 NORMENT, Department of Clinical Science, University of Bergen, Bergen, Norway
- 78 Dr. Einar Martens Research Group for Biological Psychiatry, Center for Medical  
Genetics and Molecular Medicine, Haukeland University Hospital, Bergen, Norway
- 79 Department of Clinical and Experimental Epilepsy, Institute of Neurology, University  
College London, London, UK
- 80 Department of Neurology, McGovern Medical School, UTHealth Houston, Houston,  
US
- 81 Neuroscience and Mental Health Innovation Institute, Cardiff University, Cardiff, UK
- 82 School for Mental Health and Neuroscience, Department of Psychiatry and  
Neuropsychology, Faculty of Health, Medicine and Life Sciences, Maastricht  
University, Maastricht, Netherlands
- 83 Department of Computer Science, Georgia State University, Atlanta, GA, USA
- 84 Center for Translational Research in Neuroimaging and Data Science, Georgia State  
University, Atlanta, GA, USA
- 85 Department of Cognitive Science, University of California San Diego, La Jolla, CA,  
USA
- 86 Population Neuroscience and Genetics, University of California San Diego, La Jolla,  
CA, USA

- 87 School of Clinical Sciences, Queensland University of Technology, Brisbane, QLD, Australia
- 88 Institute for Molecular Bioscience, The University of Queensland, Brisbane, Australia
- 89 Psychiatric Genetics, QIMR Berghofer Medical Research Institute, Brisbane, QLD, Australia
- 90 University of Queensland, Brisbane, QLD, Australia
- 91 Queensland University of Technology, Brisbane, QLD, Australia
- 92 Imaging Genetics Center, Mark and Mary Stevens Institute for Neuroimaging and Informatics, Keck School of Medicine, University of Southern California, Marina del Rey, CA, USA.
- 93 Centre for Neuroimaging, Cognition and Genomics, School of Biological and Chemical Sciences, University of Galway, Galway, Ireland
- 94 Queensland Brain Institute, The University of Queensland, Brisbane, QLD, Australia
- 95 Queensland Centre for Mental Health Research, The University of Queensland, QLD, Australia
- 96 Department of Biomedicine, University of Basel, Basel, Switzerland
- 97 Departments of Radiation Sciences and Integrative Medical Biology, Umeå University, Umeå, Sweden
- 98 Division of Psychological Medicine and Clinical Neurosciences, Cardiff University, Cardiff, UK
- 99 Departments of Psychiatry and Neuroscience, Faculty of Medicine and Centre Hospitalier Universitaire Sainte-Justine, University of Montreal, Montreal, QC, Canada
- 100 Departments of Psychiatry and Psychology, University of Toronto, ONT, Canada
- 101 The Hospital for Sick Children, Toronto, ON, Canada
- 102 Department of Physiology, University of Toronto, Toronto, ON, Canada
- 103 Department of Psychiatry, Erasmus University Medical Center, Rotterdam, The Netherlands
- 104 Department of Geriatric Medicine, Oslo University Hospital, Oslo, Norway
- 105 School of Psychology, The University of New South Wales (UNSW), Sydney, NSW, Australia
- 106 Melbourne Neuropsychiatry Centre, Department of Psychiatry, The University of Melbourne, Carlton South, Victoria, Australia
- 107 Psychosis Studies, Institute of Psychiatry, Psychology and Neuroscience, King's



- College London, London, UK
- 108 Neuropsychiatric Institute, The Prince of Wales Hospital, Sydney, NSW, Australia
- 109 Department of Neurology and Clinical Neurophysiology, University Hospital of Trondheim, Trondheim, Norway
- 110 Hunter Medical Research Institute, Newcastle, NSW, Australia
- 111 School of Biomedical Sciences and Pharmacy, College of Medicine, Health and Wellbeing, University of Newcastle, Newcastle, NSW, Australia
- 112 Division of Molecular Medicine, NSW Health Pathology, Newcastle, NSW, Australia
- 113 Level 3 West, Hunter Medical Research Institute, Newcastle, NSW, Australia
- 114 Norwegian National Centre for Ageing and Health, Vestfold Hospital Trust, Tønsberg, Norway
- 115 Faculty of Medicine, University of Oslo, Oslo, Norway
- 116 Department of Human Genetics, Radboud University Medical Center, Nijmegen, Netherlands
- 117 Chalfont Centre for Epilepsy, Chalfont St Peter, UK
- 118 SAMRC Unit on Risk & Resilience in Mental Disorders, Dept of Psychiatry & Neuroscience Institute, University of Cape Town, Cape Town, South Africa
- 119 Department of Genetic Epidemiology in Psychiatry, Central Institute of Mental Health, Medical Faculty Mannheim, University of Heidelberg, Mannheim, Germany
- 120 School of Psychology and Counselling, Faculty of Health, Queensland University of Technology, Brisbane, Australia
- 121 Institute for Community Medicine, University Medicine Greifswald, Greifswald, Germany
- 122 German Centre for Cardiovascular Research (DZHK), Greifswald, Germany
- 123 Hunter Medical Research Institute, New Lambton Heights, NSW, Australia
- 124 Instituto de Física de Cantabria UC-CSIC, Santander, Spain
- 125 Department of Radiology, Marqués de Valdecilla University Hospital, Valdecilla Biomedical Research Institute IDIVAL, Santander, Spain
- 126 Department of Developmental Disability Neuropsychiatry, School of Clinical Medicine, University of New South Wales, Sydney, NSW, Australia
- 127 Centre for Healthy Brain Ageing, School of Clinical Medicine, University of New South Wales, Sydney, NSW, Australia
- 128 Western Centre for Health Research and Education, Sunshine Hospital, St Albans, Victoria, Australia

- 129 Institute of Psychological Medicine and Clinical Neurosciences, Cardiff, UK
- 130 Centre for Neuropsychiatric Genetics and Genomics, Cardiff, UK
- 131 Department of Child and Adolescent Psychiatry/Psychology - Erasmus Medical Centre - Sophie, Rotterdam, Netherlands
- 132 Department of Psychiatry - University Medical Centre Utrecht, Utrecht, Netherlands
- 133 Department of Psychiatry, University Hospital Maqués de Valdecilla - IDIVAL, Santander, Spain
- 134 Departamento de Medicina y Psiquiatría, Universidad de Cantabria, Santander, Spain
- 135 University Medicine Greifswald, Institute for Community Medicine, Greifswald, Germany
- 136 KG Jebsen Centre for Neurodevelopmental Disorders, University of Oslo, Oslo, Norway.
- 137 Semel Institute for Neuroscience and Human Behavior, Departments of Psychiatry and Biobehavioral Sciences and Psychology, University of California Los Angeles, Los Angeles, CA, USA.
- 138 Department of Research and Innovation, Division of Clinical Neuroscience, Oslo University Hospital and the University of Oslo, Norway.
- 139 Kristiania University College, Oslo, Norway
- 140 Institute for Translational Neuroscience, University of Münster, Münster, Germany

\*Correspondence:

Postal address: Department of Medical Genetics, Oslo University Hospital, Postbox 4956, Nydalen, 0424 Oslo, Norway

E-mail: [boenrune@gmail.com](mailto:boenrune@gmail.com)

Keywords: copy number variants, 1q21.1 distal, 15q11.2 BP1-BP2, intra-individual variability, magnetic resonance imaging, brain structure

### Abstract

**Background:** The 1q21.1 distal and 15q11.2 BP1-BP2 CNVs exhibit regional and global brain differences compared to non-carriers. However, interpreting regional differences is challenging if a global difference drives the regional brain differences. Intra-individual variability measures can be used to test for regional differences beyond global differences in brain structure.

**Methods:** Magnetic resonance imaging data were used to obtain regional brain values for 1q21.1 distal deletion (n=30) and duplication (n=27), and 15q11.2 BP1-BP2 deletion (n=170) and duplication (n=243) carriers and matched non-carriers (n=2,350). Regional intra-deviation (RID) scores i.e., the standardized difference between an individual's regional difference and global difference, were used to test for regional differences that diverge from the global difference.

**Results:** For the 1q21.1 distal deletion carriers, cortical surface area for regions in the medial visual cortex, posterior cingulate and temporal pole differed less, and regions in the prefrontal and superior temporal cortex differed more than the global difference in cortical surface area. For the 15q11.2 BP1-BP2 deletion carriers, cortical thickness in regions in the medial visual cortex, auditory cortex and temporal pole differed less, and the prefrontal and somatosensory cortex differed more than the global difference in cortical thickness.

**Conclusion:** We find evidence for regional effects beyond differences in global brain measures in 1q21.1 distal and 15q11.2 BP1-BP2 CNVs. The results provide new insight into brain profiling of the 1q21.1 distal and 15q11.2 BP1-BP2 CNVs, with the potential to increase our understanding of mechanisms involved in altered neurodevelopment.

### Introduction

Carriers of certain rare recurrent copy number variants (CNVs) - i.e., deletions or duplications of a segment of the genome - have a higher risk of developing psychiatric and neurodevelopmental disorders, including schizophrenia and autism spectrum disorder<sup>1-5</sup>. Several rare recurrent CNVs have moderate to large effects on structural brain measures derived from magnetic resonance imaging (MRI)<sup>6,7</sup>. The effects of CNVs on brain structure have been suggested to occur primarily during early neurodevelopment<sup>8</sup>, and some rare recurrent CNVs have been associated with altered cellular function, composition and size derived from cortical organoids that models fetal and early neurodevelopment<sup>9-12</sup>. The 1q21.1 distal and 15q11.2 BP1-BP2 deletions are two of the most common recurrent CNVs<sup>1,13,14</sup>. They yield a higher risk of psychiatric and neurodevelopmental disorders<sup>1-5</sup> and show moderate to large effects on brain structure<sup>15,16</sup>. Thus, studying 1q21.1 distal and 15q11.2 BP1-BP2 deletion carriers offer a promising genetics-first approach to study deviations in neurodevelopment and brain structure, which may underlie the increased risk of developing psychiatric and neurodevelopmental disorders<sup>5,8</sup>.

To date, the neuroimaging studies on CNVs have focused on conventional mean comparisons between carriers and non-carriers, which have been informative for brain profiling of CNV carriers. For instance, several CNVs have shown global effects on the brain, as demonstrated by group differences in mean cortical thickness, total cortical surface area and total subcortical volume, in addition to wide-spread regional differences<sup>6,7</sup>. However, brain profiling may be challenging if an overall global difference on the brain drives many of the regional mean differences or if regional differences are driven by distinct subgroups in each comparison, rendering inter-regional brain profiles difficult to interpret. To overcome this challenge, detecting brain regions that diverge from the global difference could benefit from intraindividual variability measures, in which regional values represent its position within an individualized brain profile. Identification of brain regions that diverge from the overall global difference of the CNV may provide valuable insights into the regional penetrance, brain organization and functional consequences in CNV carriers. Indeed, as has been demonstrated in other fields such as cognitive science and neuropsychology, e.g.<sup>17-22</sup>, novel scientific and clinical insights can be achieved by looking beyond mean group differences through investigating intraindividual variability.

Both 1q21.1 distal and 15q11.2 BP1-BP2 deletion carriers exhibit global differences in brain structure, with the former displaying a lower total cortical surface area<sup>15</sup> and the latter showing a higher mean cortical thickness and lower total cortical surface area<sup>16</sup>. Additionally, these deletions also exhibit regional differences across the cortex<sup>15,16</sup>. However, the regional differences vary across the brain as indicated by variation in effect sizes across brain regions. This could indicate that the carriers of the 1q21.1 distal and 15q11.2 BP1-BP2 deletion exhibit higher variability in brain structure, along with systematic inter-regional differences in brain structure as measured by MRI-derived features.

In both 1q21.1 distal and 15q11.2 BP1-BP2 CNV carriers, the largest regional differences are typically found in frontal regions, associated with higher-cognitive processing. In contrast, the posterior brain regions, associated with primary sensory processing, typically do not show significant differences<sup>15,16</sup>. Insight into variation in brain structure may be useful for understanding differences in brain function as cortical morphology overlaps with the functional hierarchical gradient of the brain<sup>23</sup>. This functional hierarchical gradient reflects a sensorimotor (i.e., involved in unimodal and functional specific processes) to association axis (i.e., involved in higher-order cognitive processes) in the human brain<sup>23–25</sup>, which has been supported by anatomical, functional, and evolutionary data<sup>24</sup>. Thus, a more fine-grained brain profile of the structural differences in 1q21.1 distal and 15q11.2 BP1-BP2 CNV carriers may aid our understanding of their phenotypic profile.

Brain structural differences in 1q21.1 distal and 15q11.2 BP1-BP2 CNV carriers indicate global mean differences (i.e., cortical thickness and cortical surface area), as well as regional group differences in primarily frontal brain regions. The regional group differences indicate that some brain regions are more affected than others. Here, we define more affected brain regions as regions that differ more than the global mean difference, and less affected brain regions as regions that differ less than the global mean difference. To measure this, we use an intraindividual variability measure to detect brain regions that diverge from the global difference, where the regional values represent its position within an individualized brain profile. We expected that anterior regions within the association cortices were more affected, whereas posterior regions within the primary sensorimotor cortices were less affected in carriers of the 1q21.1 distal and 15q11.2 BP1-BP2 CNVs.

## Methods and Materials

### Sample

Individuals carrying a 1q21.1 distal or 15q11.2 CNV and a matched non-carrier group were taken from the ENIGMA-CNV working group core dataset and the UK Biobank across 61 scanner sites. Each CNV carrier was matched with five non-carriers based on age, sex, scanner site and ICV using the MatchIt package in R<sup>26</sup>. This resulted in four subsets (sample characteristics are presented in tables 1 and 2, supplementary note 1).

**Table 1. Sample characteristics for 1q21.1 distal CNVs and non-carrier comparison groups**

	1q21.1 distal deletion	1q21.1 distal deletion comparison group	1q21.1 distal duplication	1q21.1 distal duplication comparison group
N	30	150	27	135
Mean Age in years	41.6	44.6	56.4	53.7
Min-Max Age range in years	7.7-68.7	9.2-76.2	18.7-73.1	9.5-77.2
Females (%)	14 (46.7%)	73 (48.7%)	15 (55.6%)	77 (57.0%)
Intracranial Volume, mm <sup>3</sup> *10 <sup>6</sup> (SD)	1.25 (.23)	1.26 (.25)	1.59 (.16)	1.56 (.30)

**Table 2. Sample characteristics for 15q11.2 BP1-BP2 CNVs and non-carrier comparison groups**

	15q11.2 BP1-BP2 deletion	15q11.2 BP1-BP2 deletion comparison group	15q11.2 BP1-BP2 duplication	15q11.2 BP1-BP2 duplication comparison group
N	170	850	243	1,215
Mean age in years	55.9	55.9	55.8	55.9
Min-max age range in years	7.1-77.7	6.8-90.0	7.83-88.5	3.75-89.8
Females (%)	90 (52.9%)	428 (50.4%)	127 (52.3%)	608 (50.0%)
Intracranial volume, mm <sup>3</sup> *10 <sup>6</sup> (SD)	1.48 (.20)	1.50 (.20)	1.46 (.19)	1.46 (.20)

**MRI-derived features, CNVs and quality control**

Neuroimaging data were obtained from the UK Biobank, as described elsewhere<sup>27</sup>, and from the ENIGMA-CNV core dataset. The ENIGMA-CNV neuroimaging measures were collected from several sites (see appendix 1 for details) and analyzed using the standardized ENIGMA protocol (<https://enigma.ini.usc.edu/protocols/imaging-protocols/>). Details of the quality control of the MR images are provided in supplementary note 2. Briefly, the MRI data from the ENIGMA-CNV working group underwent the ENIGMA cortical quality control procedures (<https://enigma.ini.usc.edu/protocols/imaging-protocols/>), where the 68 cortical and 14 subcortical regions were extracted using the Desikan-Killiany atlas. For the UK Biobank sample, we used the Euler number as a proxy for image quality<sup>28</sup> and removed all participants with Euler numbers below minus four standard deviations from downstream analyses (n =437). To account for site effects in the samples, we ran each of the four subsets through ComBat, an instrument for data harmonization<sup>29</sup>. CNV calling in ENIGMA-CNV was based on previous publications<sup>15,16</sup>. For the UK Biobank sample, we identified CNVs based on the returned dataset from Crawford et al.<sup>30</sup> All participants with a CNV as defined in previous publications<sup>15,16,30</sup> were removed from downstream analyses, except for the individuals flagged with the 1q21.1 distal or the 15q11.2 BP1-BP2 CNV.

### Derivation of dependent variables

We adjusted for the effect of age, age<sup>2</sup>, sex and ICV on every brain regional value using linear regression across the carriers and the non-carriers. The residualized brain regional values were used to calculate the mean and standard deviation for the non-carriers only. We estimated 1) Z-scores per region (similar calculations as in<sup>31</sup>) and created 2) global index and 3) intraindividual standard deviation (similar calculations as in<sup>21</sup>) as well as 4) regional intra-deviation (RID) score.

1. *Z-scores*. Specifically, Z-scores for CNV carriers and non-carriers were calculated based on the mean and standard deviation from the non-carriers as shown in Eq. (1):

$$Z_{if} = \frac{(X_{if} - M_{if})}{SD_{if}}$$

(1)

Where  $Z_{if}$  is the standardized value for brain region  $i$  in feature  $f$  (i.e., cortical thickness, surface area, or subcortical volume), and  $X_{if}$  is the regional value for brain region  $i$  for feature  $f$ ,  $M_{if}$  and  $SD_{if}$  represent the mean and standard deviation, respectively, for brain region  $i$  using feature  $f$  across the non-carriers. Thus, for every individual we obtained a vector of standardized Z-scores across 68 cortical regions for cortical thickness and cortical surface area, and 14 subcortical regions.

2. *Global index*: We created an individualized global index (GI) for cortical thickness, cortical surface area and subcortical volume, respectively, by calculating the mean Z-score across the cortical and subcortical regions as shown in Eq. (2)

$$GI_f = \frac{1}{n_f} \sum_{i=1}^{n_f} Z_{if}$$

(2)

where  $GI_f$  is the global index for feature  $f$ ,  $n$  is the total number of brain regions for feature  $f$ , and  $Z_{if}$  is the standardized value for the brain region  $i$  for feature  $f$  derived from Eq. (1).

3. *Intraindividual standard deviation*: Furthermore, we also calculated the intraindividual standard deviation (iSD) across the Z-scores for cortical thickness, cortical surface area, and subcortical volume to obtain measures of within-individual variability, as shown in Eq. (3):



$$iSD_f = \sqrt{\frac{\sum_{i=1}^{n_f} (Z_{if} - GI_f)^2}{n_f - 1}}$$

(3)

where the  $n_f$  is total number of brain regions for feature  $f$ ,  $Z_{if}$  is the standardized value for brain region  $i$  for feature  $f$ ,  $GI_f$  is the global index for feature  $f$  (i.e., mean Z-score across brain regions for an individual) as derived from Eq. (2). A low  $iSD$  indicates that an individual's Z-scores across brain regions are relatively consistent and do not vary much across brain regions, while a high  $iSD$  indicates that the Z-score across brain regions are relatively inconsistent, indexing a more variable brain.

4. *Regional intra-deviation score*: Finally, to identify regions that diverge more than expected from an individual's global index and intraindividual standard deviation, we created a regional intra-deviation (RID) score calculated using Eq. (4) for every brain region across feature  $f$ :

$$RID_f = \frac{(Z_{if} - GI_f)}{iSD_f}$$

(4)

where the  $Z_{if}$  is the standardized value for brain region  $i$  for feature  $f$ , and  $GI_f$  is the global index for feature  $f$  as shown in Eq. (2.). The  $iSD_f$  reflects the standard deviation for the Z-score across brain regions in feature  $f$  as formulated in Eq. (3). Here, we define regions that are less affected as those that do not follow the global tendency in the data, whereas the regions that exceed the global tendency of the data are considered to be more affected. To establish brain-cognition relationships between the brain measures and cognition, we tested for associations between RID and Z-scores and cognitive ability (supplementary note 3, Figure S1, Table S1).

### Statistical analyses

All statistical analyses were conducted in R studio v4.0.0 and brain visualizations were created using the ENIGMA toolbox<sup>32</sup>. For the per-CNV analyses, we tested for group differences by including carrier status (i.e., either carrier or non-carrier) in a linear regression

model. The deletion and duplication carriers were tested separately with their corresponding matched non-carrier group used as the reference. The estimated standardized beta values were extracted from the models and are presented in the results as a measure of effect size. The p-values underwent a False Discovery Rate (FDR)<sup>33</sup> adjustment to account for multiple comparisons for each of the four CNV groups. Corrected p-values below .05 were considered statistically significant. Three main analyses were performed: First, in line with the conventional mass-univariate analysis approach, we performed group comparisons on the Z-scores across all the ROIs for cortical thickness, cortical surface area and subcortical volume (FDR corrected for 150 comparisons). Second, we compared the global index, and intraindividual standard deviation and mean corrected intraindividual standard deviation values between carriers and non-carriers (FDR corrected for 12 comparisons). The mean corrected intraindividual standard deviation represents the intraindividual standard deviation after regressing out the global index, as the mean values tend to be correlated with the standard deviation. Third, for the RID scores, group comparisons were computed between carriers and non-carriers for all ROIs for cortical thickness, cortical surface area, and subcortical volume (FDR corrected for 150 comparisons). Due to missing values in some brain regions, the analyses were restricted to individuals with complete observations for the feature that was analyzed (i.e., cortical thickness, cortical surface area, and subcortical volume). Sensitivity analyses were conducted for the significant RID score differences by adjusting for affection status (i.e., known psychiatric or neurological diagnoses). In addition, we examined the interaction term between carrier status and affection status and between carrier status and cognitive ability. Finally, we compared the brain profile of significant differences in RID scores to the significant differences in Z-scores adjusted for the global index.

## Results

### Global measures

The group differences in the global index and the intraindividual standard deviation measures are presented in Table 3 with reference values for the non-carrier groups in Table S2. The 1q21.1 distal deletion carriers had a lower global index for surface area, whereas the 15q11.2 BP1-BP2 deletion carriers had a lower global index for surface area and a higher global index for cortical thickness. In addition, the 15q11.2 BP1-BP2 duplication carriers had a lower global index for cortical thickness. Furthermore, there was a higher intraindividual standard deviation for cortical surface for both the 1q21.1 distal duplication carriers (both for the mean corrected and uncorrected measure) and the 15q11.2 BP1-BP2 deletion carriers (only for the mean corrected measure), as well as a higher intraindividual standard deviation for cortical thickness in the 15q11.2 BP1-BP2 deletion carriers (both for the mean corrected and uncorrected measure). With one exception, correlations between the intraindividual standard deviation measures across CNV groups did not show any significant differences (supplementary note 4, Figure S2).

**Table 3. Group differences in global index and intraindividual standard deviation.**

	1q21.1 distal deletion	1q21.1 distal duplication	15q11.2 BP1-BP2 deletion	15q11.2 BP1-BP2 duplication
<b>Global index</b>				
Cortical Surface Area	-1.29 (.18) <sup>d</sup>	.40 (.22)	-.22 (.09) <sup>b</sup>	-.09 (.07)
Cortical Thickness	.39 (.21)	-.04 (.22)	.35 (.09) <sup>d</sup>	-.24 (.07) <sup>b</sup>
Subcortical volume	-.15 (.20)	-.48 (.22) <sup>a</sup>	-.17 (.09) <sup>a</sup>	.02 (.07)
<b>Intraindividual standard deviation (mean uncorrected)</b>				
Cortical Surface Area	-.20 (.21)	.73 (.22) <sup>c</sup>	.15 (.09)	-.02 (.07)
Cortical Thickness	.37 (.21)	.44 (.22) <sup>a</sup>	.20 (.09) <sup>b</sup>	.00 (.07)
Subcortical volume	-.08 (.20)	.22 (.22)	.04 (.09)	.02 (.07)
<b>Intraindividual standard deviation (mean corrected)</b>				
Cortical Surface Area	.24 (.21)	.62 (.22) <sup>b</sup>	.23 (.09) <sup>b</sup>	.06 (.07)
Cortical Thickness	.37 (.21)	.46 (.22) <sup>a</sup>	.19 (.08) <sup>b</sup>	.00 (.07)
Subcortical volume	-.06 (.20)	.30 (.22)	.08 (.09)	.02 (.07)

*Notes.* The values represent the standardized beta coefficient between carriers and non-carriers, with non-carriers as the reference. Standard error is presented in parenthesis.

<sup>a</sup>  $P < .05$ , <sup>b</sup>  $P_{FDR} < .05$ , <sup>c</sup>  $P_{FDR} < .01$ , <sup>d</sup>  $P_{FDR} < .001$ .

### 1q21.1 distal copy number variant

*The 1q21.1. distal deletion* carriers showed widespread lower cortical surface area with significant differences in 63 ROIs using Z-scores (Figure 1a-b, top; Table S3), and exhibited a higher RID score for cortical surface area in regions within the occipital, superior parietal, temporal pole and posterior cingulate cortex, as well as lower RID scores in regions within the superior temporal and frontal regions (Figure 1a-c, bottom, Table S4). Further, 1q21.1. distal deletion carriers showed higher cortical thickness compared to non-carriers in 19 ROIs using Z-scores (Figure 2a-b, top, Table S3), in addition to lower RID scores for regions within the occipital lobe and paracentral lobule and higher RID scores for regions within the superior temporal and inferior frontal cortex (Figure 2a-c, bottom, Table S4). The 1q21.1 distal deletion carriers also exhibited lower subcortical volume in left thalamus and right nucleus accumbens (Table S3), and lower RID score for the left thalamus (Table S4). All the significant RID score differences survived adjustment for affection status. The interaction term between carrier status and affection status was not associated with the significant RID

scores (supplementary note 5, Table S5). A subset of the significant RID scores were implicated in the brain-cognition RID map (Figure S1). However, we did not observe any significant interactions between carrier status and cognitive ability on any of the significant RID scores (supplementary note 6, Table S6). The results yielded more significant group differences in RID scores (i.e., 24) compared to Z-scores adjusted for the global index between 15q11.2 BP1-BP2 deletion carriers and non-carriers (i.e., 13, supplementary note 7, Figure S3, Table S7). *The 1q21.1 distal duplication* carriers showed higher cortical surface area in the right pars opercularis and right superior frontal gyrus, and lower volume in the right and left hippocampus compared to non-carriers (Table S8). Using RID scores, no significant differences in the ROIs were found (Table S9).

[INSERT FIGURE 1 HERE]

[INSERT FIGURE 2 HERE]

### **15q11.2 BP1-BP2 copy number variant**

*The 15q11.2 BP1-BP2 deletion* carriers showed lower cortical surface area in 10 ROIs using Z-scores (Figure 3a-b, top, Table S10), and higher RID scores for the left frontal pole and right pars opercularis surface area, but lower RID scores for the left and right pars orbitalis surface area compared to non-carriers (Figure 3a-c, bottom, Table S11). For cortical thickness, the 15q11.2 BP1-BP2 deletion carriers showed higher cortical thickness in 30 regions using Z-scores (Figure 4a-b, top, Table S10). The RID scores for cortical thickness were lower in regions within occipital and temporal regions, and higher in motor and frontal regions compared to non-carriers (Figure 4a-c, bottom, Table S11). The 15q11.2 BP1-BP2 deletion carriers also showed lower Z-scores for left caudate, right pallidum and right nucleus accumbens (Table S10). All significant RID scores remained significant after adjustment for affection status. No significant interactions between carrier status and affection status (Table S12, supplementary note 5) nor between carrier status and cognitive ability for the 15q11.2 BP1-BP2 deletion carriers were observed (Table S13, supplementary note 6). The results yielded more significant group differences in RID scores (i.e., 14) compared to Z-scores adjusted for global index (i.e., 12) between 15q11.2 BP1-BP2 deletion carriers and non-carriers (supplementary note 7, Figure S4, Table S14). *The 15q11.2 BP1-BP2 duplication* carriers showed lower cortical thickness in 11 ROIs and higher right superior frontal cortical

surface area using Z-scores (Table S15) but showed no significant differences in the ROIs using RID-scores (Table S16).

[INSERT FIGURE 3 HERE]

[INSERT FIGURE 4 HERE]

### Discussion

The current study is the first to identify intraindividual variability differences in brain structure in CNV carriers. Using the intraindividual standard deviation measure, we observed higher variability in the regional effects for cortical surface area in both 1q21.1 distal duplication and 15q11.2 BP1-BP2 deletion carriers, and higher variability in the regional effects for cortical thickness for the 15q11.2 BP1-BP2 deletion carriers, compared to non-carriers. Using RID scores, we find that a subset of brain regions diverged significantly from non-carriers for both the 1q21.1 distal and 15q11.2 BP1-BP2 deletion carriers. We also find a higher number of significant regional differences using RID scores compared to the conventional global covariation approach. The current results hold promise for identifying specific CNV-associated brain profiles by targeting regional differences using an individualized approach, which are overlooked in studies applying conventional brain MRI measures.

In line with previous results<sup>15</sup>, the 1q21.1 distal deletion carriers showed lower global cortical surface area compared to non-carriers. The observed differences in Z-scores indicate widespread lower cortical surface area, whereas the RID scores indicate that the cortical surface area in posterior and primary sensory regions (i.e., lingual, pericalcarine, superior parietal, isthmus of the cingulate gyrus) are less affected and frontal and association cortices (i.e., caudal middle frontal, lateral orbitofrontal, rostral middle frontal, superior frontal cortex) are more affected. Thus, the observed regional Z-score group differences along lateral and medial parietal to lateral inferior temporal and motor cortex appear to be largely reflective of the global effect. A subset of the significant RID scores (i.e., the superior temporal gyri and left supramarginal gyrus cortical thickness and left lateral orbitofrontal and left lateral superior temporal gyrus cortical surface area) was associated with cognitive ability in non-carriers. However, the effect sizes are low, and the current sample size of CNV carriers is too small to reliably detect such brain-cognition associations.

The 15q11.2 BP1-BP2 deletion showed a higher global cortical thickness compared to non-carriers, primarily concentrated in the frontal cortex, recapitulating previously reported group differences in cortical thickness<sup>16</sup>. We complement these findings by showing group differences in RID scores, which indicates that the cortical thickness in sensory cortices (i.e., cuneus and pericalcarine area) are less affected, and the association cortices (i.e., rostral middle frontal and superior frontal cortex) are more affected by the deletion. The association cortices that show cortical thickness differences using RID scores are regions that underlies complex cognitive functions<sup>23–25</sup>, and may subserve the lower cognitive performance in 15q11.2 BP1-BP2 deletion carriers compared to controls<sup>14,34</sup>.

Notably, some findings deviate from the interpretation of a less affected sensorimotor cortex and a more affected association cortex. Both the 1q21.1 distal and 15q11.2 BP1-BP2 deletion carriers show evidence for a relatively less affected cortical surface area and cortical thickness, respectively, in the left temporal pole. We also find that the cortical thickness of the postcentral gyri, a primary somatosensory region, is more affected in the 15q11.2 BP1-BP2 deletion carriers. To speculate, this may be associated with the motor delay observed in clinically affected 15q11.2 BP1-BP2 deletion carriers<sup>35</sup>. For cortical surface area in the 15q11.2 BP1-BP2 deletion carriers, we find inconsistent effects for frontal regions: although we observe a relatively more different bilateral pars orbitalis, we also find evidence for a less different left frontal pole and right pars opercularis. Furthermore, we did not find significant differences in RID scores in the 15q11.2 BP1-BP2 duplication carriers, nor in the 1q21.1 distal duplication carriers. The results complement previous findings of lower effect sizes in brain measures for duplication versus deletion carriers<sup>6,7</sup>, and thus may support that deletion carriers distort the anatomical relationships in the brain more than duplication carriers.

Global and frontal regional group differences in cortical thickness are prominent brain features of several neurodevelopmental disorders, including autism spectrum disorder<sup>36</sup> and schizophrenia<sup>37</sup>. Thus, group differences in brain structure may be confounded by individuals with neurodevelopmental or psychiatric disorders. Here, all the significant RID score differences in 1q21.1 distal and 15q11.2 BP1-BP2 deletions survived adjustment for affection status, and there were no interaction effects between carrier status and affection status on the significant RID scores.

The current results implicate novel mechanisms in neurodevelopment. Compelling candidates for the changes in the 1q21.1 distal CNV are the human specific *NOTCH2NL* genes, which have been linked to the evolutionary expansion of the human neocortex<sup>38,39</sup>. NOTCH signaling is important for outer radial glia cell self-renewal, which are thought to contribute to cortical expansion<sup>40</sup>. Deletion of the *NOTCH2NL* genes in human cortical organoids yields smaller organoids compared to controls<sup>38</sup> and *NOTCH2NL* increases the number of cycling basal progenitors in the mouse embryonic neocortex<sup>41</sup>. Thus, *NOTCH2NL* could yield a potential mechanistic link between the assumed lower gene expression levels in 1q21.1 distal deletion carriers and the lower cortical surface area, possibly important for the expansion of frontal regions.

Among the four genes in the 15q11.2 BP1-BP2 loci<sup>42</sup>, *CYFIP1* has gained considerable interest due to its association to schizophrenia<sup>43,44</sup> and autism<sup>45-47</sup>. *CYFIP1* exhibits high expression levels in the developing mouse brain<sup>47</sup>. *CYFIP1* has also been linked to variation in cortical surface area<sup>48</sup>, as well as various cellular phenotypes, including myelination<sup>49</sup>, neurite length and branch number, cell size<sup>50</sup>, dendritic spine formation<sup>51</sup> and regulation of radial glia cells<sup>52</sup>. Notably, *CYFIP1* haploinsufficiency lower myelination thickness in rats<sup>49</sup>. Cortical thickness, as estimated with MRI, has been suggested to be influenced by myelination<sup>53</sup>. Thus, the higher cortical thickness observed in 15q11.2 BP1-BP2 deletion carriers may be due to altered myelination in the brain, possibly with somatosensory cortex being particularly sensitive to these alterations. *CYFIP1* deficiency has also been associated with functional connectivity deficits in motor cortices, as well as aberrant motor coordination in mice<sup>54</sup>. Finally, it should be noted that the 1q21.1 distal and the 15q11.2 BP1-BP2 loci span several genes, and genes within CNVs are likely to be involved in multifaceted genetic interactions<sup>55</sup>. More research is needed to identify the causative biological mechanisms of the brain structural phenotypes.

This study has strengths and limitations. We use an intraindividual variability approach to examine brain metrics that are related to an individual's own inter-regional brain profile. By examining metrics that consider the variation within individuals, it is possible to map the heterogeneity and deviations in CNV carriers compared to non-carriers. However, variability measures should be interpreted with caution, as some effects on the brain may be so extreme that further deviations are unlikely to be observed. That is, CNVs may yield large effects on brain structure, but only to a certain extent due to biological constraints. Thus, we urge



caution when interpreting intraindividual standard deviation in brain measures as ceiling and floor effects may bias the variability metrics. Still, we identify structures that are significantly less different or more different relative to the mean difference, indicating sufficient variability in the individualized brain metrics. About 1/2 (1q21.1 distal) and 2/3 (15q11.2 BP1-BP2) of the carriers are derived from the UK Biobank, which has a healthy volunteer bias<sup>56</sup>, possibly yielding underestimations of brain structural differences. However, this is somewhat counter-balanced by the ENIGMA-CNV dataset that is likely to increase the heterogeneity in the study sample (although some datasets are likely to have similar bias towards healthy individuals as the UK Biobank). Indeed, the variability observed in brain structure within individuals underscores the heterogeneity between and within individuals in the sample. Future studies with larger sample sizes are needed to examine the phenotypic heterogeneity observed in CNV carriers.

The results of the current study aid our understanding of 1q21.1 distal and 15q11.2 BP1-BP2 CNV brain profiles by identifying regional differences using intraindividual variability metrics, which has the potential to give better insight into the neuronal mechanisms in neurodevelopment and risk for psychiatric diseases. We find evidence for regional differences beyond the global differences in brain structure, where the spatial effects partly support the hypothesis of less affected sensorimotor cortex and more affected association cortex in both the 1q21.1 distal and 15q11.2 BP1-BP2 deletion carriers.

### Acknowledgments

**1000BRAINS:** The 1000BRAINS-Study was funded by the Institute of Neuroscience and Medicine, Research Centre Jülich, Germany. We thank the Heinz Nixdorf Foundation (Germany) for the generous support of the Heinz Nixdorf Study. We also thank the scientists and the study staff of the Heinz Nixdorf Recall Study and 1000BRAINS. Furthermore, this project has received funding from the European Union's Horizon 2020 Research and Innovation Programme under Grant Agreement No. 945539 (HBP SGA3; SC). This research was additionally supported by the Joint Lab “Supercomputing and Modeling for the Human Brain”. We gratefully acknowledge the computing time granted through JARA-HPC on the supercomputer JURECA at Forschungszentrum Jülich.

**TOP:** Centre of Excellence: RCN #23273. RCN #. 226971.

**ENIGMA-CNV working group:** IES is supported by the Research Council of Norway (#223273), South-Eastern Norway Regional Health Authority (#2020060), European Union's Horizon2020 Research and Innovation Programme (CoMorMent project; Grant #847776) and Kristian Gerhard Jebsen Stiftelsen (SKGJ-MED-021). RB is supported by South-Eastern Norway Regional Health Authority (#2020060). CEB is supported by NIMH U01MH119736, R21MH116473 and R01MH085953.

This work was performed on Services for sensitive data (TSD), University of Oslo, Norway, with resources provided by UNINETT Sigma2 - the National Infrastructure for High Performance Computing and Data Storage in Norway.

**ASRB:** the Australian Schizophrenia Research Bank (ASRB) was supported by the Australian National Health and Medical Research Council (NHMRC; Enabling Grant, ID 386500), the Pratt Foundation, Ramsay Health Care, the Viertel Charitable Foundation and the Schizophrenia Research Institute. Chief Investigators for ASRB were V. Carr., U. Schall, R. Scott, A. Jablensky, B. Mowry, P. Michie, S. Catts, F. Henskens, C. Pantelis. C.Pantelis was supported by an Australian National Health and Medical Research Council L3 Investigator Grant (Grant No. 1196508) and NHMRC Program grant (ID Number APP1150083).

**ECHO-DEFINE:** The Cardiff ECHO study acknowledges funding from the Wellcome Trust (Institutional Strategic Support Fund (ISSF)) to Marianne B.M van den Bree and Clinical Research Training Fellowship to Joanne L. Doherty (102003/Z/13/Z)), the Waterloo Foundation (WF 918- 1234 to Marianne B.M van den Bree), the Baily Thomas Charitable Fund (2315/1 to Marianne B.M van den Bree), National Institute of Mental Health (NIMH 5U01MH101724 and NIMH U01MH119738 to Marianne B.M van den Bree), the IMAGINE-ID and IMAGINE-2 studies (funded by Medical Research Council (MRC; MR/N022572/1 and MR/T033045/1 to Marianne B.M van den Bree) and a Medical Research Council (MRC) Centre Grant to Michael J. Owen (MR/P005748/1). The DEFINE study was supported by a Wellcome Trust Strategic Award (100202/Z/12/Z) to Michael J. Owen.

**FOR2107 Marburg and Münster:** This work is part of the German multicenter consortium "Neurobiology of Affective Disorders. A translational perspective on brain structure and

function“, funded by the German Research Foundation (Deutsche Forschungsgemeinschaft DFG; Forschungsgruppe/Research Unit FOR2107). Principal investigators (PIs) with respective areas of responsibility in the FOR2107 consortium are: Work Package WP1, FOR2107/MACS cohort and brainimaging: Tilo Kircher (speaker FOR2107; DFG grant numbers KI588/14-1, KI588/14-2, KI588/20-1, KI588/22-1), Udo Dannlowski (co-speaker FOR2107; DA 1151/5-1, DA 1151/5-2, DA1151/6-1), Axel Krug (KR 3822/5-1, KR 3822/7-2), Igor Nenadić (NE2254/1-2, NE2254/3-1, NE2254/4-1), Carsten Konrad (KO 4291/3-1). WP5, genetics: Marcella Rietschel (RI 908/11-1, RI 908/11-2), Markus M. Nöthen (NO 246/10-1, NO 246/10-2), Stephanie Witt (WI 3439/3-1, WI 3439/3-2). WP6, multi-method data analytics: Andreas Jansen (JA 1890/7-1, JA 1890/7-2), Tim Hahn (HA 7070/2-2). We are deeply indebted to all study participants and staff. A list of acknowledgments can be found at: [www.for2107.de/acknowledgements](http://www.for2107.de/acknowledgements).

**UCLA-Utrecht:** This study was supported by NIMH grant number: R01 MH090553 (to RAO). The NIMH had no further role in study design, in the collection, analysis and interpretation of the data, in the writing of the report, and in the decision to submit the paper for publication.

**QTIM:** The QTIM study was supported by grants from the US National Institute of Child Health and Human Development (R01 HD050735) and the Australian National Health and Medical Research Council (NHMRC) (486682, 1009064). Genotyping was supported by NHMRC (389875).

**BETULA:** Supported by a Scholar grant from Knut and Alice Wallenberg’s (KAW) foundation to Lars Nyberg. Freesurfer calculations were enabled by resources provided by the Swedish National Infrastructure for Computing (SNIC) at HPC2N, Umeå.

**SHIP:** SHIP is part of the Community Medicine Research net of the University of Greifswald, Germany, which is funded by the Federal Ministry of Education and Research (grants no. 01ZZ9603, 01ZZ0103, and 01ZZ0403), the Ministry of Cultural Affairs and the Social Ministry of the Federal State of Mecklenburg-West Pomerania. Genome-wide data in SHIP have been supported by the Federal Ministry of Education and Research (grant no. 03ZIK012) and a joint grant from Siemens Healthcare, Erlangen, Germany and the Federal State of Mecklenburg- West Pomerania. MRI scans in SHIP and SHIP-TREND have been

supported by a joint grant from Siemens Healthcare, Erlangen, Germany and the Federal State of Mecklenburg-West Pomerania.

**PAFIP:** This work was supported by the Instituto de Salud Carlos III ( 00/3095, 01/3129, PI020499, PI14/00639, PI17/01056 and PI14/00918), SENY Fundació Research Grant CI2005 0308007 and Fundación Marqués de Valdecilla . Instituto de investigación sanitaria Valdecilla (A/02/07, NCT0235832 and NCT02534363).

**OSAKA:** This research was supported by AMED (grant number JP21wm0425012 and JP18dm0307002) and JSPS KAKENHI (grant number JP20H03611). This work was partially supported by JSPS KAKENHI (Grant Number JP22H04926 and 20K15778) and by grants from the Japan Agency for Medical Research and Development (AMED) (JP22wm0425012, JP22wm0525019, and JP22dk0207060). Some computations were performed at the Research Center for Computational Science, Okazaki, Japan (Project: NIPS, 18-IMS-C162, 19-IMS-C181, 20-IMS-C162, 21-IMS-C179, 22-IMS-C195).

**IMAGEN:** received support from the European Union-funded FP6 Integrated Project IMAGEN (Reinforcement-related behavior in normal brain function and psychopathology) (LSHM-CT- 2007-037286), the Horizon 2020 funded ERC Advanced Grant ‘STRATIFY’ (Brain network based stratification of reinforcement-related disorders) (695313), the Medical Research Foundation and Medical Research Council (grants MR/R00465X/1 and MRF-058-0004-RG-DESRI: ‘Neurobiological underpinning of eating disorders: integrative biopsychosocial longitudinal analyses in adolescents’; MR/S020306/1 and MRF-058-0009-RG-DESR-C0759: ‘Establishing causal relationships between biopsychosocial predictors and correlates of eating disorders and their mediation by neural pathways’), the National Institutes of Health (NIH) funded Consortium grant U54 EB020403, supported by a cross-NIH alliance that funds Big Data to Knowledge Centres of Excellence, and 1R56AG058854-01, the National Institute for Health Research (NIHR) Biomedical Research Centre (BRC) at South London and Maudsley NHS Foundation Trust (SLaM) and King’s College London (KCL), ERANID (Understanding the Interplay between Cultural, Biological and Subjective Factors in Drug Use Pathways) (PR-ST-0416-10004), BRIDGET (JPND: BRain Imaging, cognition Dementia and next generation GENomics) (MR/N027558/1), Human Brain Project (HBP SGA 2, 785907), the FP7 project MATRICS (603016), the Medical Research Council Grant ‘c-VEDA’ (Consortium on Vulnerability to Externalizing Disorders and Addictions) (MR/N000390/1), the Bundesministerium für Bildung und Forschung (BMBF grants

01GS08152; 01EV0711; Forschungsnetz AERIAL 01EE1406A, 01EE1406B), the Deutsche Forschungsgemeinschaft (DFG grants SM 80/7-2, SFB 940/2, NE 1383/14-1), the ANR (ANR-12-SAMA-0004, AAPG2019 – GeBra), the Eranet Neuron (AF12-NEUR0008-01 – WM2NA; and ANR-18-NEUR00002-01 – ADORe), the Fondation de France (00081242), the Fondation pour la Recherche Médicale (DPA20140629802), the Mission Interministérielle de Lutte-contre-les-Drogues-et-les-Conduites-Addictives (MILDECA), the Assistance-Publique-Hôpitaux-de-Paris and INSERM (interface grant), Paris Sud University IDEX 2012, the Fondation de l’Avenir (grant AP-RM-17-013 ), the Fédération pour la Recherche sur le Cerveau. Further support was provided by grants from: ANR (project AF12-NEUR0008-01 - WM2NA, and ANR-12-SAMA-0004), the Fondation de France, the Fondation pour la Recherche Médicale, the Mission Interministérielle de Lutte-contre-les-Drogues-et-les-Conduites-Addictives (MILDECA), the Assistance-Publique-Hôpitaux-de-Paris and INSERM (interface grant), Paris Sud University IDEX 2012; ANR (project AF12-NEUR0008-01 - WM2NA, ANR-12-SAMA-0004), the Eranet Neuron (ANR-18-NEUR00002-01), the Fondation de France (00081242), the Fondation pour la Recherche Médicale (DPA20140629802), the Mission Interministérielle de Lutte-contre-les-Drogues-et-les-Conduites-Addictives (MILDECA), the Assistance-Publique-Hôpitaux-de-Paris and INSERM (interface grant), Paris Sud University IDEX 2012, the fondation de l’Avenir (grant AP-RM-17-013).

**MCIC:** The MCIC study was supported by the National Institutes of Health (NIH/NCRR P41RR14075 and R01EB005846 (to Vince D. Calhoun)), the Department of Energy (DE-FG02-99ER62764), the Mind Research Network, the Morphometry BIRN (1U24, RR021382A), the Function BIRN (U24RR021992-01, NIH.NCRR MO1 RR025758-01, NIMH 1RC1MH089257 to Vince D. Calhoun), the Deutsche Forschungsgemeinschaft (research fellowship to Stefan Ehrlich), and a NARSAD Young Investigator Award (to Stefan Ehrlich).

**NTR:** The NTR cohort was supported by the Netherlands Organization for Scientific Research (NWO) and The Netherlands Organisation for Health Research and Development (ZonMW) grants 904-61-090, 985-10-002, 912-10-020, 904-61-193, 480-04-004,463-06-001, 451-04-034, 400-05-717, Addiction-31160008, 016-115-035, 481-08-011, 056-32-010, Middelgroot-911-09-032, OCW\_NWO Gravity programme—024.001.003, NWO-Groot 480-15-001/674, Center for Medical Systems Biology (CSMB, NWO Genomics),

NBIC/BioAssist/RK(2008.024), Biobanking and Biomolecular Resources Research Infrastructure (BBMRI-NL, 184.021.007 and 184.033.111); Spinozapremie (NWO-56-464-14192), KNAW Academy Professor Award (PAH/6635) and University Research Fellow grant (URF) to Dorret I. Boomsma; Amsterdam Public Health research institute (former EMGO+), Neuroscience Amsterdam research institute (former NCA); the European Science Foundation (ESF, EU/QLRT-2001-01254), the European Community's Seventh Framework Programme (FP7- HEALTH-F4-2007-2013, grant 01413: ENGAGE and grant 602768: ACTION); the European Research Council (ERC Starting 284167, ERC Consolidator 771057, ERC Advanced 230374), Rutgers University Cell and DNA Repository (NIMH U24 MH068457-06), the National Institutes of Health (NIH, R01D0042157-01A1, R01MH58799-03, MH081802, DA018673, R01 DK092127-04, Grand Opportunity grants 1RC2 MH089951 and 1RC2 MH089995); the Avera Institute for Human Genetics, Sioux Falls, South Dakota (USA). Part of the genotyping and analyses were funded by the Genetic Association Information Network (GAIN) of the Foundation for the National Institutes of Health. Computing was supported by NWO through grant 2018/EW/00408559, BiG Grid, the Dutch e-Science Grid and SURFSARA.

**OATS:** The OATS cohort has been funded by a National Health & Medical Research Council (NHMRC) and an Australian Research Council (ARC) Strategic Award Grant of the Ageing Well, Ageing Productively Program (ID No. 401162); NHMRC Project (seed) Grants (IDs 1024224, 1025243); NHMRC Project Grants (1045325, 1085606); and NHMRC Program Grants (568969, 1093083). OATS was facilitated through access to Twins Research Australia, a national resource supported by a Centre of Research Excellence Grant (1079102) from the National Health and Medical Research Council.

**PING:** The PING Project was supported by the National Institute on Drug Abuse and the Eunice Kennedy Shriver National Institute of Child Health and Human Development with the following awards: RC2DA029475 and R01 HD061414.

**EPIGEN-UK (Sisodiya):** The work was partly undertaken at UCLH/UCL, which received a proportion of funding from the UK Department of Health's NIHR Biomedical Research Centres funding scheme. We are grateful to the Wolfson Trust and the Epilepsy Society for supporting the Epilepsy Society MRI scanner.

**Milan-OSR:** The Milan-OSR cohort was supported by the European Union H2020 EU.3.1.1 grant 754740 MOODSTRATIFICATION, the Italian Ministry of Health, grant RF-2018-12367249 and the Italian Ministry of University and Scientific Research, grant A\_201779W93T.

**Dublin:** The Dublin cohort was supported by grants to GD from the European Research Council (ERC-2015-STG-677467) and Science Foundation Ireland (SFI-16/ERCS/3787)

**Brain Imaging Genetics (BIG):** This work makes use of the BIG database, first established in Nijmegen, The Netherlands, in 2007. This resource is now part of Cognomics ([www.cognomics.nl](http://www.cognomics.nl)), a joint initiative by researchers from the Donders Centre for Cognitive Neuroimaging, the Human Genetics and Cognitive Neuroscience departments of the Radboud University Medical Centre, and the Max Planck Institute for Psycholinguistics in Nijmegen. The Cognomics Initiative has received support from the participating departments and centres and from external grants, that is, the Biobanking and Biomolecular Resources Research Infrastructure (Netherlands) (BBMRI-NL), the Hersenstichting Nederland and the Netherlands Organization for Scientific Research (NWO). The research leading to these results also receives funding from the NWO Gravitation Grant 024.001.006 ‘Language in Interaction’, the European Community’s Seventh Framework Programme (FP7/2007-2013) under grant agreement nos. 602450 (IMAGEMEND), 278948 (TACTICS) and 602805 (Aggressotype), as well as from the European Community’s Horizon 2020 programme under grant agreement no. 643051 (MiND) and from ERC-2010-AdG 268800-NEUROSCHEMA. In addition, the work was supported by a grant for the ENIGMA Consortium (grant number U54 EB020403) from the BD2K Initiative of a cross-NIH partnership.

### Disclosures

Dr. Andreassen has received speakers honorarium from Lundbeck, Janssen and Sunovion, and is a consultant to coretechs.ai. Dr. Reis Marques reports personal fees from Pfizer, Lundbeck, Astellas, Janssen and Angelini outside the submitted work. He is an employee and shareholder of Pasithea Therapeutics. Dr. Ching has received partial research support from Biogen, Inc. (Boston, USA) for work unrelated to the topic of this manuscript (PI Paul Thompson). Dr. Thompson has received partial research support from Biogen, Inc. (Boston, USA) for work unrelated to the topic of this manuscript. Dr. van den Bree reports grants from Takeda Pharmaceuticals, outside the submitted work. Dr. Grabe has received travel grants and

speakers honoraria from Fresenius Medical Care, Neuraxpharm, Servier and Janssen Cilag as well as research funding from Fresenius Medical Care. Dr Selbæk has received honoraria for participating at advisory board meetings from Roche and Biogen regarding new Alzheimer drugs. All other authors declare no competing financial interests. Dr. Selmer has received consultant and speaker's honoraria from Roche and OrionPharma, as well as reimbursement of travel and accommodation cost at a meeting from Kolpharma, and finally received sponsorships for arranging conferences from Desitin and Eisai AB. Dr. Agartz has received speakers honorarium from Lundbeck. Dr. Nöthen has received fees for membership in an advisory board from HMG Systems Engineering GmbH (Fürth, Germany), for membership in the Medical-Scientific Editorial Office of the Deutsches Ärzteblatt, and for serving as a consultant for EVERIS Belgique SPRL in a project of the European Commission (REFORM/SC2020/029). MMN receives salary payments from Life & Brain GmbH and holds shares in Life & Brain GmbH. All these concerned activities outside the submitted work. Dr. Pantelis received honoraria for talks from Lundbeck, Australia Pty Ltd. outside the submitted work.

#### References

1. Calle Sánchez, X. *et al.* Comparing Copy Number Variations in a Danish Case Cohort of Individuals With Psychiatric Disorders. *JAMA Psychiatry* **79**, 59–69 (2022).
2. Stefansson, H. *et al.* Large recurrent microdeletions associated with schizophrenia. *Nature* **455**, 232–236 (2008).
3. Marshall, C. R. *et al.* Contribution of copy number variants to schizophrenia from a genome-wide study of 41,321 subjects. *Nat. Genet.* **49**, 27–35 (2017).
4. Singh, T. *et al.* Rare coding variants in ten genes confer substantial risk for schizophrenia. *Nature* **604**, 509–516 (2022).
5. Mollon, J., Almasy, L., Jacquemont, S. & Glahn, D. C. The contribution of copy number variants to psychiatric symptoms and cognitive ability. *Mol. Psychiatry* 1–14 (2023) doi:10.1038/s41380-023-01978-4.
6. Modenato, C. *et al.* Lessons Learned From Neuroimaging Studies of Copy Number Variants: A Systematic Review. *Biol. Psychiatry* **90**, 596–610 (2021).
7. Sønderby, I. E. *et al.* Effects of copy number variations on brain structure and risk for psychiatric illness: Large-scale studies from the ENIGMA working groups on CNVs. *Hum. Brain Mapp.* **43**, 300–328 (2022).



8. Moreau, C. A., Ching, C. R., Kumar, K., Jacquemont, S. & Bearden, C. E. Structural and functional brain alterations revealed by neuroimaging in CNV carriers. *Curr. Opin. Genet. Dev.* **68**, 88–98 (2021).
9. Chapman, G. *et al.* Using induced pluripotent stem cells to investigate human neuronal phenotypes in 1q21.1 deletion and duplication syndrome. *Mol. Psychiatry* **27**, 819–830 (2022).
10. Urresti, J. *et al.* Cortical organoids model early brain development disrupted by 16p11.2 copy number variants in autism. *Mol. Psychiatry* **26**, 7560–7580 (2021).
11. Khan, T. A. *et al.* Neuronal defects in a human cellular model of 22q11.2 deletion syndrome. *Nat. Med.* **26**, 1888–1898 (2020).
12. Sundberg, M. *et al.* 16p11.2 deletion is associated with hyperactivation of human iPSC-derived dopaminergic neuron networks and is rescued by RHOA inhibition in vitro. *Nat. Commun.* **12**, 2897 (2021).
13. Smajlagić, D. *et al.* Population prevalence and inheritance pattern of recurrent CNVs associated with neurodevelopmental disorders in 12,252 newborns and their parents. *Eur. J. Hum. Genet.* **29**, 205–215 (2021).
14. Kendall, K. M. *et al.* Cognitive Performance Among Carriers of Pathogenic Copy Number Variants: Analysis of 152,000 UK Biobank Subjects. *Biol. Psychiatry* **82**, 103–110 (2017).
15. Sønderby, I. E. *et al.* 1q21.1 distal copy number variants are associated with cerebral and cognitive alterations in humans. *Transl. Psychiatry* **11**, 1–16 (2021).
16. Writing Committee for the ENIGMA-CNV Working Group *et al.* Association of Copy Number Variation of the 15q11.2 BP1-BP2 Region With Cortical and Subcortical Morphology and Cognition. *JAMA Psychiatry* **77**, 420–430 (2020).
17. Anderson, A. E. *et al.* Intra-individual variability in neuropsychological performance predicts cognitive decline and death in HIV. *Neuropsychology* **32**, 966–972 (2018).
18. Dykiert, D., Der, G., Starr, J. M. & Deary, I. J. Sex differences in reaction time mean and intraindividual variability across the life span. *Dev. Psychol.* **48**, 1262–1276 (2012).
19. Hilborn, J. V., Strauss, E., Hultsch, D. F. & Hunter, M. A. Intraindividual variability across cognitive domains: Investigation of dispersion levels and performance profiles in older adults. *J. Clin. Exp. Neuropsychol.* **31**, 412–424 (2009).
20. MacDonald, S. W. S., Nyberg, L. & Bäckman, L. Intra-individual variability in behavior: links to brain structure, neurotransmission and neuronal activity. *Trends*

- Neurosci.* **29**, 474–480 (2006).
21. Roalf, D. R. *et al.* Within-Individual Variability: An Index for Subtle Change in Neurocognition in Mild Cognitive Impairment. *J. Alzheimers Dis. JAD* **54**, 325–335 (2016).
  22. Tamnes, C. K., Fjell, A. M., Westlye, L. T., Østby, Y. & Walhovd, K. B. Becoming Consistent: Developmental Reductions in Intraindividual Variability in Reaction Time Are Related to White Matter Integrity. *J. Neurosci.* **32**, 972–982 (2012).
  23. Keller, A. S. *et al.* Hierarchical functional system development supports executive function. *Trends Cogn. Sci.* **27**, 160–174 (2023).
  24. Sydnor, V. J. *et al.* Neurodevelopment of the association cortices: Patterns, mechanisms, and implications for psychopathology. *Neuron* **109**, 2820–2846 (2021).
  25. Yeo, B. T. T. *et al.* Functional Specialization and Flexibility in Human Association Cortex. *Cereb. Cortex* **25**, 3654–3672 (2015).
  26. Ho, D., Imai, K., King, G. & Stuart, E. A. MatchIt: Nonparametric Preprocessing for Parametric Causal Inference. *J. Stat. Softw.* **42**, 1–28 (2011).
  27. Alfaro-Almagro, F. *et al.* Image processing and Quality Control for the first 10,000 brain imaging datasets from UK Biobank. *NeuroImage* **166**, 400–424 (2018).
  28. Monereo-Sánchez, J. *et al.* Quality control strategies for brain MRI segmentation and parcellation: Practical approaches and recommendations - insights from the Maastricht study. *NeuroImage* **237**, 118174 (2021).
  29. Radua, J. *et al.* Increased power by harmonizing structural MRI site differences with the ComBat batch adjustment method in ENIGMA. *NeuroImage* **218**, 116956 (2020).
  30. Crawford, K. *et al.* Medical consequences of pathogenic CNVs in adults: analysis of the UK Biobank. *J. Med. Genet.* **56**, 131–138 (2019).
  31. Kochunov, P. *et al.* White Matter in Schizophrenia Treatment Resistance. *Am. J. Psychiatry* **176**, 829–838 (2019).
  32. Larivière, S. *et al.* The ENIGMA Toolbox: multiscale neural contextualization of multisite neuroimaging datasets. *Nat. Methods* **18**, 698–700 (2021).
  33. Benjamini, Y. & Hochberg, Y. Controlling the False Discovery Rate: A Practical and Powerful Approach to Multiple Testing. *J. R. Stat. Soc. Ser. B Methodol.* **57**, 289–300 (1995).
  34. Stefansson, H. *et al.* CNVs conferring risk of autism or schizophrenia affect cognition in controls. *Nature* **505**, 361–366 (2014).
  35. Cox, D. M. & Butler, M. G. The 15q11.2 BP1–BP2 Microdeletion Syndrome: A

- Review. *Int. J. Mol. Sci.* **16**, 4068–4082 (2015).
36. van Rooij, D. *et al.* Cortical and Subcortical Brain Morphometry Differences Between Patients With Autism Spectrum Disorder and Healthy Individuals Across the Lifespan: Results From the ENIGMA ASD Working Group. *Am. J. Psychiatry* **175**, 359–369 (2018).
  37. van Erp, T. G. M. *et al.* Cortical Brain Abnormalities in 4474 Individuals With Schizophrenia and 5098 Control Subjects via the Enhancing Neuro Imaging Genetics Through Meta Analysis (ENIGMA) Consortium. *Biol. Psychiatry* **84**, 644–654 (2018).
  38. Fiddes, I. T. *et al.* Human-Specific NOTCH2NL Genes Affect Notch Signaling and Cortical Neurogenesis. *Cell* **173**, 1356–1369.e22 (2018).
  39. Suzuki, I. K. *et al.* Human-Specific NOTCH2NL Genes Expand Cortical Neurogenesis through Delta/Notch Regulation. *Cell* **173**, 1370–1384.e16 (2018).
  40. Hansen, D. V., Lui, J. H., Parker, P. R. L. & Kriegstein, A. R. Neurogenic radial glia in the outer subventricular zone of human neocortex. *Nature* **464**, 554–561 (2010).
  41. Florio, M. *et al.* Evolution and cell-type specificity of human-specific genes preferentially expressed in progenitors of fetal neocortex. *eLife* **7**, e32332 (2018).
  42. Chai, J.-H. *et al.* Identification of Four Highly Conserved Genes between Breakpoint Hotspots BP1 and BP2 of the Prader-Willi/Angelman Syndromes Deletion Region That Have Undergone Evolutionary Transposition Mediated by Flanking Duplicons. *Am. J. Hum. Genet.* **73**, 898–925 (2003).
  43. Tam, G. W. C. *et al.* Confirmed rare copy number variants implicate novel genes in schizophrenia. *Biochem. Soc. Trans.* **38**, 445–451 (2010).
  44. Nebel, R. A. *et al.* Reduced CYFIP1 in Human Neural Progenitors Results in Dysregulation of Schizophrenia and Epilepsy Gene Networks. *PLOS ONE* **11**, e0148039 (2016).
  45. Wang, J. *et al.* Common Regulatory Variants of CYFIP1 Contribute to Susceptibility for Autism Spectrum Disorder (ASD) and Classical Autism. *Ann. Hum. Genet.* **79**, 329–340 (2015).
  46. Toma, C. *et al.* Exome sequencing in multiplex autism families suggests a major role for heterozygous truncating mutations. *Mol. Psychiatry* **19**, 784–790 (2014).
  47. Zwaag, B. van der *et al.* A co-segregating microduplication of chromosome 15q11.2 pinpoints two risk genes for autism spectrum disorder. *Am. J. Med. Genet. B Neuropsychiatr. Genet.* **153B**, 960–966 (2010).
  48. Woo, Y. J. *et al.* A Common CYFIP1 Variant at the 15q11.2 Disease Locus Is

- Associated with Structural Variation at the Language-Related Left Supramarginal Gyrus. *PLOS ONE* **11**, e0158036 (2016).
49. Silva, A. I. *et al.* Cyfip1 haploinsufficient rats show white matter changes, myelin thinning, abnormal oligodendrocytes and behavioural inflexibility. *Nat. Commun.* **10**, 3455 (2019).
  50. Oguro-Ando, A. *et al.* Increased CYFIP1 dosage alters cellular and dendritic morphology and dysregulates mTOR. *Mol. Psychiatry* **20**, 1069–1078 (2015).
  51. De Rubeis, S. *et al.* CYFIP1 Coordinates mRNA Translation and Cytoskeleton Remodeling to Ensure Proper Dendritic Spine Formation. *Neuron* **79**, 1169–1182 (2013).
  52. Yoon, K.-J. *et al.* Modeling a Genetic Risk for Schizophrenia in iPSCs and Mice Reveals Neural Stem Cell Deficits Associated with Adherens Junctions and Polarity. *Cell Stem Cell* **15**, 79–91 (2014).
  53. Natu, V. S. *et al.* Apparent thinning of human visual cortex during childhood is associated with myelination. *Proc. Natl. Acad. Sci.* 201904931 (2019)  
doi:10.1073/pnas.1904931116.
  54. Domínguez-Iturza, N. *et al.* The autism- and schizophrenia-associated protein CYFIP1 regulates bilateral brain connectivity and behaviour. *Nat. Commun.* **10**, 3454 (2019).
  55. Jensen, M. & Girirajan, S. An interaction-based model for neuropsychiatric features of copy-number variants. *PLOS Genet.* **15**, e1007879 (2019).
  56. Fry, A. *et al.* Comparison of Sociodemographic and Health-Related Characteristics of UK Biobank Participants With Those of the General Population. *Am. J. Epidemiol.* **186**, 1026–1034 (2017).



**Figure 1. Cortical surface area comparison between 1q21.1 distal deletion carriers and non-carriers.** A) Top panel shows z-scores - group differences in regional cortical surface area. Bottom panel shows RID-scores - group differences in regional cortical surface area that are scaled to the individual's own global index. Non-carriers are represented by gray lines, and 1q21.1 distal deletion carriers are represented by black lines. Blue dots indicate significant differences. The insular cortex is included under frontal cortex for visualization purposes. B) Top panel displays the significant differences in Z-scores, and the bottom panel shows the significant differences in RID-scores. Blue-red diverging maps represent the effect size. C) Spatial distribution of all the mean differences in RID scores. Please note that all values are shown regardless of significance. Yellow-purple diverging maps represent the direction of the mean differences. Increased yellow intensity represents values that are less deviant than the overall global mean difference in cortical surface area, and increased purple intensity represents values that are more deviant than the overall global mean difference in cortical surface area. Z- and RID-scores are based on raw values adjusted for age, age<sup>2</sup>, sex, and intracranial volume on site harmonized data.





**Figure 2. Cortical thickness comparison between 1q21.1 distal deletion carriers and non-carriers.** A) Top panel shows z-scores - group differences in regional cortical thickness. Bottom panel shows RID-scores - group differences in regional cortical thickness that are scaled to the individual's own global index. Non-carriers are represented by gray lines, and 1q21.1 distal deletion carriers are represented by black lines. Blue dots indicate significant differences. The insular cortex is included under frontal cortex for visualization purposes. B) Top panel displays the significant differences in Z-scores, and the bottom panel shows the significant differences in RID-scores. Blue-red diverging maps represent the effect size. C) Spatial distribution of all the mean differences in RID scores. Please note that all values are shown regardless of significance. Yellow-purple diverging maps represent the direction of the mean differences. Increased yellow intensity represents values that are less deviant than the overall global mean difference in cortical thickness, and increased purple intensity represents values that are more deviant than the overall global mean difference in cortical thickness. Z- and RID-scores are based on raw values adjusted for age, age<sup>2</sup>, sex, and intracranial volume on site harmonized data.





**Figure 3. Cortical surface area comparison between 15q11.2 BP1-BP2 deletion carriers and non-carriers.** A) Top panel shows z-scores - group differences in regional cortical surface area. Bottom panel shows RID-scores - group differences in regional cortical surface area that are scaled to the individual's own global index. Non-carriers are represented by gray lines, and 15q11.2 BP1-BP2 deletion carriers are represented by black lines. Blue dots indicate significant differences. The insular cortex is included under frontal cortex for visualization purposes. B) Top panel displays the significant differences in Z-scores, and the bottom panel shows the significant differences in RID-scores. Blue-red diverging maps represent the effect size. C) Spatial distribution of all the mean differences in RID scores. Please note that all values are shown regardless of significance. Yellow-purple diverging maps represent the direction of the mean differences. Increased yellow intensity represents values that are less deviant than the overall global mean difference in cortical surface area, and increased purple intensity represents values that are more deviant than the overall global mean difference in cortical surface area. Z- and RID-scores are based on raw values adjusted for age, age<sup>2</sup>, sex, and intracranial volume on site harmonized data.





**Figure 4. Cortical thickness comparison between 15q11.2 BP1-BP2 deletion carriers and non-carriers.** A) Top panel shows z-scores - group differences in regional cortical thickness. Bottom panel shows RID-scores - group differences in regional cortical thickness that are scaled to the individual's own global index. Non-carriers are represented by gray lines, and 15q11.2 BP1-BP2 deletion carriers are represented by black lines. Blue dots indicate significant differences. The insular cortex is included under frontal cortex for visualization purposes. B) Top panel displays the significant differences in Z-scores, and the bottom panel shows the significant differences in RID-scores. Blue-red diverging maps represent the effect size. C) Spatial distribution of all the mean differences in RID scores. Please note that all values are shown regardless of significance. Yellow-purple diverging maps represent the direction of the mean differences. Increased yellow intensity represents values that are less deviant than the overall global mean difference in cortical thickness, and increased purple intensity represents values that are more deviant than the overall global mean difference in cortical thickness. Z- and RID-scores are based on raw values adjusted for age, age<sup>2</sup>, sex, and intracranial volume on site harmonized data.

## SUPPLEMENTARY INFORMATION

### **Beyond the Global Brain Differences: Intra-individual Variability Differences in 1q21.1 Distal and 15q11.2 BP1-BP2 Deletion Carriers**

Boen *et al.*

#### ***Content in this file:***

**Supplementary note 1:** Sampling procedure

**Supplementary note 2:** MRI quality control

**Supplementary note 3.** Association between RID scores and Z-scores and cognitive ability.

**Supplementary note 4:** Associations between the intraindividual standard deviation values for cortical surface area, cortical thickness, and subcortical volume.

**Supplementary note 5.** RID scores and affection status

**Supplementary note 6.** RID scores and cognitive ability in 1q21.1 distal deletion and 15q11.2 BP1-BP2 deletion carriers.

**Supplementary note 7.** Comparison between the conventional case-control analysis adjusted for the global index and the RID score approach.

#### **Supplementary references**

**Supplementary Appendix 1:** Technical details of the scanners and acquisition parameters used at the participating sites.

**Table S1.** Associations between cognitive ability and Z-scores and RID-scores in the UK Biobank.

**Table S2.** Reference values for the global index and intraindividual standard deviation

**Table S3.** Group differences in Z-scores for 1q21.1 distal deletion carriers.

**Table S4.** Group differences in RID-scores for 1q21.1 distal deletion carriers.

**Table S5.** Carrier status (i.e., 1q21.1 distal deletion vs non-carriers) and affection status on RID-scores.

**Table S6.** Carrier status (i.e., 1q21.1 distal deletion vs non-carriers) and cognitive ability on RID-scores.

**Table S7.** Group differences in Z-scores for 1q21.1 distal deletion carriers, adjusted for the global index.

**Table S8.** Group differences in Z-scores for 1q21.1 distal duplication carriers.

**Table S9.** Group differences in RID-scores for 1q21.1 distal duplication carriers.

**Table S10.** Group differences in Z-scores for 15q11.2 BP1-BP2 deletion carriers.

**Table S11.** Group differences in RID-scores for 15q11.2 BP1-BP2 deletion carriers.

**Table S12.** Carrier status (i.e., 15q11.2 BP1-BP2 deletion vs non-carriers) and affection status on RID-scores.

**Table S13.** Carrier status (i.e., 15q11.2 BP1-BP2 deletion vs non-carriers) and cognitive ability on RID-scores.

**Table S14.** Group differences in Z-scores for 15q11.2 BP1-BP2 deletion carriers, adjusted for the global index.

**Table S15.** Group differences in Z-scores for 15q11.2 BP1-BP2 duplication carriers.

**Table S16.** Group differences in RID-scores for 15q11.2 BP1-BP2 duplication carriers.

### **Supplementary note 1: Sampling procedure**

The included samples were drawn from a pool of participants from the ENIGMA-CNV working group and the UK Biobank. Participants flagged with either a 1q21.1 distal deletion, 1q21.1 distal duplication, 15q11.2 BP1-BP2 deletion or 15q11.2 BP1-BP2 duplication were included in the study. For the participants pooled from the ENIGMA-CNV consortium, identification of the CNV carriers was derived as described in previously published articles on the 1q21.1 distal and 15q11.2 BP1-BP2. For the UK Biobank sample, we identified CNVs based on the returned dataset from Crawford et al.(1). All participants flagged to have a CNV as previously reported in Crawford et al. were removed from downstream analyses, except for those flagged with the 1q21.1 distal or the 15q11.2 BP1-BP2 CNVs. A matched non-carrier group for each of the four CNV samples were extracted using the MatchIt function in R(2). The non-carrier group was matched to each carrier on age, sex, scanner site and ICV. The sample size of the non-carrier group is based on previous published studies. For the 1q21.1 distal deletion, sensitivity analyses indicated that group differences can be detected using 1:1 ratio sample comparison due to large effect sizes(3). For the 15q11.2 BP1-BP2 deletion, previous power analysis has found a 1:4 ratio sample comparison suitable detect small to medium effect sizes(4). Here, we used a matched non-carrier group that was five times larger than the carrier group as we expected some reduction in sample size due to missing data (see below). Furthermore, we also harmonized the data across scanner sites and use a mega-analytical approach to test for group differences, which has been reported to yield increased power compared to studies using a meta-analytical approach with scanner site included as a covariate(5).

### **Supplementary note 2: MRI quality control**

The MRI data from the UK Biobank underwent an automatic quality control procedure, using the derived Euler numbers to exclude participants with Euler numbers that dropped below four standard deviations from the rest of the sample. For the ENIGMA-CNV sample, all cohorts were asked to complete the cortical quality control that includes visual and statistical evaluation of the included participants (<https://enigma.ini.usc.edu/protocols/imaging-protocols/>). Further, after matching each carrier to five non-carriers, we examined the distribution of the Z-score in each of the four derived samples. Here, non-carriers that exhibited a highly atypical Z-score distribution (i.e., severe change in a regional Z-score within participants, i.e., > 6SD) were removed from the sample. The non-carriers were removed from the sampling pool, and we reran the matching procedure to obtain five non-

carriers per carrier. We detected one regional value with a severe change in Z-score (i.e., > 7SD) among one 15q11.2 BP1-BP2 deletion carrier from the UK Biobank. This region was excluded for this participant (i.e., regional value was set to NA) in downstream analyses. As the statistical procedure used in the current study is sensitive to individuals that do not have a full observation across the feature of interest (i.e., cortical thickness, surface area, and subcortical volume), we only included individuals with full observations for the feature of interest. Thus, the number of individuals included in the analyses differs between features. The number of individuals included in the analyses is included in the supplementary tables. The four samples were derived from a total of 61 scanner sites (including scanner sites from the UK Biobank). Thus, to account for systematic differences between scanner sites, we ran each of the four subsamples through ComBat, which is an instrument for data harmonization that increases the statistical power and can harmonize data with missing values(5).

### **Supplementary note 3. Association between RID scores and Z-scores and cognitive ability.**

To test the associations between the RID-scores and Z-scores and cognitive ability, we utilized data from the UK Biobank.

First, we created RID scores across all participants without a pathogenic CNV and with available imaging data (n = 40,312) using the sample's own mean and standard deviation to generate the Z-scores.

Second, we extracted cognitive scores from four different cognitive tasks that were available from the imaging visit (i.e., Data-Field 20016: fluid intelligence test (verbal and numeric reasoning), Data-Field 20023: reaction time test (simple processing speed), Data-Field 4282: digit span test (numeric working memory) and Data-Field 399: pairs matching test (episodic memory)). The intelligence measure is based on the number of correct responses on 13 questions, reaction time is based on the log transformed mean reaction time after the removal of trials with responses <50 ms and >2000 ms, digit span is based on the maximum number of digits remembered, and pairs matching is based on errors in the second round using a log+1 transformation. Further, we imputed values for the missing data using multivariate imputation by chained equations with classification and regression trees(6).

Third, we ran a principal component analysis across the test scores to get the first principal component across the four tasks, which we used as a measure of cognitive ability(7,8). We transformed the first principal component, such that higher values indicate better cognitive performance. The first principal component was highly correlated with number of correct



responses on the intelligence task ( $r = .985$ ,  $p < .001$ ) and maximum number of digits remembered in the digit span task ( $r = .506$ ,  $p < .001$ ). Moreover, higher values of the first principal component were associated with fewer errors in the pairs matching task ( $r = -.175$ ,  $p < .001$ ) and faster reaction time in the reaction time test ( $r = -.165$ ,  $p < .001$ ).

Fourth, the data were divided into two samples, 75% of the participants went into a discovery sample, and the remaining 25% of the participants went into a replication sample, yielding two groups consisting of 30,234 and 10,078 participants, respectively. We created a linear regression model, where the measure of cognitive ability was included as the independent variable and the RID scores included as the dependent variable. This resulted in 150 comparisons. Here, we report the brain regions that were significant in the discovery sample after FDR correction (i.e.,  $P_{\text{FDR}} < .05$ ) across the 150 comparisons and were below the uncorrected  $p < .05$  threshold in the replication sample (Table S1, left). The values were scaled to get a standardized beta value, serving as a measure of effect size. To compare the associations and effect sizes to conventional brain-cognition analyses, we redid the analysis using Z-scores (Table S1, right). The results are visualized in Figure S1. Interestingly, a subset of the RID scores that differed significantly between 1q21.1 distal deletion and non-carriers (i.e., left and right superior temporal gyri and left supramarginal gyrus cortical thickness and left lateral orbitofrontal and left lateral superior temporal gyrus cortical surface area) also displayed significant associations with cognitive ability in the UK Biobank non-carrier sample.

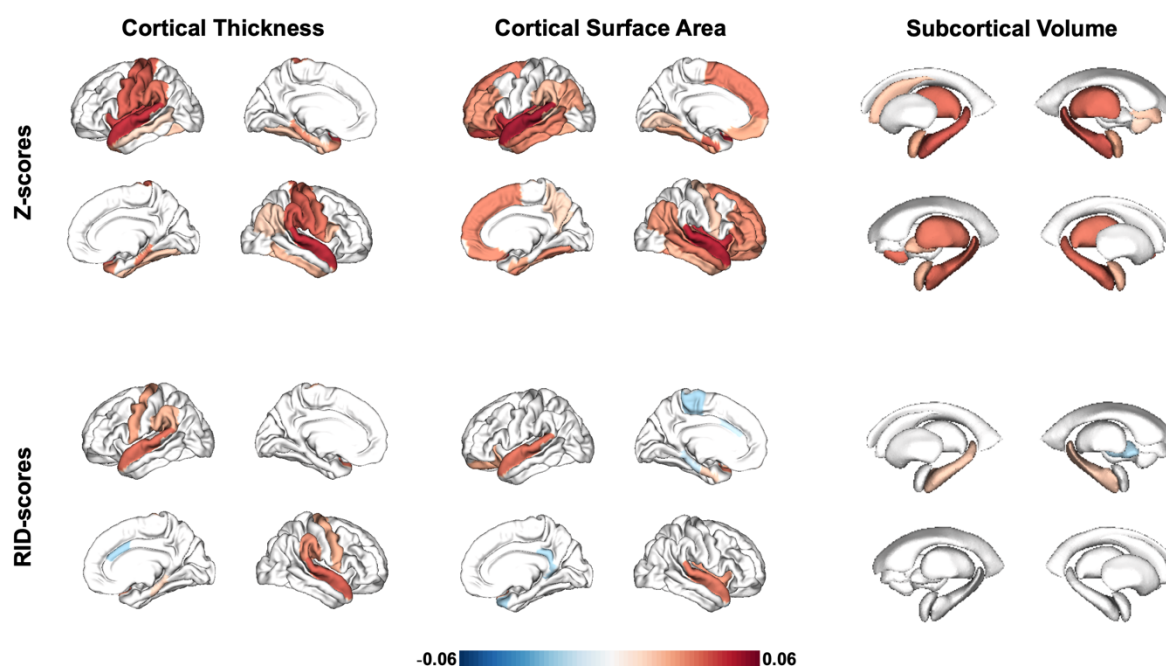


**Figure S1.** Associations between brain Z-scores (top) and RID scores (bottom) and cognitive ability measure [as estimated by the first principal component across the four tasks: Intelligence, reaction time, digit span and match pairing]. Blue-red diverging maps represent the effect size as derived from the discovery sample.

**Supplementary note 4: Associations between the intraindividual standard deviation values for cortical surface area, cortical thickness, and subcortical volume.**

To examine the associations between the intraindividual standard deviation values across the MRI-derived features, we correlated the iSD measures for cortical surface area, cortical thickness, and subcortical volumes for both CNVs. To increase statistical power for the non-carriers, we merged the two non-carrier groups in the 1q21.1 distal and 15q11.2 BP1-BP2 CNV groups, respectively. To test if the correlations between deletions and duplication carriers statistically differ from each other, we used the Fisher's Z test in the cocor package in R(9). The associations across CNV carriers and non-carriers are visualized in Figure S2.

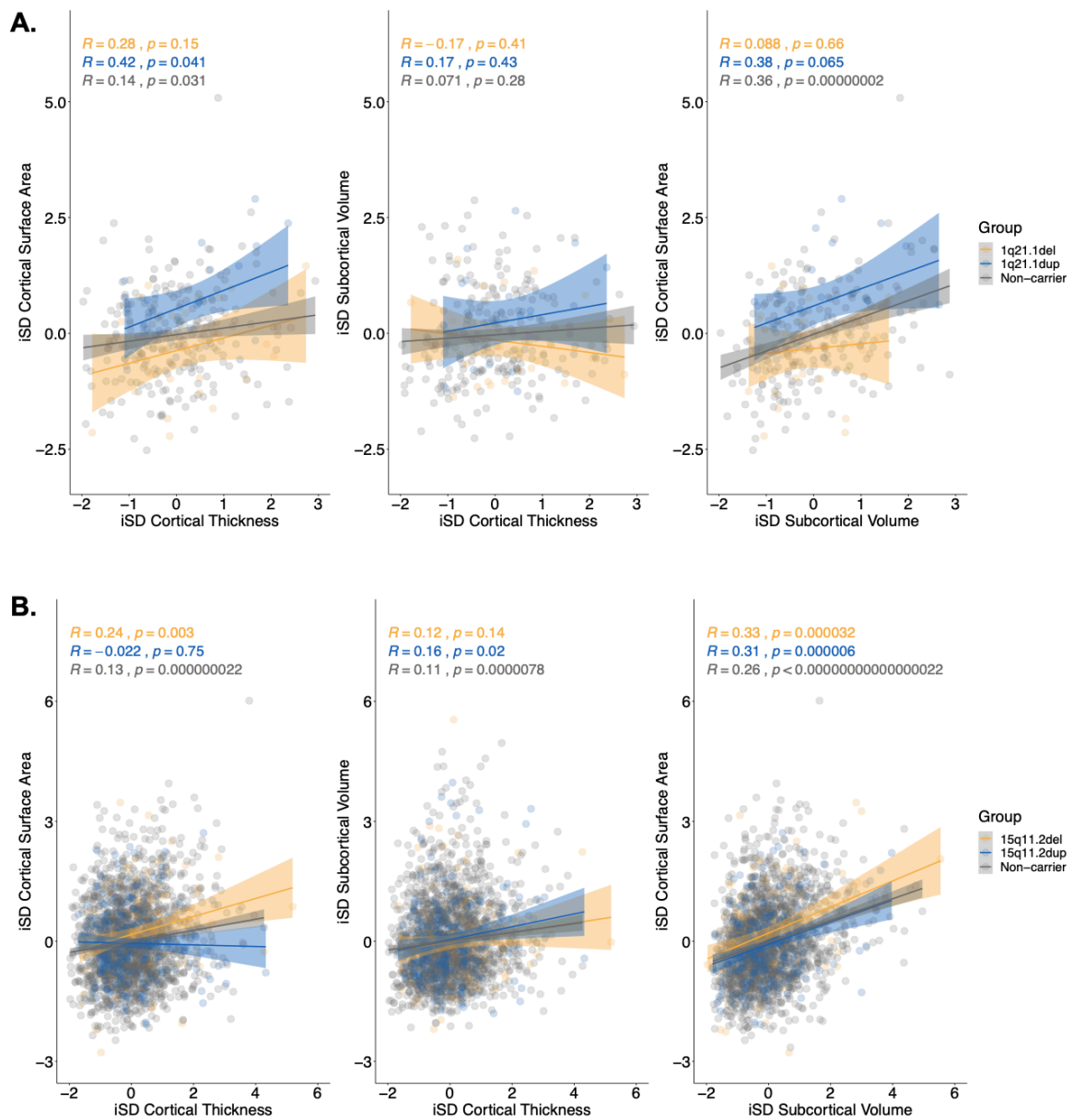


**Figure S2.** Correlations between intraindividual standard deviation values (iSDs) for cortical thickness, surface area, and subcortical volume. A) Correlations across 1q21.1 distal deletion and duplication carriers and non-carriers. B) Correlations across 15q11.2 BP1-BP2 deletion and duplication carriers and non-carriers. Correlation coefficients and p-values for each group are presented in the figures and are matched to the color of each group. Yellow = deletion carriers, blue = duplication carrier, grey = non-carrier. iSD = intraindividual standard deviation.

For the 1q21.1 distal deletion and duplication, we did not find evidence for a statistical difference in the correlations between iSD cortical thickness and iSD cortical surface area ( $Z = -0.934$ ,  $p = 0.350$ ), iSD cortical thickness and iSD subcortical volume ( $Z = 0.962$ ,  $p = 0.336$ ), or iSD subcortical volume and iSD surface area ( $Z = -1.053$ ,  $p = 0.292$ ).

For the 15q11.2 BP1-BP2 deletion and duplication, the correlation between iSD cortical thickness and iSD surface area were significantly different from each other ( $Z = 3.207$ ,  $p = 0.001$ ,  $P_{FDR} = 0.004$ ), whereas there was no statistical difference between the correlations of iSD cortical thickness and iSD subcortical volume ( $Z = 0.477$ ,  $p = 0.633$ ) or iSD cortical surface area and iSD subcortical volume ( $Z = 0.271$ ,  $p = 0.786$ ).

The overall pattern of the results indicates that a more variable brain, as indicated by regional variability across ROIs, tend to be a feature of the whole brain, as indicated by the correlations between the MRI-derived measures (i.e., cortical surface area, cortical thickness, subcortical volume). This is supported by the consistent positive correlations between the MRI-derived measures from the well-powered non-carrier groups. However, for the 15q11.2 BP1-BP2 CNV, this pattern appears to be slightly different, as the 15q11.2 BP1-BP2 duplication does not show evidence for an association between the regional variability across ROIs using cortical surface area and regional variability across ROIs using cortical thickness, which significantly differed from the pattern observed in the 15q11.2 BP1-BP2 deletion.

### **Supplementary note 5. RID scores and affection status**

To further examine the significant RID results between the 1q21.1 distal deletion carriers and non-carriers and 15q11.2 BP1-BP2 deletion carriers, we ran additional analyses to test the effect of affection status on the significant RID scores. Here, we included 1) affection status (i.e., having a known psychiatric or neurological diagnosis, or an F or G-ICD diagnosis for the UK Biobank participants, coded as 0 (none) and 1 (dx)) as a covariate and 2) an interaction term between affection status and copy number. The affection status was distributed as follows: 10 (33.3%) 1q21.1 distal deletion carriers and 18 (12%) non-carriers, and 19 (11.2%) 15q11.2 BP1-BP2 deletion carriers and 91 (10.7%) non-carriers.

All significant RID scores survived the adjustment for affection status for both the 1q21.1 distal deletion (Table S5, top) and the 15q11.2 BP1-BP2 deletion (Table S12, top). None of the RID scores showed an interaction effect between copy number status (i.e., deletion or non-carrier, non-carrier group used as the reference) and affection status (affection status 0 (none) used as the reference) for either the 1q21.1 distal deletion (Table S5, top) or the 15q11.2 BP1-BP2 deletion (Table S12, bottom).

### **Supplementary note 6. RID scores and cognitive ability in 1q21.1 distal deletion and 15q11.2 BP1-BP2 deletion carriers.**

The low effect sizes for the brain-cognition relationship described in supplementary note 3, indicate that brain-cognition associations are underpowered for the CNV groups. Nevertheless, to explore the possibility that the brain-cognition relationships are stronger in the 1q21.1 distal deletion and 15q11.2 BP1-BP2 deletion carriers compared to the non-carriers, we tested for a significant interaction effect between our calculated measure of cognitive ability and carrier status using linear regression. A significant interaction term would indicate that the brain-cognition relationship is stronger for one of the groups. For each of the 1q21.1 distal deletion and 15q11.2 BP1-BP2 deletion samples, including their corresponding matched non-carrier group, we followed the same approach for imputation and principal component procedure as outlined in supplementary note 3. The cognitive ability measure was lower for the 1q21.1 distal deletion carriers (Estimate = -.667, S.E. = .307, t-value = -2.169,  $p = .033$ ) and the 15q11.2 BP1-BP2 deletion carriers (Estimate = -.392, S.E. = .097, t-value = -4.030,  $p < .001$ ) compared to non-carriers. However, we did not find evidence for an interaction effect between copy number and cognitive ability on the RID scores for either the 1q21.1 distal deletion (Table S6) or the 15q11.2 BP1-BP2 deletion carriers (Table S13). These results - the effect sizes between RID scores and the cognitive ability measure using the full UK Biobank sample (standardized beta values  $> .06$ ) and the lack of interaction term between carrier status and cognitive ability - indicate that the 1q21.1 distal deletion and 15q11.2 BP1-BP2 deletion samples are likely underpowered to detect reliable brain-cognition relationships.

### **Supplementary note 7. Comparison between the conventional case-control analysis adjusted for the global index and the RID score approach.**

To compare the significant RID scores to the conventional case-control analyses, adjusted for the global index, we created a linear regression model using copy number status as the independent variable with the global index as covariate and Z-scores as the dependent variable. The global index for cortical surface area, cortical thickness, and subcortical volume was included for cortical surface area, cortical thickness, and subcortical volume Z-scores, respectively. The continuous values were scaled and P-values that were below .05 after FDR correction were considered significant.

The Z-score results and RID score results are visualized in Figure S3 for the 1q21.1 distal deletion and in Figure S4 for the 15q11.2 BP1-BP2 deletion. The results indicate that the regions with the largest effect sizes remained significant after adjusting for the global index, but also showed some non-overlapping brain regions with their corresponding RID profile. That is, for the adjusted Z-scores the right paracentral cortical surface area was also significantly different between the 1q21.1 distal deletion and non-carriers, and the lateral occipital cortical thickness, right caudal anterior cingulate cortical surface area, and right nucleus accumbens subcortical volume differed significantly between the 15q11.2 BP1-BP2 deletion and non-carriers.

There are some key differences in the methodological approach between the estimations of RID scores and mean correcting for the global effect using linear regression. Of note, in contrast to the RID score approach, which use the estimated global index for each individual as the reference, the global covariation approach utilizes the linear relationship between the global index and the regional Z-scores across the sample to adjust for the global index. Here, we observe that the standardized beta values were smaller for the adjusted Z-scores and yielded a lower number of significant ROIs compared to the group differences using RID scores.

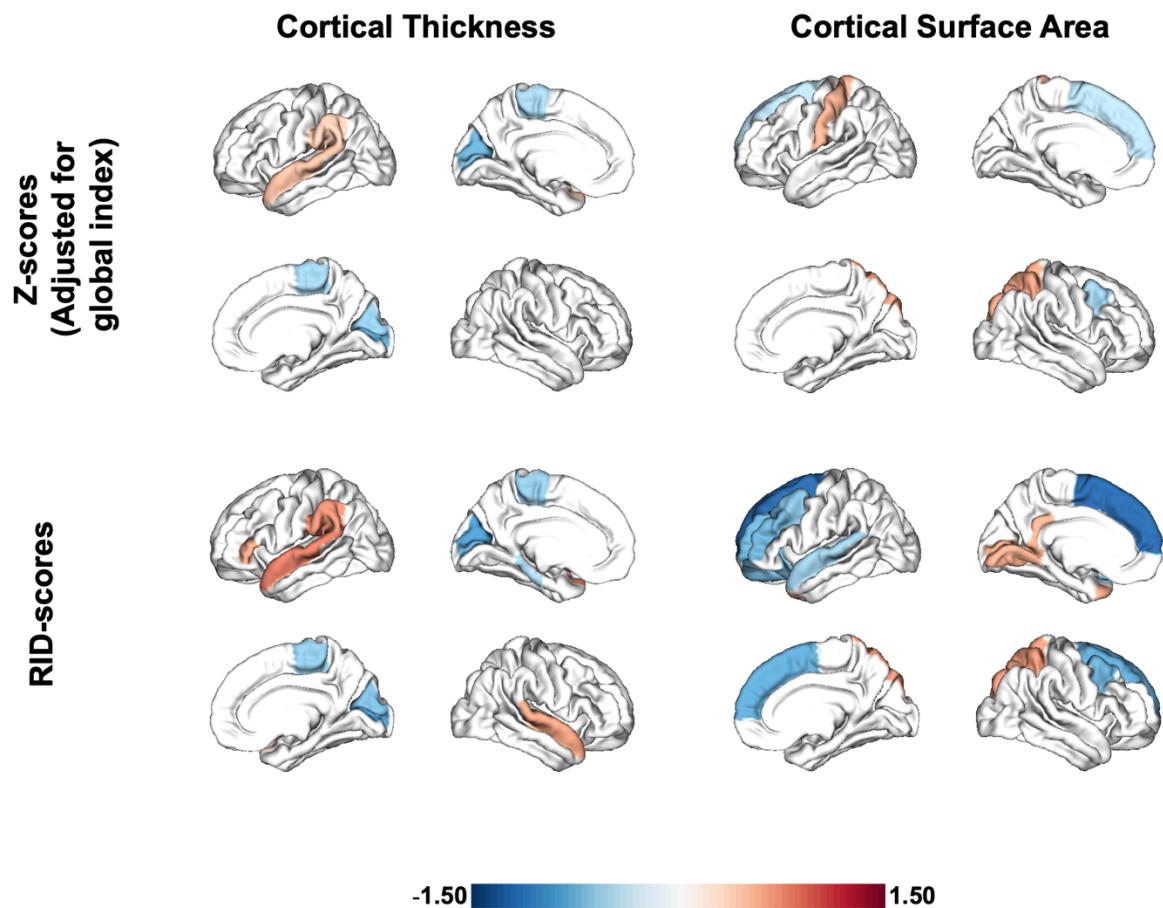


**Figure S3.** Comparison between the brain profile derived from adjusted Z-scores (top) and RID scores (bottom) derived from significant group differences between 1q21.1 distal deletion and non-carriers. Blue-red diverging maps represent the effect size.

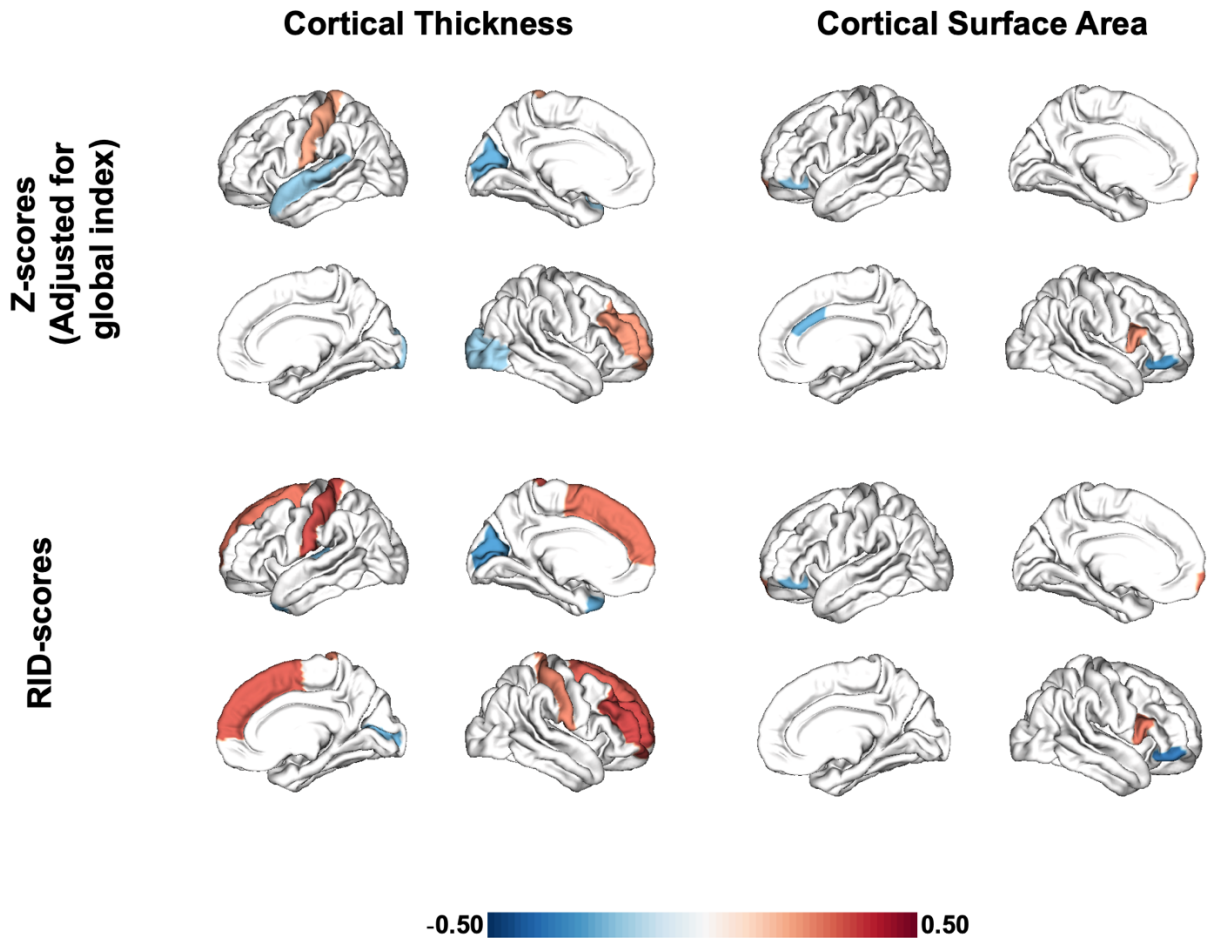


**Figure S4.** Comparison between the brain profile derived from adjusted Z-scores (top) and RID scores (bottom) derived from significant group differences between 15q11.2 BP1-BP2 deletion and non-carriers. Blue-red diverging maps represent the effect size.

### Supplementary References

1. Crawford K, Bracher-Smith M, Owen D, Kendall KM, Rees E, Pardiñas AF, et al. Medical consequences of pathogenic CNVs in adults: analysis of the UK Biobank. *J Med Genet.* 2019 Mar 1;56(3):131–8.
2. Ho D, Imai K, King G, Stuart EA. MatchIt: Nonparametric Preprocessing for Parametric Causal Inference. *J Stat Softw.* 2011 Jun 14;42(1):1–28.
3. Sønderby IE, van der Meer D, Moreau C, Kaufmann T, Walters GB, Ellegaard M, et al. 1q21.1 distal copy number variants are associated with cerebral and cognitive alterations in humans. *Transl Psychiatry.* 2021 Mar 22;11(1):1–16.



4. Boen R, Kaufmann T, Frei O, van der Meer D, Djurovic S, Andreassen OA, et al. No signs of neurodegenerative effects in 15q11.2 BP1-BP2 copy number variant carriers in the UK Biobank. *Transl Psychiatry*. 2023 Feb 18;13(1):1–6.
5. Radua J, Vieta E, Shinohara R, Kochunov P, Quidé Y, Green MJ, et al. Increased power by harmonizing structural MRI site differences with the ComBat batch adjustment method in ENIGMA. *NeuroImage*. 2020 Sep 1;218:116956.
6. Buuren S van, Groothuis-Oudshoorn K. mice: Multivariate Imputation by Chained Equations in R. *J Stat Softw*. 2011 Dec 12;45:1–67.
7. Hepsomali P, Groeger JA. Diet and general cognitive ability in the UK Biobank dataset. *Sci Rep*. 2021 Jun 3;11(1):11786.
8. Fawns-Ritchie C, Deary IJ. Reliability and validity of the UK Biobank cognitive tests. *PLOS ONE*. 2020 Apr 20;15(4):e0231627.
9. Diedenhofen B, Musch J. cocor: A Comprehensive Solution for the Statistical Comparison of Correlations. *PLOS ONE*. 2015 Apr 2;10(4):e0121945.

## APPENDIX 1

WRITING COMMITTEE FOR THE ENIGMA-CNV WORKING GROUP  
 TECHNICAL DETAILS CONCERNING SCANNERS AND ACQUISITION PARAMETERS USED AT THE PARTICIPATING SITES  
 PLEASE NOTE THAT SCANNERSITES ASRB\_1-5 FOR2107-MARBURG, FOR2107-MUENSTER, MILAN-OSR\_1-2 AND READING WERE NOT INCLUDED IN PREVIOUS  
 PUBLICATIONS. ALSO NOTE THAT DATASETS BETULA, ADHD\_BERGEN AND LIFESPAN DO NOT HAVE DATA INCLUDED IN THIS ANALYSIS.

NOTE: MM= MILLIMETER, MS=MILLISECOND

DATASET	Study design	Scanner site	Sequence	Field strength	Acq. direction	Number of slices	Slice gap	Voxel size in mm3	TI	TE	TR	Flip angle	Segmentation
<b>1000BRAINS</b>	Population-based	1000 BRAINS	3D T1-weighted magnetization prepared rapid acquisition gradient echo MPRAGE	3T	Sagittal	176	0mm	1x1x1	900 ms	3.03 ms	2.25 ms	9	FreeSurfer (5.3.0)
<b>16P11.2 EUROPEAN CONSORTIUM</b>	Neuro-developmental cohort	16p11_consortium_b	3D T1-weighted magnetization prepared rapid acquisition gradient echo MPRAGE	3T Siemens Magnetom Prisma Syngo	Sagittal	176	0.5	1x1x1	920 ms	2.39 ms	2000 ms	9	FreeSurfer (5.1.0) freesurfer-x86_64-redhat-linux-gnu-stable5-20110522
		16p11_consortium_a	3D T1-weight multi-Echo Magnetization Prepared RApid Gradient Echo sequence ME-MPRAGE	3T Magnetom TIM Trio	Sagittal	176	0.5	1x1x1	120 ms	TE1 = 1.64 ms, TE2 = 3.5 ms, TE3 = 5.36 ms, TE4 = 7.22 ms	2530 ms	7	FreeSurfer (5.1.0) freesurfer-x86_64-redhat-linux-gnu-stable5-20110522

<b>ADHD_ BERGEN</b>	Bergen	3D SPGR	3T GE Medical systems	sagittal	180	1 mm	1x1x1	500 ms	3.15 ms	7.95 ms	11	FreeSurfer (5.3.0)
<b>AHUS</b>	Ahus	3D turbo field echo	3T Philips Achieva	Sagittal	170	0 mm	1x1.2x1.2	853 ms	2.2 ms	4.5	8	FreeSurfer (5.3.0)
<b>ASRB</b>	ASRB_1	3D T1-weighted magnetization prepared rapid acquisition gradient echo MPRAGE	1.5T Siemens Avanto	Sagittal	176	0 mm	0.98*0.98*1	4.3	4.3	1980	15	FreeSurfer (5.1.0)
	ASRB_2	3D T1-weighted magnetization prepared rapid acquisition gradient echo MPRAGE	1.5T Siemens Avanto	Sagittal	176	0 mm	0.98*0.98*1	4.3	4.3	1980	15	FreeSurfer (5.1.0)
	ASRB_3	3D T1-weighted magnetization prepared rapid acquisition gradient echo MPRAGE	1.5T Siemens Avanto	Sagittal	176	0 mm	0.98*0.98*1	4.3	4.3	1980	15	FreeSurfer (5.1.0)
	ASRB_4	3D T1-weighted magnetization prepared rapid acquisition gradient echo MPRAGE	1.5T Siemens Avanto	Sagittal	176	0 mm	0.98*0.98*1	4.3	4.3	1980	15	FreeSurfer (5.1.0)

ASRB_5	3D T1-weighted magnetization prepared rapid acquisition gradient echo MPRAGE	1.5T Siemens Avanto	Sagittal	176	0 mm	0.98*0.98*1	450	3.2	8.2	15	FreeSurfer (5.1.0)		
<b>BETULA</b>	Population-based	Betula	FSPGR 3D	3T GE	Axial	180	1	0.49x0.49x1.0	450	3.2	8.2	12	FreeSurfer (5.3.0)
<b>BIG</b>	Population-based	BIG_T3	3D T1-weighted magnetization prepared rapid acquisition gradient echo MPRAGE	3T Siemens Trio	Sagittal	192	1.0 x 1.0 x 1.0	110	3.03	2300	8	FreeSurfer (5.3.0)	
	Population-based		3D T1-weighted magnetization prepared rapid acquisition gradient echo MPRAGE	3T Siemens Trio	Sagittal	192	1.0 x 1.0 x 1.0	110	2.92	2300	8	FreeSurfer (5.3.0)	
	Population-based		3D T1-weighted magnetization prepared rapid acquisition gradient echo MPRAGE	3T Siemens Trio	Sagittal	192	1.0 x 1.0 x 1.0	110	2.96	2300	8	FreeSurfer (5.3.0)	

	3D T1-weighted magnetization prepared rapid acquisition gradient echo MPRAGE	3T Siemens Trio	Sagittal	192	$1.0 \times 1.0 \times 1.0$	110 0ms	2.99 ms	2300 ms	8	FreeSurfer (5.3.0)
	3D T1-weighted magnetization prepared rapid acquisition gradient echo MPRAGE	3T Siemens Trio	Sagittal	176	$1.0 \times 1.0 \times 1.0$	110 0ms	3.93 ms	1940 ms	8	FreeSurfer (5.3.0)
	3D T1-weighted magnetization prepared rapid acquisition gradient echo MPRAGE	3T Siemens Trio	Sagittal	176	$1.0 \times 1.0 \times 1.0$	110 0ms	4.58 ms	1960 ms	8	FreeSurfer (5.3.0)
<b>BIG</b>	Population-based BIG_T1.5	1.5T Siemens Avanto	Sagittal	176	$1.0 \times 1.0 \times 1.0$	100 0ms	2.95 ms	2730 ms	7	FreeSurfer (5.3.0)
	3D T1-weighted magnetization prepared rapid acquisition gradient echo MPRAGE	1.5T Siemens Avanto	Sagittal	176	$1.0 \times 1.0 \times 1.0$	100 0ms	2.95 ms	2730 ms	7	FreeSurfer (5.3.0)
	3D T1-weighted magnetization prepared rapid acquisition gradient echo MPRAGE	1.5T Siemens Avanto	Sagittal	176	$1.0 \times 1.0 \times 1.0$	850 ms	2.95 ms	2250 ms	15	FreeSurfer (5.3.0)

	3D T1-weighted magnetization prepared rapid acquisition gradient echo MPRAGE	1.5T Siemens Sonata	Sagittal	176	$1.0 \times 1.0 \times 1.0$	850 ms	3.93 ms	2250 ms	15	FreeSurfer (5.3.0)		
	3D T1-weighted magnetization prepared rapid acquisition gradient echo MPRAGE	1.5T Siemens Sonata	Sagittal	176	$1.0 \times 1.0 \times 1.0$	850 ms	3.68 ms	2250 ms	15	FreeSurfer (5.3.0)		
<b>COBRE</b>	Case-control (SCZ and healthy controls)	COBRE	3T Siemens Trio	192	sagittal	1x1x1	0	5 ech oes, 1.64 /3.5 /5.3 6/7. 22/ 9.08 ms	2520 ms	7	FreeSurfer (5.3.0)	
<b>DEMGEN</b>	Case-control (Dementia and healthy controls)	DemGene_Ullevaal	3T GE Signa HDxT	170	Sagittal	1x1x1,2	0	450 ms	2,95 6	7.8	12	FreeSurfer (5.3.0)
<b>DUBLIN</b>	Case-control (SCZ, BD, other psychoses, and healthy controls)	Dublin	Philips Achieva 3T system	180	sagittal	0.9x0.9x0.9	0	516 ms	3ms	8.4ms	8	FreeSurfer (5.4.0)
<b>ECHO_DEFINE</b>	Neurodevelopmental cohort	ECHO_DEFINE	3T GE SIGNA HDx	256	1mm	1x1x1	0	450 ms	2.98 4ms	7.816 ms	20	FreeSurfer (5.3.0)

<b>EPIGEN</b>	Epilepsy cases	EPIGEN_London	whole-brain T1-weighted IR-prepared FSPGR	1.5T GE Signa	Coronal	128	0mm	0.9375×0.9375×1.1	450 ms	3ms	8ms	20	FreeSurfer (4.5.0)
<b>EPIGEN-DUBLIN</b>	Epilepsy cases	EPIGEN_Dublin											FreeSurfer (5.3.0)
<b>GAP</b>	Case-control (Schizophrenia and healthy controls)	GAP	3D T1-weighted magnetization prepared rapid acquisition gradient echo MPRAGE	3T Siemens Tim Trio	Coronal	180	0mm	1.25x1.25x1.2	500 ms	4ms	500ms	8	FreeSurfer (5.1.0)
<b>GOBS</b>	Family study	GOBS	T1-weighted MPRAGE (also, "3D turbo-flash sequences with an adiabatic inversion contrast pulse")	3T TIM Treo	Axial	160	0mm	1.7x1.7x3	785	3.04	2100 ms	13	FreeSurfer (5.3.0)
<b>GSP</b>	Population-based (volunteers)	GSP_1	Multi-echo MPRAGE	3T Siemens Tim Trio	Sagittal	144		1.2x1.2x1.2	110 0ms	1.5/ 3.4/ 5.2/ 7.0 ms	2200 ms	7	FreeSurfer (4.5.0)
		GSP_2	Multi-echo MPRAGE	3T Siemens Tim Trio	Sagittal	144		1.2x1.2x1.2	110 0ms	1.5/ 3.4/ 5.2/ 7.0 ms	2200 ms	7	FreeSurfer (4.5.0)
		GSP_3	Multi-echo MPRAGE	3T Siemens Tim Trio	Sagittal	144		1.2x1.2x1.2	110 0ms	1.5/ 3.4/ 5.2/ 7.0 ms	2200 ms	7	FreeSurfer (4.5.0)
		GSP_4	Multi-echo MPRAGE	3T Siemens Tim Trio	Sagittal	144		1.2x1.2x1.2	110 0ms	1.5/ 3.4/ 5.2/ 7.0 ms	2200 ms	7	FreeSurfer (4.5.0)

<b>FOR2107</b>	Case-control (SCZ, BD, MD, and healthy controls)	GSP_5	Multi-echo MPRAGE	3T Siemens Tim Trio	Sagittal	144	1.2x1.2x1.2	110 0ms	1.5/ 3.4/ 5.2/ 7.0 ms	2200 ms	7	FreeSurfer (4.5.0)
		Marburg	3D T1-weighted magnetization prepared rapid acquisition gradient echo MPRAGE	3T	Sagittal	176	1.0x1.0x1.0	900 ms	2.26 ms	1900 ms	9	FreeSurfer (5.3.0)
		Muenster	3D T1-weighted magnetization prepared rapid acquisition gradient echo MPRAGE	3T	Sagittal	192	1.0x1.0x1.0	900 ms	2.28 ms	2130 ms	8	FreeSurfer (5.3.0)
<b>HUBIN</b>	Case-control (SCZ and healthy controls)	Hubin	3D T1-weighted fast spoiled gradient recall (3D FSPGR)	1.5T GE signa Echo-speed	Coronal	124	0.975 x 1.5 x 0.975	6	6	24	35	FreeSurfer (5.3.0)
		HUNT	Population-based	3D T1-weighted inversion recovery prepared fast spoiled gradient recalled sequence (IR-FSPGR)	1.5T GE Signa HDx	Sagittal	162	0.9375*0.9375*1.2	4.2 ms	10.2 ms	10	FreeSurfer (5.3.0)
<b>IMAGEN</b>	Population-based	IMAGEN_a	ADNI MPRAGE	3T	Sagittal	170	1.1x1.1x1.1 mm	900 ms	3.01 6 ms	7,16 ms	8	FreeSurfer
		IMAGEN_b	ADNI MPRAGE	3T	Sagittal	160	1.1x1.1x1.1 mm	900 ms	2.93 ms	2300 ms	9	FreeSurfer



	IMAGEN_c	ADNI MPRAGE	3T	Sagittal	160	0mm	1.1x1.1x1.1 mm	900 ms	2.93 ms	2300 ms	9	FreeSurfer
	IMAGEN_d	ADNI MPRAGE	3T	Sagittal	137	0mm	1.1x1.1x1.1 mm	900 ms	2.78 ms	6,9 ms	9	FreeSurfer
	IMAGEN_e	ADNI MPRAGE	3T	Sagittal	160	0mm	1.1x1.1x1.1 mm	900 ms	2.93 ms	2300 ms	9	FreeSurfer
	IMAGEN_f	ADNI MPRAGE	3T	Sagittal	170	0mm	1.1x1.1x1.1 mm	900 ms	2.81 ms	6,608 ms	8	FreeSurfer
	IMAGEN_g	ADNI MPRAGE	3T	Sagittal	160	0mm	1.1x1.1x1.1 mm	900 ms	2.93 ms	2300 ms	9	FreeSurfer
	IMAGEN_h	ADNI MPRAGE	3T	Sagittal	137	0mm	1.1x1.1x1.1 mm	900 ms	2.78 ms	6,9 ms	9	FreeSurfer
	IMAGEN_i	ADNI MPRAGE	3T	Sagittal	160	0mm	1.1x1.1x1.1 mm	900 ms	2.93 ms	2300 ms	9	FreeSurfer
<b>MAS</b>	Population-based MAS_0, MAS_1	3D T1-weighted	3T Philips Achieva Quasar	Coronal	190	0mm	1x1x1	439	2.9	6.39	8	FreeSurfer (5.3.0)
<b>MCIC</b>	Case-control (SCZ and healthy controls)	Gradient Echo MGH	1.5T Siemens	coronal	128	0mm	0.625 x 0.625 x 1.5		4.76 ms	12ms	20	FreeSurfer (5.3.0)
	MCIC_IA	Gradient Echo	1.5T GE Signa	coronal	128	0mm	0.6641 x 0.6641 x 1.6		6ms	20ms	30	FreeSurfer (5.3.0)
	MCIC_UMN	3D T1-weighted magnetization prepared rapid acquisition gradient echo MPRAGE	3T Siemens Trio	coronal	128	0mm	0.625 x 0.625 x 1.5	110 0ms	3.79 ms	2530 ms	7	FreeSurfer (5.3.0)
	MCIC_UNM	Gradient Echo	1.5T Siemens	coronal	128	0mm	0.625 x 0.625 x 1.5		4.76 ms	12ms	20	FreeSurfer (5.3.0)

<b>METH-CT</b>	Case-control (schizophrenia including individuals with methamphetamine dependence (MA) or methamphetamine-associated psychosis (MAP) and healthy controls)	METH-CT	3D T1-weighted multi-echo magnetization prepared rapid acquisition gradient echo MEM PRAGE	3T Siemens MAGNET OM Allegra	Sagittal	160	0.5mm	1x1x1	110 0ms	1.53 ms, 3.21 ms, 4.89 ms, 6.57 ms	2530 ms	7	FreeSurfer (5.3.0)
<b>MILAN-OSR</b>	Bipolar	Milan-OSR_1	3D T1-weighted MPRAGE	3T	axial	182	0 mm	1x1x1	3.7 ms	8 ms	8 ms	8	FreeSurfer (7.2.0)
<b>NCNG</b>	Population-based	NCNG1	3D T1-weighted MPRAGE	3T	axial	220	-0.8 mm		4.6 ms	25 ms	30	30	FreeSurfer (7.2.0)
			3D T1-weighted magnetization prepared rapid acquisition gradient echo MPRAGE	1.5T Siemens Avanto	Sagittal	160	0mm	1.3x1.3x1.2	100 0ms	3.60 ms	2400 ms	8	FreeSurfer (5.3.0)
		NCNG_b	3D T1-weighted magnetization prepared rapid acquisition gradient echo MPRAGE	1.5T Siemens Sonata	Sagittal	128	0mm	1.0x1.0x1.33	100 0ms	3.43 ms	2730 ms	7	FreeSurfer (5.3.0)

<b>NTR</b>	NCNG_c	T1-weighted 3D inversion recovery-prepared fast spoiled gradient-recalled acquisitions	1.5T GE Sigma	Sagittal	124	0mm	0.94x0.94x1.4	450 ms	1.77 ms	9.11 ms	7	FreeSurfer (5.3.0)
	NTR_1	3D T1-weighted magnetization prepared rapid acquisition gradient echo MPRAGE	1.5T Siemens Sonata	Sagittal	160	0mm	1.00x1.00x1.00	110 ms	3.93 ms	1900 ms	15	FreeSurfer (5.1.0)
	NTR_2	3D gradient-echo T1-weighted sequence (technique: T1TFF)	3.0T Philips Intera	Coronal	182	0mm	1.00x1.00x1.20	4.60 ms	4.60 ms	9.69 ms	8	FreeSurfer (5.1.0)
	NTR_3	3D T1-weighted magnetization prepared rapid acquisition gradient echo MPRAGE	1.5T Siemens Sonata	Coronal	160	0mm	1.00x1.00x1.50	300 ms	7.00 ms	15ms	8	FreeSurfer (5.1.0)
	NTR_41	3D spoiled gradient-echo T1-weighted sequence (technique: T1TFF)	1.5T Philips GyroScan Intera	Coronal	170-180	0mm	1.00x1.00x1.20	4.6 ms	4.6 ms	30ms	30	FreeSurfer (5.1.0)

	NTR_42	3D spoiled gradient-echo T1-weighted sequence (technique: T1FFE)	1.5T Philips GyroScan Intera	Coronal	170-180	0mm	1.00x1.00x1.20	4.6 ms	30ms	30	FreeSurfer (5.3.0)
	Brainscale	3D T1-weighted coronal spoiled gradient echo	1.5T Philips Achieva	Coronal	160-180	0mm	1.00x1.00x1.20	0ms	30ms	30	FreeSurfer (5.3.0)
<b>OSAKA</b>	OSAKA	3D T1-weighted fast spoiled gradient recall (3D FSPGR)	1.5T GE Signa EXCITE	Sagittal	124	1.4mm	0.9375x0.9375x1.4	400 ms	12.6 ms	15	FreeSurfer (5.3.0)
<b>OATS</b>	OATS_a	3D T1-weighted volumetric	Siemens Sonata 1.5T	Coronal	144	0mm	1x1x1.5mm	780 ms	3.24 ms	8	FreeSurfer (5.3.0)
	OATS_b	3D T1-weighted	1.5T Siemens Magnetom Avanto	Coronal	144	0	1x1x1.5	3.24	1530 ms	8	FreeSurfer (5.3.0)
	OATS_c	3D T1-weighted	3T Philips Achieva Quasar	Coronal	190	0	1x1x1	439	2.9 ms	8	FreeSurfer (5.3.0)
	OATS_d	T1FFE	1.5T Philips Gyroscan	Coronal	150	0	1x1x1.5	385	3.7 ms	8	FreeSurfer (5.3.0)
<b>PAFIP</b>	PAFIP	3D T1-weighted turbo field echo (TFE)	3T Philips Achieva	Sagittal	160	1	0.9375x0.9375x1	3.70 4ms	8.104 ms	8	FreeSurfer (5.3)
<b>PING</b>	PING_a	MPRAGE	3T Philips Achieva	Sagittal	170	0mm	1x1x1.2	845 ms	3.1 ms	8	FreeSurfer (4.5.0)
	PING_c	IRSPGR	3T GE Signa HDx	Sagittal	170	0mm	1x1x1.2	640 ms	3.45 2ms	8	FreeSurfer (4.5.0)
	PING_d	MPRAGE	3T Siemens TrioTim	Sagittal	160	0mm	1x1x1.2	110 0ms	4.33 ms	7	FreeSurfer (4.5.0)

	PING_f	MPRAGE	3T Siemens TrioTim	Sagittal	160	0mm	1x1x1.2	110 0ms	4.33 ms	2170 ms	7	FreeSurfer (4.5.0)
	PING_g	MPRAGE	3T Siemens TrioTim	Sagittal	160	0mm	1x1x1.2	110 0ms	4.33 ms	2170 ms	7	FreeSurfer (4.5.0)
	PING_h	MPRAGE	3T Phillips Achieva	Sagittal	170	0mm	1x1x1.2	845 ms	3.1 ms	6.8ms	8	FreeSurfer (4.5.0)
	PING_i	IRSPGR	3T GE Discovery MR750	Sagittal	170	0mm	1x1x1.2	640 ms	2.98 4ms	7.38 ms	8	FreeSurfer (4.5.0)
	PING_j	MPRAGE	3T Siemens TrioTim	Sagittal	160	0mm	1x1x1.2	110 0ms	4.33 ms	2170 ms	7	FreeSurfer (4.5.0)
	PING_l	MPRAGE	3T Siemens TrioTim	Sagittal	160	0mm	1x1x1.2	110 0ms	4.33 ms	2170 ms	7	FreeSurfer (4.5.0)
	PING_m	MPRAGE	3T Siemens TrioTim	Sagittal	160	0mm	1x1x1.2	110 0ms	4.33 ms	2170 ms	7	FreeSurfer (4.5.0)
<b>QTIM</b>	Population-based Twin Study	3D T1-weighted MPRAGE	4T Bruker Medspec	Coronal (85%), Sagittal (15%)	256 (coronal) , 240 (sagittal)	0.45m m	0.9375x0.9375x0.9	700 ms	3.35 ms	1500 ms	8	FreeSurfer (5.3)
<b>SHIP</b>	Population-based	3D T1-weighted magnetization prepared rapid acquisition gradient echo MPRAGE	1.5T Siemens Magnetom Avanto	Axial	176	0mm	1x1x1	110 0ms	3.4 ms	1900 ms	15	Subcortical: FreeSurfer (5.1.0); Cortical: FreeSurfer (5.3.0)
<b>STROKEMRI/ TOP3T</b>	Stroke project (only healthy controls)	3D gradient echo (TFE) sequence (FSPGR)	3T GE Signa HDxT	Sagittal	170	0 mm	1x1x1,2	450 6	2.95 ms	7.8 ms	12	FreeSurfer (5.3.0)

<b>SYS_ADOLESCENTS</b>	Population-based	SYS_CNG	3D T1-weighted RF-spoiled gradient-echo scan	Phillips 1.0-T superconducting magnet (Gyroscan NT; Philips Medical Systems, Best, the Netherlands)	Sagittal	140–160	0 mm	1x1x1	N/A	5ms	25ms	30	FreeSurfer (5.1.0)
<b>SYS_PARENTS</b>	Population-based	SYS_Reisch I	3D Magnetization Prepared Rapid Gradient Echo sequence	1.5 T Siemens (Avanto) scanner	Sagittal	176	0 mm	1x1x1	100	2.65	2400	8	FreeSurfer (5.1.0)
<b>TOP</b>	Case-control (SCZ, BD, other psychoses, and healthy controls)	TOP_1.5	3D T1-weighted magnetization prepared rapid acquisition gradient echo MPRAGE	1.5T GE Signa	Coronal	180	0mm	1.25x1.25x1.2	500	4ms	500ms	8	FreeSurfer (5.1.0)
<b>TROENDER BRAIN</b>	Case-control (Dementia and healthy controls)	StOlav	ADNI 3DT1	3T Philips Intera	Sagittal	170	0 mm	1,2x1,2x1,2		3,13	6,75	8	FreeSurfer (5.3.0)
<b>UCLA_UTRECHT</b>	Case-control (BP and healthy controls)	UCLA UTR ECHT_T3	3D T1-weighted fast field echo	3T Philips Achieva	Sagittal	220	0 mm	0.75x0.75x0.8		4.6	10	8	FreeSurfer (5.3.0)
		UCLA UTR ECHT_T1.5 I	3D T1-weighted fast field echo	1.5T Philips Achieva	Coronal	160-180	0 mm	1x1x1.2		4.6	30	30	FreeSurfer (5.1.0)
		UCLA UTR ECHT_T1.5 II	3D T1-weighted fast field echo	1.5T Philips NT	Coronal	160-180	0 mm	1x1x1.2		4.6	30	30	FreeSurfer (5.3.0)
		UCLA UTR ECHT_T1.5 III	3D T1-weighted fast field echo	1.5T Philips NT	Coronal	160-180	0 mm	1x1x1.2		4.6	30	30	FreeSurfer (5.3.0)

UCLA UTR ECHT_T1.5 IV	3D T1-weighted fast field echo	1.5T Philips NT	Coronal	160-180	0 mm	1x1x1.2	4.6 ms	30 ms	30	FreeSurfer (5.3.0)
UCLA UTR ECHT_T1.5 V	3D T1-weighted fast field echo	1.5T Philips NT	Coronal	160-180	0 mm	1x1x1.2	4.6 ms	30 ms	30	FreeSurfer (5.3.0)
UK BIOBANK Population-based volunteers	Cheadle 3D T1-weighted magnetization prepared rapid acquisition gradient echo MPRAGE	3T SIEMENS MAGNET OM Skyra syngo MR D13	Sagittal			1.0x1.0x1.0 mm	880 ms	2.01 ms	2000. 8 0 ms	FreeSurfer (5.3.0)
Newcastle	3D T1-weighted magnetization prepared rapid acquisition gradient echo MPRAGE	3T SIEMENS MAGNET OM Skyra syngo MR D13	Sagittal			1.0x1.0x1.0 mm	880 ms	2.01 ms	2000. 8 0 ms	FreeSurfer (5.3.0)
Reading	3D T1-weighted magnetization prepared rapid acquisition gradient echo MPRAGE	3T SIEMENS MAGNET OM Skyra syngo MR D13	Sagittal			1.0x1.0x1.0 mm	880 ms	2.01 ms	2000. 8 0 ms	FreeSurfer (5.3.0)

**Table S1.**

Association between RID scores and cognitive ability derived from the UK Biobank (using a discovery and replication sample).

<b>Region</b>	<b>Estimate</b>	<b>StdError</b>	<b>tvalue</b>	<b>pvalue</b>	<b>IndVar</b>	<b>pcorr</b>
lh_bankssts_thickness	-0.003	0.006	-0.566	0.571	Cognitive Ability	0.685
lh_caudalanteriorcingulate_thickness	-0.023	0.006	-3.939	0.000	Cognitive Ability	0.001
lh_caudalmiddlefrontal_thickness	-0.008	0.006	-1.341	0.180	Cognitive Ability	0.298
lh_cuneus_thickness	0.005	0.006	0.939	0.348	Cognitive Ability	0.488
lh_entorhinal_thickness	0.001	0.006	0.111	0.912	Cognitive Ability	0.957
lh_fusiform_thickness	-0.002	0.006	-0.371	0.710	Cognitive Ability	0.820
lh_inferiorparietal_thickness	-0.009	0.006	-1.613	0.107	Cognitive Ability	0.204
lh_inferiortemporal_thickness	-0.015	0.006	-2.593	0.010	Cognitive Ability	0.041
lh_isthmuscingulate_thickness	-0.017	0.006	-3.002	0.003	Cognitive Ability	0.015
lh_lateraloccipital_thickness	-0.036	0.006	-6.236	0.000	Cognitive Ability	0.000
lh_lateralorbitofrontal_thickness	-0.003	0.006	-0.542	0.588	Cognitive Ability	0.700
lh_lingual_thickness	-0.010	0.006	-1.781	0.075	Cognitive Ability	0.161
lh_medialorbitofrontal_thickness	-0.006	0.006	-0.991	0.322	Cognitive Ability	0.469
lh_middletemporal_thickness	-0.007	0.006	-1.300	0.194	Cognitive Ability	0.309
lh_parahippocampal_thickness	0.011	0.006	1.997	0.046	Cognitive Ability	0.115
lh_paracentral_thickness	0.009	0.006	1.484	0.138	Cognitive Ability	0.249
lh_parsopercularis_thickness	0.005	0.006	0.945	0.344	Cognitive Ability	0.487
lh_parsorbitalis_thickness	0.003	0.006	0.482	0.630	Cognitive Ability	0.744
lh_parstriangularis_thickness	-0.002	0.006	-0.329	0.742	Cognitive Ability	0.837
lh_pericalcarine_thickness	-0.008	0.006	-1.472	0.141	Cognitive Ability	0.249
lh_postcentral_thickness	0.025	0.006	4.391	0.000	Cognitive Ability	0.000
lh_posteriorcingulate_thickness	-0.008	0.006	-1.477	0.140	Cognitive Ability	0.249
lh_precentral_thickness	0.026	0.006	4.473	0.000	Cognitive Ability	0.000
lh_precuneus_thickness	0.002	0.006	0.344	0.730	Cognitive Ability	0.830
lh_rostralanteriorcingulate_thickness	-0.014	0.006	-2.454	0.014	Cognitive Ability	0.050
lh_rostralmiddlefrontal_thickness	0.012	0.006	2.012	0.044	Cognitive Ability	0.112
lh_superiorfrontal_thickness	-0.005	0.006	-0.922	0.357	Cognitive Ability	0.495
lh_superiorparietal_thickness	-0.001	0.006	-0.261	0.794	Cognitive Ability	0.870



lh_superiortemporal_thickness	0.035	0.006	6.110	0.000	Cognitive Ability	0.000
lh_supramarginal_thickness	0.021	0.006	3.724	0.000	Cognitive Ability	0.001
lh_frontalpole_thickness	-0.009	0.006	-1.623	0.105	Cognitive Ability	0.204
lh_temporalpole_thickness	0.011	0.006	1.900	0.057	Cognitive Ability	0.134
lh_transversetemporal_thickness	0.028	0.006	4.874	0.000	Cognitive Ability	0.000
lh_insula_thickness	0.028	0.006	4.865	0.000	Cognitive Ability	0.000
rh_bankssts_thickness	0.001	0.006	0.204	0.838	Cognitive Ability	0.892
rh_caudalanteriorcingulate_thickness	-0.022	0.006	-3.768	0.000	Cognitive Ability	0.001
rh_caudalmiddlefrontal_thickness	-0.012	0.006	-2.122	0.034	Cognitive Ability	0.094
rh_cuneus_thickness	-0.002	0.006	-0.314	0.753	Cognitive Ability	0.840
rh_entorhinal_thickness	-0.016	0.006	-2.735	0.006	Cognitive Ability	0.028
rh_fusiform_thickness	-0.002	0.006	-0.310	0.756	Cognitive Ability	0.840
rh_inferioparietal_thickness	-0.006	0.006	-0.967	0.333	Cognitive Ability	0.476
rh_inferiortemporal_thickness	0.004	0.006	0.652	0.515	Cognitive Ability	0.654
rh_isthmusingulate_thickness	-0.004	0.006	-0.619	0.536	Cognitive Ability	0.659
rh_lateraloccipital_thickness	-0.028	0.006	-4.819	0.000	Cognitive Ability	0.000
rh_lateralorbitofrontal_thickness	-0.005	0.006	-0.892	0.372	Cognitive Ability	0.507
rh_lingual_thickness	0.002	0.006	0.408	0.683	Cognitive Ability	0.794
rh_medialorbitofrontal_thickness	0.000	0.006	0.009	0.993	Cognitive Ability	0.993
rh_middletemporal_thickness	0.000	0.006	0.060	0.952	Cognitive Ability	0.974
rh parahippocampal_thickness	0.015	0.006	2.575	0.010	Cognitive Ability	0.041
rh_paracentral_thickness	-0.001	0.006	-0.214	0.831	Cognitive Ability	0.892
rh_parsopercularis_thickness	0.000	0.006	-0.036	0.971	Cognitive Ability	0.978
rh_parsorbitalis_thickness	-0.002	0.006	-0.356	0.722	Cognitive Ability	0.826
rh_parstriangularis_thickness	-0.018	0.006	-3.191	0.001	Cognitive Ability	0.008
rh_pericalcarine_thickness	-0.014	0.006	-2.422	0.015	Cognitive Ability	0.054
rh_postcentral_thickness	0.025	0.006	4.271	0.000	Cognitive Ability	0.000
rh_posteriorcingulate_thickness	-0.004	0.006	-0.621	0.534	Cognitive Ability	0.659
rh_precentral_thickness	0.023	0.006	3.979	0.000	Cognitive Ability	0.001
rh_precuneus_thickness	0.001	0.006	0.246	0.805	Cognitive Ability	0.875
rh_rostralanteriorcingulate_thickness	-0.009	0.006	-1.636	0.102	Cognitive Ability	0.201
rh_rostralmiddlefrontal_thickness	-0.002	0.006	-0.286	0.775	Cognitive Ability	0.855

rh_superiorfrontal_thickness	-0.008	0.006	-1.339	0.181	Cognitive Ability	0.298
rh_superiorparietal_thickness	-0.013	0.006	-2.331	0.020	Cognitive Ability	0.062
rh_superiortemporal_thickness	0.037	0.006	6.479	0.000	Cognitive Ability	0.000
rh_supramarginal_thickness	0.029	0.006	4.979	0.000	Cognitive Ability	0.000
rh_frontalpole_thickness	-0.011	0.006	-1.859	0.063	Cognitive Ability	0.144
rh_temporalpole_thickness	0.014	0.006	2.354	0.019	Cognitive Ability	0.060
rh_transversetemporal_thickness	0.010	0.006	1.723	0.085	Cognitive Ability	0.172
rh_insula_thickness	0.009	0.006	1.596	0.110	Cognitive Ability	0.207
lh_bankssts_area	-0.007	0.006	-1.191	0.233	Cognitive Ability	0.354
lh_caudalanteriorcingulate_area	-0.014	0.006	-2.512	0.012	Cognitive Ability	0.045
lh_caudalmiddlefrontal_area	-0.008	0.006	-1.363	0.173	Cognitive Ability	0.292
lh_cuneus_area	-0.013	0.006	-2.220	0.026	Cognitive Ability	0.079
lh_entorhinal_area	0.016	0.006	2.787	0.005	Cognitive Ability	0.026
lh_fusiform_area	0.005	0.006	0.799	0.424	Cognitive Ability	0.568
lh_inferiorparietal_area	0.005	0.006	0.897	0.370	Cognitive Ability	0.507
lh_inferiortemporal_area	0.011	0.006	1.851	0.064	Cognitive Ability	0.144
lh_isthmuscingulate_area	-0.012	0.006	-2.072	0.038	Cognitive Ability	0.102
lh_lateraloccipital_area	0.006	0.006	0.971	0.331	Cognitive Ability	0.476
lh_lateralorbitofrontal_area	0.024	0.006	4.157	0.000	Cognitive Ability	0.000
lh_lingual_area	-0.007	0.006	-1.254	0.210	Cognitive Ability	0.328
lh_medialorbitofrontal_area	0.004	0.006	0.666	0.505	Cognitive Ability	0.648
lh_middletemporal_area	0.013	0.006	2.240	0.025	Cognitive Ability	0.077
lh parahippocampal_area	-0.016	0.006	-2.744	0.006	Cognitive Ability	0.028
lh_paracentral_area	-0.022	0.006	-3.803	0.000	Cognitive Ability	0.001
lh_parsopercularis_area	0.000	0.006	0.039	0.969	Cognitive Ability	0.978
lh_parsorbitalis_area	0.010	0.006	1.759	0.079	Cognitive Ability	0.166
lh_parstriangularis_area	0.010	0.006	1.738	0.082	Cognitive Ability	0.171
lh_pericalcarine_area	0.004	0.006	0.640	0.522	Cognitive Ability	0.658
lh_postcentral_area	-0.012	0.006	-2.029	0.042	Cognitive Ability	0.111
lh_posteriorcingulate_area	-0.014	0.006	-2.380	0.017	Cognitive Ability	0.058
lh_precentral_area	0.003	0.006	0.470	0.638	Cognitive Ability	0.748
lh_precuneus_area	-0.014	0.006	-2.348	0.019	Cognitive Ability	0.060

lh_rostralanteriorcingulate_area	-0.008	0.006	-1.400	0.162	Cognitive Ability	0.279
lh_rostralmiddlefrontal_area	0.009	0.006	1.553	0.121	Cognitive Ability	0.223
lh_superiorfrontal_area	0.015	0.006	2.582	0.010	Cognitive Ability	0.041
lh_superiorparietal_area	-0.019	0.006	-3.284	0.001	Cognitive Ability	0.006
lh_superiortemporal_area	0.034	0.006	5.974	0.000	Cognitive Ability	0.000
lh_supramarginal_area	-0.001	0.006	-0.195	0.845	Cognitive Ability	0.893
lh_frontalpole_area	-0.007	0.006	-1.200	0.230	Cognitive Ability	0.352
lh_temporalpole_area	-0.004	0.006	-0.734	0.463	Cognitive Ability	0.609
lh_transversetemporal_area	0.004	0.006	0.710	0.478	Cognitive Ability	0.623
lh_insula_area	0.028	0.006	4.844	0.000	Cognitive Ability	0.000
rh_bankssts_area	0.008	0.006	1.379	0.168	Cognitive Ability	0.286
rh_caudalanteriorcingulate_area	-0.010	0.006	-1.680	0.093	Cognitive Ability	0.186
rh_caudalmiddlefrontal_area	-0.008	0.006	-1.310	0.190	Cognitive Ability	0.307
rh_cuneus_area	-0.017	0.006	-2.921	0.003	Cognitive Ability	0.019
rh_entorhinal_area	0.003	0.006	0.579	0.563	Cognitive Ability	0.680
rh_fusiform_area	0.011	0.006	1.944	0.052	Cognitive Ability	0.126
rh_inferioparietal_area	0.007	0.006	1.237	0.216	Cognitive Ability	0.334
rh_inferiortemporal_area	0.000	0.006	0.072	0.943	Cognitive Ability	0.974
rh_isthmuscingulate_area	-0.020	0.006	-3.520	0.000	Cognitive Ability	0.003
rh_lateraloccipital_area	0.012	0.006	2.127	0.033	Cognitive Ability	0.094
rh_lateralorbitofrontal_area	0.009	0.006	1.510	0.131	Cognitive Ability	0.240
rh_lingual_area	-0.015	0.006	-2.524	0.012	Cognitive Ability	0.045
rh_medialorbitofrontal_area	0.010	0.006	1.725	0.085	Cognitive Ability	0.172
rh_middletemporal_area	0.014	0.006	2.379	0.017	Cognitive Ability	0.058
rh parahippocampal_area	-0.009	0.006	-1.611	0.107	Cognitive Ability	0.204
rh_paracentral_area	-0.008	0.006	-1.402	0.161	Cognitive Ability	0.279
rh_parsopercularis_area	-0.005	0.006	-0.887	0.375	Cognitive Ability	0.507
rh_parsorbitalis_area	0.008	0.006	1.333	0.183	Cognitive Ability	0.298
rh_parsstriangularis_area	0.011	0.006	1.977	0.048	Cognitive Ability	0.118
rh_pericalcarine_area	-0.004	0.006	-0.625	0.532	Cognitive Ability	0.659
rh_postcentral_area	-0.012	0.006	-2.093	0.036	Cognitive Ability	0.099
rh_posteriorcingulate_area	-0.012	0.006	-2.023	0.043	Cognitive Ability	0.111

rh_precentral_area	-0.005	0.006	-0.793	0.428	Cognitive Ability	0.568
rh_precuneus_area	-0.007	0.006	-1.291	0.197	Cognitive Ability	0.311
rh_rostralanteriorcingulate_area	-0.010	0.006	-1.818	0.069	Cognitive Ability	0.150
rh_rostralmiddlefrontal_area	0.011	0.006	1.930	0.054	Cognitive Ability	0.128
rh_superiorfrontal_area	0.016	0.006	2.766	0.006	Cognitive Ability	0.027
rh_superiorparietal_area	-0.024	0.006	-4.203	0.000	Cognitive Ability	0.000
rh_superiortemporal_area	0.032	0.006	5.641	0.000	Cognitive Ability	0.000
rh_supramarginal_area	-0.007	0.006	-1.148	0.251	Cognitive Ability	0.373
rh_frontalpole_area	-0.003	0.006	-0.586	0.558	Cognitive Ability	0.680
rh_temporalpole_area	-0.021	0.006	-3.717	0.000	Cognitive Ability	0.001
rh_transverse temporal_area	0.007	0.006	1.169	0.242	Cognitive Ability	0.364
rh_insula_area	0.028	0.006	4.848	0.000	Cognitive Ability	0.000
Left-Thalamus-Proper	0.011	0.006	1.847	0.065	Cognitive Ability	0.144
Right-Thalamus-Proper	0.011	0.006	1.844	0.065	Cognitive Ability	0.144
Left-Caudate	0.000	0.006	-0.077	0.939	Cognitive Ability	0.974
Right-Caudate	0.004	0.006	0.688	0.491	Cognitive Ability	0.635
Left-Putamen	-0.017	0.006	-2.904	0.004	Cognitive Ability	0.019
Right-Putamen	-0.013	0.006	-2.181	0.029	Cognitive Ability	0.084
Left-Pallidum	-0.020	0.006	-3.551	0.000	Cognitive Ability	0.003
Right-Pallidum	0.000	0.006	0.057	0.955	Cognitive Ability	0.974
Left-Hippocampus	0.017	0.006	2.899	0.004	Cognitive Ability	0.019
Right-Hippocampus	0.014	0.006	2.477	0.013	Cognitive Ability	0.049
Left-Amygdala	-0.001	0.006	-0.205	0.838	Cognitive Ability	0.892
Right-Amygdala	-0.007	0.006	-1.138	0.255	Cognitive Ability	0.375
Left-Accumbens-area	-0.013	0.006	-2.212	0.027	Cognitive Ability	0.079
Right-Accumbens-area	0.015	0.006	2.539	0.011	Cognitive Ability	0.044

Test_Region	Test_Estimate	Test_StdError	Test_tvalue	Test_pvalue	Test_IndVar	Pdic
lh_bankssts_thickness	0.006	0.010	0.572	0.567	Cognitive Ability	P > .05
lh_caudalanteriorcingulate_thickness	-0.007	0.010	-0.711	0.477	Cognitive Ability	P > .05
lh_caudalmiddlefrontal_thickness	-0.006	0.010	-0.642	0.521	Cognitive Ability	P > .05
lh_cuneus_thickness	-0.011	0.010	-1.094	0.274	Cognitive Ability	P > .05

lh_entorhinal_thickness	0.006	0.010	0.651	0.515	Cognitive Ability	P > .05
lh_fusiform_thickness	0.009	0.010	0.887	0.375	Cognitive Ability	P > .05
lh_inferiorparietal_thickness	0.002	0.010	0.161	0.872	Cognitive Ability	P > .05
lh_inferiortemporal_thickness	0.012	0.010	1.238	0.216	Cognitive Ability	P > .05
lh_isthmuscingulate_thickness	-0.017	0.010	-1.669	0.095	Cognitive Ability	P > .05
lh_lateraloccipital_thickness	-0.013	0.010	-1.283	0.200	Cognitive Ability	P > .05
lh_lateralorbitofrontal_thickness	-0.001	0.010	-0.127	0.899	Cognitive Ability	P > .05
lh_lingual_thickness	0.002	0.010	0.206	0.837	Cognitive Ability	P > .05
lh_medialorbitofrontal_thickness	-0.007	0.010	-0.665	0.506	Cognitive Ability	P > .05
lh_middletemporal_thickness	0.026	0.010	2.579	0.010	Cognitive Ability	P > .05
lh parahippocampal_thickness	0.024	0.010	2.426	0.015	Cognitive Ability	P > .05
lh_paracentral_thickness	0.005	0.010	0.543	0.587	Cognitive Ability	P > .05
lh_parsopercularis_thickness	0.002	0.010	0.212	0.832	Cognitive Ability	P > .05
lh_parsorbitalis_thickness	0.002	0.010	0.168	0.866	Cognitive Ability	P > .05
lh_parsotriangularis_thickness	0.005	0.010	0.533	0.594	Cognitive Ability	P > .05
lh_pericalcarine_thickness	-0.011	0.010	-1.102	0.271	Cognitive Ability	P > .05
lh_postcentral_thickness	0.017	0.010	1.666	0.096	Cognitive Ability	P > .05
lh_posteriorcingulate_thickness	-0.029	0.010	-2.872	0.004	Cognitive Ability	P > .05
lh_precentral_thickness	0.035	0.010	3.483	0.000	Cognitive Ability	P < .05
lh_precuneus_thickness	-0.010	0.010	-1.050	0.294	Cognitive Ability	P > .05
lh_rostralanteriorcingulate_thickness	-0.015	0.010	-1.473	0.141	Cognitive Ability	P > .05
lh_rostralmiddlefrontal_thickness	-0.002	0.010	-0.208	0.835	Cognitive Ability	P > .05
lh_superiorfrontal_thickness	-0.010	0.010	-0.960	0.337	Cognitive Ability	P > .05
lh_superiorparietal_thickness	-0.014	0.010	-1.358	0.174	Cognitive Ability	P > .05
lh_superiortemporal_thickness	0.049	0.010	4.880	0.000	Cognitive Ability	P < .05
lh_supramarginal_thickness	0.027	0.010	2.759	0.006	Cognitive Ability	P < .05
lh_frontalpole_thickness	-0.014	0.010	-1.400	0.162	Cognitive Ability	P > .05
lh_temporalpole_thickness	0.018	0.010	1.843	0.065	Cognitive Ability	P > .05
lh_transversetemporal_thickness	0.006	0.010	0.597	0.551	Cognitive Ability	P > .05
lh_insula_thickness	0.014	0.010	1.393	0.164	Cognitive Ability	P > .05
rh_bankssts_thickness	-0.019	0.010	-1.859	0.063	Cognitive Ability	P > .05
rh_caudalanteriorcingulate_thickness	-0.031	0.010	-3.121	0.002	Cognitive Ability	P < .05

rh_caudalmiddlefrontal_thickness	-0.019	0.010	-1.869	0.062	Cognitive Ability	P > .05
rh_cuneus_thickness	-0.004	0.010	-0.390	0.697	Cognitive Ability	P > .05
rh_entorhinal_thickness	-0.011	0.010	-1.148	0.251	Cognitive Ability	P > .05
rh_fusiform_thickness	0.009	0.010	0.884	0.377	Cognitive Ability	P > .05
rh_inferiorparietal_thickness	0.003	0.010	0.351	0.726	Cognitive Ability	P > .05
rh_inferiortemporal_thickness	0.008	0.010	0.822	0.411	Cognitive Ability	P > .05
rh_isthmuscingulate_thickness	0.001	0.010	0.052	0.959	Cognitive Ability	P > .05
rh_lateraloccipital_thickness	-0.005	0.010	-0.505	0.614	Cognitive Ability	P > .05
rh_lateralorbitofrontal_thickness	-0.016	0.010	-1.635	0.102	Cognitive Ability	P > .05
rh_lingual_thickness	0.004	0.010	0.407	0.684	Cognitive Ability	P > .05
rh_medialorbitofrontal_thickness	-0.023	0.010	-2.328	0.020	Cognitive Ability	P > .05
rh_middletemporal_thickness	0.005	0.010	0.496	0.620	Cognitive Ability	P > .05
rh_parahippocampal_thickness	0.025	0.010	2.559	0.011	Cognitive Ability	P < .05
rh_paracentral_thickness	-0.004	0.010	-0.410	0.682	Cognitive Ability	P > .05
rh_parsopercularis_thickness	0.009	0.010	0.860	0.390	Cognitive Ability	P > .05
rh_parsorbitalis_thickness	0.005	0.010	0.499	0.618	Cognitive Ability	P > .05
rh_parstriangularis_thickness	-0.008	0.010	-0.805	0.421	Cognitive Ability	P > .05
rh_pericalcarine_thickness	-0.002	0.010	-0.212	0.832	Cognitive Ability	P > .05
rh_postcentral_thickness	0.005	0.010	0.492	0.623	Cognitive Ability	P > .05
rh_posteriorcingulate_thickness	-0.018	0.010	-1.851	0.064	Cognitive Ability	P > .05
rh_precentral_thickness	0.027	0.010	2.741	0.006	Cognitive Ability	P < .05
rh_precuneus_thickness	0.000	0.010	-0.001	0.999	Cognitive Ability	P > .05
rh_rostralanteriorcingulate_thickness	-0.022	0.010	-2.252	0.024	Cognitive Ability	P > .05
rh_rostralmiddlefrontal_thickness	-0.011	0.010	-1.093	0.274	Cognitive Ability	P > .05
rh_superiorfrontal_thickness	-0.012	0.010	-1.245	0.213	Cognitive Ability	P > .05
rh_superiorparietal_thickness	-0.019	0.010	-1.918	0.055	Cognitive Ability	P > .05
rh_superiortemporal_thickness	0.051	0.010	5.090	0.000	Cognitive Ability	P < .05
rh_supramarginal_thickness	0.020	0.010	2.000	0.045	Cognitive Ability	P < .05
rh_frontalpole_thickness	-0.013	0.010	-1.283	0.199	Cognitive Ability	P > .05
rh_temporalpole_thickness	0.013	0.010	1.303	0.193	Cognitive Ability	P > .05
rh_transversetemporal_thickness	-0.011	0.010	-1.149	0.250	Cognitive Ability	P > .05
rh_insula_thickness	-0.008	0.010	-0.778	0.437	Cognitive Ability	P > .05

lh_bankssts_area	0.009	0.010	0.898	0.369	Cognitive Ability	P > .05
lh_caudalanteriorcingulate_area	-0.024	0.010	-2.420	0.016	Cognitive Ability	P < .05
lh_caudalmiddlefrontal_area	-0.013	0.010	-1.352	0.176	Cognitive Ability	P > .05
lh_cuneus_area	-0.012	0.010	-1.236	0.216	Cognitive Ability	P > .05
lh_entorhinal_area	0.030	0.010	2.992	0.003	Cognitive Ability	P < .05
lh_fusiform_area	0.022	0.010	2.164	0.030	Cognitive Ability	P > .05
lh_inferiorparietal_area	0.002	0.010	0.239	0.811	Cognitive Ability	P > .05
lh_inferiortemporal_area	0.016	0.010	1.644	0.100	Cognitive Ability	P > .05
lh_isthmuscingulate_area	-0.003	0.010	-0.305	0.761	Cognitive Ability	P > .05
lh_lateraloccipital_area	-0.006	0.010	-0.556	0.578	Cognitive Ability	P > .05
lh_lateralorbitofrontal_area	0.027	0.010	2.717	0.007	Cognitive Ability	P < .05
lh_lingual_area	0.007	0.010	0.710	0.478	Cognitive Ability	P > .05
lh_medialorbitofrontal_area	-0.009	0.010	-0.855	0.392	Cognitive Ability	P > .05
lh_middletemporal_area	0.002	0.010	0.244	0.807	Cognitive Ability	P > .05
lh parahippocampal_area	-0.027	0.010	-2.704	0.007	Cognitive Ability	P < .05
lh_paracentral_area	-0.042	0.010	-4.256	0.000	Cognitive Ability	P < .05
lh_parsopercularis_area	-0.017	0.010	-1.722	0.085	Cognitive Ability	P > .05
lh_parsorbitalis_area	0.020	0.010	2.052	0.040	Cognitive Ability	P > .05
lh_parstriangularis_area	0.025	0.010	2.472	0.013	Cognitive Ability	P > .05
lh_pericalcarine_area	-0.006	0.010	-0.629	0.530	Cognitive Ability	P > .05
lh_postcentral_area	-0.011	0.010	-1.140	0.254	Cognitive Ability	P > .05
lh_posteriorcingulate_area	-0.001	0.010	-0.051	0.959	Cognitive Ability	P > .05
lh_precentral_area	-0.013	0.010	-1.306	0.192	Cognitive Ability	P > .05
lh_precuneus_area	0.002	0.010	0.214	0.831	Cognitive Ability	P > .05
lh_rostralanteriorcingulate_area	-0.025	0.010	-2.517	0.012	Cognitive Ability	P > .05
lh_rostralmiddlefrontal_area	0.019	0.010	1.942	0.052	Cognitive Ability	P > .05
lh_superiorfrontal_area	0.010	0.010	0.973	0.331	Cognitive Ability	P > .05
lh_superiorparietal_area	-0.014	0.010	-1.360	0.174	Cognitive Ability	P > .05
lh_superiortemporal_area	0.042	0.010	4.207	0.000	Cognitive Ability	P < .05
lh_supramarginal_area	0.008	0.010	0.851	0.395	Cognitive Ability	P > .05
lh_frontalpole_area	0.001	0.010	0.120	0.904	Cognitive Ability	P > .05
lh_temporalpole_area	-0.007	0.010	-0.688	0.491	Cognitive Ability	P > .05

lh_transversetemporal_area	0.010	0.010	1.028	0.304	Cognitive Ability	P > .05
lh_insula_area	0.015	0.010	1.490	0.136	Cognitive Ability	P > .05
rh_bankssts_area	0.001	0.010	0.096	0.923	Cognitive Ability	P > .05
rh_caudalanteriorcingulate_area	-0.005	0.010	-0.526	0.599	Cognitive Ability	P > .05
rh_caudalmiddlefrontal_area	-0.029	0.010	-2.866	0.004	Cognitive Ability	P > .05
rh_cuneus_area	-0.008	0.010	-0.845	0.398	Cognitive Ability	P > .05
rh_entorhinal_area	0.012	0.010	1.230	0.219	Cognitive Ability	P > .05
rh_fusiform_area	0.012	0.010	1.244	0.213	Cognitive Ability	P > .05
rh_inferiorparietal_area	0.014	0.010	1.377	0.169	Cognitive Ability	P > .05
rh_inferiortemporal_area	0.017	0.010	1.744	0.081	Cognitive Ability	P > .05
rh_isthmuscingulate_area	-0.042	0.010	-4.232	0.000	Cognitive Ability	P < .05
rh_lateraloccipital_area	-0.007	0.010	-0.717	0.473	Cognitive Ability	P > .05
rh_lateralorbitofrontal_area	0.035	0.010	3.509	0.000	Cognitive Ability	P > .05
rh_lingual_area	-0.017	0.010	-1.694	0.090	Cognitive Ability	P > .05
rh_medialorbitofrontal_area	0.011	0.010	1.089	0.276	Cognitive Ability	P > .05
rh_middletemporal_area	0.011	0.010	1.076	0.282	Cognitive Ability	P > .05
rh parahippocampal_area	-0.012	0.010	-1.241	0.214	Cognitive Ability	P > .05
rh_paracentral_area	-0.025	0.010	-2.506	0.012	Cognitive Ability	P > .05
rh_parsopercularis_area	-0.027	0.010	-2.690	0.007	Cognitive Ability	P > .05
rh_parsorbitalis_area	0.034	0.010	3.369	0.001	Cognitive Ability	P > .05
rh_parstriangularis_area	0.015	0.010	1.556	0.120	Cognitive Ability	P > .05
rh_pericalcarine_area	-0.008	0.010	-0.850	0.396	Cognitive Ability	P > .05
rh_postcentral_area	-0.009	0.010	-0.888	0.375	Cognitive Ability	P > .05
rh_posteriorcingulate_area	-0.010	0.010	-0.977	0.329	Cognitive Ability	P > .05
rh_precentral_area	-0.005	0.010	-0.493	0.622	Cognitive Ability	P > .05
rh_precuneus_area	0.003	0.010	0.291	0.771	Cognitive Ability	P > .05
rh_rostralanteriorcingulate_area	-0.022	0.010	-2.237	0.025	Cognitive Ability	P > .05
rh_rostralmiddlefrontal_area	0.019	0.010	1.917	0.055	Cognitive Ability	P > .05
rh_superiorfrontal_area	0.014	0.010	1.386	0.166	Cognitive Ability	P > .05
rh_superiorparietal_area	-0.005	0.010	-0.471	0.638	Cognitive Ability	P > .05
rh_superiortemporal_area	0.031	0.010	3.133	0.002	Cognitive Ability	P < .05
rh_supramarginal_area	-0.010	0.010	-0.982	0.326	Cognitive Ability	P > .05



rh_frontalpole_area	-0.028	0.010	-2.826	0.005	Cognitive Ability	P > .05
rh_temporalpole_area	-0.024	0.010	-2.422	0.015	Cognitive Ability	P < .05
rh_transversetemporal_area	0.028	0.010	2.798	0.005	Cognitive Ability	P > .05
rh_insula_area	0.021	0.010	2.147	0.032	Cognitive Ability	P < .05
Left-Thalamus-Proper	0.015	0.010	1.532	0.126	Cognitive Ability	P > .05
Right-Thalamus-Proper	0.012	0.010	1.233	0.218	Cognitive Ability	P > .05
Left-Caudate	-0.005	0.010	-0.527	0.599	Cognitive Ability	P > .05
Right-Caudate	-0.017	0.010	-1.661	0.097	Cognitive Ability	P > .05
Left-Putamen	-0.015	0.010	-1.530	0.126	Cognitive Ability	P > .05
Right-Putamen	-0.008	0.010	-0.757	0.449	Cognitive Ability	P > .05
Left-Pallidum	-0.033	0.010	-3.348	0.001	Cognitive Ability	P < .05
Right-Pallidum	-0.007	0.010	-0.729	0.466	Cognitive Ability	P > .05
Left-Hippocampus	0.027	0.010	2.676	0.007	Cognitive Ability	P < .05
Right-Hippocampus	0.014	0.010	1.358	0.174	Cognitive Ability	P > .05
Left-Amygdala	0.003	0.010	0.320	0.749	Cognitive Ability	P > .05
Right-Amygdala	0.006	0.010	0.607	0.544	Cognitive Ability	P > .05
Left-Accumbens-area	-0.005	0.010	-0.551	0.582	Cognitive Ability	P > .05
Right-Accumbens-area	0.015	0.010	1.500	0.134	Cognitive Ability	P > .05

Association between Z scores and cognitive ability derived from the UK Biobank (using a discovery and replication sample).

Region	Estimate	StdError	tvalue	pvalue	IndVar	pcorr
lh_bankssts_thickness	0.017	0.006	2.938	0.003	Cognitive Ability	0.006
lh_caudalanteriorcingulate_thickness	-0.005	0.006	-0.923	0.356	Cognitive Ability	0.393
lh_caudalmiddlefrontal_thickness	0.013	0.006	2.299	0.022	Cognitive Ability	0.031
lh_cuneus_thickness	0.023	0.006	4.001	0.000	Cognitive Ability	0.000
lh_entorhinal_thickness	0.019	0.006	3.314	0.001	Cognitive Ability	0.002
lh_fusiform_thickness	0.018	0.006	3.084	0.002	Cognitive Ability	0.004
lh_inferiorparietal_thickness	0.012	0.006	2.159	0.031	Cognitive Ability	0.042
lh_inferiortemporal_thickness	0.006	0.006	1.062	0.288	Cognitive Ability	0.320
lh_isthmusingulate_thickness	0.002	0.006	0.411	0.681	Cognitive Ability	0.699
lh_lateraloccipital_thickness	-0.009	0.006	-1.611	0.107	Cognitive Ability	0.131

lh_lateralorbitofrontal_thickness	0.015	0.006	2.573	0.010	Cognitive Ability	0.016
lh_lingual_thickness	0.009	0.006	1.637	0.102	Cognitive Ability	0.126
lh_medialorbitofrontal_thickness	0.012	0.006	2.044	0.041	Cognitive Ability	0.055
lh_middletemporal_thickness	0.013	0.006	2.248	0.025	Cognitive Ability	0.034
lh parahippocampal_thickness	0.029	0.006	5.084	0.000	Cognitive Ability	0.000
lh_paracentral_thickness	0.024	0.006	4.200	0.000	Cognitive Ability	0.000
lh_parsopercularis_thickness	0.023	0.006	4.072	0.000	Cognitive Ability	0.000
lh_parsorbitalis_thickness	0.020	0.006	3.547	0.000	Cognitive Ability	0.001
lh_parstriangularis_thickness	0.016	0.006	2.773	0.006	Cognitive Ability	0.010
lh_pericalcarine_thickness	0.010	0.006	1.735	0.083	Cognitive Ability	0.105
lh_postcentral_thickness	0.037	0.006	6.479	0.000	Cognitive Ability	0.000
lh_posteriorcingulate_thickness	0.010	0.006	1.717	0.086	Cognitive Ability	0.109
lh_precentral_thickness	0.037	0.006	6.445	0.000	Cognitive Ability	0.000
lh_precuneus_thickness	0.020	0.006	3.480	0.001	Cognitive Ability	0.001
lh_rostralanteriorcingulate_thickness	0.004	0.006	0.612	0.540	Cognitive Ability	0.567
lh_rostralmiddlefrontal_thickness	0.026	0.006	4.472	0.000	Cognitive Ability	0.000
lh_superiorfrontal_thickness	0.015	0.006	2.612	0.009	Cognitive Ability	0.014
lh_superiorparietal_thickness	0.017	0.006	3.025	0.002	Cognitive Ability	0.005
lh_superiortemporal_thickness	0.046	0.006	7.991	0.000	Cognitive Ability	0.000
lh_supramarginal_thickness	0.034	0.006	5.920	0.000	Cognitive Ability	0.000
lh_frontalpole_thickness	0.009	0.006	1.552	0.121	Cognitive Ability	0.143
lh_temporalpole_thickness	0.027	0.006	4.647	0.000	Cognitive Ability	0.000
lh_transversetemporal_thickness	0.043	0.006	7.406	0.000	Cognitive Ability	0.000
lh_insula_thickness	0.042	0.006	7.356	0.000	Cognitive Ability	0.000
rh_bankssts_thickness	0.020	0.006	3.489	0.000	Cognitive Ability	0.001
rh_caudalanteriorcingulate_thickness	-0.004	0.006	-0.753	0.451	Cognitive Ability	0.487
rh_caudalmiddlefrontal_thickness	0.009	0.006	1.573	0.116	Cognitive Ability	0.139
rh_cuneus_thickness	0.016	0.006	2.775	0.006	Cognitive Ability	0.010
rh_entorhinal_thickness	0.003	0.006	0.567	0.571	Cognitive Ability	0.595
rh_fusiform_thickness	0.017	0.006	3.030	0.002	Cognitive Ability	0.005
rh_inferiorparietal_thickness	0.016	0.006	2.702	0.007	Cognitive Ability	0.011
rh_inferiortemporal_thickness	0.021	0.006	3.632	0.000	Cognitive Ability	0.001

rh_isthmusingulate_thickness	0.015	0.006	2.560	0.010	Cognitive Ability	0.016
rh_lateraloccipital_thickness	-0.002	0.006	-0.422	0.673	Cognitive Ability	0.696
rh_lateralorbitofrontal_thickness	0.013	0.006	2.198	0.028	Cognitive Ability	0.038
rh_lingual_thickness	0.019	0.006	3.374	0.001	Cognitive Ability	0.002
rh_medialorbitofrontal_thickness	0.016	0.006	2.792	0.005	Cognitive Ability	0.009
rh_middletemporal_thickness	0.019	0.006	3.238	0.001	Cognitive Ability	0.002
rh_parahippocampal_thickness	0.032	0.006	5.604	0.000	Cognitive Ability	0.000
rh_paracentral_thickness	0.018	0.006	3.131	0.002	Cognitive Ability	0.003
rh_parsopercularis_thickness	0.020	0.006	3.430	0.001	Cognitive Ability	0.001
rh_parsorbitalis_thickness	0.014	0.006	2.468	0.014	Cognitive Ability	0.020
rh_parsotriangularis_thickness	0.004	0.006	0.627	0.531	Cognitive Ability	0.560
rh_pericalcarine_thickness	0.004	0.006	0.693	0.488	Cognitive Ability	0.523
rh_postcentral_thickness	0.037	0.006	6.509	0.000	Cognitive Ability	0.000
rh_posteriorcingulate_thickness	0.016	0.006	2.696	0.007	Cognitive Ability	0.012
rh_precentral_thickness	0.034	0.006	5.999	0.000	Cognitive Ability	0.000
rh_precuneus_thickness	0.019	0.006	3.248	0.001	Cognitive Ability	0.002
rh_rostralanteriorcingulate_thickness	0.007	0.006	1.273	0.203	Cognitive Ability	0.232
rh_rostralmiddlefrontal_thickness	0.016	0.006	2.720	0.007	Cognitive Ability	0.011
rh_superiorfrontal_thickness	0.013	0.006	2.294	0.022	Cognitive Ability	0.031
rh_superiorparietal_thickness	0.009	0.006	1.557	0.120	Cognitive Ability	0.142
rh_superiotemporal_thickness	0.047	0.006	8.122	0.000	Cognitive Ability	0.000
rh_supramarginal_thickness	0.039	0.006	6.744	0.000	Cognitive Ability	0.000
rh_frontalpole_thickness	0.006	0.006	1.082	0.279	Cognitive Ability	0.313
rh_temporalpole_thickness	0.030	0.006	5.194	0.000	Cognitive Ability	0.000
rh_transversetemporal_thickness	0.027	0.006	4.659	0.000	Cognitive Ability	0.000
rh_insula_thickness	0.027	0.006	4.632	0.000	Cognitive Ability	0.000
lh_bankssts_area	0.015	0.006	2.680	0.007	Cognitive Ability	0.012
lh_caudalanteriorcingulate_area	0.008	0.006	1.319	0.187	Cognitive Ability	0.219
lh_caudalmiddlefrontal_area	0.015	0.006	2.657	0.008	Cognitive Ability	0.013
lh_cuneus_area	0.007	0.006	1.154	0.249	Cognitive Ability	0.280
lh_entorhinal_area	0.037	0.006	6.480	0.000	Cognitive Ability	0.000
lh_fusiform_area	0.024	0.006	4.146	0.000	Cognitive Ability	0.000

lh_inferioparietal_area	0.026	0.006	4.548	0.000	Cognitive Ability	0.000
lh_inferiortemporal_area	0.030	0.006	5.256	0.000	Cognitive Ability	0.000
lh_isthmuscingulate_area	0.011	0.006	1.925	0.054	Cognitive Ability	0.071
lh_lateraloccipital_area	0.025	0.006	4.365	0.000	Cognitive Ability	0.000
lh_lateralorbitofrontal_area	0.042	0.006	7.277	0.000	Cognitive Ability	0.000
lh_lingual_area	0.014	0.006	2.511	0.012	Cognitive Ability	0.018
lh_medialorbitofrontal_area	0.024	0.006	4.169	0.000	Cognitive Ability	0.000
lh_middletemporal_area	0.032	0.006	5.591	0.000	Cognitive Ability	0.000
lh parahippocampal_area	0.007	0.006	1.181	0.237	Cognitive Ability	0.270
lh_paracentral_area	0.001	0.006	0.222	0.824	Cognitive Ability	0.833
lh_parsopercularis_area	0.022	0.006	3.772	0.000	Cognitive Ability	0.000
lh_parsorbitalis_area	0.030	0.006	5.217	0.000	Cognitive Ability	0.000
lh_parsstriangularis_area	0.029	0.006	5.093	0.000	Cognitive Ability	0.000
lh_pericalcarine_area	0.023	0.006	3.928	0.000	Cognitive Ability	0.000
lh_postcentral_area	0.011	0.006	1.855	0.064	Cognitive Ability	0.083
lh_posteriorcingulate_area	0.009	0.006	1.623	0.105	Cognitive Ability	0.129
lh_precentral_area	0.023	0.006	3.951	0.000	Cognitive Ability	0.000
lh_precuneus_area	0.009	0.006	1.593	0.111	Cognitive Ability	0.134
lh_rostralanteriorcingulate_area	0.014	0.006	2.458	0.014	Cognitive Ability	0.021
lh_rostralmiddlefrontal_area	0.027	0.006	4.732	0.000	Cognitive Ability	0.000
lh_superiorfrontal_area	0.032	0.006	5.640	0.000	Cognitive Ability	0.000
lh_superiorparietal_area	0.005	0.006	0.811	0.417	Cognitive Ability	0.457
lh_superiortemporal_area	0.052	0.006	9.064	0.000	Cognitive Ability	0.000
lh_supramarginal_area	0.020	0.006	3.438	0.001	Cognitive Ability	0.001
lh_frontalpole_area	0.016	0.006	2.759	0.006	Cognitive Ability	0.010
lh_temporalpole_area	0.016	0.006	2.845	0.004	Cognitive Ability	0.008
lh_transversetemporal_area	0.028	0.006	4.828	0.000	Cognitive Ability	0.000
lh_insula_area	0.046	0.006	7.925	0.000	Cognitive Ability	0.000
rh_bankssts_area	0.031	0.006	5.364	0.000	Cognitive Ability	0.000
rh_caudalanteriorcingulate_area	0.012	0.006	2.014	0.044	Cognitive Ability	0.058
rh_caudalmiddlefrontal_area	0.014	0.006	2.404	0.016	Cognitive Ability	0.024
rh_cuneus_area	0.005	0.006	0.784	0.433	Cognitive Ability	0.471

rh_entorhinal_area	0.024	0.006	4.228	0.000	Cognitive Ability	0.000
rh_fusiform_area	0.030	0.006	5.295	0.000	Cognitive Ability	0.000
rh_inferioparietal_area	0.027	0.006	4.763	0.000	Cognitive Ability	0.000
rh_inferiortemporal_area	0.021	0.006	3.656	0.000	Cognitive Ability	0.001
rh_isthmuscingulate_area	0.004	0.006	0.673	0.501	Cognitive Ability	0.533
rh_lateraloccipital_area	0.030	0.006	5.242	0.000	Cognitive Ability	0.000
rh_lateralorbitofrontal_area	0.029	0.006	4.994	0.000	Cognitive Ability	0.000
rh_lingual_area	0.007	0.006	1.275	0.202	Cognitive Ability	0.232
rh_medialorbitofrontal_area	0.030	0.006	5.143	0.000	Cognitive Ability	0.000
rh_middletemporal_area	0.032	0.006	5.645	0.000	Cognitive Ability	0.000
rh parahippocampal_area	0.013	0.006	2.230	0.026	Cognitive Ability	0.035
rh_paracentral_area	0.013	0.006	2.304	0.021	Cognitive Ability	0.031
rh_parsopercularis_area	0.017	0.006	2.926	0.003	Cognitive Ability	0.006
rh_parsorbitalis_area	0.027	0.006	4.705	0.000	Cognitive Ability	0.000
rh_parsstriangularis_area	0.033	0.006	5.705	0.000	Cognitive Ability	0.000
rh_pericalcarine_area	0.015	0.006	2.647	0.008	Cognitive Ability	0.013
rh_postcentral_area	0.010	0.006	1.801	0.072	Cognitive Ability	0.092
rh_posteriorcingulate_area	0.010	0.006	1.652	0.099	Cognitive Ability	0.123
rh_precentral_area	0.017	0.006	2.886	0.004	Cognitive Ability	0.007
rh_precuneus_area	0.015	0.006	2.579	0.010	Cognitive Ability	0.015
rh_rostralanteriorcingulate_area	0.011	0.006	1.841	0.066	Cognitive Ability	0.085
rh_rostralmiddlefrontal_area	0.029	0.006	5.084	0.000	Cognitive Ability	0.000
rh_superiorfrontal_area	0.031	0.006	5.435	0.000	Cognitive Ability	0.000
rh_superioparietal_area	0.001	0.006	0.218	0.827	Cognitive Ability	0.833
rh_superiortemporal_area	0.049	0.006	8.469	0.000	Cognitive Ability	0.000
rh_supramarginal_area	0.016	0.006	2.767	0.006	Cognitive Ability	0.010
rh_frontalpole_area	0.018	0.006	3.082	0.002	Cognitive Ability	0.004
rh_temporalpole_area	-0.001	0.006	-0.115	0.908	Cognitive Ability	0.908
rh_transversetemporal_area	0.029	0.006	5.075	0.000	Cognitive Ability	0.000
rh_insula_area	0.046	0.006	8.032	0.000	Cognitive Ability	0.000
Left-Thalamus-Proper	0.035	0.006	6.167	0.000	Cognitive Ability	0.000
Right-Thalamus-Proper	0.033	0.006	5.797	0.000	Cognitive Ability	0.000

Left-Caudate	0.019	0.006	3.227	0.001	Cognitive Ability	0.003
Right-Caudate	0.022	0.006	3.755	0.000	Cognitive Ability	0.000
Left-Putamen	0.007	0.006	1.296	0.195	Cognitive Ability	0.227
Right-Putamen	0.013	0.006	2.279	0.023	Cognitive Ability	0.032
Left-Pallidum	0.002	0.006	0.370	0.712	Cognitive Ability	0.726
Right-Pallidum	0.020	0.006	3.547	0.000	Cognitive Ability	0.001
Left-Hippocampus	0.039	0.006	6.759	0.000	Cognitive Ability	0.000
Right-Hippocampus	0.037	0.006	6.354	0.000	Cognitive Ability	0.000
Left-Amygdala	0.024	0.006	4.148	0.000	Cognitive Ability	0.000
Right-Amygdala	0.021	0.006	3.611	0.000	Cognitive Ability	0.001
Left-Accumbens-area	0.014	0.006	2.392	0.017	Cognitive Ability	0.024
Right-Accumbens-area	0.036	0.006	6.269	0.000	Cognitive Ability	0.000

Test_Region	Test_Estimate	Test_StdError	Test_tvalue	Test_pvalue	Test_IndVar	Pdic
lh_bankssts_thickness	0.019	0.010	1.945	0.052	Cognitive Ability	P > .05
lh_caudalanteriorcingulate_thickness	0.007	0.010	0.663	0.507	Cognitive Ability	P > .05
lh_caudalmiddlefrontal_thickness	0.012	0.010	1.235	0.217	Cognitive Ability	P > .05
lh_cuneus_thickness	0.004	0.010	0.369	0.712	Cognitive Ability	P > .05
lh_entorhinal_thickness	0.022	0.010	2.239	0.025	Cognitive Ability	P < .05
lh_fusiform_thickness	0.024	0.010	2.362	0.018	Cognitive Ability	P < .05
lh_inferiorparietal_thickness	0.019	0.010	1.861	0.063	Cognitive Ability	P > .05
lh_inferiortemporal_thickness	0.024	0.010	2.456	0.014	Cognitive Ability	P > .05
lh_isthmuscingulate_thickness	-0.003	0.010	-0.286	0.775	Cognitive Ability	P > .05
lh_lateraloccipital_thickness	0.007	0.010	0.733	0.463	Cognitive Ability	P > .05
lh_lateralorbitofrontal_thickness	0.011	0.010	1.070	0.285	Cognitive Ability	P > .05
lh_lingual_thickness	0.016	0.010	1.597	0.110	Cognitive Ability	P > .05
lh_medialorbitofrontal_thickness	0.004	0.010	0.389	0.697	Cognitive Ability	P > .05
lh_middletemporal_thickness	0.036	0.010	3.568	0.000	Cognitive Ability	P < .05
lh parahippocampal_thickness	0.039	0.010	3.884	0.000	Cognitive Ability	P < .05
lh_paracentral_thickness	0.019	0.010	1.910	0.056	Cognitive Ability	P > .05
lh_parsopercularis_thickness	0.016	0.010	1.581	0.114	Cognitive Ability	P > .05
lh_parsorbitalis_thickness	0.014	0.010	1.403	0.161	Cognitive Ability	P > .05

lh_parstriangularis_thickness	0.015	0.010	1.496	0.135	Cognitive Ability	P > .05
lh_pericalcarine_thickness	0.001	0.010	0.131	0.896	Cognitive Ability	P > .05
lh_postcentral_thickness	0.030	0.010	2.967	0.003	Cognitive Ability	P < .05
lh_posteriorcingulate_thickness	-0.011	0.010	-1.102	0.270	Cognitive Ability	P > .05
lh_precentral_thickness	0.042	0.010	4.255	0.000	Cognitive Ability	P < .05
lh_precuneus_thickness	0.011	0.010	1.093	0.274	Cognitive Ability	P > .05
lh_rostralanteriorcingulate_thickness	-0.001	0.010	-0.081	0.935	Cognitive Ability	P > .05
lh_rostralmiddlefrontal_thickness	0.012	0.010	1.217	0.224	Cognitive Ability	P > .05
lh_superiorfrontal_thickness	0.010	0.010	1.043	0.297	Cognitive Ability	P > .05
lh_superiorparietal_thickness	0.009	0.010	0.907	0.364	Cognitive Ability	P > .05
lh_superiortemporal_thickness	0.054	0.010	5.452	0.000	Cognitive Ability	P < .05
lh_supramarginal_thickness	0.036	0.010	3.661	0.000	Cognitive Ability	P < .05
lh_frontalpole_thickness	-0.002	0.010	-0.157	0.875	Cognitive Ability	P > .05
lh_temporalpole_thickness	0.032	0.010	3.196	0.001	Cognitive Ability	P < .05
lh_transversetemporal_thickness	0.023	0.010	2.303	0.021	Cognitive Ability	P < .05
lh_insula_thickness	0.024	0.010	2.444	0.015	Cognitive Ability	P < .05
rh_bankssts_thickness	0.001	0.010	0.117	0.907	Cognitive Ability	P > .05
rh_caudalanteriorcingulate_thickness	-0.020	0.010	-2.031	0.042	Cognitive Ability	P > .05
rh_caudalmiddlefrontal_thickness	0.003	0.010	0.252	0.801	Cognitive Ability	P > .05
rh_cuneus_thickness	0.010	0.010	1.030	0.303	Cognitive Ability	P > .05
rh_entorhinal_thickness	0.006	0.010	0.555	0.579	Cognitive Ability	P > .05
rh_fusiform_thickness	0.022	0.010	2.219	0.027	Cognitive Ability	P < .05
rh_inferiorparietal_thickness	0.020	0.010	2.003	0.045	Cognitive Ability	P < .05
rh_inferiortemporal_thickness	0.020	0.010	1.963	0.050	Cognitive Ability	P < .05
rh_isthmuscingulate_thickness	0.012	0.010	1.171	0.242	Cognitive Ability	P > .05
rh_lateraloccipital_thickness	0.011	0.010	1.136	0.256	Cognitive Ability	P > .05
rh_lateralorbitofrontal_thickness	-0.003	0.010	-0.273	0.785	Cognitive Ability	P > .05
rh_lingual_thickness	0.016	0.010	1.640	0.101	Cognitive Ability	P > .05
rh_medialorbitofrontal_thickness	-0.009	0.010	-0.912	0.362	Cognitive Ability	P > .05
rh_middletemporal_thickness	0.017	0.010	1.737	0.082	Cognitive Ability	P > .05
rh parahippocampal_thickness	0.038	0.010	3.798	0.000	Cognitive Ability	P < .05
rh_paracentral_thickness	0.012	0.010	1.159	0.247	Cognitive Ability	P > .05

rh_parsopercularis_thickness	0.021	0.010	2.141	0.032	Cognitive Ability	P < .05
rh_parsorbitalis_thickness	0.018	0.010	1.801	0.072	Cognitive Ability	P > .05
rh_parstriangularis_thickness	0.008	0.010	0.763	0.446	Cognitive Ability	P > .05
rh_pericalcarine_thickness	0.010	0.010	0.976	0.329	Cognitive Ability	P > .05
rh_postcentral_thickness	0.020	0.010	2.010	0.044	Cognitive Ability	P < .05
rh_posteriorcingulate_thickness	-0.005	0.010	-0.493	0.622	Cognitive Ability	P > .05
rh_precentral_thickness	0.037	0.010	3.697	0.000	Cognitive Ability	P < .05
rh_precuneus_thickness	0.016	0.010	1.654	0.098	Cognitive Ability	P > .05
rh_rostralanteriorcingulate_thickness	-0.010	0.010	-1.026	0.305	Cognitive Ability	P > .05
rh_rostralmiddlefrontal_thickness	0.005	0.010	0.549	0.583	Cognitive Ability	P > .05
rh_superiorfrontal_thickness	0.006	0.010	0.606	0.544	Cognitive Ability	P > .05
rh_superiorparietal_thickness	0.005	0.010	0.466	0.641	Cognitive Ability	P > .05
rh_superiortemporal_thickness	0.054	0.010	5.437	0.000	Cognitive Ability	P < .05
rh_supramarginal_thickness	0.030	0.010	3.010	0.003	Cognitive Ability	P < .05
rh_frontalpole_thickness	-0.002	0.010	-0.169	0.866	Cognitive Ability	P > .05
rh_temporalpole_thickness	0.026	0.010	2.626	0.009	Cognitive Ability	P < .05
rh_transverse temporal_thickness	0.005	0.010	0.543	0.587	Cognitive Ability	P > .05
rh_insula_thickness	0.007	0.010	0.742	0.458	Cognitive Ability	P > .05
lh_bankssts_area	0.037	0.010	3.761	0.000	Cognitive Ability	P < .05
lh_caudalanteriorcingulate_area	-0.001	0.010	-0.080	0.936	Cognitive Ability	P > .05
lh_caudalmiddlefrontal_area	0.014	0.010	1.395	0.163	Cognitive Ability	P > .05
lh_cuneus_area	0.012	0.010	1.178	0.239	Cognitive Ability	P > .05
lh_entorhinal_area	0.053	0.010	5.352	0.000	Cognitive Ability	P < .05
lh_fusiform_area	0.044	0.010	4.433	0.000	Cognitive Ability	P < .05
lh_inferiorparietal_area	0.028	0.010	2.809	0.005	Cognitive Ability	P < .05
lh_inferiortemporal_area	0.041	0.010	4.165	0.000	Cognitive Ability	P < .05
lh_isthmuscingulate_area	0.023	0.010	2.289	0.022	Cognitive Ability	P > .05
lh_lateraloccipital_area	0.019	0.010	1.909	0.056	Cognitive Ability	P > .05
lh_lateralorbitofrontal_area	0.050	0.010	5.052	0.000	Cognitive Ability	P < .05
lh_lingual_area	0.033	0.010	3.274	0.001	Cognitive Ability	P < .05
lh_medialorbitofrontal_area	0.020	0.010	2.012	0.044	Cognitive Ability	P < .05
lh_middletemporal_area	0.029	0.010	2.949	0.003	Cognitive Ability	P < .05



lh parahippocampal_area	0.003	0.010	0.271	0.786	Cognitive Ability	P > .05
lh paracentral_area	-0.014	0.010	-1.429	0.153	Cognitive Ability	P > .05
lh parsopercularis_area	0.010	0.010	0.980	0.327	Cognitive Ability	P > .05
lh parsorbitalis_area	0.047	0.010	4.694	0.000	Cognitive Ability	P < .05
lh parstriangularis_area	0.048	0.010	4.802	0.000	Cognitive Ability	P < .05
lh pericalcarine_area	0.018	0.010	1.782	0.075	Cognitive Ability	P > .05
lh postcentral_area	0.015	0.010	1.476	0.140	Cognitive Ability	P > .05
lh posteriorcingulate_area	0.024	0.010	2.375	0.018	Cognitive Ability	P > .05
lh precentral_area	0.014	0.010	1.432	0.152	Cognitive Ability	P > .05
lh precuneus_area	0.028	0.010	2.811	0.005	Cognitive Ability	P > .05
lh rostralanteriorcingulate_area	0.004	0.010	0.449	0.653	Cognitive Ability	P > .05
lh rostralmiddlefrontal_area	0.042	0.010	4.172	0.000	Cognitive Ability	P < .05
lh superiorfrontal_area	0.034	0.010	3.443	0.001	Cognitive Ability	P < .05
lh superiorparietal_area	0.015	0.010	1.511	0.131	Cognitive Ability	P > .05
lh superiortemporal_area	0.064	0.010	6.426	0.000	Cognitive Ability	P < .05
lh supramarginal_area	0.034	0.010	3.374	0.001	Cognitive Ability	P < .05
lh frontalpole_area	0.028	0.010	2.832	0.005	Cognitive Ability	P < .05
lh temporalpole_area	0.019	0.010	1.878	0.060	Cognitive Ability	P > .05
lh transversetemporal_area	0.039	0.010	3.922	0.000	Cognitive Ability	P < .05
lh insula_area	0.043	0.010	4.369	0.000	Cognitive Ability	P < .05
rh bankssts_area	0.029	0.010	2.869	0.004	Cognitive Ability	P < .05
rh caudalanteriorcingulate_area	0.017	0.010	1.667	0.096	Cognitive Ability	P > .05
rh caudalmiddlefrontal_area	0.000	0.010	-0.001	0.999	Cognitive Ability	P > .05
rh cuneus_area	0.014	0.010	1.423	0.155	Cognitive Ability	P > .05
rh entorhinal_area	0.038	0.010	3.798	0.000	Cognitive Ability	P < .05
rh fusiform_area	0.037	0.010	3.757	0.000	Cognitive Ability	P < .05
rh inferiorparietal_area	0.037	0.010	3.677	0.000	Cognitive Ability	P < .05
rh inferiortemporal_area	0.041	0.010	4.097	0.000	Cognitive Ability	P < .05
rh isthmuscingulate_area	-0.009	0.010	-0.877	0.380	Cognitive Ability	P > .05
rh lateraloccipital_area	0.017	0.010	1.699	0.089	Cognitive Ability	P > .05
rh lateralorbitofrontal_area	0.060	0.010	6.019	0.000	Cognitive Ability	P < .05
rh lingual_area	0.010	0.010	0.954	0.340	Cognitive Ability	P > .05

rh_medialorbitofrontal_area	0.035	0.010	3.500	0.000	Cognitive Ability	P < .05
rh_middletemporal_area	0.035	0.010	3.520	0.000	Cognitive Ability	P < .05
rh parahippocampal_area	0.019	0.010	1.919	0.055	Cognitive Ability	P > .05
rh_paracentral_area	0.007	0.010	0.715	0.475	Cognitive Ability	P > .05
rh_parsopercularis_area	0.004	0.010	0.438	0.662	Cognitive Ability	P > .05
rh_parsorbitalis_area	0.058	0.010	5.855	0.000	Cognitive Ability	P < .05
rh_parstriangularis_area	0.040	0.010	3.992	0.000	Cognitive Ability	P < .05
rh_pericalcarine_area	0.016	0.010	1.628	0.103	Cognitive Ability	P > .05
rh_postcentral_area	0.018	0.010	1.820	0.069	Cognitive Ability	P > .05
rh_posteriorcingulate_area	0.015	0.010	1.530	0.126	Cognitive Ability	P > .05
rh_precentral_area	0.020	0.010	1.973	0.049	Cognitive Ability	P < .05
rh_precuneus_area	0.031	0.010	3.074	0.002	Cognitive Ability	P < .05
rh_rostralanteriorcingulate_area	0.002	0.010	0.182	0.856	Cognitive Ability	P > .05
rh_rostralmiddlefrontal_area	0.039	0.010	3.895	0.000	Cognitive Ability	P < .05
rh_superiorfrontal_area	0.037	0.010	3.715	0.000	Cognitive Ability	P < .05
rh_superiorparietal_area	0.023	0.010	2.277	0.023	Cognitive Ability	P > .05
rh_superiortemporal_area	0.055	0.010	5.496	0.000	Cognitive Ability	P < .05
rh_supramarginal_area	0.018	0.010	1.790	0.073	Cognitive Ability	P > .05
rh_frontalpole_area	-0.002	0.010	-0.239	0.811	Cognitive Ability	P > .05
rh_temporalpole_area	0.004	0.010	0.362	0.718	Cognitive Ability	P > .05
rh_transversetemporal_area	0.053	0.010	5.367	0.000	Cognitive Ability	P < .05
rh_insula_area	0.048	0.010	4.872	0.000	Cognitive Ability	P < .05
Left-Thalamus-Proper	0.047	0.010	4.731	0.000	Cognitive Ability	P < .05
Right-Thalamus-Proper	0.043	0.010	4.339	0.000	Cognitive Ability	P < .05
Left-Caudate	0.027	0.010	2.722	0.006	Cognitive Ability	P < .05
Right-Caudate	0.017	0.010	1.734	0.083	Cognitive Ability	P > .05
Left-Putamen	0.018	0.010	1.836	0.066	Cognitive Ability	P > .05
Right-Putamen	0.019	0.010	1.916	0.055	Cognitive Ability	P > .05
Left-Pallidum	-0.003	0.010	-0.272	0.786	Cognitive Ability	P > .05
Right-Pallidum	0.021	0.010	2.098	0.036	Cognitive Ability	P < .05
Left-Hippocampus	0.054	0.010	5.467	0.000	Cognitive Ability	P < .05
Right-Hippocampus	0.045	0.010	4.554	0.000	Cognitive Ability	P < .05

Left-Amygdala	0.036	0.010	3.568	0.000	Cognitive Ability	P < .05
Right-Amygdala	0.036	0.010	3.577	0.000	Cognitive Ability	P < .05
Left-Accumbens-area	0.027	0.010	2.669	0.008	Cognitive Ability	P < .05
Right-Accumbens-area	0.040	0.010	4.052	0.000	Cognitive Ability	P < .05

**Table S2.**

Reference values for the global index and intraindividual standard deviation.

	1q21.1 distal deletion matched control group	1q21.1 distal duplication matched control group	15q11.2 BP1-BP2 deletion matched control group	15q11.2 BP1-BP2 duplication matched control group
<b>Global Index</b>				
Cortical Surface Area	-0.00 (.59)	.00 (.58)	-0.01 (.46)	-0.01 (.49)
Cortical Thickness	.01 (.58)	.00 (.56)	.01 (.53)	-0.00 (.55)
Subcortical volume	.01 (.65)	-0.01 (.62)	-0.00 (.58)	.00 (.56)
<b>Intraindividual standard deviation (mean uncorrected)</b>				
Cortical Surface Area	.80 (.14)	.82 (.12)	.87 (.15)	.85 (.15)
Cortical Thickness	.81 (.11)	.82 (.12)	.84 (.14)	.83 (.13)
Subcortical volume	.75 (.24)	.77 (.24)	.81 (.25)	.82 (.26)
<b>Intraindividual standard deviation (mean corrected)</b>				
Cortical Surface Area	-0.01 (.65)	-0.01 (.11)	-0.00 (.14)	-0.00 (.14)
Cortical Thickness	-0.01 (.11)	-0.01 (.12)	-0.00 (.14)	-0.00 (.13)
Subcortical volume	.00 (.23)	-0.01 (.24)	-0.00 (.24)	-0.00 (.26)

Note. Mean values for the non-carrier groups. Standard deviation is presented in parenthesis.

**Table S3.**

Group differences in Z-scores for 1q21.1 distal deletion carriers.

<b>CNV</b>	<b>Estimate</b>	<b>S.E.</b>	<b>T-value</b>	<b>P-value</b>	<b>Region of Interest</b>	<b>Cases</b>	<b>Controls</b>	<b>PFDR</b>	<b>Pcorrected_dic</b>
1q21.1del	0.595	0.203	2.936	0.004	lh_bankssts_thickness	28	136	0.010	Sig
1q21.1del	0.195	0.208	0.940	0.349	lh_caudalanteriorcingulate_thickness	28	136	0.429	NonSig
1q21.1del	0.514	0.204	2.516	0.013	lh_caudalmiddlefrontal_thickness	28	136	0.026	Sig
1q21.1del	-0.542	0.204	-2.660	0.009	lh_cuneus_thickness	28	136	0.018	Sig
1q21.1del	0.073	0.208	0.350	0.727	lh_entorhinal_thickness	28	136	0.767	NonSig
1q21.1del	0.019	0.208	0.093	0.926	lh_fusiform_thickness	28	136	0.932	NonSig
1q21.1del	0.255	0.207	1.230	0.220	lh_inferiorparietal_thickness	28	136	0.291	NonSig
1q21.1del	0.424	0.205	2.065	0.040	lh_inferiortemporal_thickness	28	136	0.071	NonSig
1q21.1del	0.335	0.206	1.624	0.106	lh_isthmusingulate_thickness	28	136	0.161	NonSig
1q21.1del	-0.105	0.208	-0.503	0.616	lh_lateraloccipital_thickness	28	136	0.695	NonSig
1q21.1del	0.465	0.205	2.270	0.025	lh_lateralorbitofrontal_thickness	28	136	0.045	Sig
1q21.1del	0.076	0.208	0.363	0.717	lh_lingual_thickness	28	136	0.763	NonSig
1q21.1del	0.501	0.204	2.452	0.015	lh_medialorbitofrontal_thickness	28	136	0.030	Sig
1q21.1del	0.587	0.203	2.890	0.004	lh_middletemporal_thickness	28	136	0.012	Sig
1q21.1del	-0.332	0.207	-1.610	0.109	lh parahippocampal_thickness	28	136	0.164	NonSig
1q21.1del	-0.311	0.207	-1.505	0.134	lh_paracentral_thickness	28	136	0.195	NonSig
1q21.1del	0.136	0.208	0.653	0.514	lh_parsopercularis_thickness	28	136	0.612	NonSig
1q21.1del	0.063	0.208	0.304	0.761	lh_parsorbitalis_thickness	28	136	0.798	NonSig
1q21.1del	0.683	0.201	3.397	0.001	lh_parsotriangularis_thickness	28	136	0.003	Sig
1q21.1del	-0.554	0.204	-2.723	0.007	lh_pericalcarine_thickness	28	136	0.016	Sig
1q21.1del	0.288	0.207	1.390	0.167	lh_postcentral_thickness	28	136	0.236	NonSig
1q21.1del	-0.022	0.208	-0.108	0.914	lh_posteriorcingulate_thickness	28	136	0.927	NonSig
1q21.1del	0.118	0.208	0.566	0.572	lh_precentral_thickness	28	136	0.660	NonSig
1q21.1del	0.350	0.206	1.697	0.092	lh_precuneus_thickness	28	136	0.143	NonSig
1q21.1del	0.549	0.204	2.693	0.008	lh_rostralanteriorcingulate_thickness	28	136	0.017	Sig
1q21.1del	0.485	0.205	2.370	0.019	lh_rostralmiddlefrontal_thickness	28	136	0.036	Sig
1q21.1del	0.375	0.206	1.822	0.070	lh_superiorfrontal_thickness	28	136	0.116	NonSig
1q21.1del	0.152	0.208	0.732	0.465	lh_superiorparietal_thickness	28	136	0.568	NonSig

1q21.1del	0.759	0.199	3.805	0.000	lh_superiortemporal_thickness	28	136	0.001	Sig
1q21.1del	0.694	0.201	3.452	0.001	lh_supramarginal_thickness	28	136	0.002	Sig
1q21.1del	0.374	0.206	1.815	0.071	lh_frontalpole_thickness	28	136	0.116	NonSig
1q21.1del	0.457	0.205	2.227	0.027	lh_temporalpole_thickness	28	136	0.049	Sig
1q21.1del	0.283	0.207	1.370	0.173	lh_transversetemporal_thickness	28	136	0.242	NonSig
1q21.1del	0.102	0.208	0.489	0.626	lh_insula_thickness	28	136	0.701	NonSig
1q21.1del	0.416	0.206	2.023	0.045	rh_bankssts_thickness	28	136	0.076	NonSig
1q21.1del	0.365	0.206	1.770	0.079	rh_caudalanteriorcingulate_thickness	28	136	0.125	NonSig
1q21.1del	0.213	0.207	1.025	0.307	rh_caudalmiddlefrontal_thickness	28	136	0.383	NonSig
1q21.1del	-0.376	0.206	-1.822	0.070	rh_cuneus_thickness	28	136	0.116	NonSig
1q21.1del	0.082	0.208	0.393	0.695	rh_entorhinal_thickness	28	136	0.750	NonSig
1q21.1del	0.028	0.208	0.133	0.894	rh_fusiform_thickness	28	136	0.912	NonSig
1q21.1del	0.253	0.207	1.223	0.223	rh_inferioparietal_thickness	28	136	0.291	NonSig
1q21.1del	0.260	0.207	1.255	0.211	rh_inferiortemporal_thickness	28	136	0.286	NonSig
1q21.1del	0.509	0.204	2.492	0.014	rh_isthmuscingulate_thickness	28	136	0.027	Sig
1q21.1del	-0.150	0.208	-0.724	0.470	rh_lateraloccipital_thickness	28	136	0.569	NonSig
1q21.1del	0.462	0.205	2.254	0.026	rh_lateralorbitofrontal_thickness	28	136	0.046	Sig
1q21.1del	-0.218	0.207	-1.052	0.294	rh_lingual_thickness	28	136	0.371	NonSig
1q21.1del	0.654	0.202	3.245	0.001	rh_medialorbitofrontal_thickness	28	136	0.004	Sig
1q21.1del	0.446	0.205	2.171	0.031	rh_middletemporal_thickness	28	136	0.055	NonSig
1q21.1del	-0.037	0.208	-0.177	0.859	rh parahippocampal_thickness	28	136	0.883	NonSig
1q21.1del	-0.313	0.207	-1.513	0.132	rh_paracentral_thickness	28	136	0.195	NonSig
1q21.1del	0.259	0.207	1.249	0.214	rh_parsopercularis_thickness	28	136	0.286	NonSig
1q21.1del	0.275	0.207	1.329	0.186	rh_parsorbitalis_thickness	28	136	0.256	NonSig
1q21.1del	0.416	0.206	2.023	0.045	rh_parstriangularis_thickness	28	136	0.076	NonSig
1q21.1del	-0.677	0.201	-3.366	0.001	rh_pericalcarine_thickness	28	136	0.003	Sig
1q21.1del	0.240	0.207	1.157	0.249	rh_postcentral_thickness	28	136	0.319	NonSig
1q21.1del	0.271	0.207	1.307	0.193	rh_posteriorcingulate_thickness	28	136	0.263	NonSig
1q21.1del	0.142	0.208	0.683	0.495	rh_precentral_thickness	28	136	0.594	NonSig
1q21.1del	0.121	0.208	0.579	0.563	rh_precuneus_thickness	28	136	0.655	NonSig
1q21.1del	0.298	0.207	1.442	0.151	rh_rostralanteriorcingulate_thickness	28	136	0.216	NonSig
1q21.1del	0.355	0.206	1.721	0.087	rh_rostralmiddlefrontal_thickness	28	136	0.138	NonSig

1q21.1del	0.323	0.207	1.565	0.119	rh_superiorfrontal_thickness	28	136	0.177	NonSig
1q21.1del	0.133	0.208	0.640	0.523	rh_superiorparietal_thickness	28	136	0.618	NonSig
1q21.1del	0.664	0.202	3.294	0.001	rh_superiortemporal_thickness	28	136	0.004	Sig
1q21.1del	0.078	0.208	0.373	0.709	rh_supramarginal_thickness	28	136	0.760	NonSig
1q21.1del	0.575	0.203	2.829	0.005	rh_frontalpole_thickness	28	136	0.014	Sig
1q21.1del	0.349	0.206	1.690	0.093	rh_temporalpole_thickness	28	136	0.144	NonSig
1q21.1del	0.227	0.207	1.094	0.276	rh_transversetemporal_thickness	28	136	0.350	NonSig
1q21.1del	0.127	0.208	0.610	0.543	rh_insula_thickness	28	136	0.636	NonSig
1q21.1del	-0.588	0.203	-2.896	0.004	lh_bankssts_area	28	135	0.012	Sig
1q21.1del	-0.569	0.203	-2.798	0.006	lh_caudalanteriorcingulate_area	28	135	0.014	Sig
1q21.1del	-1.250	0.184	-6.810	0.000	lh_caudalmiddlefrontal_area	28	135	0.000	Sig
1q21.1del	-0.495	0.205	-2.417	0.017	lh_cuneus_area	28	135	0.032	Sig
1q21.1del	-0.534	0.204	-2.615	0.010	lh_entorhinal_area	28	135	0.020	Sig
1q21.1del	-0.991	0.193	-5.131	0.000	lh_fusiform_area	28	135	0.000	Sig
1q21.1del	-0.560	0.204	-2.753	0.007	lh_inferiorparietal_area	28	135	0.016	Sig
1q21.1del	-0.909	0.196	-4.645	0.000	lh_inferiortemporal_area	28	135	0.000	Sig
1q21.1del	-0.378	0.206	-1.832	0.069	lh_isthmuscingulate_area	28	135	0.116	NonSig
1q21.1del	-1.024	0.192	-5.330	0.000	lh_lateraloccipital_area	28	135	0.000	Sig
1q21.1del	-1.225	0.185	-6.640	0.000	lh_lateralorbitofrontal_area	28	135	0.000	Sig
1q21.1del	-0.372	0.206	-1.806	0.073	lh_lingual_area	28	135	0.118	NonSig
1q21.1del	-1.040	0.192	-5.428	0.000	lh_medialorbitofrontal_area	28	135	0.000	Sig
1q21.1del	-0.690	0.201	-3.431	0.001	lh_middletemporal_area	28	135	0.003	Sig
1q21.1del	-0.553	0.204	-2.713	0.007	lh parahippocampal_area	28	135	0.016	Sig
1q21.1del	-0.966	0.194	-4.981	0.000	lh_paracentral_area	28	135	0.000	Sig
1q21.1del	-0.921	0.195	-4.720	0.000	lh_parsopercularis_area	28	135	0.000	Sig
1q21.1del	-0.878	0.196	-4.467	0.000	lh_parsorbitalis_area	28	135	0.000	Sig
1q21.1del	-0.571	0.203	-2.807	0.006	lh_parstriangularis_area	28	135	0.014	Sig
1q21.1del	-0.275	0.207	-1.328	0.186	lh_pericalcarine_area	28	135	0.256	NonSig
1q21.1del	-0.477	0.205	-2.330	0.021	lh_postcentral_area	28	135	0.039	Sig
1q21.1del	-0.642	0.202	-3.180	0.002	lh_posteriorcingulate_area	28	135	0.005	Sig
1q21.1del	-0.970	0.194	-5.007	0.000	lh_precentral_area	28	135	0.000	Sig
1q21.1del	-0.655	0.202	-3.246	0.001	lh_precuneus_area	28	135	0.004	Sig

1q21.1del	-0.975	0.194	-5.038	0.000	lh_rostralanteriorcingulate_area	28	135	0.000	Sig
1q21.1del	-1.242	0.184	-6.752	0.000	lh_rostralmiddlefrontal_area	28	135	0.000	Sig
1q21.1del	-1.442	0.175	-8.257	0.000	lh_superiorfrontal_area	28	135	0.000	Sig
1q21.1del	-0.662	0.202	-3.283	0.001	lh_superiorparietal_area	28	135	0.004	Sig
1q21.1del	-1.173	0.187	-6.284	0.000	lh_superiortemporal_area	28	135	0.000	Sig
1q21.1del	-0.785	0.199	-3.944	0.000	lh_supramarginal_area	28	135	0.000	Sig
1q21.1del	-0.557	0.204	-2.734	0.007	lh_frontalpole_area	28	135	0.016	Sig
1q21.1del	-0.299	0.207	-1.443	0.151	lh_temporalpole_area	28	135	0.216	NonSig
1q21.1del	-1.096	0.190	-5.783	0.000	lh_transversetemporal_area	28	135	0.000	Sig
1q21.1del	-0.944	0.195	-4.852	0.000	lh_insula_area	28	135	0.000	Sig
1q21.1del	-0.844	0.197	-4.275	0.000	rh_bankssts_area	28	135	0.000	Sig
1q21.1del	-0.825	0.198	-4.170	0.000	rh_caudalanteriorcingulate_area	28	135	0.000	Sig
1q21.1del	-1.278	0.182	-7.012	0.000	rh_caudalmiddlefrontal_area	28	135	0.000	Sig
1q21.1del	-0.849	0.197	-4.306	0.000	rh_cuneus_area	28	135	0.000	Sig
1q21.1del	-0.516	0.204	-2.526	0.013	rh_entorhinal_area	28	135	0.025	Sig
1q21.1del	-0.983	0.193	-5.084	0.000	rh_fusiform_area	28	135	0.000	Sig
1q21.1del	-0.919	0.195	-4.703	0.000	rh_inferioparietal_area	28	135	0.000	Sig
1q21.1del	-0.922	0.195	-4.723	0.000	rh_inferiortemporal_area	28	135	0.000	Sig
1q21.1del	-0.557	0.204	-2.736	0.007	rh_isthmuscingulate_area	28	135	0.016	Sig
1q21.1del	-0.727	0.200	-3.629	0.000	rh_lateraloccipital_area	28	135	0.001	Sig
1q21.1del	-1.041	0.191	-5.435	0.000	rh_lateralorbitofrontal_area	28	135	0.000	Sig
1q21.1del	-0.559	0.204	-2.744	0.007	rh_lingual_area	28	135	0.016	Sig
1q21.1del	-0.986	0.193	-5.105	0.000	rh_medialorbitofrontal_area	28	135	0.000	Sig
1q21.1del	-0.823	0.198	-4.157	0.000	rh_middletemporal_area	28	135	0.000	Sig
1q21.1del	-0.641	0.202	-3.170	0.002	rh parahippocampal_area	28	135	0.005	Sig
1q21.1del	-0.827	0.198	-4.180	0.000	rh_paracentral_area	28	135	0.000	Sig
1q21.1del	-1.042	0.191	-5.440	0.000	rh_parsopercularis_area	28	135	0.000	Sig
1q21.1del	-0.706	0.201	-3.518	0.001	rh_parsorbitalis_area	28	135	0.002	Sig
1q21.1del	-1.040	0.192	-5.430	0.000	rh_parstriangularis_area	28	135	0.000	Sig
1q21.1del	-0.470	0.205	-2.291	0.023	rh_pericalcarine_area	28	135	0.043	Sig
1q21.1del	-0.675	0.201	-3.352	0.001	rh_postcentral_area	28	135	0.003	Sig
1q21.1del	-0.857	0.197	-4.350	0.000	rh_posteriorcingulate_area	28	135	0.000	Sig



1q21.1del	-1.022	0.192	-5.322	0.000	rh_precentral_area	28	135	0.000	Sig
1q21.1del	-0.700	0.201	-3.483	0.001	rh_precuneus_area	28	135	0.002	Sig
1q21.1del	-0.830	0.198	-4.198	0.000	rh_rostralanteriorcingulate_area	28	135	0.000	Sig
1q21.1del	-1.132	0.188	-6.014	0.000	rh_rostralmiddlefrontal_area	28	135	0.000	Sig
1q21.1del	-1.241	0.184	-6.747	0.000	rh_superiorfrontal_area	28	135	0.000	Sig
1q21.1del	-0.342	0.207	-1.657	0.099	rh_superiorparietal_area	28	135	0.152	NonSig
1q21.1del	-0.983	0.193	-5.085	0.000	rh_superiortemporal_area	28	135	0.000	Sig
1q21.1del	-0.820	0.198	-4.138	0.000	rh_supramarginal_area	28	135	0.000	Sig
1q21.1del	-0.570	0.203	-2.800	0.006	rh_frontalpole_area	28	135	0.014	Sig
1q21.1del	-0.552	0.204	-2.709	0.007	rh_temporalpole_area	28	135	0.016	Sig
1q21.1del	-0.904	0.196	-4.617	0.000	rh_transversetemporal_area	28	135	0.000	Sig
1q21.1del	-0.770	0.199	-3.862	0.000	rh_insula_area	28	135	0.001	Sig
1q21.1del	-0.540	0.200	-2.693	0.008	Left-Thalamus-Proper	29	139	0.017	Sig
1q21.1del	-0.250	0.204	-1.228	0.221	Right-Thalamus-Proper	29	139	0.291	NonSig
1q21.1del	0.203	0.204	0.995	0.321	Left-Caudate	29	139	0.398	NonSig
1q21.1del	0.082	0.205	0.400	0.690	Right-Caudate	29	139	0.750	NonSig
1q21.1del	-0.092	0.205	-0.450	0.653	Left-Putamen	29	139	0.722	NonSig
1q21.1del	-0.083	0.205	-0.404	0.686	Right-Putamen	29	139	0.750	NonSig
1q21.1del	-0.058	0.205	-0.282	0.778	Left-Pallidum	29	139	0.811	NonSig
1q21.1del	-0.092	0.205	-0.449	0.654	Right-Pallidum	29	139	0.722	NonSig
1q21.1del	0.104	0.205	0.508	0.612	Left-Hippocampus	29	139	0.695	NonSig
1q21.1del	0.041	0.205	0.200	0.842	Right-Hippocampus	29	139	0.871	NonSig
1q21.1del	0.112	0.205	0.547	0.585	Left-Amygdala	29	139	0.670	NonSig
1q21.1del	-0.015	0.205	-0.074	0.941	Right-Amygdala	29	139	0.941	NonSig
1q21.1del	-0.236	0.204	-1.159	0.248	Left-Accumbens-area	29	139	0.319	NonSig
1q21.1del	-0.525	0.201	-2.616	0.010	Right-Accumbens-area	29	139	0.020	Sig

**Table S4.**

Group differences in RID-scores for 1q21.1 distal deletion carriers.

<b>CNV</b>	<b>Estimate</b>	<b>S.E.</b>	<b>T-value</b>	<b>P-value</b>	<b>Region of Interest</b>	<b>Cases</b>	<b>Controls</b>	<b>PFDR</b>	<b>Pcorrected</b>	<b>dic</b>
1q21.1del	0.387	0.206	1.881	0.062	lh_bankssts_thickness	28	136	0.227		NonSig
1q21.1del	-0.036	0.208	-0.175	0.861	lh_caudalanteriorcingulate_thickness	28	136	0.926		NonSig
1q21.1del	0.362	0.206	1.754	0.081	lh_caudalmiddlefrontal_thickness	28	136	0.254		NonSig
1q21.1del	-0.906	0.196	-4.633	0.000	lh_cuneus_thickness	28	136	0.000		Sig
1q21.1del	-0.197	0.208	-0.949	0.344	lh_entorhinal_thickness	28	136	0.561		NonSig
1q21.1del	-0.264	0.207	-1.277	0.203	lh_fusiform_thickness	28	136	0.418		NonSig
1q21.1del	0.090	0.208	0.431	0.667	lh_inferiorparietal_thickness	28	136	0.794		NonSig
1q21.1del	0.195	0.208	0.938	0.350	lh_inferiortemporal_thickness	28	136	0.564		NonSig
1q21.1del	0.090	0.208	0.434	0.665	lh_isthmuscingulate_thickness	28	136	0.794		NonSig
1q21.1del	-0.408	0.206	-1.985	0.049	lh_lateraloccipital_thickness	28	136	0.206		NonSig
1q21.1del	0.279	0.207	1.350	0.179	lh_lateralorbitofrontal_thickness	28	136	0.394		NonSig
1q21.1del	-0.153	0.208	-0.737	0.462	lh_lingual_thickness	28	136	0.648		NonSig
1q21.1del	0.301	0.207	1.458	0.147	lh_medialorbitofrontal_thickness	28	136	0.373		NonSig
1q21.1del	0.501	0.204	2.453	0.015	lh_middletemporal_thickness	28	136	0.082		NonSig
1q21.1del	-0.562	0.203	-2.765	0.006	lh_parahippocampal_thickness	28	136	0.040		Sig
1q21.1del	-0.640	0.202	-3.169	0.002	lh_paracentral_thickness	28	136	0.017		Sig
1q21.1del	-0.116	0.208	-0.559	0.577	lh_parsopercularis_thickness	28	136	0.752		NonSig
1q21.1del	-0.185	0.208	-0.892	0.374	lh_parsorbitalis_thickness	28	136	0.590		NonSig
1q21.1del	0.609	0.203	3.005	0.003	lh_parstriangularis_thickness	28	136	0.026		Sig
1q21.1del	-0.788	0.199	-3.965	0.000	lh_pericalcarine_thickness	28	136	0.002		Sig
1q21.1del	0.101	0.208	0.484	0.629	lh_postcentral_thickness	28	136	0.776		NonSig
1q21.1del	-0.229	0.207	-1.106	0.271	lh_posteriorcingulate_thickness	28	136	0.489		NonSig
1q21.1del	-0.165	0.208	-0.793	0.429	lh_precentral_thickness	28	136	0.631		NonSig
1q21.1del	0.188	0.208	0.907	0.366	lh_precuneus_thickness	28	136	0.584		NonSig
1q21.1del	0.321	0.207	1.553	0.122	lh_rostralanteriorcingulate_thickness	28	136	0.334		NonSig
1q21.1del	0.391	0.206	1.902	0.059	lh_rostralmiddlefrontal_thickness	28	136	0.227		NonSig
1q21.1del	0.246	0.207	1.186	0.237	lh_superiorfrontal_thickness	28	136	0.450		NonSig
1q21.1del	-0.075	0.208	-0.362	0.718	lh_superiorparietal_thickness	28	136	0.828		NonSig

1q21.1del	0.803	0.198	4.048	0.000	lh_superiortemporal_thickness	28	136	0.002	Sig
1q21.1del	0.709	0.201	3.534	0.001	lh_supramarginal_thickness	28	136	0.007	Sig
1q21.1del	0.168	0.208	0.808	0.420	lh_frontalpole_thickness	28	136	0.625	NonSig
1q21.1del	0.247	0.207	1.189	0.236	lh_temporalpole_thickness	28	136	0.450	NonSig
1q21.1del	0.083	0.208	0.398	0.691	lh_transversetemporal_thickness	28	136	0.806	NonSig
1q21.1del	-0.161	0.208	-0.776	0.439	lh_insula_thickness	28	136	0.639	NonSig
1q21.1del	0.179	0.208	0.863	0.390	rh_bankssts_thickness	28	136	0.596	NonSig
1q21.1del	0.168	0.208	0.807	0.421	rh_caudalanteriorcingulate_thickness	28	136	0.625	NonSig
1q21.1del	0.036	0.208	0.174	0.862	rh_caudalmiddlefrontal_thickness	28	136	0.926	NonSig
1q21.1del	-0.726	0.200	-3.626	0.000	rh_cuneus_thickness	28	136	0.006	Sig
1q21.1del	-0.143	0.208	-0.689	0.492	rh_entorhinal_thickness	28	136	0.671	NonSig
1q21.1del	-0.278	0.207	-1.341	0.182	rh_fusiform_thickness	28	136	0.394	NonSig
1q21.1del	0.131	0.208	0.631	0.529	rh_inferiorparietal_thickness	28	136	0.696	NonSig
1q21.1del	0.012	0.208	0.057	0.954	rh_inferiortemporal_thickness	28	136	0.974	NonSig
1q21.1del	0.272	0.207	1.312	0.191	rh_isthmuscingulate_thickness	28	136	0.404	NonSig
1q21.1del	-0.502	0.204	-2.456	0.015	rh_lateraloccipital_thickness	28	136	0.082	NonSig
1q21.1del	0.286	0.207	1.381	0.169	rh_lateralorbitofrontal_thickness	28	136	0.385	NonSig
1q21.1del	-0.509	0.204	-2.492	0.014	rh_lingual_thickness	28	136	0.079	NonSig
1q21.1del	0.485	0.205	2.371	0.019	rh_medialorbitofrontal_thickness	28	136	0.098	NonSig
1q21.1del	0.287	0.207	1.387	0.167	rh_middletemporal_thickness	28	136	0.385	NonSig
1q21.1del	-0.238	0.207	-1.146	0.253	rh parahippocampal_thickness	28	136	0.469	NonSig
1q21.1del	-0.652	0.202	-3.233	0.001	rh_paracentral_thickness	28	136	0.015	Sig
1q21.1del	0.052	0.208	0.250	0.803	rh_parsopercularis_thickness	28	136	0.892	NonSig
1q21.1del	0.029	0.208	0.141	0.888	rh_parsorbitalis_thickness	28	136	0.926	NonSig
1q21.1del	0.209	0.208	1.009	0.314	rh_parstriangularis_thickness	28	136	0.529	NonSig
1q21.1del	-0.932	0.195	-4.784	0.000	rh_pericalcarine_thickness	28	136	0.000	Sig
1q21.1del	0.055	0.208	0.263	0.793	rh_postcentral_thickness	28	136	0.888	NonSig
1q21.1del	0.064	0.208	0.305	0.761	rh_posteriorcingulate_thickness	28	136	0.859	NonSig
1q21.1del	-0.042	0.208	-0.204	0.839	rh_precentral_thickness	28	136	0.925	NonSig
1q21.1del	-0.151	0.208	-0.728	0.467	rh_precuneus_thickness	28	136	0.649	NonSig
1q21.1del	0.087	0.208	0.420	0.675	rh_rostralanteriorcingulate_thickness	28	136	0.798	NonSig
1q21.1del	0.170	0.208	0.817	0.415	rh_rostralmiddlefrontal_thickness	28	136	0.625	NonSig

1q21.1del	0.148	0.208	0.714	0.476	rh_superiorfrontal_thickness	28	136	0.655	NonSig
1q21.1del	-0.100	0.208	-0.480	0.632	rh_superiorparietal_thickness	28	136	0.776	NonSig
1q21.1del	0.621	0.202	3.071	0.003	rh_superiortemporal_thickness	28	136	0.022	Sig
1q21.1del	-0.114	0.208	-0.547	0.585	rh_supramarginal_thickness	28	136	0.757	NonSig
1q21.1del	0.368	0.206	1.783	0.076	rh_frontalpole_thickness	28	136	0.249	NonSig
1q21.1del	0.101	0.208	0.486	0.628	rh_temporalpole_thickness	28	136	0.776	NonSig
1q21.1del	0.019	0.208	0.093	0.926	rh_transversetemporal_thickness	28	136	0.952	NonSig
1q21.1del	-0.155	0.208	-0.747	0.456	rh_insula_thickness	28	136	0.646	NonSig
1q21.1del	0.295	0.207	1.424	0.156	lh_bankssts_area	28	135	0.373	NonSig
1q21.1del	0.297	0.207	1.435	0.153	lh_caudalanteriorcingulate_area	28	135	0.373	NonSig
1q21.1del	-0.670	0.201	-3.327	0.001	lh_caudalmiddlefrontal_area	28	135	0.012	Sig
1q21.1del	0.330	0.207	1.596	0.112	lh_cuneus_area	28	135	0.318	NonSig
1q21.1del	0.376	0.206	1.824	0.070	lh_entorhinal_area	28	135	0.244	NonSig
1q21.1del	-0.343	0.207	-1.663	0.098	lh_fusiform_area	28	135	0.284	NonSig
1q21.1del	0.410	0.206	1.991	0.048	lh_inferiorparietal_area	28	135	0.206	NonSig
1q21.1del	-0.104	0.208	-0.501	0.617	lh_inferiortemporal_area	28	135	0.776	NonSig
1q21.1del	0.585	0.203	2.882	0.004	lh_isthmuscingulate_area	28	135	0.034	Sig
1q21.1del	-0.387	0.206	-1.878	0.062	lh_lateraloccipital_area	28	135	0.227	NonSig
1q21.1del	-0.746	0.200	-3.732	0.000	lh_lateralorbitofrontal_area	28	135	0.004	Sig
1q21.1del	0.570	0.203	2.800	0.006	lh_lingual_area	28	135	0.038	Sig
1q21.1del	-0.408	0.206	-1.981	0.049	lh_medialorbitofrontal_area	28	135	0.206	NonSig
1q21.1del	0.218	0.208	1.052	0.294	lh_middletemporal_area	28	135	0.525	NonSig
1q21.1del	0.389	0.206	1.890	0.061	lh parahippocampal_area	28	135	0.227	NonSig
1q21.1del	-0.110	0.208	-0.527	0.599	lh_paracentral_area	28	135	0.761	NonSig
1q21.1del	-0.182	0.208	-0.877	0.382	lh_parsopercularis_area	28	135	0.593	NonSig
1q21.1del	-0.034	0.208	-0.162	0.872	lh_parsorbitalis_area	28	135	0.926	NonSig
1q21.1del	0.323	0.207	1.561	0.121	lh_parstriangularis_area	28	135	0.334	NonSig
1q21.1del	0.595	0.203	2.931	0.004	lh_pericalcarine_area	28	135	0.031	Sig
1q21.1del	0.423	0.206	2.059	0.041	lh_postcentral_area	28	135	0.187	NonSig
1q21.1del	0.208	0.208	1.003	0.317	lh_posteriorcingulate_area	28	135	0.529	NonSig
1q21.1del	-0.253	0.207	-1.218	0.225	lh_precentral_area	28	135	0.444	NonSig
1q21.1del	0.239	0.207	1.152	0.251	lh_precuneus_area	28	135	0.469	NonSig

1q21.1del	-0.297	0.207	-1.433	0.154	lh_rostralanteriorcingulate_area	28	135	0.373	NonSig
1q21.1del	-0.769	0.199	-3.861	0.000	lh_rostralmiddlefrontal_area	28	135	0.003	Sig
1q21.1del	-1.239	0.184	-6.734	0.000	lh_superiorfrontal_area	28	135	0.000	Sig
1q21.1del	0.206	0.208	0.990	0.324	lh_superiorparietal_area	28	135	0.534	NonSig
1q21.1del	-0.578	0.203	-2.846	0.005	lh_superiortemporal_area	28	135	0.036	Sig
1q21.1del	0.066	0.208	0.319	0.750	lh_supramarginal_area	28	135	0.859	NonSig
1q21.1del	0.371	0.206	1.798	0.074	lh_frontalpole_area	28	135	0.247	NonSig
1q21.1del	0.568	0.203	2.794	0.006	lh_temporalpole_area	28	135	0.038	Sig
1q21.1del	-0.371	0.206	-1.797	0.074	lh_transversetemporal_area	28	135	0.247	NonSig
1q21.1del	-0.111	0.208	-0.535	0.593	lh_insula_area	28	135	0.761	NonSig
1q21.1del	-0.063	0.208	-0.304	0.762	rh_bankssts_area	28	135	0.859	NonSig
1q21.1del	-0.029	0.208	-0.140	0.889	rh_caudalanteriorcingulate_area	28	135	0.926	NonSig
1q21.1del	-0.787	0.199	-3.956	0.000	rh_caudalmiddlefrontal_area	28	135	0.002	Sig
1q21.1del	-0.210	0.208	-1.013	0.313	rh_cuneus_area	28	135	0.529	NonSig
1q21.1del	0.448	0.205	2.181	0.031	rh_entorhinal_area	28	135	0.144	NonSig
1q21.1del	-0.299	0.207	-1.443	0.151	rh_fusiform_area	28	135	0.373	NonSig
1q21.1del	-0.132	0.208	-0.635	0.527	rh_inferioparietal_area	28	135	0.696	NonSig
1q21.1del	-0.157	0.208	-0.756	0.451	rh_inferiortemporal_area	28	135	0.644	NonSig
1q21.1del	0.349	0.206	1.689	0.093	rh_isthmusingulate_area	28	135	0.274	NonSig
1q21.1del	0.096	0.208	0.459	0.647	rh_lateraloccipital_area	28	135	0.789	NonSig
1q21.1del	-0.365	0.206	-1.769	0.079	rh_lateralorbitofrontal_area	28	135	0.252	NonSig
1q21.1del	0.303	0.207	1.466	0.145	rh_lingual_area	28	135	0.373	NonSig
1q21.1del	-0.247	0.207	-1.191	0.235	rh_medialorbitofrontal_area	28	135	0.450	NonSig
1q21.1del	0.001	0.208	0.003	0.998	rh_middletemporal_area	28	135	0.998	NonSig
1q21.1del	0.233	0.207	1.125	0.262	rh parahippocampal_area	28	135	0.480	NonSig
1q21.1del	0.001	0.208	0.005	0.996	rh_paracentral_area	28	135	0.998	NonSig
1q21.1del	-0.391	0.206	-1.897	0.060	rh_parsopercularis_area	28	135	0.227	NonSig
1q21.1del	0.182	0.208	0.874	0.384	rh_parsorbitalis_area	28	135	0.593	NonSig
1q21.1del	-0.358	0.206	-1.734	0.085	rh_parstriangularis_area	28	135	0.257	NonSig
1q21.1del	0.382	0.206	1.852	0.066	rh_pericalcarine_area	28	135	0.235	NonSig
1q21.1del	0.214	0.208	1.031	0.304	rh_postcentral_area	28	135	0.529	NonSig
1q21.1del	0.026	0.208	0.127	0.899	rh_posteriorcingulate_area	28	135	0.930	NonSig

1q21.1del	-0.357	0.206	-1.730	0.086	rh_precentral_area	28	135	0.257	NonSig
1q21.1del	0.159	0.208	0.764	0.446	rh_precuneus_area	28	135	0.643	NonSig
1q21.1del	-0.092	0.208	-0.442	0.659	rh_rostralanteriorcingulate_area	28	135	0.794	NonSig
1q21.1del	-0.532	0.204	-2.608	0.010	rh_rostralmiddlefrontal_area	28	135	0.060	NonSig
1q21.1del	-0.832	0.198	-4.206	0.000	rh_superiorfrontal_area	28	135	0.002	Sig
1q21.1del	0.674	0.201	3.346	0.001	rh_superiorparietal_area	28	135	0.012	Sig
1q21.1del	-0.211	0.208	-1.018	0.310	rh_superiortemporal_area	28	135	0.529	NonSig
1q21.1del	0.033	0.208	0.161	0.873	rh_supramarginal_area	28	135	0.926	NonSig
1q21.1del	0.293	0.207	1.414	0.159	rh_frontalpole_area	28	135	0.373	NonSig
1q21.1del	0.266	0.207	1.285	0.201	rh_temporalpole_area	28	135	0.418	NonSig
1q21.1del	-0.134	0.208	-0.642	0.522	rh_transversetemporal_area	28	135	0.696	NonSig
1q21.1del	0.134	0.208	0.644	0.521	rh_insula_area	28	135	0.696	NonSig
1q21.1del	-0.667	0.198	-3.367	0.001	Left-Thalamus-Proper	29	139	0.012	Sig
1q21.1del	-0.253	0.204	-1.239	0.217	Right-Thalamus-Proper	29	139	0.440	NonSig
1q21.1del	0.444	0.202	2.199	0.029	Left-Caudate	29	139	0.142	NonSig
1q21.1del	0.274	0.204	1.346	0.180	Right-Caudate	29	139	0.394	NonSig
1q21.1del	-0.081	0.205	-0.395	0.693	Left-Putamen	29	139	0.806	NonSig
1q21.1del	-0.006	0.205	-0.027	0.978	Right-Putamen	29	139	0.991	NonSig
1q21.1del	0.035	0.205	0.169	0.866	Left-Pallidum	29	139	0.926	NonSig
1q21.1del	-0.031	0.205	-0.151	0.880	Right-Pallidum	29	139	0.926	NonSig
1q21.1del	0.272	0.204	1.334	0.184	Left-Hippocampus	29	139	0.394	NonSig
1q21.1del	0.310	0.203	1.524	0.129	Right-Hippocampus	29	139	0.346	NonSig
1q21.1del	0.291	0.204	1.431	0.154	Left-Amygdala	29	139	0.373	NonSig
1q21.1del	0.213	0.204	1.044	0.298	Right-Amygdala	29	139	0.526	NonSig
1q21.1del	-0.250	0.204	-1.225	0.222	Left-Accumbens-area	29	139	0.444	NonSig
1q21.1del	-0.464	0.202	-2.303	0.023	Right-Accumbens-area	29	139	0.113	NonSig

**Table S5.**

Group differences in RID-scores for 1q21.1 distal deletion carriers, adjusted for affection status.

<b>CNV</b>	<b>Estimate</b>	<b>S.E.</b>	<b>T-value</b>	<b>P-value</b>	<b>Region of Interest</b>	<b>Cases</b>	<b>Controls</b>	<b>PFDR</b>	<b>Pcorrected</b>	<b>dic</b>
1q21.1del	-0.929	0.202	-4.591	0.000	lh_cuneus_thickness	28	136	0.000		Sig
1q21.1del	-0.532	0.210	-2.529	0.012	lh_parahippocampal_thickness	28	136	0.012		Sig
1q21.1del	-0.660	0.209	-3.160	0.002	lh_paracentral_thickness	28	136	0.003		Sig
1q21.1del	0.568	0.209	2.715	0.007	lh_parstriangularis_thickness	28	136	0.009		Sig
1q21.1del	-0.800	0.206	-3.889	0.000	lh_pericalcarine_thickness	28	136	0.000		Sig
1q21.1del	0.833	0.205	4.060	0.000	lh_superiortemporal_thickness	28	136	0.000		Sig
1q21.1del	0.715	0.208	3.442	0.001	lh_supramarginal_thickness	28	136	0.002		Sig
1q21.1del	-0.653	0.206	-3.173	0.002	rh_cuneus_thickness	28	136	0.003		Sig
1q21.1del	-0.737	0.207	-3.557	0.000	rh_paracentral_thickness	28	136	0.001		Sig
1q21.1del	-0.925	0.202	-4.589	0.000	rh_pericalcarine_thickness	28	136	0.000		Sig
1q21.1del	0.704	0.208	3.389	0.001	rh_superiortemporal_thickness	28	136	0.002		Sig
1q21.1del	-0.642	0.209	-3.074	0.002	lh_caudalmiddlefrontal_area	28	136	0.004		Sig
1q21.1del	0.566	0.210	2.694	0.008	lh_isthmuscingulate_area	28	136	0.009		Sig
1q21.1del	-0.715	0.206	-3.465	0.001	lh_lateralorbitofrontal_area	28	136	0.002		Sig
1q21.1del	0.621	0.210	2.961	0.004	lh_lingual_area	28	136	0.005		Sig
1q21.1del	0.590	0.210	2.810	0.006	lh_pericalcarine_area	28	136	0.007		Sig
1q21.1del	-0.799	0.206	-3.877	0.000	lh_rostralmiddlefrontal_area	28	136	0.000		Sig
1q21.1del	-1.214	0.191	-6.364	0.000	lh_superiorfrontal_area	28	136	0.000		Sig
1q21.1del	-0.592	0.210	-2.816	0.005	lh_superiortemporal_area	28	136	0.007		Sig
1q21.1del	0.546	0.210	2.594	0.010	lh_temporalpole_area	28	136	0.011		Sig
1q21.1del	-0.842	0.205	-4.108	0.000	rh_caudalmiddlefrontal_area	28	136	0.000		Sig
1q21.1del	-0.871	0.204	-4.262	0.000	rh_superiorfrontal_area	28	136	0.000		Sig
1q21.1del	0.667	0.208	3.198	0.002	rh_superiorparietal_area	28	136	0.003		Sig
1q21.1del	-0.551	0.212	-2.603	0.010	Left-Thalamus-Proper	28	136	0.011		Sig

Interaction effect between copy number status (i.e., 1q21.1 distal deletion vs non-carriers) and affection status on RID-scores.

CNV	Estimate	S.E.	T-value	P-value	Region of Interest	Cases	Controls	PFDR	Pcorrected_dic
1q21.1del	-0.632	0.448	-1.409	0.161	lh_cuneus_thickness	28	136	0.643	NonSig
1q21.1del	0.146	0.469	0.312	0.756	lh_parahippocampal_thickness	28	136	0.940	NonSig
1q21.1del	0.476	0.464	1.026	0.306	lh_paracentral_thickness	28	136	0.766	NonSig
1q21.1del	-0.037	0.466	-0.078	0.938	lh_parstriangularis_thickness	28	136	0.940	NonSig
1q21.1del	0.081	0.458	0.178	0.859	lh_pericalcarine_thickness	28	136	0.940	NonSig
1q21.1del	0.658	0.454	1.449	0.149	lh_superiortemporal_thickness	28	136	0.643	NonSig
1q21.1del	0.099	0.463	0.214	0.831	lh_supramarginal_thickness	28	136	0.940	NonSig
1q21.1del	-0.035	0.459	-0.076	0.940	rh_cuneus_thickness	28	136	0.940	NonSig
1q21.1del	0.076	0.462	0.166	0.869	rh_paracentral_thickness	28	136	0.940	NonSig
1q21.1del	-0.079	0.449	-0.175	0.861	rh_pericalcarine_thickness	28	136	0.940	NonSig
1q21.1del	1.193	0.453	2.632	0.009	rh_superiortemporal_thickness	28	136	0.224	NonSig
1q21.1del	-0.183	0.465	-0.393	0.695	lh_caudalmiddlefrontal_area	28	136	0.940	NonSig
1q21.1del	-0.732	0.464	-1.576	0.117	lh_isthmuscingulate_area	28	136	0.643	NonSig
1q21.1del	-0.078	0.460	-0.169	0.866	lh_lateralorbitofrontal_area	28	136	0.940	NonSig
1q21.1del	0.120	0.468	0.257	0.797	lh_lingual_area	28	136	0.940	NonSig
1q21.1del	0.184	0.468	0.394	0.694	lh_pericalcarine_area	28	136	0.940	NonSig
1q21.1del	-0.684	0.456	-1.500	0.136	lh_rostralmiddlefrontal_area	28	136	0.643	NonSig
1q21.1del	-0.307	0.424	-0.723	0.471	lh_superiorfrontal_area	28	136	0.940	NonSig
1q21.1del	-0.567	0.466	-1.216	0.226	lh_superiortemporal_area	28	136	0.766	NonSig
1q21.1del	0.467	0.468	0.999	0.319	lh_temporalpole_area	28	136	0.766	NonSig
1q21.1del	-0.255	0.456	-0.558	0.578	rh_caudalmiddlefrontal_area	28	136	0.940	NonSig
1q21.1del	0.468	0.454	1.031	0.304	rh_superiorfrontal_area	28	136	0.766	NonSig
1q21.1del	-0.988	0.458	-2.158	0.032	rh_superiorparietal_area	28	136	0.389	NonSig
1q21.1del	-0.298	0.471	-0.632	0.529	Left-Thalamus-Proper	28	136	0.940	NonSig



**Table S6.**

Interaction effect between copy number status (i.e., 1q21.1 distal deletion vs non-carriers) and cognitive ability on RID-scores.

<b>CNV</b>	<b>Estimate</b>	<b>S.E.</b>	<b>T-value</b>	<b>P-value</b>	<b>Region of Interest</b>	<b>PFDR</b>	<b>Pcorrected</b>	<b>dic</b>
1q21.1del	0.223	0.425	0.524	0.602	lh_cuneus_thickness	1	1	NonSig
1q21.1del	0.161	0.428	0.376	0.708	lh parahippocampal_thickness	1	1	NonSig
1q21.1del	-0.527	0.416	-1.269	0.209	lh_paracentral_thickness	1	1	NonSig
1q21.1del	-0.545	0.419	-1.299	0.198	lh_parstriangularis_thickness	1	1	NonSig
1q21.1del	0.426	0.407	1.044	0.300	lh_pericalcarine_thickness	1	1	NonSig
1q21.1del	-0.453	0.412	-1.100	0.275	lh_superiortemporal_thickness	1	1	NonSig
1q21.1del	-0.192	0.415	-0.464	0.644	lh_supramarginal_thickness	1	1	NonSig
1q21.1del	0.358	0.419	0.854	0.396	rh_cuneus_thickness	1	1	NonSig
1q21.1del	-0.342	0.421	-0.811	0.420	rh_paracentral_thickness	1	1	NonSig
1q21.1del	0.401	0.412	0.975	0.333	rh_pericalcarine_thickness	1	1	NonSig
1q21.1del	0.440	0.418	1.052	0.296	rh_superiortemporal_thickness	1	1	NonSig
1q21.1del	-0.217	0.428	-0.508	0.613	lh_caudalmiddlefrontal_area	1	1	NonSig
1q21.1del	-0.025	0.429	-0.058	0.954	lh_isthmuscingulate_area	1	1	NonSig
1q21.1del	0.333	0.415	0.803	0.425	lh_lateralorbitofrontal_area	1	1	NonSig
1q21.1del	0.213	0.420	0.508	0.613	lh_lingual_area	1	1	NonSig
1q21.1del	0.373	0.424	0.879	0.383	lh_pericalcarine_area	1	1	NonSig
1q21.1del	0.305	0.425	0.716	0.476	lh_rostralmiddlefrontal_area	1	1	NonSig
1q21.1del	0.007	0.392	0.018	0.985	lh_superiorfrontal_area	1	1	NonSig
1q21.1del	-0.307	0.422	-0.729	0.469	lh_superiortemporal_area	1	1	NonSig
1q21.1del	-0.405	0.427	-0.948	0.346	lh_temporalpole_area	1	1	NonSig
1q21.1del	-0.095	0.416	-0.229	0.819	rh_caudalmiddlefrontal_area	1	1	NonSig
1q21.1del	0.301	0.412	0.731	0.467	rh_superiorfrontal_area	1	1	NonSig
1q21.1del	0.629	0.423	1.484	0.142	rh_superiorparietal_area	1	1	NonSig
1q21.1del	0.415	0.399	1.040	0.302	Left-Thalamus-Proper	1	1	NonSig

**Table s7.**

Group differences in Z-scores for 1q21.1 distal deletion carriers, adjusted for the global effect (i.e., global index of cortical thickness for cortical thickness measures, global index of cortical surface area for cortical surface area measures, global index of subcortical volume for subcortical volume measures).

<b>CNV</b>	<b>Estimate</b>	<b>S.E.</b>	<b>T-value</b>	<b>P-value</b>	<b>Region of Interest</b>	<b>Cases</b>	<b>Controls</b>	<b>PFDR</b>	<b>Pcorrected dic</b>
1q21.1del	0.421	0.183	2.305	0.022	lh_bankssts_thickness	28	136	0.143	NonSig
1q21.1del	0.050	0.195	0.255	0.799	lh_caudalanteriorcingulate_thickness	28	136	0.922	NonSig
1q21.1del	0.261	0.155	1.678	0.095	lh_caudalmiddlefrontal_thickness	28	136	0.348	NonSig
1q21.1del	-0.791	0.157	-5.050	0.000	lh_cuneus_thickness	28	136	0.000	Sig
1q21.1del	-0.070	0.196	-0.358	0.721	lh_entorhinal_thickness	28	136	0.886	NonSig
1q21.1del	-0.203	0.173	-1.169	0.244	lh_fusiform_thickness	28	136	0.572	NonSig
1q21.1del	-0.045	0.134	-0.335	0.738	lh_inferioparietal_thickness	28	136	0.890	NonSig
1q21.1del	0.198	0.169	1.175	0.242	lh_inferiortemporal_thickness	28	136	0.572	NonSig
1q21.1del	0.267	0.206	1.297	0.196	lh_isthmusingulate_thickness	28	136	0.520	NonSig
1q21.1del	-0.359	0.160	-2.249	0.026	lh_lateraloccipital_thickness	28	136	0.155	NonSig
1q21.1del	0.238	0.167	1.421	0.157	lh_lateralorbitofrontal_thickness	28	136	0.472	NonSig
1q21.1del	-0.139	0.176	-0.790	0.430	lh_lingual_thickness	28	136	0.710	NonSig
1q21.1del	0.293	0.174	1.683	0.094	lh_medialorbitofrontal_thickness	28	136	0.348	NonSig
1q21.1del	0.346	0.160	2.171	0.031	lh_middletemporal_thickness	28	136	0.168	NonSig
1q21.1del	-0.496	0.190	-2.616	0.010	lh parahippocampal_thickness	28	136	0.073	NonSig
1q21.1del	-0.556	0.162	-3.430	0.001	lh_paracentral_thickness	28	136	0.013	Sig
1q21.1del	-0.133	0.153	-0.871	0.385	lh_parsopercularis_thickness	28	136	0.680	NonSig
1q21.1del	-0.139	0.180	-0.768	0.443	lh_parsorbitalis_thickness	28	136	0.723	NonSig
1q21.1del	0.459	0.164	2.801	0.006	lh_parstriangularis_thickness	28	136	0.056	NonSig
1q21.1del	-0.717	0.187	-3.847	0.000	lh_pericalcarine_thickness	28	136	0.006	Sig
1q21.1del	0.010	0.147	0.071	0.944	lh_postcentral_thickness	28	136	0.975	NonSig
1q21.1del	-0.198	0.188	-1.052	0.294	lh_posteriorcingulate_thickness	28	136	0.603	NonSig
1q21.1del	-0.141	0.158	-0.894	0.373	lh_precentral_thickness	28	136	0.666	NonSig
1q21.1del	0.056	0.136	0.415	0.679	lh_precuneus_thickness	28	136	0.871	NonSig
1q21.1del	0.371	0.183	2.029	0.044	lh_rostralanteriorcingulate_thickness	28	136	0.213	NonSig
1q21.1del	0.204	0.141	1.445	0.150	lh_rostralmiddlefrontal_thickness	28	136	0.462	NonSig
1q21.1del	0.075	0.131	0.571	0.569	lh_superiorfrontal_thickness	28	136	0.823	NonSig
1q21.1del	-0.121	0.150	-0.801	0.424	lh_superioparietal_thickness	28	136	0.710	NonSig

1q21.1del	0.483	0.136	3.544	0.001	lh_superiortemporal_thickness	28	136	0.011	Sig
1q21.1del	0.406	0.131	3.094	0.002	lh_supramarginal_thickness	28	136	0.029	Sig
1q21.1del	0.193	0.185	1.047	0.297	lh_frontalpole_thickness	28	136	0.603	NonSig
1q21.1del	0.289	0.187	1.545	0.124	lh_temporalpole_thickness	28	136	0.406	NonSig
1q21.1del	0.053	0.169	0.314	0.754	lh_transversetemporal_thickness	28	136	0.890	NonSig
1q21.1del	-0.081	0.186	-0.437	0.663	lh_insula_thickness	28	136	0.865	NonSig
1q21.1del	0.239	0.185	1.291	0.198	rh_bankssts_thickness	28	136	0.520	NonSig
1q21.1del	0.239	0.198	1.208	0.229	rh_caudalanteriorcingulate_thickness	28	136	0.554	NonSig
1q21.1del	-0.044	0.158	-0.280	0.780	rh_caudalmiddlefrontal_thickness	28	136	0.914	NonSig
1q21.1del	-0.625	0.160	-3.911	0.000	rh_cuneus_thickness	28	136	0.006	Sig
1q21.1del	-0.015	0.204	-0.074	0.941	rh_entorhinal_thickness	28	136	0.975	NonSig
1q21.1del	-0.213	0.166	-1.287	0.200	rh_fusiform_thickness	28	136	0.520	NonSig
1q21.1del	-0.028	0.145	-0.192	0.848	rh_inferioparietal_thickness	28	136	0.942	NonSig
1q21.1del	0.037	0.172	0.217	0.829	rh_inferiortemporal_thickness	28	136	0.935	NonSig
1q21.1del	0.450	0.205	2.200	0.029	rh_isthmuscingulate_thickness	28	136	0.162	NonSig
1q21.1del	-0.420	0.152	-2.768	0.006	rh_lateraloccipital_thickness	28	136	0.056	NonSig
1q21.1del	0.235	0.168	1.401	0.163	rh_lateralorbitofrontal_thickness	28	136	0.479	NonSig
1q21.1del	-0.428	0.177	-2.417	0.017	rh_lingual_thickness	28	136	0.119	NonSig
1q21.1del	0.450	0.172	2.616	0.010	rh_medialorbitofrontal_thickness	28	136	0.073	NonSig
1q21.1del	0.194	0.157	1.233	0.219	rh_middletemporal_thickness	28	136	0.539	NonSig
1q21.1del	-0.181	0.196	-0.924	0.357	rh parahippocampal_thickness	28	136	0.654	NonSig
1q21.1del	-0.575	0.154	-3.730	0.000	rh_paracentral_thickness	28	136	0.007	Sig
1q21.1del	-0.009	0.152	-0.062	0.951	rh_parsopercularis_thickness	28	136	0.975	NonSig
1q21.1del	0.040	0.167	0.237	0.813	rh_parsorbitalis_thickness	28	136	0.927	NonSig
1q21.1del	0.166	0.158	1.045	0.298	rh_parstriangularis_thickness	28	136	0.603	NonSig
1q21.1del	-0.839	0.184	-4.555	0.000	rh_pericalcarine_thickness	28	136	0.001	Sig
1q21.1del	0.000	0.165	0.001	0.999	rh_postcentral_thickness	28	136	0.999	NonSig
1q21.1del	0.111	0.191	0.579	0.563	rh_posteriorcingulate_thickness	28	136	0.823	NonSig
1q21.1del	-0.111	0.160	-0.692	0.490	rh_precentral_thickness	28	136	0.790	NonSig
1q21.1del	-0.182	0.133	-1.369	0.173	rh_precuneus_thickness	28	136	0.489	NonSig
1q21.1del	0.123	0.187	0.656	0.513	rh_rostralanteriorcingulate_thickness	28	136	0.801	NonSig
1q21.1del	0.082	0.148	0.553	0.581	rh_rostralmiddlefrontal_thickness	28	136	0.823	NonSig

1q21.1del	0.032	0.138	0.234	0.816	rh_superiorfrontal_thickness	28	136	0.927	NonSig
1q21.1del	-0.153	0.143	-1.069	0.287	rh_superiorparietal_thickness	28	136	0.603	NonSig
1q21.1del	0.392	0.142	2.763	0.006	rh_superiortemporal_thickness	28	136	0.056	NonSig
1q21.1del	-0.220	0.137	-1.608	0.110	rh_supramarginal_thickness	28	136	0.374	NonSig
1q21.1del	0.419	0.188	2.229	0.027	rh_frontalpole_thickness	28	136	0.157	NonSig
1q21.1del	0.188	0.190	0.988	0.325	rh_temporalpole_thickness	28	136	0.624	NonSig
1q21.1del	0.031	0.182	0.173	0.863	rh_transversetemporal_thickness	28	136	0.952	NonSig
1q21.1del	-0.075	0.180	-0.414	0.680	rh_insula_thickness	28	136	0.871	NonSig
1q21.1del	0.112	0.204	0.549	0.584	lh_bankssts_area	28	135	0.823	NonSig
1q21.1del	0.110	0.207	0.530	0.597	lh_caudalanteriorcingulate_area	28	135	0.829	NonSig
1q21.1del	-0.492	0.172	-2.861	0.005	lh_caudalmiddlefrontal_area	28	135	0.051	NonSig
1q21.1del	0.134	0.212	0.629	0.530	lh_cuneus_area	28	135	0.815	NonSig
1q21.1del	-0.104	0.224	-0.463	0.644	lh_entorhinal_area	28	135	0.855	NonSig
1q21.1del	-0.074	0.165	-0.449	0.654	lh_fusiform_area	28	135	0.861	NonSig
1q21.1del	0.416	0.173	2.403	0.017	lh_inferiorparietal_area	28	135	0.119	NonSig
1q21.1del	-0.028	0.174	-0.162	0.871	lh_inferiortemporal_area	28	135	0.952	NonSig
1q21.1del	0.418	0.199	2.100	0.037	lh_isthmuscingulate_area	28	135	0.193	NonSig
1q21.1del	-0.195	0.176	-1.110	0.269	lh_lateraloccipital_area	28	135	0.602	NonSig
1q21.1del	-0.200	0.133	-1.508	0.134	lh_lateralorbitofrontal_area	28	135	0.426	NonSig
1q21.1del	0.451	0.196	2.296	0.023	lh_lingual_area	28	135	0.143	NonSig
1q21.1del	-0.131	0.164	-0.796	0.427	lh_medialorbitofrontal_area	28	135	0.710	NonSig
1q21.1del	0.287	0.169	1.702	0.091	lh_middletemporal_area	28	135	0.348	NonSig
1q21.1del	0.170	0.203	0.839	0.403	lh parahippocampal_area	28	135	0.703	NonSig
1q21.1del	-0.244	0.190	-1.284	0.201	lh_paracentral_area	28	135	0.520	NonSig
1q21.1del	-0.148	0.186	-0.794	0.429	lh_parsopercularis_area	28	135	0.710	NonSig
1q21.1del	0.107	0.160	0.664	0.507	lh_parsorbitalis_area	28	135	0.801	NonSig
1q21.1del	0.219	0.196	1.120	0.264	lh_parsstriangularis_area	28	135	0.601	NonSig
1q21.1del	0.399	0.212	1.884	0.061	lh_pericalcarine_area	28	135	0.256	NonSig
1q21.1del	0.551	0.167	3.298	0.001	lh_postcentral_area	28	135	0.017	Sig
1q21.1del	0.108	0.198	0.544	0.587	lh_posteriorcingulate_area	28	135	0.823	NonSig
1q21.1del	-0.024	0.162	-0.145	0.885	lh_precentral_area	28	135	0.952	NonSig
1q21.1del	0.315	0.171	1.844	0.067	lh_precuneus_area	28	135	0.272	NonSig

1q21.1del	-0.181	0.182	-0.994	0.322	lh_rostralanteriorcingulate_area	28	135	0.624	NonSig
1q21.1del	-0.229	0.134	-1.709	0.089	lh_rostralmiddlefrontal_area	28	135	0.348	NonSig
1q21.1del	-0.460	0.123	-3.740	0.000	lh_superiorfrontal_area	28	135	0.007	Sig
1q21.1del	0.227	0.182	1.250	0.213	lh_superiorparietal_area	28	135	0.533	NonSig
1q21.1del	-0.252	0.155	-1.630	0.105	lh_superiortemporal_area	28	135	0.369	NonSig
1q21.1del	0.102	0.178	0.570	0.569	lh_supramarginal_area	28	135	0.823	NonSig
1q21.1del	-0.104	0.222	-0.466	0.642	lh_frontalpole_area	28	135	0.855	NonSig
1q21.1del	0.218	0.223	0.979	0.329	lh_temporalpole_area	28	135	0.624	NonSig
1q21.1del	-0.355	0.182	-1.948	0.053	lh_transversetemporal_area	28	135	0.240	NonSig
1q21.1del	-0.065	0.173	-0.375	0.708	lh_insula_area	28	135	0.886	NonSig
1q21.1del	-0.098	0.192	-0.511	0.610	rh_bankssts_area	28	135	0.831	NonSig
1q21.1del	-0.216	0.205	-1.051	0.295	rh_caudalanteriorcingulate_area	28	135	0.603	NonSig
1q21.1del	-0.580	0.177	-3.281	0.001	rh_caudalmiddlefrontal_area	28	135	0.017	Sig
1q21.1del	-0.075	0.189	-0.398	0.691	rh_cuneus_area	28	135	0.878	NonSig
1q21.1del	-0.044	0.222	-0.196	0.845	rh_entorhinal_area	28	135	0.942	NonSig
1q21.1del	0.012	0.154	0.077	0.939	rh_fusiform_area	28	135	0.975	NonSig
1q21.1del	0.060	0.160	0.374	0.709	rh_inferioparietal_area	28	135	0.886	NonSig
1q21.1del	-0.092	0.180	-0.511	0.610	rh_inferiortemporal_area	28	135	0.831	NonSig
1q21.1del	0.119	0.207	0.576	0.565	rh_isthmuscingulate_area	28	135	0.823	NonSig
1q21.1del	0.064	0.192	0.333	0.739	rh_lateraloccipital_area	28	135	0.890	NonSig
1q21.1del	-0.078	0.156	-0.501	0.617	rh_lateralorbitofrontal_area	28	135	0.834	NonSig
1q21.1del	0.301	0.188	1.596	0.112	rh_lingual_area	28	135	0.375	NonSig
1q21.1del	-0.052	0.163	-0.319	0.750	rh_medialorbitofrontal_area	28	135	0.890	NonSig
1q21.1del	0.173	0.161	1.078	0.283	rh_middletemporal_area	28	135	0.603	NonSig
1q21.1del	-0.008	0.209	-0.039	0.969	rh parahippocampal_area	28	135	0.975	NonSig
1q21.1del	-0.069	0.192	-0.362	0.718	rh_paracentral_area	28	135	0.886	NonSig
1q21.1del	-0.368	0.191	-1.924	0.056	rh_parsopercularis_area	28	135	0.240	NonSig
1q21.1del	0.118	0.189	0.625	0.533	rh_parsorbitalis_area	28	135	0.815	NonSig
1q21.1del	-0.398	0.194	-2.047	0.042	rh_parstriangularis_area	28	135	0.211	NonSig
1q21.1del	0.280	0.202	1.382	0.169	rh_pericalcarine_area	28	135	0.487	NonSig
1q21.1del	0.206	0.183	1.125	0.262	rh_postcentral_area	28	135	0.601	NonSig
1q21.1del	0.014	0.178	0.077	0.939	rh_posteriorcingulate_area	28	135	0.975	NonSig

1q21.1del	-0.111	0.165	-0.675	0.501	rh_precentral_area	28	135	0.799	NonSig
1q21.1del	0.320	0.162	1.979	0.050	rh_precuneus_area	28	135	0.232	NonSig
1q21.1del	-0.121	0.196	-0.617	0.538	rh_rostralanteriorcingulate_area	28	135	0.815	NonSig
1q21.1del	-0.140	0.145	-0.963	0.337	rh_rostralmiddlefrontal_area	28	135	0.631	NonSig
1q21.1del	-0.213	0.131	-1.627	0.106	rh_superiorfrontal_area	28	135	0.369	NonSig
1q21.1del	0.621	0.179	3.465	0.001	rh_superiorparietal_area	28	135	0.013	Sig
1q21.1del	0.022	0.152	0.145	0.885	rh_superiortemporal_area	28	135	0.952	NonSig
1q21.1del	0.010	0.184	0.054	0.957	rh_supramarginal_area	28	135	0.975	NonSig
1q21.1del	-0.070	0.220	-0.319	0.750	rh_frontalpole_area	28	135	0.890	NonSig
1q21.1del	-0.210	0.228	-0.923	0.358	rh_temporalpole_area	28	135	0.654	NonSig
1q21.1del	-0.190	0.193	-0.983	0.327	rh_transversetemporal_area	28	135	0.624	NonSig
1q21.1del	0.141	0.176	0.803	0.423	rh_insula_area	28	135	0.710	NonSig
1q21.1del	-0.440	0.150	-2.935	0.004	Left-Thalamus-Proper	29	139	0.044	Sig
1q21.1del	-0.144	0.146	-0.988	0.325	Right-Thalamus-Proper	29	139	0.624	NonSig
1q21.1del	0.301	0.156	1.929	0.055	Left-Caudate	29	139	0.240	NonSig
1q21.1del	0.187	0.149	1.254	0.211	Right-Caudate	29	139	0.533	NonSig
1q21.1del	0.020	0.139	0.140	0.888	Left-Putamen	29	139	0.952	NonSig
1q21.1del	0.034	0.131	0.260	0.795	Right-Putamen	29	139	0.922	NonSig
1q21.1del	0.019	0.177	0.109	0.914	Left-Pallidum	29	139	0.972	NonSig
1q21.1del	0.007	0.156	0.048	0.962	Right-Pallidum	29	139	0.975	NonSig
1q21.1del	0.211	0.146	1.443	0.151	Left-Hippocampus	29	139	0.462	NonSig
1q21.1del	0.151	0.142	1.060	0.290	Right-Hippocampus	29	139	0.603	NonSig
1q21.1del	0.207	0.161	1.287	0.200	Left-Amygdala	29	139	0.520	NonSig
1q21.1del	0.085	0.155	0.545	0.586	Right-Amygdala	29	139	0.823	NonSig
1q21.1del	-0.152	0.170	-0.894	0.373	Left-Accumbens-area	29	139	0.666	NonSig
1q21.1del	-0.441	0.167	-2.646	0.009	Right-Accumbens-area	29	139	0.073	NonSig

**Table S8.**

Group differences in Z-scores for 1q21.1 distal duplication carriers.

<b>CNV</b>	<b>Estimate</b>	<b>S.E.</b>	<b>T-value</b>	<b>P-value</b>	<b>Region of Interest</b>	<b>Cases</b>	<b>Controls</b>	<b>PFDR</b>	<b>Pcorrected</b>	<b>dic</b>
1q21.1.dup	-0.091	0.222	-0.410	0.682	lh_bankssts_thickness	25	114	0.890	NonSig	NonSig
1q21.1.dup	0.134	0.221	0.604	0.547	lh_caudalanteriorcingulate_thickness	25	114	0.811	NonSig	NonSig
1q21.1.dup	-0.003	0.222	-0.015	0.988	lh_caudalmiddlefrontal_thickness	25	114	0.995	NonSig	NonSig
1q21.1.dup	0.182	0.221	0.824	0.411	lh_cuneus_thickness	25	114	0.771	NonSig	NonSig
1q21.1.dup	-0.428	0.219	-1.957	0.052	lh_entorhinal_thickness	25	114	0.293	NonSig	NonSig
1q21.1.dup	-0.168	0.221	-0.761	0.448	lh_fusiform_thickness	25	114	0.785	NonSig	NonSig
1q21.1.dup	0.009	0.222	0.040	0.968	lh_inferiorparietal_thickness	25	114	0.995	NonSig	NonSig
1q21.1.dup	0.086	0.222	0.388	0.698	lh_inferiortemporal_thickness	25	114	0.895	NonSig	NonSig
1q21.1.dup	0.408	0.219	1.863	0.065	lh_isthmusingulate_thickness	25	114	0.293	NonSig	NonSig
1q21.1.dup	0.112	0.221	0.507	0.613	lh_lateraloccipital_thickness	25	114	0.855	NonSig	NonSig
1q21.1.dup	0.128	0.221	0.576	0.565	lh_lateralorbitofrontal_thickness	25	114	0.823	NonSig	NonSig
1q21.1.dup	0.233	0.221	1.054	0.294	lh_lingual_thickness	25	114	0.680	NonSig	NonSig
1q21.1.dup	0.471	0.218	2.163	0.032	lh_medialorbitofrontal_thickness	25	114	0.220	NonSig	NonSig
1q21.1.dup	-0.073	0.222	-0.332	0.741	lh_middletemporal_thickness	25	114	0.926	NonSig	NonSig
1q21.1.dup	0.148	0.221	0.671	0.504	lh_parahippocampal_thickness	25	114	0.798	NonSig	NonSig
1q21.1.dup	-0.221	0.221	-0.999	0.320	lh_paracentral_thickness	25	114	0.695	NonSig	NonSig
1q21.1.dup	0.164	0.221	0.740	0.460	lh_parsopercularis_thickness	25	114	0.785	NonSig	NonSig
1q21.1.dup	-0.140	0.221	-0.631	0.529	lh_parsorbitalis_thickness	25	114	0.806	NonSig	NonSig
1q21.1.dup	0.012	0.222	0.054	0.957	lh_parstriangularis_thickness	25	114	0.995	NonSig	NonSig
1q21.1.dup	0.294	0.220	1.336	0.184	lh_pericalcarine_thickness	25	114	0.520	NonSig	NonSig
1q21.1.dup	-0.322	0.220	-1.465	0.145	lh_postcentral_thickness	25	114	0.469	NonSig	NonSig
1q21.1.dup	0.082	0.222	0.369	0.713	lh_posteriorcingulate_thickness	25	114	0.906	NonSig	NonSig
1q21.1.dup	-0.313	0.220	-1.421	0.158	lh_precentral_thickness	25	114	0.473	NonSig	NonSig
1q21.1.dup	0.116	0.221	0.523	0.602	lh_precuneus_thickness	25	114	0.852	NonSig	NonSig
1q21.1.dup	0.278	0.220	1.261	0.209	lh_rostralanteriorcingulate_thickness	25	114	0.576	NonSig	NonSig
1q21.1.dup	0.162	0.221	0.732	0.466	lh_rostralmiddlefrontal_thickness	25	114	0.785	NonSig	NonSig
1q21.1.dup	0.035	0.222	0.159	0.874	lh_superiorfrontal_thickness	25	114	0.962	NonSig	NonSig
1q21.1.dup	0.041	0.222	0.186	0.853	lh_superiorparietal_thickness	25	114	0.962	NonSig	NonSig

1q21.1.dup	-0.271	0.220	-1.229	0.221	lh_superiortemporal_thickness	25	114	0.592	NonSig
1q21.1.dup	-0.153	0.221	-0.693	0.489	lh_supramarginal_thickness	25	114	0.798	NonSig
1q21.1.dup	0.147	0.221	0.666	0.506	lh_frontalpole_thickness	25	114	0.798	NonSig
1q21.1.dup	-0.514	0.217	-2.365	0.019	lh_temporalpole_thickness	25	114	0.208	NonSig
1q21.1.dup	-0.418	0.219	-1.912	0.058	lh_transversetemporal_thickness	25	114	0.293	NonSig
1q21.1.dup	-0.126	0.221	-0.568	0.571	lh_insula_thickness	25	114	0.824	NonSig
1q21.1.dup	-0.239	0.221	-1.083	0.281	rh_bankssts_thickness	25	114	0.680	NonSig
1q21.1.dup	-0.139	0.221	-0.626	0.532	rh_caudalanteriorcingulate_thickness	25	114	0.806	NonSig
1q21.1.dup	-0.193	0.221	-0.871	0.385	rh_caudalmiddlefrontal_thickness	25	114	0.771	NonSig
1q21.1.dup	0.228	0.221	1.032	0.304	rh_cuneus_thickness	25	114	0.680	NonSig
1q21.1.dup	-0.427	0.219	-1.955	0.053	rh_entorhinal_thickness	25	114	0.293	NonSig
1q21.1.dup	-0.303	0.220	-1.376	0.171	rh_fusiform_thickness	25	114	0.493	NonSig
1q21.1.dup	0.091	0.222	0.410	0.682	rh_inferioparietal_thickness	25	114	0.890	NonSig
1q21.1.dup	-0.018	0.222	-0.080	0.937	rh_inferiortemporal_thickness	25	114	0.995	NonSig
1q21.1.dup	0.234	0.221	1.061	0.290	rh_isthmusingulate_thickness	25	114	0.680	NonSig
1q21.1.dup	0.474	0.218	2.174	0.031	rh_lateraloccipital_thickness	25	114	0.220	NonSig
1q21.1.dup	-0.009	0.222	-0.043	0.966	rh_lateralorbitofrontal_thickness	25	114	0.995	NonSig
1q21.1.dup	-0.097	0.221	-0.437	0.663	rh_lingual_thickness	25	114	0.888	NonSig
1q21.1.dup	0.143	0.221	0.648	0.518	rh_medialorbitofrontal_thickness	25	114	0.801	NonSig
1q21.1.dup	-0.047	0.222	-0.214	0.831	rh_middletemporal_thickness	25	114	0.962	NonSig
1q21.1.dup	-0.190	0.221	-0.861	0.391	rh parahippocampal_thickness	25	114	0.771	NonSig
1q21.1.dup	-0.176	0.221	-0.794	0.428	rh_paracentral_thickness	25	114	0.780	NonSig
1q21.1.dup	0.267	0.220	1.210	0.228	rh_parsopercularis_thickness	25	114	0.597	NonSig
1q21.1.dup	-0.119	0.221	-0.538	0.592	rh_parsorbitalis_thickness	25	114	0.845	NonSig
1q21.1.dup	-0.055	0.222	-0.250	0.803	rh_parstriangularis_thickness	25	114	0.962	NonSig
1q21.1.dup	0.501	0.217	2.303	0.023	rh_pericalcarine_thickness	25	114	0.218	NonSig
1q21.1.dup	-0.133	0.221	-0.601	0.549	rh_postcentral_thickness	25	114	0.811	NonSig
1q21.1.dup	-0.036	0.222	-0.161	0.872	rh_posteriorcingulate_thickness	25	114	0.962	NonSig
1q21.1.dup	-0.175	0.221	-0.789	0.431	rh_precentral_thickness	25	114	0.780	NonSig
1q21.1.dup	-0.216	0.221	-0.979	0.330	rh_precuneus_thickness	25	114	0.706	NonSig
1q21.1.dup	-0.186	0.221	-0.840	0.402	rh_rostralanteriorcingulate_thickness	25	114	0.771	NonSig
1q21.1.dup	-0.146	0.221	-0.659	0.511	rh_rostralmiddlefrontal_thickness	25	114	0.798	NonSig



1q21.1.dup	-0.059	0.222	-0.266	0.791	rh_superiorfrontal_thickness	25	114	0.962	NonSig
1q21.1.dup	-0.044	0.222	-0.200	0.842	rh_superiorparietal_thickness	25	114	0.962	NonSig
1q21.1.dup	-0.186	0.221	-0.842	0.401	rh_superiortemporal_thickness	25	114	0.771	NonSig
1q21.1.dup	-0.023	0.222	-0.103	0.918	rh_supramarginal_thickness	25	114	0.984	NonSig
1q21.1.dup	0.231	0.221	1.044	0.298	rh_frontalpole_thickness	25	114	0.680	NonSig
1q21.1.dup	-0.321	0.220	-1.461	0.146	rh_temporalpole_thickness	25	114	0.469	NonSig
1q21.1.dup	-0.405	0.219	-1.850	0.066	rh_transversetemporal_thickness	25	114	0.293	NonSig
1q21.1.dup	0.049	0.222	0.223	0.824	rh_insula_thickness	25	114	0.962	NonSig
1q21.1.dup	0.046	0.222	0.207	0.836	lh_bankssts_area	25	111	0.962	NonSig
1q21.1.dup	0.326	0.220	1.479	0.142	lh_caudalanteriorcingulate_area	25	111	0.469	NonSig
1q21.1.dup	0.490	0.218	2.246	0.026	lh_caudalmiddlefrontal_area	25	111	0.220	NonSig
1q21.1.dup	0.183	0.222	0.824	0.411	lh_cuneus_area	25	111	0.771	NonSig
1q21.1.dup	-0.103	0.222	-0.463	0.644	lh_entorhinal_area	25	111	0.878	NonSig
1q21.1.dup	0.188	0.222	0.847	0.399	lh_fusiform_area	25	111	0.771	NonSig
1q21.1.dup	-0.012	0.222	-0.055	0.956	lh_inferiorparietal_area	25	111	0.995	NonSig
1q21.1.dup	-0.038	0.222	-0.173	0.863	lh_inferiortemporal_area	25	111	0.962	NonSig
1q21.1.dup	-0.419	0.219	-1.912	0.058	lh_isthmuscingulate_area	25	111	0.293	NonSig
1q21.1.dup	0.060	0.222	0.270	0.788	lh_lateraloccipital_area	25	111	0.962	NonSig
1q21.1.dup	0.166	0.222	0.749	0.455	lh_lateralorbitofrontal_area	25	111	0.785	NonSig
1q21.1.dup	-0.075	0.222	-0.338	0.736	lh_lingual_area	25	111	0.926	NonSig
1q21.1.dup	0.278	0.221	1.257	0.211	lh_medialorbitofrontal_area	25	111	0.576	NonSig
1q21.1.dup	0.000	0.222	0.001	0.999	lh_middletemporal_area	25	111	0.999	NonSig
1q21.1.dup	-0.173	0.222	-0.778	0.438	lh parahippocampal_area	25	111	0.782	NonSig
1q21.1.dup	0.671	0.215	3.129	0.002	lh_paracentral_area	25	111	0.065	NonSig
1q21.1.dup	0.597	0.216	2.761	0.007	lh_parsopercularis_area	25	111	0.141	NonSig
1q21.1.dup	0.097	0.222	0.439	0.661	lh_parsorbitalis_area	25	111	0.888	NonSig
1q21.1.dup	0.167	0.222	0.751	0.454	lh_parstriangularis_area	25	111	0.785	NonSig
1q21.1.dup	0.244	0.221	1.105	0.271	lh_pericalcarine_area	25	111	0.678	NonSig
1q21.1.dup	-0.050	0.222	-0.224	0.823	lh_postcentral_area	25	111	0.962	NonSig
1q21.1.dup	0.483	0.218	2.212	0.029	lh_posteriorcingulate_area	25	111	0.220	NonSig
1q21.1.dup	0.266	0.221	1.204	0.231	lh_precentral_area	25	111	0.597	NonSig
1q21.1.dup	-0.032	0.222	-0.146	0.884	lh_precuneus_area	25	111	0.962	NonSig

1q21.1.dup	0.316	0.221	1.434	0.154	lh_rostralanteriorcingulate_area	25	111	0.473	NonSig
1q21.1.dup	0.587	0.216	2.714	0.008	lh_rostralmiddlefrontal_area	25	111	0.141	NonSig
1q21.1.dup	0.501	0.218	2.296	0.023	lh_superiorfrontal_area	25	111	0.218	NonSig
1q21.1.dup	0.335	0.220	1.522	0.130	lh_superioparietal_area	25	111	0.466	NonSig
1q21.1.dup	0.156	0.222	0.703	0.484	lh_superiortemporal_area	25	111	0.798	NonSig
1q21.1.dup	0.524	0.218	2.409	0.017	lh_supramarginal_area	25	111	0.200	NonSig
1q21.1.dup	0.407	0.219	1.855	0.066	lh_frontalpole_area	25	111	0.293	NonSig
1q21.1.dup	-0.175	0.222	-0.789	0.432	lh_temporalpole_area	25	111	0.780	NonSig
1q21.1.dup	0.627	0.216	2.909	0.004	lh_transversetemporal_area	25	111	0.106	NonSig
1q21.1.dup	0.112	0.222	0.504	0.615	lh_insula_area	25	111	0.855	NonSig
1q21.1.dup	0.032	0.222	0.144	0.885	rh_bankssts_area	25	111	0.962	NonSig
1q21.1.dup	-0.006	0.222	-0.026	0.979	rh_caudalanteriorcingulate_area	25	111	0.995	NonSig
1q21.1.dup	0.544	0.217	2.505	0.013	rh_caudalmiddlefrontal_area	25	111	0.168	NonSig
1q21.1.dup	0.380	0.220	1.728	0.086	rh_cuneus_area	25	111	0.359	NonSig
1q21.1.dup	0.089	0.222	0.399	0.691	rh_entorhinal_area	25	111	0.893	NonSig
1q21.1.dup	-0.374	0.220	-1.702	0.091	rh_fusiform_area	25	111	0.369	NonSig
1q21.1.dup	-0.107	0.222	-0.482	0.631	rh_inferioparietal_area	25	111	0.868	NonSig
1q21.1.dup	0.154	0.222	0.696	0.487	rh_inferiortemporal_area	25	111	0.798	NonSig
1q21.1.dup	-0.052	0.222	-0.236	0.814	rh_isthmuscingulate_area	25	111	0.962	NonSig
1q21.1.dup	0.188	0.222	0.850	0.397	rh_lateraloccipital_area	25	111	0.771	NonSig
1q21.1.dup	0.256	0.221	1.156	0.250	rh_lateralorbitofrontal_area	25	111	0.635	NonSig
1q21.1.dup	0.337	0.220	1.529	0.129	rh_lingual_area	25	111	0.466	NonSig
1q21.1.dup	0.052	0.222	0.232	0.817	rh_medialorbitofrontal_area	25	111	0.962	NonSig
1q21.1.dup	0.230	0.221	1.038	0.301	rh_middletemporal_area	25	111	0.680	NonSig
1q21.1.dup	0.474	0.218	2.169	0.032	rh_parahippocampal_area	25	111	0.220	NonSig
1q21.1.dup	0.452	0.219	2.065	0.041	rh_paracentral_area	25	111	0.266	NonSig
1q21.1.dup	0.701	0.214	3.281	0.001	rh_parsopercularis_area	25	111	0.049	Sig
1q21.1.dup	-0.148	0.222	-0.669	0.505	rh_parsorbitalis_area	25	111	0.798	NonSig
1q21.1.dup	0.040	0.222	0.182	0.856	rh_parstriangularis_area	25	111	0.962	NonSig
1q21.1.dup	0.355	0.220	1.611	0.110	rh_pericalcarine_area	25	111	0.421	NonSig
1q21.1.dup	0.093	0.222	0.417	0.677	rh_postcentral_area	25	111	0.890	NonSig
1q21.1.dup	0.485	0.218	2.222	0.028	rh_posteriorcingulate_area	25	111	0.220	NonSig

1q21.1.dup	0.231	0.221	1.043	0.299	rh_precentral_area	25	111	0.680	NonSig
1q21.1.dup	0.407	0.219	1.853	0.066	rh_precuneus_area	25	111	0.293	NonSig
1q21.1.dup	0.183	0.222	0.825	0.411	rh_rostralanteriorcingulate_area	25	111	0.771	NonSig
1q21.1.dup	0.550	0.217	2.532	0.012	rh_rostralmiddlefrontal_area	25	111	0.168	NonSig
1q21.1.dup	0.759	0.212	3.575	0.000	rh_superiorfrontal_area	25	111	0.025	Sig
1q21.1.dup	0.329	0.220	1.494	0.138	rh_superiorparietal_area	25	111	0.469	NonSig
1q21.1.dup	0.221	0.221	1.000	0.319	rh_superiortemporal_area	25	111	0.695	NonSig
1q21.1.dup	0.371	0.220	1.687	0.094	rh_supramarginal_area	25	111	0.371	NonSig
1q21.1.dup	0.567	0.217	2.614	0.010	rh_frontalpole_area	25	111	0.166	NonSig
1q21.1.dup	0.057	0.222	0.255	0.799	rh_temporalpole_area	25	111	0.962	NonSig
1q21.1.dup	0.547	0.217	2.520	0.013	rh_transversetemporal_area	25	111	0.168	NonSig
1q21.1.dup	0.005	0.222	0.022	0.982	rh_insula_area	25	111	0.995	NonSig
1q21.1.dup	-0.025	0.225	-0.109	0.913	Left-Thalamus-Proper	24	118	0.984	NonSig
1q21.1.dup	-0.015	0.225	-0.065	0.948	Right-Thalamus-Proper	24	118	0.995	NonSig
1q21.1.dup	-0.404	0.222	-1.817	0.071	Left-Caudate	24	118	0.306	NonSig
1q21.1.dup	-0.204	0.224	-0.909	0.365	Right-Caudate	24	118	0.771	NonSig
1q21.1.dup	-0.414	0.222	-1.867	0.064	Left-Putamen	24	118	0.293	NonSig
1q21.1.dup	-0.420	0.222	-1.892	0.061	Right-Putamen	24	118	0.293	NonSig
1q21.1.dup	-0.351	0.223	-1.577	0.117	Left-Pallidum	24	118	0.439	NonSig
1q21.1.dup	-0.314	0.223	-1.406	0.162	Right-Pallidum	24	118	0.477	NonSig
1q21.1.dup	-0.861	0.213	-4.049	0.000	Left-Hippocampus	24	118	0.013	Sig
1q21.1.dup	-0.766	0.215	-3.562	0.001	Right-Hippocampus	24	118	0.025	Sig
1q21.1.dup	-0.439	0.222	-1.981	0.050	Left-Amygdala	24	118	0.293	NonSig
1q21.1.dup	0.134	0.224	0.597	0.551	Right-Amygdala	24	118	0.811	NonSig
1q21.1.dup	-0.325	0.223	-1.459	0.147	Left-Accumbens-area	24	118	0.469	NonSig
1q21.1.dup	0.317	0.223	1.422	0.157	Right-Accumbens-area	24	118	0.473	NonSig

**Table S9.**

Group differences in RID-scores for 1q21.1 distal duplication carriers.

<b>CNV</b>	<b>Estimate</b>	<b>S.E.</b>	<b>T-value</b>	<b>P-value</b>	<b>Region of Interest</b>	<b>Cases</b>	<b>Controls</b>	<b>PFDR</b>	<b>Pcorrected</b>	<b>dic</b>
1q21.1.dup	-0.048	0.222	-0.216	0.829	lh_bankssts_thickness	25	114	0.962	NonSig	NonSig
1q21.1.dup	0.134	0.221	0.605	0.546	lh_caudalanteriorcingulate_thickness	25	114	0.759	NonSig	NonSig
1q21.1.dup	0.053	0.222	0.240	0.811	lh_caudalmiddlefrontal_thickness	25	114	0.962	NonSig	NonSig
1q21.1.dup	0.261	0.221	1.185	0.238	lh_cuneus_thickness	25	114	0.644	NonSig	NonSig
1q21.1.dup	-0.431	0.219	-1.970	0.051	lh_entorhinal_thickness	25	114	0.364	NonSig	NonSig
1q21.1.dup	-0.167	0.221	-0.757	0.451	lh_fusiform_thickness	25	114	0.718	NonSig	NonSig
1q21.1.dup	0.069	0.222	0.310	0.757	lh_inferiorparietal_thickness	25	114	0.938	NonSig	NonSig
1q21.1.dup	0.117	0.221	0.530	0.597	lh_inferiortemporal_thickness	25	114	0.793	NonSig	NonSig
1q21.1.dup	0.491	0.218	2.256	0.026	lh_isthmuscingulate_thickness	25	114	0.248	NonSig	NonSig
1q21.1.dup	0.213	0.221	0.966	0.336	lh_lateraloccipital_thickness	25	114	0.662	NonSig	NonSig
1q21.1.dup	0.175	0.221	0.793	0.429	lh_lateralorbitofrontal_thickness	25	114	0.718	NonSig	NonSig
1q21.1.dup	0.352	0.220	1.603	0.111	lh_lingual_thickness	25	114	0.467	NonSig	NonSig
1q21.1.dup	0.550	0.217	2.537	0.012	lh_medialorbitofrontal_thickness	25	114	0.186	NonSig	NonSig
1q21.1.dup	-0.062	0.222	-0.278	0.782	lh_middletemporal_thickness	25	114	0.953	NonSig	NonSig
1q21.1.dup	0.162	0.221	0.734	0.464	lh_parahippocampal_thickness	25	114	0.718	NonSig	NonSig
1q21.1.dup	-0.234	0.221	-1.059	0.292	lh_paracentral_thickness	25	114	0.662	NonSig	NonSig
1q21.1.dup	0.241	0.221	1.092	0.277	lh_parsopercularis_thickness	25	114	0.662	NonSig	NonSig
1q21.1.dup	-0.171	0.221	-0.774	0.441	lh_parsorbitalis_thickness	25	114	0.718	NonSig	NonSig
1q21.1.dup	0.008	0.222	0.037	0.971	lh_parstriangularis_thickness	25	114	0.983	NonSig	NonSig
1q21.1.dup	0.340	0.220	1.547	0.124	lh_pericalcarine_thickness	25	114	0.467	NonSig	NonSig
1q21.1.dup	-0.392	0.219	-1.791	0.076	lh_postcentral_thickness	25	114	0.453	NonSig	NonSig
1q21.1.dup	0.127	0.221	0.573	0.567	lh_posteriorcingulate_thickness	25	114	0.774	NonSig	NonSig
1q21.1.dup	-0.362	0.219	-1.650	0.101	lh_precentral_thickness	25	114	0.467	NonSig	NonSig
1q21.1.dup	0.220	0.221	0.994	0.322	lh_precuneus_thickness	25	114	0.662	NonSig	NonSig
1q21.1.dup	0.267	0.220	1.210	0.228	lh_rostralanteriorcingulate_thickness	25	114	0.634	NonSig	NonSig
1q21.1.dup	0.216	0.221	0.977	0.330	lh_rostralmiddlefrontal_thickness	25	114	0.662	NonSig	NonSig
1q21.1.dup	0.091	0.222	0.412	0.681	lh_superiorfrontal_thickness	25	114	0.865	NonSig	NonSig
1q21.1.dup	0.098	0.221	0.442	0.659	lh_superiorparietal_thickness	25	114	0.845	NonSig	NonSig

lq21.1.dup	-0.327	0.220	-1.486	0.140	lh_superiortemporal_thickness	25	114	0.476	NonSig
lq21.1.dup	-0.172	0.221	-0.779	0.438	lh_supramarginal_thickness	25	114	0.718	NonSig
lq21.1.dup	0.247	0.221	1.121	0.264	lh_frontalpole_thickness	25	114	0.660	NonSig
lq21.1.dup	-0.485	0.218	-2.227	0.028	lh_temporalpole_thickness	25	114	0.248	NonSig
lq21.1.dup	-0.514	0.217	-2.368	0.019	lh_transversetemporal_thickness	25	114	0.248	NonSig
lq21.1.dup	-0.162	0.221	-0.732	0.466	lh_insula_thickness	25	114	0.718	NonSig
lq21.1.dup	-0.229	0.221	-1.036	0.302	rh_bankssts_thickness	25	114	0.662	NonSig
lq21.1.dup	-0.164	0.221	-0.742	0.459	rh_caudalanteriorcingulate_thickness	25	114	0.718	NonSig
lq21.1.dup	-0.209	0.221	-0.947	0.345	rh_caudalmiddlefrontal_thickness	25	114	0.664	NonSig
lq21.1.dup	0.329	0.220	1.494	0.137	rh_cuneus_thickness	25	114	0.476	NonSig
lq21.1.dup	-0.382	0.219	-1.740	0.084	rh_entorhinal_thickness	25	114	0.467	NonSig
lq21.1.dup	-0.357	0.220	-1.625	0.106	rh_fusiform_thickness	25	114	0.467	NonSig
lq21.1.dup	0.258	0.221	1.168	0.245	rh_inferioparietal_thickness	25	114	0.644	NonSig
lq21.1.dup	-0.005	0.222	-0.024	0.981	rh_inferiortemporal_thickness	25	114	0.983	NonSig
lq21.1.dup	0.340	0.220	1.549	0.124	rh_isthmuscingulate_thickness	25	114	0.467	NonSig
lq21.1.dup	0.633	0.215	2.946	0.004	rh_lateraloccipital_thickness	25	114	0.085	NonSig
lq21.1.dup	0.017	0.222	0.075	0.940	rh_lateralorbitofrontal_thickness	25	114	0.980	NonSig
lq21.1.dup	-0.062	0.222	-0.282	0.778	rh_lingual_thickness	25	114	0.953	NonSig
lq21.1.dup	0.178	0.221	0.804	0.423	rh_medialorbitofrontal_thickness	25	114	0.718	NonSig
lq21.1.dup	-0.015	0.222	-0.066	0.948	rh_middletemporal_thickness	25	114	0.980	NonSig
lq21.1.dup	-0.149	0.221	-0.675	0.501	rh parahippocampal_thickness	25	114	0.740	NonSig
lq21.1.dup	-0.217	0.221	-0.981	0.328	rh_paracentral_thickness	25	114	0.662	NonSig
lq21.1.dup	0.366	0.219	1.666	0.098	rh_parsopercularis_thickness	25	114	0.467	NonSig
lq21.1.dup	-0.086	0.222	-0.389	0.698	rh_parsorbitalis_thickness	25	114	0.872	NonSig
lq21.1.dup	-0.039	0.222	-0.178	0.859	rh_parstriangularis_thickness	25	114	0.962	NonSig
lq21.1.dup	0.556	0.217	2.567	0.011	rh_pericalcarine_thickness	25	114	0.186	NonSig
lq21.1.dup	-0.147	0.221	-0.665	0.507	rh_postcentral_thickness	25	114	0.740	NonSig
lq21.1.dup	0.016	0.222	0.074	0.941	rh_posteriorcingulate_thickness	25	114	0.980	NonSig
lq21.1.dup	-0.228	0.221	-1.032	0.304	rh_precentral_thickness	25	114	0.662	NonSig
lq21.1.dup	-0.239	0.221	-1.082	0.281	rh_precuneus_thickness	25	114	0.662	NonSig
lq21.1.dup	-0.157	0.221	-0.709	0.479	rh_rostralanteriorcingulate_thickness	25	114	0.719	NonSig
lq21.1.dup	-0.159	0.221	-0.717	0.474	rh_rostralmiddlefrontal_thickness	25	114	0.719	NonSig

1q21.1.dup	-0.049	0.222	-0.221	0.826	rh_superiorfrontal_thickness	25	114	0.962	NonSig
1q21.1.dup	0.010	0.222	0.047	0.963	rh_superiorparietal_thickness	25	114	0.983	NonSig
1q21.1.dup	-0.225	0.221	-1.021	0.309	rh_superiortemporal_thickness	25	114	0.662	NonSig
1q21.1.dup	-0.017	0.222	-0.077	0.939	rh_supramarginal_thickness	25	114	0.980	NonSig
1q21.1.dup	0.216	0.221	0.980	0.329	rh_frontalpole_thickness	25	114	0.662	NonSig
1q21.1.dup	-0.349	0.220	-1.591	0.114	rh_temporalpole_thickness	25	114	0.467	NonSig
1q21.1.dup	-0.483	0.218	-2.220	0.028	rh_transversetemporal_thickness	25	114	0.248	NonSig
1q21.1.dup	0.037	0.222	0.167	0.868	rh_insula_thickness	25	114	0.964	NonSig
1q21.1.dup	-0.244	0.221	-1.105	0.271	lh_bankssts_area	25	111	0.662	NonSig
1q21.1.dup	0.087	0.222	0.392	0.696	lh_caudalanteriorcingulate_area	25	111	0.872	NonSig
1q21.1.dup	0.277	0.221	1.252	0.213	lh_caudalmiddlefrontal_area	25	111	0.602	NonSig
1q21.1.dup	0.017	0.222	0.075	0.940	lh_cuneus_area	25	111	0.980	NonSig
1q21.1.dup	-0.360	0.220	-1.636	0.104	lh_entorhinal_area	25	111	0.467	NonSig
1q21.1.dup	-0.040	0.222	-0.181	0.857	lh_fusiform_area	25	111	0.962	NonSig
1q21.1.dup	-0.288	0.221	-1.306	0.194	lh_inferiorparietal_area	25	111	0.581	NonSig
1q21.1.dup	-0.334	0.220	-1.515	0.132	lh_inferiortemporal_area	25	111	0.472	NonSig
1q21.1.dup	-0.693	0.214	-3.240	0.002	lh_isthmuscingulate_area	25	111	0.056	NonSig
1q21.1.dup	-0.206	0.221	-0.928	0.355	lh_lateraloccipital_area	25	111	0.672	NonSig
1q21.1.dup	-0.032	0.222	-0.143	0.886	lh_lateralorbitofrontal_area	25	111	0.965	NonSig
1q21.1.dup	-0.291	0.221	-1.319	0.190	lh_lingual_area	25	111	0.580	NonSig
1q21.1.dup	0.106	0.222	0.477	0.634	lh_medialorbitofrontal_area	25	111	0.827	NonSig
1q21.1.dup	-0.254	0.221	-1.151	0.252	lh_middletemporal_area	25	111	0.644	NonSig
1q21.1.dup	-0.408	0.219	-1.861	0.065	lh parahippocampal_area	25	111	0.412	NonSig
1q21.1.dup	0.487	0.218	2.230	0.027	lh_paracentral_area	25	111	0.248	NonSig
1q21.1.dup	0.371	0.220	1.689	0.093	lh_parsopercularis_area	25	111	0.467	NonSig
1q21.1.dup	-0.140	0.222	-0.630	0.530	lh_parsorbitalis_area	25	111	0.748	NonSig
1q21.1.dup	-0.050	0.222	-0.226	0.822	lh_parstriangularis_area	25	111	0.962	NonSig
1q21.1.dup	0.033	0.222	0.150	0.881	lh_pericalcarine_area	25	111	0.965	NonSig
1q21.1.dup	-0.336	0.220	-1.526	0.129	lh_postcentral_area	25	111	0.472	NonSig
1q21.1.dup	0.254	0.221	1.151	0.252	lh_posteriorcingulate_area	25	111	0.644	NonSig
1q21.1.dup	0.055	0.222	0.248	0.805	lh_precentral_area	25	111	0.962	NonSig
1q21.1.dup	-0.199	0.222	-0.899	0.370	lh_precuneus_area	25	111	0.678	NonSig

1q21.1.dup	0.122	0.222	0.549	0.584	lh_rostralanteriorcingulate_area	25	111	0.782	NonSig
1q21.1.dup	0.489	0.218	2.243	0.027	lh_rostralmiddlefrontal_area	25	111	0.248	NonSig
1q21.1.dup	0.364	0.220	1.657	0.100	lh_superiorfrontal_area	25	111	0.467	NonSig
1q21.1.dup	0.182	0.222	0.823	0.412	lh_superioparietal_area	25	111	0.718	NonSig
1q21.1.dup	-0.113	0.222	-0.509	0.612	lh_superiortemporal_area	25	111	0.805	NonSig
1q21.1.dup	0.385	0.220	1.751	0.082	lh_supramarginal_area	25	111	0.467	NonSig
1q21.1.dup	0.138	0.222	0.624	0.534	lh_frontalpole_area	25	111	0.748	NonSig
1q21.1.dup	-0.407	0.219	-1.854	0.066	lh_temporalpole_area	25	111	0.412	NonSig
1q21.1.dup	0.478	0.218	2.191	0.030	lh_transversetemporal_area	25	111	0.252	NonSig
1q21.1.dup	-0.122	0.222	-0.550	0.583	lh_insula_area	25	111	0.782	NonSig
1q21.1.dup	-0.187	0.222	-0.845	0.400	rh_bankssts_area	25	111	0.715	NonSig
1q21.1.dup	-0.238	0.221	-1.077	0.284	rh_caudalanteriorcingulate_area	25	111	0.662	NonSig
1q21.1.dup	0.316	0.221	1.433	0.154	rh_caudalmiddlefrontal_area	25	111	0.514	NonSig
1q21.1.dup	0.199	0.222	0.898	0.371	rh_cuneus_area	25	111	0.678	NonSig
1q21.1.dup	-0.129	0.222	-0.583	0.561	rh_entorhinal_area	25	111	0.772	NonSig
1q21.1.dup	-0.632	0.215	-2.932	0.004	rh_fusiform_area	25	111	0.085	NonSig
1q21.1.dup	-0.416	0.219	-1.896	0.060	rh_inferioparietal_area	25	111	0.410	NonSig
1q21.1.dup	-0.167	0.222	-0.753	0.453	rh_inferiortemporal_area	25	111	0.718	NonSig
1q21.1.dup	-0.299	0.221	-1.353	0.178	rh_isthmuscingulate_area	25	111	0.557	NonSig
1q21.1.dup	-0.021	0.222	-0.096	0.923	rh_lateraloccipital_area	25	111	0.980	NonSig
1q21.1.dup	0.040	0.222	0.181	0.857	rh_lateralorbitofrontal_area	25	111	0.962	NonSig
1q21.1.dup	0.142	0.222	0.638	0.524	rh_lingual_area	25	111	0.748	NonSig
1q21.1.dup	-0.254	0.221	-1.147	0.253	rh_medialorbitofrontal_area	25	111	0.644	NonSig
1q21.1.dup	-0.043	0.222	-0.191	0.848	rh_middletemporal_area	25	111	0.962	NonSig
1q21.1.dup	0.236	0.221	1.066	0.289	rh parahippocampal_area	25	111	0.662	NonSig
1q21.1.dup	0.301	0.221	1.363	0.175	rh_paracentral_area	25	111	0.557	NonSig
1q21.1.dup	0.550	0.217	2.534	0.012	rh_parsopercularis_area	25	111	0.186	NonSig
1q21.1.dup	-0.432	0.219	-1.970	0.051	rh_parsorbitalis_area	25	111	0.364	NonSig
1q21.1.dup	-0.204	0.222	-0.921	0.359	rh_parsstriangularis_area	25	111	0.672	NonSig
1q21.1.dup	0.145	0.222	0.655	0.513	rh_pericalcarine_area	25	111	0.740	NonSig
1q21.1.dup	-0.104	0.222	-0.470	0.639	rh_postcentral_area	25	111	0.827	NonSig
1q21.1.dup	0.280	0.221	1.266	0.208	rh_posteriorcingulate_area	25	111	0.602	NonSig

1q21.1.dup	-0.005	0.222	-0.022	0.983	rh_precentral_area	25	111	0.983	NonSig
1q21.1.dup	0.187	0.222	0.844	0.400	rh_precuneus_area	25	111	0.715	NonSig
1q21.1.dup	0.040	0.222	0.178	0.859	rh_rostralanteriorcingulate_area	25	111	0.962	NonSig
1q21.1.dup	0.449	0.219	2.054	0.042	rh_rostralmiddlefrontal_area	25	111	0.331	NonSig
1q21.1.dup	0.753	0.212	3.543	0.001	rh_superiorfrontal_area	25	111	0.056	NonSig
1q21.1.dup	0.161	0.222	0.726	0.469	rh_superiorparietal_area	25	111	0.718	NonSig
1q21.1.dup	-0.015	0.222	-0.070	0.945	rh_superiortemporal_area	25	111	0.980	NonSig
1q21.1.dup	0.169	0.222	0.763	0.447	rh_supramarginal_area	25	111	0.718	NonSig
1q21.1.dup	0.309	0.221	1.400	0.164	rh_frontalpole_area	25	111	0.534	NonSig
1q21.1.dup	-0.214	0.221	-0.968	0.335	rh_temporalpole_area	25	111	0.662	NonSig
1q21.1.dup	0.340	0.220	1.545	0.125	rh_transversetemporal_area	25	111	0.467	NonSig
1q21.1.dup	-0.211	0.221	-0.952	0.343	rh_insula_area	25	111	0.664	NonSig
1q21.1.dup	0.352	0.223	1.579	0.117	Left-Thalamus-Proper	24	118	0.467	NonSig
1q21.1.dup	0.378	0.222	1.700	0.091	Right-Thalamus-Proper	24	118	0.467	NonSig
1q21.1.dup	-0.177	0.224	-0.790	0.431	Left-Caudate	24	118	0.718	NonSig
1q21.1.dup	0.147	0.224	0.657	0.512	Right-Caudate	24	118	0.740	NonSig
1q21.1.dup	-0.216	0.224	-0.966	0.335	Left-Putamen	24	118	0.662	NonSig
1q21.1.dup	-0.282	0.223	-1.261	0.209	Right-Putamen	24	118	0.602	NonSig
1q21.1.dup	-0.032	0.225	-0.141	0.888	Left-Pallidum	24	118	0.965	NonSig
1q21.1.dup	-0.054	0.225	-0.239	0.812	Right-Pallidum	24	118	0.962	NonSig
1q21.1.dup	-0.707	0.217	-3.263	0.001	Left-Hippocampus	24	118	0.056	NonSig
1q21.1.dup	-0.662	0.218	-3.040	0.003	Right-Hippocampus	24	118	0.085	NonSig
1q21.1.dup	-0.167	0.224	-0.746	0.457	Left-Amygdala	24	118	0.718	NonSig
1q21.1.dup	0.502	0.221	2.275	0.024	Right-Amygdala	24	118	0.248	NonSig
1q21.1.dup	0.007	0.225	0.033	0.974	Left-Accumbens-area	24	118	0.983	NonSig
1q21.1.dup	0.709	0.217	3.275	0.001	Right-Accumbens-area	24	118	0.056	NonSig



**Table s10.**

Group differences in Z-scores for 15q11.2 BP1-BP2 deletion carriers.

CNV	Estimate	S.E.	T-value	P-value	Region of Interest	Cases	Controls	PFDR	Pcorrected_dic
15q11.2del	0.097	0.088	1.095	0.274	lh_bankssts_thickness	153	790	0.401	NonSig
15q11.2del	0.231	0.088	2.626	0.009	lh_caudalanteriorcingulate_thickness	153	790	0.036	Sig
15q11.2del	0.303	0.088	3.456	0.001	lh_caudalmiddlefrontal_thickness	153	790	0.005	Sig
15q11.2del	-0.111	0.088	-1.262	0.207	lh_cuneus_thickness	153	790	0.331	NonSig
15q11.2del	0.068	0.088	0.772	0.440	lh_entorhinal_thickness	153	790	0.584	NonSig
15q11.2del	0.183	0.088	2.075	0.038	lh_fusiform_thickness	153	790	0.094	NonSig
15q11.2del	0.117	0.088	1.330	0.184	lh_inferioparietal_thickness	153	790	0.303	NonSig
15q11.2del	0.029	0.088	0.327	0.744	lh_inferiortemporal_thickness	153	790	0.851	NonSig
15q11.2del	0.299	0.088	3.407	0.001	lh_isthmusingulate_thickness	153	790	0.005	Sig
15q11.2del	0.026	0.088	0.295	0.768	lh_lateraloccipital_thickness	153	790	0.857	NonSig
15q11.2del	0.250	0.088	2.845	0.005	lh_lateralorbitofrontal_thickness	153	790	0.024	Sig
15q11.2del	0.014	0.088	0.154	0.878	lh_lingual_thickness	153	790	0.908	NonSig
15q11.2del	0.345	0.088	3.934	0.000	lh_medialorbitofrontal_thickness	153	790	0.001	Sig
15q11.2del	0.256	0.088	2.910	0.004	lh_middletemporal_thickness	153	790	0.021	Sig
15q11.2del	0.025	0.088	0.283	0.777	lh parahippocampal_thickness	153	790	0.857	NonSig
15q11.2del	0.077	0.088	0.868	0.385	lh_paracentral_thickness	153	790	0.535	NonSig
15q11.2del	0.275	0.088	3.133	0.002	lh_parsopercularis_thickness	153	790	0.012	Sig
15q11.2del	0.297	0.088	3.378	0.001	lh_parsorbitalis_thickness	153	790	0.005	Sig
15q11.2del	0.223	0.088	2.526	0.012	lh_parsstriangularis_thickness	153	790	0.041	Sig
15q11.2del	-0.128	0.088	-1.452	0.147	lh_pericalcarine_thickness	153	790	0.259	NonSig
15q11.2del	0.429	0.087	4.918	0.000	lh_postcentral_thickness	153	790	0.000	Sig
15q11.2del	0.359	0.088	4.104	0.000	lh_posteriorcingulate_thickness	153	790	0.001	Sig
15q11.2del	0.179	0.088	2.031	0.043	lh_precentral_thickness	153	790	0.100	NonSig
15q11.2del	0.299	0.088	3.401	0.001	lh_precuneus_thickness	153	790	0.005	Sig
15q11.2del	0.145	0.088	1.641	0.101	lh_rostralanteriorcingulate_thickness	153	790	0.196	NonSig
15q11.2del	0.344	0.088	3.926	0.000	lh_rostralmiddlefrontal_thickness	153	790	0.001	Sig
15q11.2del	0.390	0.087	4.459	0.000	lh_superiorfrontal_thickness	153	790	0.000	Sig
15q11.2del	0.207	0.088	2.352	0.019	lh_superioparietal_thickness	153	790	0.060	NonSig

15q11.2del	0.022	0.088	0.253	0.800	lh_superiortemporal_thickness	153	790	0.863	NonSig
15q11.2del	0.131	0.088	1.488	0.137	lh_supramarginal_thickness	153	790	0.251	NonSig
15q11.2del	0.319	0.088	3.629	0.000	lh_frontalpole_thickness	153	790	0.003	Sig
15q11.2del	-0.104	0.088	-1.177	0.240	lh_temporalpole_thickness	153	790	0.367	NonSig
15q11.2del	-0.029	0.088	-0.329	0.742	lh_transversetemporal_thickness	153	790	0.851	NonSig
15q11.2del	0.310	0.088	3.528	0.000	lh_insula_thickness	153	790	0.004	Sig
15q11.2del	0.200	0.088	2.264	0.024	rh_bankssts_thickness	153	790	0.070	NonSig
15q11.2del	0.130	0.088	1.472	0.141	rh_caudalanteriorcingulate_thickness	153	790	0.252	NonSig
15q11.2del	0.262	0.088	2.982	0.003	rh_caudalmiddlefrontal_thickness	153	790	0.018	Sig
15q11.2del	0.024	0.088	0.276	0.782	rh_cuneus_thickness	153	790	0.857	NonSig
15q11.2del	0.101	0.088	1.143	0.253	rh_entorhinal_thickness	153	790	0.376	NonSig
15q11.2del	0.189	0.088	2.148	0.032	rh_fusiform_thickness	153	790	0.089	NonSig
15q11.2del	0.204	0.088	2.315	0.021	rh_inferioparietal_thickness	153	790	0.064	NonSig
15q11.2del	0.047	0.088	0.528	0.597	rh_inferiortemporal_thickness	153	790	0.723	NonSig
15q11.2del	0.199	0.088	2.259	0.024	rh_isthmuscingulate_thickness	153	790	0.070	NonSig
15q11.2del	0.029	0.088	0.330	0.742	rh_lateraloccipital_thickness	153	790	0.851	NonSig
15q11.2del	0.225	0.088	2.552	0.011	rh_lateralorbitofrontal_thickness	153	790	0.041	Sig
15q11.2del	0.199	0.088	2.257	0.024	rh_lingual_thickness	153	790	0.070	NonSig
15q11.2del	0.233	0.088	2.650	0.008	rh_medialorbitofrontal_thickness	153	790	0.036	Sig
15q11.2del	0.231	0.088	2.628	0.009	rh_middletemporal_thickness	153	790	0.036	Sig
15q11.2del	0.207	0.088	2.347	0.019	rh parahippocampal_thickness	153	790	0.060	NonSig
15q11.2del	0.070	0.088	0.794	0.428	rh_paracentral_thickness	153	790	0.573	NonSig
15q11.2del	0.335	0.088	3.826	0.000	rh_parsopercularis_thickness	153	790	0.002	Sig
15q11.2del	0.232	0.088	2.631	0.009	rh_parsorbitalis_thickness	153	790	0.036	Sig
15q11.2del	0.367	0.088	4.196	0.000	rh_parstriangularis_thickness	153	790	0.001	Sig
15q11.2del	-0.076	0.088	-0.858	0.391	rh_pericalcarine_thickness	153	790	0.538	NonSig
15q11.2del	0.392	0.087	4.487	0.000	rh_postcentral_thickness	153	790	0.000	Sig
15q11.2del	0.133	0.088	1.505	0.133	rh_posteriorcingulate_thickness	153	790	0.250	NonSig
15q11.2del	0.226	0.088	2.570	0.010	rh_precentral_thickness	153	790	0.040	Sig
15q11.2del	0.246	0.088	2.801	0.005	rh_precuneus_thickness	153	790	0.026	Sig
15q11.2del	0.157	0.088	1.775	0.076	rh_rostralanteriorcingulate_thickness	153	790	0.161	NonSig
15q11.2del	0.467	0.087	5.369	0.000	rh_rostralmiddlefrontal_thickness	153	790	0.000	Sig

15q11.2del	0.422	0.087	4.837	0.000	rh_superiorfrontal_thickness	153	790	0.000	Sig
15q11.2del	0.242	0.088	2.746	0.006	rh_superiorparietal_thickness	153	790	0.030	Sig
15q11.2del	0.188	0.088	2.137	0.033	rh_superiortemporal_thickness	153	790	0.090	NonSig
15q11.2del	0.165	0.088	1.874	0.061	rh_supramarginal_thickness	153	790	0.133	NonSig
15q11.2del	0.186	0.088	2.106	0.035	rh_frontalpole_thickness	153	790	0.090	NonSig
15q11.2del	0.013	0.088	0.146	0.884	rh_temporalpole_thickness	153	790	0.908	NonSig
15q11.2del	0.133	0.088	1.503	0.133	rh_transversetemporal_thickness	153	790	0.250	NonSig
15q11.2del	0.393	0.087	4.493	0.000	rh_insula_thickness	153	790	0.000	Sig
15q11.2del	0.023	0.089	0.260	0.795	lh_bankssts_area	151	787	0.863	NonSig
15q11.2del	-0.191	0.089	-2.159	0.031	lh_caudalanteriorcingulate_area	151	787	0.088	NonSig
15q11.2del	-0.087	0.089	-0.983	0.326	lh_caudalmiddlefrontal_area	151	787	0.465	NonSig
15q11.2del	-0.158	0.089	-1.777	0.076	lh_cuneus_area	151	787	0.161	NonSig
15q11.2del	0.039	0.089	0.442	0.658	lh_entorhinal_area	151	787	0.778	NonSig
15q11.2del	-0.114	0.089	-1.280	0.201	lh_fusiform_area	151	787	0.324	NonSig
15q11.2del	-0.003	0.089	-0.038	0.970	lh_inferiorparietal_area	151	787	0.976	NonSig
15q11.2del	-0.151	0.089	-1.699	0.090	lh_inferiortemporal_area	151	787	0.179	NonSig
15q11.2del	-0.066	0.089	-0.747	0.455	lh_isthmuscingulate_area	151	787	0.599	NonSig
15q11.2del	-0.025	0.089	-0.277	0.782	lh_lateraloccipital_area	151	787	0.857	NonSig
15q11.2del	-0.179	0.089	-2.013	0.044	lh_lateralorbitofrontal_area	151	787	0.102	NonSig
15q11.2del	-0.103	0.089	-1.163	0.245	lh_lingual_area	151	787	0.371	NonSig
15q11.2del	-0.115	0.089	-1.298	0.195	lh_medialorbitofrontal_area	151	787	0.317	NonSig
15q11.2del	-0.021	0.089	-0.241	0.810	lh_middletemporal_area	151	787	0.868	NonSig
15q11.2del	-0.241	0.089	-2.719	0.007	lh parahippocampal_area	151	787	0.031	Sig
15q11.2del	-0.088	0.089	-0.989	0.323	lh_paracentral_area	151	787	0.465	NonSig
15q11.2del	-0.054	0.089	-0.606	0.545	lh_parsopercularis_area	151	787	0.682	NonSig
15q11.2del	-0.333	0.088	-3.778	0.000	lh_parsorbitalis_area	151	787	0.002	Sig
15q11.2del	-0.282	0.088	-3.195	0.001	lh_parsstriangularis_area	151	787	0.010	Sig
15q11.2del	-0.185	0.089	-2.091	0.037	lh_pericalcarine_area	151	787	0.092	NonSig
15q11.2del	-0.188	0.089	-2.119	0.034	lh_postcentral_area	151	787	0.090	NonSig
15q11.2del	-0.124	0.089	-1.397	0.163	lh_posteriorcingulate_area	151	787	0.284	NonSig
15q11.2del	-0.054	0.089	-0.604	0.546	lh_precentral_area	151	787	0.682	NonSig
15q11.2del	-0.133	0.089	-1.493	0.136	lh_precuneus_area	151	787	0.251	NonSig

15q11.2del	-0.181	0.089	-2.037	0.042	lh_rostralanteriorcingulate_area	151	787	0.100	NonSig
15q11.2del	-0.230	0.089	-2.601	0.009	lh_rostralmiddlefrontal_area	151	787	0.037	Sig
15q11.2del	0.025	0.089	0.279	0.780	lh_superiorfrontal_area	151	787	0.857	NonSig
15q11.2del	-0.233	0.089	-2.634	0.009	lh_superiorparietal_area	151	787	0.036	Sig
15q11.2del	0.017	0.089	0.191	0.849	lh_superiortemporal_area	151	787	0.890	NonSig
15q11.2del	-0.040	0.089	-0.447	0.655	lh_supramarginal_area	151	787	0.778	NonSig
15q11.2del	0.208	0.089	2.351	0.019	lh_frontalpole_area	151	787	0.060	NonSig
15q11.2del	-0.097	0.089	-1.092	0.275	lh_temporalpole_area	151	787	0.401	NonSig
15q11.2del	0.072	0.089	0.814	0.416	lh_transversetemporal_area	151	787	0.562	NonSig
15q11.2del	0.050	0.089	0.557	0.578	lh_insula_area	151	787	0.710	NonSig
15q11.2del	-0.085	0.089	-0.961	0.337	rh_bankssts_area	151	787	0.472	NonSig
15q11.2del	-0.339	0.088	-3.844	0.000	rh_caudalanteriorcingulate_area	151	787	0.002	Sig
15q11.2del	-0.102	0.089	-1.152	0.249	rh_caudalmiddlefrontal_area	151	787	0.374	NonSig
15q11.2del	-0.107	0.089	-1.200	0.230	rh_cuneus_area	151	787	0.356	NonSig
15q11.2del	-0.050	0.089	-0.568	0.570	rh_entorhinal_area	151	787	0.707	NonSig
15q11.2del	-0.016	0.089	-0.180	0.857	rh_fusiform_area	151	787	0.893	NonSig
15q11.2del	-0.182	0.089	-2.047	0.041	rh_inferioparietal_area	151	787	0.099	NonSig
15q11.2del	-0.108	0.089	-1.214	0.225	rh_inferiortemporal_area	151	787	0.355	NonSig
15q11.2del	0.120	0.089	1.347	0.178	rh_isthmuscingulate_area	151	787	0.301	NonSig
15q11.2del	-0.120	0.089	-1.350	0.177	rh_lateraloccipital_area	151	787	0.301	NonSig
15q11.2del	-0.250	0.089	-2.824	0.005	rh_lateralorbitofrontal_area	151	787	0.025	Sig
15q11.2del	-0.018	0.089	-0.199	0.842	rh_lingual_area	151	787	0.890	NonSig
15q11.2del	-0.155	0.089	-1.751	0.080	rh_medialorbitofrontal_area	151	787	0.165	NonSig
15q11.2del	-0.072	0.089	-0.816	0.415	rh_middletemporal_area	151	787	0.562	NonSig
15q11.2del	-0.152	0.089	-1.714	0.087	rh parahippocampal_area	151	787	0.176	NonSig
15q11.2del	-0.132	0.089	-1.482	0.139	rh_paracentral_area	151	787	0.251	NonSig
15q11.2del	0.157	0.089	1.764	0.078	rh_parsopercularis_area	151	787	0.163	NonSig
15q11.2del	-0.406	0.088	-4.618	0.000	rh_parsorbitalis_area	151	787	0.000	Sig
15q11.2del	-0.086	0.089	-0.965	0.335	rh_parsstriangularis_area	151	787	0.472	NonSig
15q11.2del	-0.224	0.089	-2.533	0.011	rh_pericalcarine_area	151	787	0.041	Sig
15q11.2del	-0.175	0.089	-1.975	0.049	rh_postcentral_area	151	787	0.110	NonSig
15q11.2del	-0.188	0.089	-2.119	0.034	rh_posteriorcingulate_area	151	787	0.090	NonSig

15q11.2del	-0.169	0.089	-1.910	0.056	rh_precentral_area	151	787	0.124	NonSig
15q11.2del	-0.056	0.089	-0.635	0.526	rh_precuneus_area	151	787	0.668	NonSig
15q11.2del	-0.214	0.089	-2.412	0.016	rh_rostralanteriorcingulate_area	151	787	0.055	NonSig
15q11.2del	-0.266	0.088	-3.010	0.003	rh_rostralmiddlefrontal_area	151	787	0.017	Sig
15q11.2del	-0.007	0.089	-0.081	0.935	rh_superiorfrontal_area	151	787	0.954	NonSig
15q11.2del	-0.209	0.089	-2.356	0.019	rh_superiorparietal_area	151	787	0.060	NonSig
15q11.2del	0.017	0.089	0.192	0.848	rh_superiortemporal_area	151	787	0.890	NonSig
15q11.2del	0.040	0.089	0.450	0.653	rh_supramarginal_area	151	787	0.778	NonSig
15q11.2del	0.001	0.089	0.012	0.991	rh_frontalpole_area	151	787	0.991	NonSig
15q11.2del	-0.175	0.089	-1.971	0.049	rh_temporalpole_area	151	787	0.110	NonSig
15q11.2del	0.049	0.089	0.547	0.584	rh_transversetemporal_area	151	787	0.713	NonSig
15q11.2del	0.059	0.089	0.668	0.504	rh_insula_area	151	787	0.652	NonSig
15q11.2del	-0.142	0.085	-1.669	0.095	Left-Thalamus-Proper	165	815	0.188	NonSig
15q11.2del	0.029	0.085	0.343	0.732	Right-Thalamus-Proper	165	815	0.851	NonSig
15q11.2del	-0.247	0.085	-2.899	0.004	Left-Caudate	165	815	0.021	Sig
15q11.2del	-0.102	0.085	-1.201	0.230	Right-Caudate	165	815	0.356	NonSig
15q11.2del	-0.114	0.085	-1.340	0.181	Left-Putamen	165	815	0.301	NonSig
15q11.2del	-0.140	0.085	-1.637	0.102	Right-Putamen	165	815	0.196	NonSig
15q11.2del	-0.117	0.085	-1.368	0.172	Left-Pallidum	165	815	0.296	NonSig
15q11.2del	-0.216	0.085	-2.537	0.011	Right-Pallidum	165	815	0.041	Sig
15q11.2del	-0.026	0.085	-0.301	0.764	Left-Hippocampus	165	815	0.857	NonSig
15q11.2del	-0.006	0.085	-0.070	0.944	Right-Hippocampus	165	815	0.957	NonSig
15q11.2del	0.057	0.085	0.662	0.508	Left-Amygdala	165	815	0.652	NonSig
15q11.2del	0.062	0.085	0.728	0.467	Right-Amygdala	165	815	0.608	NonSig
15q11.2del	-0.180	0.085	-2.111	0.035	Left-Accumbens-area	165	815	0.090	NonSig
15q11.2del	-0.304	0.085	-3.583	0.000	Right-Accumbens-area	165	815	0.003	Sig

**Table s11.**

Group differences in RID-scores for 15q11.2 BP1-BP2 deletion carriers.

CNV	Estimate	S.E.	T-value	P-value	Region of Interest	Cases	Controls	PFDR	Pcorrected_dic
15q11.2del	-0.085	0.088	-0.965	0.335	lh_bankssts_thickness	153	790	0.628	NonSig
15q11.2del	0.025	0.088	0.285	0.776	lh_caudalanteriorcingulate_thickness	153	790	0.899	NonSig
15q11.2del	0.177	0.088	2.012	0.044	lh_caudalmiddlefrontal_thickness	153	790	0.203	NonSig
15q11.2del	-0.311	0.088	-3.540	0.000	lh_cuneus_thickness	153	790	0.010	Sig
15q11.2del	-0.115	0.088	-1.307	0.191	lh_entorhinal_thickness	153	790	0.456	NonSig
15q11.2del	-0.020	0.088	-0.224	0.823	lh_fusiform_thickness	153	790	0.914	NonSig
15q11.2del	-0.073	0.088	-0.824	0.410	lh_inferiorparietal_thickness	153	790	0.643	NonSig
15q11.2del	-0.192	0.088	-2.176	0.030	lh_inferiortemporal_thickness	153	790	0.181	NonSig
15q11.2del	0.102	0.088	1.154	0.249	lh_isthmusingulate_thickness	153	790	0.526	NonSig
15q11.2del	-0.184	0.088	-2.084	0.037	lh_lateraloccipital_thickness	153	790	0.198	NonSig
15q11.2del	0.053	0.088	0.597	0.551	lh_lateralorbitofrontal_thickness	153	790	0.748	NonSig
15q11.2del	-0.213	0.088	-2.414	0.016	lh_lingual_thickness	153	790	0.120	NonSig
15q11.2del	0.138	0.088	1.567	0.117	lh_medialorbitofrontal_thickness	153	790	0.346	NonSig
15q11.2del	0.087	0.088	0.989	0.323	lh_middletemporal_thickness	153	790	0.619	NonSig
15q11.2del	-0.160	0.088	-1.815	0.070	lh_parahippocampal_thickness	153	790	0.249	NonSig
15q11.2del	-0.103	0.088	-1.167	0.243	lh_paracentral_thickness	153	790	0.526	NonSig
15q11.2del	0.138	0.088	1.563	0.118	lh_parsopercularis_thickness	153	790	0.346	NonSig
15q11.2del	0.120	0.088	1.357	0.175	lh_parsorbitalis_thickness	153	790	0.453	NonSig
15q11.2del	0.075	0.088	0.851	0.395	lh_parsotriangularis_thickness	153	790	0.643	NonSig
15q11.2del	-0.328	0.088	-3.743	0.000	lh_pericalcarine_thickness	153	790	0.007	Sig
15q11.2del	0.338	0.088	3.852	0.000	lh_postcentral_thickness	153	790	0.006	Sig
15q11.2del	0.187	0.088	2.123	0.034	lh_posteriorcingulate_thickness	153	790	0.189	NonSig
15q11.2del	0.024	0.088	0.273	0.785	lh_precentral_thickness	153	790	0.899	NonSig
15q11.2del	0.137	0.088	1.557	0.120	lh_precuneus_thickness	153	790	0.346	NonSig
15q11.2del	-0.059	0.088	-0.673	0.501	lh_rostralanteriorcingulate_thickness	153	790	0.723	NonSig
15q11.2del	0.218	0.088	2.474	0.014	lh_rostralmiddlefrontal_thickness	153	790	0.107	NonSig
15q11.2del	0.289	0.088	3.286	0.001	lh_superiorfrontal_thickness	153	790	0.023	Sig
15q11.2del	0.064	0.088	0.719	0.472	lh_superiorparietal_thickness	153	790	0.694	NonSig

15q11.2del	-0.203	0.088	-2.300	0.022	lh_superiortemporal_thickness	153	790	0.148	NonSig
15q11.2del	-0.073	0.088	-0.822	0.411	lh_supramarginal_thickness	153	790	0.643	NonSig
15q11.2del	0.116	0.088	1.313	0.190	lh_frontalpole_thickness	153	790	0.456	NonSig
15q11.2del	-0.275	0.088	-3.124	0.002	lh_temporalpole_thickness	153	790	0.028	Sig
15q11.2del	-0.253	0.088	-2.880	0.004	lh_transversetemporal_thickness	153	790	0.044	Sig
15q11.2del	0.130	0.088	1.472	0.141	lh_insula_thickness	153	790	0.385	NonSig
15q11.2del	0.027	0.088	0.304	0.761	rh_bankssts_thickness	153	790	0.899	NonSig
15q11.2del	-0.050	0.088	-0.566	0.572	rh_caudalanteriorcingulate_thickness	153	790	0.752	NonSig
15q11.2del	0.102	0.088	1.155	0.248	rh_caudalmiddlefrontal_thickness	153	790	0.526	NonSig
15q11.2del	-0.152	0.088	-1.720	0.086	rh_cuneus_thickness	153	790	0.286	NonSig
15q11.2del	-0.079	0.088	-0.897	0.370	rh_entorhinal_thickness	153	790	0.643	NonSig
15q11.2del	0.001	0.088	0.010	0.992	rh_fusiform_thickness	153	790	0.996	NonSig
15q11.2del	0.037	0.088	0.413	0.679	rh_inferioparietal_thickness	153	790	0.822	NonSig
15q11.2del	-0.169	0.088	-1.912	0.056	rh_inferiortemporal_thickness	153	790	0.222	NonSig
15q11.2del	0.012	0.088	0.135	0.893	rh_isthmuscingulate_thickness	153	790	0.942	NonSig
15q11.2del	-0.192	0.088	-2.183	0.029	rh_lateraloccipital_thickness	153	790	0.181	NonSig
15q11.2del	0.043	0.088	0.482	0.630	rh_lateralorbitofrontal_thickness	153	790	0.788	NonSig
15q11.2del	0.014	0.088	0.155	0.877	rh_lingual_thickness	153	790	0.942	NonSig
15q11.2del	0.043	0.088	0.487	0.626	rh_medialorbitofrontal_thickness	153	790	0.788	NonSig
15q11.2del	0.048	0.088	0.538	0.591	rh_middletemporal_thickness	153	790	0.764	NonSig
15q11.2del	0.010	0.088	0.113	0.910	rh parahippocampal_thickness	153	790	0.942	NonSig
15q11.2del	-0.118	0.088	-1.340	0.181	rh_paracentral_thickness	153	790	0.456	NonSig
15q11.2del	0.161	0.088	1.821	0.069	rh_parsopercularis_thickness	153	790	0.249	NonSig
15q11.2del	0.046	0.088	0.520	0.603	rh_parsorbitalis_thickness	153	790	0.774	NonSig
15q11.2del	0.206	0.088	2.338	0.020	rh_parstriangularis_thickness	153	790	0.140	NonSig
15q11.2del	-0.263	0.088	-2.989	0.003	rh_pericalcarine_thickness	153	790	0.036	Sig
15q11.2del	0.261	0.088	2.964	0.003	rh_postcentral_thickness	153	790	0.036	Sig
15q11.2del	-0.069	0.088	-0.783	0.434	rh_posteriorcingulate_thickness	153	790	0.664	NonSig
15q11.2del	0.073	0.088	0.829	0.407	rh_precentral_thickness	153	790	0.643	NonSig
15q11.2del	0.077	0.088	0.869	0.385	rh_precuneus_thickness	153	790	0.643	NonSig
15q11.2del	-0.039	0.088	-0.436	0.663	rh_rostralanteriorcingulate_thickness	153	790	0.809	NonSig
15q11.2del	0.348	0.088	3.974	0.000	rh_rostralmiddlefrontal_thickness	153	790	0.006	Sig

15q11.2del	0.319	0.088	3.631	0.000	rh_superiorfrontal_thickness	153	790	0.009	Sig
15q11.2del	0.084	0.088	0.950	0.342	rh_superiorparietal_thickness	153	790	0.634	NonSig
15q11.2del	0.009	0.088	0.097	0.923	rh_superiortemporal_thickness	153	790	0.942	NonSig
15q11.2del	-0.068	0.088	-0.765	0.444	rh_supramarginal_thickness	153	790	0.666	NonSig
15q11.2del	-0.041	0.088	-0.459	0.646	rh_frontalpole_thickness	153	790	0.794	NonSig
15q11.2del	-0.170	0.088	-1.929	0.054	rh_temporalpole_thickness	153	790	0.219	NonSig
15q11.2del	-0.060	0.088	-0.675	0.500	rh_transversetemporal_thickness	153	790	0.723	NonSig
15q11.2del	0.220	0.088	2.501	0.013	rh_insula_thickness	153	790	0.105	NonSig
15q11.2del	0.118	0.089	1.331	0.184	lh_bankssts_area	151	787	0.456	NonSig
15q11.2del	-0.103	0.089	-1.159	0.247	lh_caudalanteriorcingulate_area	151	787	0.526	NonSig
15q11.2del	0.043	0.089	0.481	0.630	lh_caudalmiddlefrontal_area	151	787	0.788	NonSig
15q11.2del	-0.050	0.089	-0.567	0.571	lh_cuneus_area	151	787	0.752	NonSig
15q11.2del	0.129	0.089	1.453	0.146	lh_entorhinal_area	151	787	0.392	NonSig
15q11.2del	-0.029	0.089	-0.325	0.745	lh_fusiform_area	151	787	0.887	NonSig
15q11.2del	0.097	0.089	1.096	0.274	lh_inferiorparietal_area	151	787	0.562	NonSig
15q11.2del	-0.078	0.089	-0.882	0.378	lh_inferiortemporal_area	151	787	0.643	NonSig
15q11.2del	0.055	0.089	0.620	0.536	lh_isthmuscingulate_area	151	787	0.744	NonSig
15q11.2del	0.095	0.089	1.066	0.287	lh_lateraloccipital_area	151	787	0.574	NonSig
15q11.2del	-0.083	0.089	-0.936	0.349	lh_lateralorbitofrontal_area	151	787	0.639	NonSig
15q11.2del	-0.009	0.089	-0.105	0.916	lh_lingual_area	151	787	0.942	NonSig
15q11.2del	-0.022	0.089	-0.252	0.801	lh_medialorbitofrontal_area	151	787	0.906	NonSig
15q11.2del	0.077	0.089	0.868	0.386	lh_middletemporal_area	151	787	0.643	NonSig
15q11.2del	-0.141	0.089	-1.584	0.113	lh parahippocampal_area	151	787	0.346	NonSig
15q11.2del	-0.008	0.089	-0.088	0.930	lh_paracentral_area	151	787	0.942	NonSig
15q11.2del	0.065	0.089	0.732	0.464	lh_parsopercularis_area	151	787	0.689	NonSig
15q11.2del	-0.265	0.088	-2.992	0.003	lh_parsorbitalis_area	151	787	0.036	Sig
15q11.2del	-0.176	0.089	-1.985	0.047	lh_parietangularis_area	151	787	0.203	NonSig
15q11.2del	-0.110	0.089	-1.239	0.216	lh_pericalcarine_area	151	787	0.506	NonSig
15q11.2del	-0.117	0.089	-1.313	0.190	lh_postcentral_area	151	787	0.456	NonSig
15q11.2del	-0.011	0.089	-0.118	0.906	lh_posteriorcingulate_area	151	787	0.942	NonSig
15q11.2del	0.072	0.089	0.805	0.421	lh_precentral_area	151	787	0.651	NonSig
15q11.2del	-0.024	0.089	-0.273	0.785	lh_precuneus_area	151	787	0.899	NonSig



15q11.2del	-0.078	0.089	-0.875	0.382	lh_rostralanteriorcingulate_area	151	787	0.643	NonSig
15q11.2del	-0.140	0.089	-1.577	0.115	lh_rostralmiddlefrontal_area	151	787	0.346	NonSig
15q11.2del	0.176	0.089	1.986	0.047	lh_superiorfrontal_area	151	787	0.203	NonSig
15q11.2del	-0.123	0.089	-1.387	0.166	lh_superiorparietal_area	151	787	0.436	NonSig
15q11.2del	0.145	0.089	1.638	0.102	lh_superiortemporal_area	151	787	0.325	NonSig
15q11.2del	0.080	0.089	0.899	0.369	lh_supramarginal_area	151	787	0.643	NonSig
15q11.2del	0.285	0.088	3.225	0.001	lh_frontalpole_area	151	787	0.024	Sig
15q11.2del	-0.009	0.089	-0.096	0.923	lh_temporalpole_area	151	787	0.942	NonSig
15q11.2del	0.183	0.089	2.068	0.039	lh_transversetemporal_area	151	787	0.198	NonSig
15q11.2del	0.189	0.089	2.133	0.033	lh_insula_area	151	787	0.189	NonSig
15q11.2del	0.012	0.089	0.137	0.891	rh_bankssts_area	151	787	0.942	NonSig
15q11.2del	-0.228	0.089	-2.577	0.010	rh_caudalanteriorcingulate_area	151	787	0.089	NonSig
15q11.2del	0.022	0.089	0.249	0.804	rh_caudalmiddlefrontal_area	151	787	0.906	NonSig
15q11.2del	-0.021	0.089	-0.242	0.809	rh_cuneus_area	151	787	0.906	NonSig
15q11.2del	0.052	0.089	0.589	0.556	rh_entorhinal_area	151	787	0.748	NonSig
15q11.2del	0.074	0.089	0.832	0.406	rh_fusiform_area	151	787	0.643	NonSig
15q11.2del	-0.081	0.089	-0.912	0.362	rh_inferioparietal_area	151	787	0.643	NonSig
15q11.2del	-0.013	0.089	-0.142	0.887	rh_inferiortemporal_area	151	787	0.942	NonSig
15q11.2del	0.248	0.089	2.803	0.005	rh_isthmuscingulate_area	151	787	0.052	NonSig
15q11.2del	-0.025	0.089	-0.281	0.779	rh_lateraloccipital_area	151	787	0.899	NonSig
15q11.2del	-0.166	0.089	-1.866	0.062	rh_lateralorbitofrontal_area	151	787	0.240	NonSig
15q11.2del	0.096	0.089	1.086	0.278	rh_lingual_area	151	787	0.563	NonSig
15q11.2del	-0.057	0.089	-0.642	0.521	rh_medialorbitofrontal_area	151	787	0.730	NonSig
15q11.2del	0.029	0.089	0.326	0.744	rh_middletemporal_area	151	787	0.887	NonSig
15q11.2del	-0.054	0.089	-0.606	0.545	rh parahippocampal_area	151	787	0.748	NonSig
15q11.2del	-0.009	0.089	-0.105	0.916	rh_paracentral_area	151	787	0.942	NonSig
15q11.2del	0.281	0.088	3.172	0.002	rh_parsopercularis_area	151	787	0.026	Sig
15q11.2del	-0.377	0.088	-4.284	0.000	rh_parsorbitalis_area	151	787	0.003	Sig
15q11.2del	0.000	0.089	0.005	0.996	rh_parstriangularis_area	151	787	0.996	NonSig
15q11.2del	-0.177	0.089	-1.991	0.047	rh_pericalcarine_area	151	787	0.203	NonSig
15q11.2del	-0.092	0.089	-1.041	0.298	rh_postcentral_area	151	787	0.589	NonSig
15q11.2del	-0.089	0.089	-1.000	0.318	rh_posteriorcingulate_area	151	787	0.619	NonSig

15q11.2del	-0.078	0.089	-0.880	0.379	rh_precentral_area	151	787	0.643	NonSig
15q11.2del	0.058	0.089	0.649	0.516	rh_precuneus_area	151	787	0.730	NonSig
15q11.2del	-0.103	0.089	-1.156	0.248	rh_rostralanteriorcingulate_area	151	787	0.526	NonSig
15q11.2del	-0.183	0.089	-2.060	0.040	rh_rostralmiddlefrontal_area	151	787	0.198	NonSig
15q11.2del	0.108	0.089	1.213	0.225	rh_superiorfrontal_area	151	787	0.520	NonSig
15q11.2del	-0.098	0.089	-1.106	0.269	rh_superiorparietal_area	151	787	0.561	NonSig
15q11.2del	0.158	0.089	1.785	0.075	rh_superiortemporal_area	151	787	0.260	NonSig
15q11.2del	0.133	0.089	1.502	0.134	rh_supramarginal_area	151	787	0.373	NonSig
15q11.2del	0.087	0.089	0.983	0.326	rh_frontalpole_area	151	787	0.619	NonSig
15q11.2del	-0.076	0.089	-0.860	0.390	rh_temporalpole_area	151	787	0.643	NonSig
15q11.2del	0.174	0.089	1.964	0.050	rh_transversetemporal_area	151	787	0.208	NonSig
15q11.2del	0.157	0.089	1.766	0.078	rh_insula_area	151	787	0.265	NonSig
15q11.2del	-0.056	0.085	-0.658	0.511	Left-Thalamus-Proper	165	815	0.730	NonSig
15q11.2del	0.170	0.085	2.000	0.046	Right-Thalamus-Proper	165	815	0.203	NonSig
15q11.2del	-0.128	0.085	-1.499	0.134	Left-Caudate	165	815	0.373	NonSig
15q11.2del	0.047	0.085	0.553	0.581	Right-Caudate	165	815	0.757	NonSig
15q11.2del	0.016	0.085	0.190	0.849	Left-Putamen	165	815	0.936	NonSig
15q11.2del	-0.040	0.085	-0.464	0.642	Right-Putamen	165	815	0.794	NonSig
15q11.2del	0.016	0.085	0.183	0.855	Left-Pallidum	165	815	0.936	NonSig
15q11.2del	-0.155	0.085	-1.823	0.069	Right-Pallidum	165	815	0.249	NonSig
15q11.2del	0.050	0.085	0.585	0.559	Left-Hippocampus	165	815	0.748	NonSig
15q11.2del	0.066	0.085	0.772	0.441	Right-Hippocampus	165	815	0.666	NonSig
15q11.2del	0.185	0.085	2.170	0.030	Left-Amygdala	165	815	0.181	NonSig
15q11.2del	0.144	0.085	1.692	0.091	Right-Amygdala	165	815	0.297	NonSig
15q11.2del	-0.100	0.085	-1.169	0.243	Left-Accumbens-area	165	815	0.526	NonSig
15q11.2del	-0.220	0.085	-2.589	0.010	Right-Accumbens-area	165	815	0.089	NonSig

**Table S12.**

Group differences in RID-scores for 15q11.2 BP1-BP2 deletion carriers, adjusted for affection status.

CNV	Estimate	S.E.	T-value	P-value	Region of Interest	Cases	Controls	PFDR	Pcorrected_dic
15q11.2del	-0.313	0.088	-3.562	0.000	lh_cuneus_thickness	153	790	0.001	Sig
15q11.2del	-0.330	0.088	-3.765	0.000	lh_pericalcarine_thickness	153	790	0.001	Sig
15q11.2del	0.337	0.088	3.846	0.000	lh_postcentral_thickness	153	790	0.001	Sig
15q11.2del	0.290	0.088	3.300	0.001	lh_superiorfrontal_thickness	153	790	0.002	Sig
15q11.2del	-0.275	0.088	-3.125	0.002	lh_temporalpole_thickness	153	790	0.003	Sig
15q11.2del	-0.254	0.088	-2.884	0.004	lh_transversetemporal_thickness	153	790	0.004	Sig
15q11.2del	-0.265	0.088	-3.011	0.003	rh_pericalcarine_thickness	153	790	0.003	Sig
15q11.2del	0.260	0.088	2.953	0.003	rh_postcentral_thickness	153	790	0.003	Sig
15q11.2del	0.350	0.088	3.994	0.000	rh_rostralmiddlefrontal_thickness	153	790	0.000	Sig
15q11.2del	0.320	0.088	3.643	0.000	rh_superiorfrontal_thickness	153	790	0.001	Sig
15q11.2del	-0.278	0.088	-3.164	0.002	lh_parsorbitalis_area	153	790	0.002	Sig
15q11.2del	0.296	0.088	3.375	0.001	lh_frontalpole_area	153	790	0.002	Sig
15q11.2del	0.263	0.088	2.983	0.003	rh_parsopercularis_area	153	790	0.003	Sig
15q11.2del	-0.361	0.088	-4.121	0.000	rh_parsorbitalis_area	153	790	0.000	Sig

Interaction effect between copy number status (i.e., 15q11.2 BP1-BP2 deletion vs non-carriers) and affection status on RID-scores.

CNV	Estimate	S.E.	T-value	P-value	Region of Interest	Cases	Controls	PFDR	Pcorrected_dic
15q11.2del	-0.014	0.268	-0.053	0.958	lh_cuneus_thickness	153	790	0.992	NonSig
15q11.2del	-0.063	0.268	-0.236	0.814	lh_pericalcarine_thickness	153	790	0.992	NonSig
15q11.2del	-0.003	0.268	-0.010	0.992	lh_postcentral_thickness	153	790	0.992	NonSig
15q11.2del	-0.439	0.268	-1.634	0.103	lh_superiorfrontal_thickness	153	790	0.431	NonSig
15q11.2del	0.140	0.269	0.520	0.603	lh_temporalpole_thickness	153	790	0.992	NonSig
15q11.2del	-0.025	0.269	-0.094	0.925	lh_transversetemporal_thickness	153	790	0.992	NonSig
15q11.2del	-0.216	0.269	-0.804	0.421	rh_pericalcarine_thickness	153	790	0.843	NonSig
15q11.2del	0.553	0.268	2.061	0.040	rh_postcentral_thickness	153	790	0.431	NonSig
15q11.2del	-0.413	0.268	-1.543	0.123	rh_rostralmiddlefrontal_thickness	153	790	0.431	NonSig
15q11.2del	-0.500	0.268	-1.865	0.062	rh_superiorfrontal_thickness	153	790	0.431	NonSig
15q11.2del	0.247	0.269	0.918	0.359	lh_parsorbitalis_area	153	790	0.837	NonSig
15q11.2del	0.020	0.269	0.074	0.941	lh_frontalpole_area	153	790	0.992	NonSig

15q11.2del	0.297	0.269	1.103	0.270	rh_parsopercularis_area	153	790	0.756	NonSig
15q11.2del	-0.011	0.268	-0.041	0.967	rh_parsorbitalis_area	153	790	0.992	NonSig

**Table s13.**

Interaction effect between copy number status (i.e., 15q11.2 BP1-BP2 deletion vs non-carriers) and cognitive ability on RID-scores.

CNV	Estimate	S.E.	T-value	P-value	Region of Interest	PFDR	Pcorrected	dic
15q11.2del	-0.036	0.099	-0.362	0.717	lh_cuneus_thickness	1	NonSig	
15q11.2del	0.011	0.099	0.112	0.911	lh_pericalcarine_thickness	1	NonSig	
15q11.2del	-0.070	0.098	-0.710	0.478	lh_postcentral_thickness	1	NonSig	
15q11.2del	0.025	0.099	0.248	0.804	lh_superiorfrontal_thickness	1	NonSig	
15q11.2del	0.038	0.099	0.384	0.701	lh_temporalpole_thickness	1	NonSig	
15q11.2del	-0.093	0.099	-0.934	0.350	lh_transversetemporal_thickness	1	NonSig	
15q11.2del	0.061	0.100	0.609	0.543	rh_pericalcarine_thickness	1	NonSig	
15q11.2del	-0.151	0.099	-1.524	0.128	rh_postcentral_thickness	1	NonSig	
15q11.2del	-0.048	0.099	-0.481	0.630	rh_rostralmiddlefrontal_thickness	1	NonSig	
15q11.2del	0.067	0.099	0.674	0.500	rh_superiorfrontal_thickness	1	NonSig	
15q11.2del	-0.152	0.099	-1.535	0.125	lh_parsorbitalis_area	1	NonSig	
15q11.2del	-0.076	0.099	-0.770	0.441	lh_frontalpole_area	1	NonSig	
15q11.2del	-0.087	0.099	-0.880	0.379	rh_parsopercularis_area	1	NonSig	
15q11.2del	0.040	0.098	0.407	0.684	rh_parsorbitalis_area	1	NonSig	

**Table s14.**

Group differences in Z-scores for 15q11.2 BP1-BP2 deletion carriers, adjusted for the global effect (i.e., global index of cortical thickness for cortical thickness measures, global index of cortical surface area for cortical surface area measures, global index of subcortical volume for subcortical volume measures).

CNV	Estimate	S.E.	T-value	P-value	Region of Interest	Cases	Controls	PFDR	Pcorrected_dic
15q11.2del	-0.092	0.075	-1.226	0.221	lh_bankssts_thickness	153	790	0.460	NonSig
15q11.2del	0.126	0.085	1.485	0.138	lh_caudalanteriorcingulate_thickness	153	790	0.345	NonSig
15q11.2del	0.081	0.068	1.180	0.238	lh_caudalmiddlefrontal_thickness	153	790	0.464	NonSig
15q11.2del	-0.277	0.079	-3.525	0.000	lh_cuneus_thickness	153	790	0.022	Sig
15q11.2del	-0.026	0.086	-0.304	0.761	lh_entorhinal_thickness	153	790	0.921	NonSig
15q11.2del	-0.025	0.072	-0.355	0.723	lh_fusiform_thickness	153	790	0.901	NonSig
15q11.2del	-0.136	0.062	-2.206	0.028	lh_inferioparietal_thickness	153	790	0.130	NonSig
15q11.2del	-0.158	0.076	-2.097	0.036	lh_inferiortemporal_thickness	153	790	0.147	NonSig
15q11.2del	0.164	0.082	2.005	0.045	lh_isthmusingulate_thickness	153	790	0.161	NonSig
15q11.2del	-0.190	0.071	-2.690	0.007	lh_lateraloccipital_thickness	153	790	0.063	NonSig
15q11.2del	0.069	0.076	0.909	0.364	lh_lateralorbitofrontal_thickness	153	790	0.621	NonSig
15q11.2del	-0.185	0.074	-2.502	0.013	lh_lingual_thickness	153	790	0.080	NonSig
15q11.2del	0.190	0.079	2.397	0.017	lh_medialorbitofrontal_thickness	153	790	0.093	NonSig
15q11.2del	0.045	0.071	0.632	0.527	lh_middletemporal_thickness	153	790	0.750	NonSig
15q11.2del	-0.056	0.087	-0.642	0.521	lh_parahippocampal_thickness	153	790	0.750	NonSig
15q11.2del	-0.132	0.072	-1.844	0.065	lh_paracentral_thickness	153	790	0.207	NonSig
15q11.2del	0.055	0.069	0.799	0.424	lh_parsopercularis_thickness	153	790	0.650	NonSig
15q11.2del	0.132	0.078	1.684	0.092	lh_parsorbitalis_thickness	153	790	0.255	NonSig
15q11.2del	0.026	0.074	0.349	0.727	lh_parstriangularis_thickness	153	790	0.901	NonSig
15q11.2del	-0.268	0.082	-3.276	0.001	lh_pericalcarine_thickness	153	790	0.041	Sig
15q11.2del	0.210	0.068	3.066	0.002	lh_postcentral_thickness	153	790	0.042	Sig
15q11.2del	0.199	0.078	2.531	0.012	lh_posteriorcingulate_thickness	153	790	0.080	NonSig
15q11.2del	-0.062	0.065	-0.949	0.343	lh_precentral_thickness	153	790	0.613	NonSig
15q11.2del	0.057	0.064	0.890	0.373	lh_precuneus_thickness	153	790	0.621	NonSig
15q11.2del	0.021	0.083	0.248	0.805	lh_rostralanteriorcingulate_thickness	153	790	0.950	NonSig
15q11.2del	0.111	0.066	1.679	0.093	lh_rostralmiddlefrontal_thickness	153	790	0.255	NonSig
15q11.2del	0.141	0.062	2.277	0.023	lh_superiorfrontal_thickness	153	790	0.115	NonSig

15q11.2del	-0.026	0.067	-0.394	0.693	lh_superioparietal_thickness	153	790	0.877	NonSig
15q11.2del	-0.210	0.067	-3.126	0.002	lh_superiortemporal_thickness	153	790	0.042	Sig
15q11.2del	-0.127	0.061	-2.098	0.036	lh_supramarginal_thickness	153	790	0.147	NonSig
15q11.2del	0.211	0.084	2.501	0.013	lh_frontalpole_thickness	153	790	0.080	NonSig
15q11.2del	-0.212	0.085	-2.494	0.013	lh_temporalpole_thickness	153	790	0.080	NonSig
15q11.2del	-0.206	0.077	-2.676	0.008	lh_transversetemporal_thickness	153	790	0.063	NonSig
15q11.2del	0.104	0.072	1.455	0.146	lh_insula_thickness	153	790	0.359	NonSig
15q11.2del	0.016	0.076	0.215	0.830	rh_bankssts_thickness	153	790	0.965	NonSig
15q11.2del	0.036	0.086	0.422	0.673	rh_caudalanteriorcingulate_thickness	153	790	0.870	NonSig
15q11.2del	0.038	0.068	0.552	0.581	rh_caudalmiddlefrontal_thickness	153	790	0.796	NonSig
15q11.2del	-0.143	0.079	-1.818	0.069	rh_cuneus_thickness	153	790	0.212	NonSig
15q11.2del	0.006	0.086	0.066	0.948	rh_entorhinal_thickness	153	790	0.995	NonSig
15q11.2del	-0.028	0.070	-0.395	0.693	rh_fusiform_thickness	153	790	0.877	NonSig
15q11.2del	-0.048	0.062	-0.768	0.442	rh_inferioparietal_thickness	153	790	0.667	NonSig
15q11.2del	-0.155	0.073	-2.113	0.035	rh_inferiortemporal_thickness	153	790	0.147	NonSig
15q11.2del	0.077	0.083	0.918	0.359	rh_isthmuscingulate_thickness	153	790	0.621	NonSig
15q11.2del	-0.199	0.068	-2.914	0.004	rh_lateraloccipital_thickness	153	790	0.047	Sig
15q11.2del	0.045	0.076	0.594	0.552	rh_lateralorbitofrontal_thickness	153	790	0.767	NonSig
15q11.2del	-0.004	0.073	-0.060	0.952	rh_lingual_thickness	153	790	0.995	NonSig
15q11.2del	0.083	0.080	1.034	0.301	rh_medialorbitofrontal_thickness	153	790	0.558	NonSig
15q11.2del	0.000	0.067	-0.001	1.000	rh_middletemporal_thickness	153	790	1.000	NonSig
15q11.2del	0.097	0.085	1.152	0.250	rh parahippocampal_thickness	153	790	0.474	NonSig
15q11.2del	-0.151	0.070	-2.169	0.030	rh_paracentral_thickness	153	790	0.138	NonSig
15q11.2del	0.117	0.069	1.692	0.091	rh_parsopercularis_thickness	153	790	0.255	NonSig
15q11.2del	0.047	0.076	0.627	0.531	rh_parsorbitalis_thickness	153	790	0.750	NonSig
15q11.2del	0.157	0.071	2.228	0.026	rh_parsotriangularis_thickness	153	790	0.126	NonSig
15q11.2del	-0.213	0.082	-2.600	0.009	rh_pericalcarine_thickness	153	790	0.075	NonSig
15q11.2del	0.197	0.073	2.694	0.007	rh_postcentral_thickness	153	790	0.063	NonSig
15q11.2del	-0.022	0.080	-0.269	0.788	rh_posteriorcingulate_thickness	153	790	0.943	NonSig
15q11.2del	-0.005	0.067	-0.081	0.935	rh_precentral_thickness	153	790	0.995	NonSig
15q11.2del	0.000	0.063	0.004	0.997	rh_precuneus_thickness	153	790	1.000	NonSig
15q11.2del	0.039	0.084	0.463	0.644	rh_rostralanteriorcingulate_thickness	153	790	0.840	NonSig

15q11.2del	0.236	0.066	3.601	0.000	rh_rostralmiddlefrontal_thickness	153	790	0.022	Sig
15q11.2del	0.173	0.061	2.807	0.005	rh_superiorfrontal_thickness	153	790	0.055	NonSig
15q11.2del	0.016	0.068	0.237	0.813	rh_superiorparietal_thickness	153	790	0.952	NonSig
15q11.2del	-0.056	0.064	-0.872	0.383	rh_superiortemporal_thickness	153	790	0.625	NonSig
15q11.2del	-0.086	0.062	-1.387	0.166	rh_supramarginal_thickness	153	790	0.388	NonSig
15q11.2del	0.072	0.084	0.860	0.390	rh_frontalpole_thickness	153	790	0.629	NonSig
15q11.2del	-0.107	0.084	-1.271	0.204	rh_temporalpole_thickness	153	790	0.437	NonSig
15q11.2del	-0.027	0.079	-0.342	0.733	rh_transversetemporal_thickness	153	790	0.901	NonSig
15q11.2del	0.216	0.076	2.839	0.005	rh_insula_thickness	153	790	0.053	NonSig
15q11.2del	0.101	0.083	1.210	0.227	lh_bankssts_area	151	787	0.464	NonSig
15q11.2del	-0.116	0.083	-1.388	0.165	lh_caudalanteriorcingulate_area	151	787	0.388	NonSig
15q11.2del	0.010	0.080	0.121	0.904	lh_caudalmiddlefrontal_area	151	787	0.995	NonSig
15q11.2del	-0.072	0.082	-0.885	0.377	lh_cuneus_area	151	787	0.621	NonSig
15q11.2del	0.113	0.084	1.350	0.177	lh_entorhinal_area	151	787	0.403	NonSig
15q11.2del	-0.004	0.077	-0.049	0.961	lh_fusiform_area	151	787	0.995	NonSig
15q11.2del	0.109	0.076	1.433	0.152	lh_inferiorparietal_area	151	787	0.368	NonSig
15q11.2del	-0.040	0.077	-0.524	0.601	lh_inferiortemporal_area	151	787	0.800	NonSig
15q11.2del	0.031	0.080	0.391	0.696	lh_isthmuscingulate_area	151	787	0.877	NonSig
15q11.2del	0.085	0.077	1.095	0.274	lh_lateraloccipital_area	151	787	0.513	NonSig
15q11.2del	-0.043	0.070	-0.620	0.535	lh_lateralorbitofrontal_area	151	787	0.750	NonSig
15q11.2del	0.000	0.078	0.004	0.997	lh_lingual_area	151	787	1.000	NonSig
15q11.2del	-0.007	0.077	-0.087	0.931	lh_medialorbitofrontal_area	151	787	0.995	NonSig
15q11.2del	0.098	0.075	1.311	0.190	lh_middletemporal_area	151	787	0.419	NonSig
15q11.2del	-0.169	0.084	-2.017	0.044	lh parahippocampal_area	151	787	0.161	NonSig
15q11.2del	-0.005	0.082	-0.062	0.951	lh_paracentral_area	151	787	0.995	NonSig
15q11.2del	0.027	0.083	0.329	0.742	lh_parsopercularis_area	151	787	0.905	NonSig
15q11.2del	-0.234	0.079	-2.976	0.003	lh_parsorbitalis_area	151	787	0.047	Sig
15q11.2del	-0.198	0.082	-2.423	0.016	lh_parstriangularis_area	151	787	0.093	NonSig
15q11.2del	-0.096	0.081	-1.183	0.237	lh_pericalcarine_area	151	787	0.464	NonSig
15q11.2del	-0.061	0.072	-0.845	0.398	lh_postcentral_area	151	787	0.629	NonSig
15q11.2del	-0.039	0.082	-0.475	0.635	lh_posteriorcingulate_area	151	787	0.836	NonSig
15q11.2del	0.062	0.075	0.827	0.408	lh_precentral_area	151	787	0.636	NonSig

15q11.2del	-0.003	0.071	-0.038	0.969	lh_precuneus_area	151	787	0.996	NonSig
15q11.2del	-0.080	0.079	-1.014	0.311	lh_rostralanteriorcingulate_area	151	787	0.569	NonSig
15q11.2del	-0.090	0.068	-1.327	0.185	lh_rostralmiddlefrontal_area	151	787	0.414	NonSig
15q11.2del	0.169	0.067	2.541	0.011	lh_superiorfrontal_area	151	787	0.080	NonSig
15q11.2del	-0.114	0.074	-1.536	0.125	lh_superiorparietal_area	151	787	0.323	NonSig
15q11.2del	0.143	0.073	1.958	0.051	lh_superiortemporal_area	151	787	0.176	NonSig
15q11.2del	0.064	0.078	0.822	0.411	lh_supramarginal_area	151	787	0.636	NonSig
15q11.2del	0.264	0.086	3.069	0.002	lh_frontalpole_area	151	787	0.042	Sig
15q11.2del	-0.022	0.084	-0.264	0.792	lh_temporalpole_area	151	787	0.943	NonSig
15q11.2del	0.154	0.083	1.867	0.062	lh_transversestemporal_area	151	787	0.203	NonSig
15q11.2del	0.171	0.074	2.311	0.021	lh_insula_area	151	787	0.113	NonSig
15q11.2del	-0.006	0.083	-0.074	0.941	rh_bankssts_area	151	787	0.995	NonSig
15q11.2del	-0.268	0.084	-3.208	0.001	rh_caudalanteriorcingulate_area	151	787	0.041	Sig
15q11.2del	-0.008	0.080	-0.098	0.922	rh_caudalmiddlefrontal_area	151	787	0.995	NonSig
15q11.2del	-0.007	0.079	-0.090	0.928	rh_cuneus_area	151	787	0.995	NonSig
15q11.2del	0.012	0.086	0.135	0.893	rh_entorhinal_area	151	787	0.995	NonSig
15q11.2del	0.098	0.076	1.287	0.198	rh_fusiform_area	151	787	0.431	NonSig
15q11.2del	-0.072	0.077	-0.934	0.350	rh_inferiorparietal_area	151	787	0.618	NonSig
15q11.2del	-0.002	0.078	-0.028	0.977	rh_inferiortemporal_area	151	787	0.997	NonSig
15q11.2del	0.216	0.080	2.706	0.007	rh_isthmuscingulate_area	151	787	0.063	NonSig
15q11.2del	-0.012	0.077	-0.150	0.881	rh_lateraloccipital_area	151	787	0.995	NonSig
15q11.2del	-0.135	0.075	-1.794	0.073	rh_lateralorbitofrontal_area	151	787	0.219	NonSig
15q11.2del	0.090	0.077	1.167	0.243	rh_lingual_area	151	787	0.468	NonSig
15q11.2del	-0.039	0.075	-0.521	0.603	rh_medialorbitofrontal_area	151	787	0.800	NonSig
15q11.2del	0.063	0.070	0.906	0.365	rh_middletemporal_area	151	787	0.621	NonSig
15q11.2del	-0.070	0.082	-0.847	0.397	rh parahippocampal_area	151	787	0.629	NonSig
15q11.2del	-0.042	0.081	-0.522	0.602	rh_paracentral_area	151	787	0.800	NonSig
15q11.2del	0.241	0.082	2.932	0.003	rh_parsopercularis_area	151	787	0.047	Sig
15q11.2del	-0.314	0.080	-3.934	0.000	rh_parsorbitalis_area	151	787	0.013	Sig
15q11.2del	-0.008	0.083	-0.098	0.922	rh_parstriangularis_area	151	787	0.995	NonSig
15q11.2del	-0.135	0.081	-1.667	0.096	rh_pericalcarine_area	151	787	0.257	NonSig
15q11.2del	-0.054	0.074	-0.729	0.466	rh_postcentral_area	151	787	0.692	NonSig



15q11.2del	-0.075	0.076	-0.982	0.326	rh_posteriorcingulate_area	151	787	0.590	NonSig
15q11.2del	-0.059	0.077	-0.764	0.445	rh_precentral_area	151	787	0.667	NonSig
15q11.2del	0.066	0.074	0.893	0.372	rh_precuneus_area	151	787	0.621	NonSig
15q11.2del	-0.141	0.084	-1.686	0.092	rh_rostralanteriorcingulate_area	151	787	0.255	NonSig
15q11.2del	-0.130	0.069	-1.884	0.060	rh_rostralmiddlefrontal_area	151	787	0.200	NonSig
15q11.2del	0.135	0.067	2.007	0.045	rh_superiorfrontal_area	151	787	0.161	NonSig
15q11.2del	-0.087	0.074	-1.184	0.237	rh_superiorparietal_area	151	787	0.464	NonSig
15q11.2del	0.151	0.070	2.142	0.032	rh_superiortemporal_area	151	787	0.143	NonSig
15q11.2del	0.148	0.078	1.905	0.057	rh_supramarginal_area	151	787	0.195	NonSig
15q11.2del	0.061	0.086	0.717	0.474	rh_frontalpole_area	151	787	0.692	NonSig
15q11.2del	-0.117	0.086	-1.366	0.172	rh_temporalpole_area	151	787	0.397	NonSig
15q11.2del	0.137	0.081	1.686	0.092	rh_transversetemporal_area	151	787	0.255	NonSig
15q11.2del	0.160	0.079	2.015	0.044	rh_insula_area	151	787	0.161	NonSig
15q11.2del	-0.053	0.074	-0.715	0.475	Left-Thalamus-Proper	165	815	0.692	NonSig
15q11.2del	0.130	0.071	1.838	0.066	Right-Thalamus-Proper	165	815	0.207	NonSig
15q11.2del	-0.135	0.066	-2.037	0.042	Left-Caudate	165	815	0.161	NonSig
15q11.2del	0.005	0.068	0.077	0.938	Right-Caudate	165	815	0.995	NonSig
15q11.2del	0.003	0.064	0.048	0.962	Left-Putamen	165	815	0.995	NonSig
15q11.2del	-0.011	0.059	-0.194	0.846	Right-Putamen	165	815	0.977	NonSig
15q11.2del	-0.043	0.078	-0.548	0.584	Left-Pallidum	165	815	0.796	NonSig
15q11.2del	-0.114	0.070	-1.631	0.103	Right-Pallidum	165	815	0.271	NonSig
15q11.2del	0.082	0.068	1.197	0.232	Left-Hippocampus	165	815	0.464	NonSig
15q11.2del	0.103	0.068	1.525	0.127	Right-Hippocampus	165	815	0.324	NonSig
15q11.2del	0.160	0.070	2.289	0.022	Left-Amygdala	165	815	0.115	NonSig
15q11.2del	0.167	0.069	2.404	0.016	Right-Amygdala	165	815	0.093	NonSig
15q11.2del	-0.094	0.075	-1.259	0.208	Left-Accumbens-area	165	815	0.440	NonSig
15q11.2del	-0.204	0.070	-2.907	0.004	Right-Accumbens-area	165	815	0.047	Sig

**Table s15.**

Group differences in Z-scores for 15q11.2 BP1-BP2 duplication carriers.

CNV	Estimate	S.E.	T-value	P-value	Region of Interest	Cases	Controls	PFDR	Pcorrected_dic
15q11.2dup	-0.229	0.074	-3.085	0.002	lh_bankssts_thickness	217	1081	0.039	Sig
15q11.2dup	-0.196	0.074	-2.639	0.008	lh_caudalanteriorcingulate_thickness	217	1081	0.082	NonSig
15q11.2dup	-0.088	0.074	-1.182	0.237	lh_caudalmiddlefrontal_thickness	217	1081	0.438	NonSig
15q11.2dup	-0.097	0.074	-1.300	0.194	lh_cuneus_thickness	217	1081	0.415	NonSig
15q11.2dup	-0.067	0.074	-0.901	0.368	lh_entorhinal_thickness	217	1081	0.531	NonSig
15q11.2dup	-0.148	0.074	-1.992	0.047	lh_fusiform_thickness	217	1081	0.233	NonSig
15q11.2dup	0.026	0.074	0.347	0.729	lh_inferiorparietal_thickness	217	1081	0.776	NonSig
15q11.2dup	-0.079	0.074	-1.067	0.286	lh_inferiortemporal_thickness	217	1081	0.477	NonSig
15q11.2dup	-0.100	0.074	-1.350	0.177	lh_isthmuscingulate_thickness	217	1081	0.403	NonSig
15q11.2dup	-0.001	0.074	-0.017	0.986	lh_lateraloccipital_thickness	217	1081	0.986	NonSig
15q11.2dup	-0.179	0.074	-2.412	0.016	lh_lateralorbitofrontal_thickness	217	1081	0.121	NonSig
15q11.2dup	-0.105	0.074	-1.412	0.158	lh_lingual_thickness	217	1081	0.390	NonSig
15q11.2dup	-0.056	0.074	-0.747	0.455	lh_medialorbitofrontal_thickness	217	1081	0.594	NonSig
15q11.2dup	-0.186	0.074	-2.506	0.012	lh_middletemporal_thickness	217	1081	0.103	NonSig
15q11.2dup	-0.164	0.074	-2.203	0.028	lh parahippocampal_thickness	217	1081	0.189	NonSig
15q11.2dup	-0.140	0.074	-1.878	0.061	lh_paracentral_thickness	217	1081	0.233	NonSig
15q11.2dup	-0.188	0.074	-2.536	0.011	lh_parsopercularis_thickness	217	1081	0.100	NonSig
15q11.2dup	-0.140	0.074	-1.887	0.059	lh_parsorbitalis_thickness	217	1081	0.233	NonSig
15q11.2dup	-0.166	0.074	-2.231	0.026	lh_parstriangularis_thickness	217	1081	0.185	NonSig
15q11.2dup	-0.055	0.074	-0.741	0.459	lh_pericalcarine_thickness	217	1081	0.594	NonSig
15q11.2dup	-0.237	0.074	-3.200	0.001	lh_postcentral_thickness	217	1081	0.037	Sig
15q11.2dup	-0.138	0.074	-1.852	0.064	lh_posteriorcingulate_thickness	217	1081	0.234	NonSig
15q11.2dup	-0.126	0.074	-1.694	0.091	lh_precentral_thickness	217	1081	0.295	NonSig
15q11.2dup	-0.091	0.074	-1.224	0.221	lh_precuneus_thickness	217	1081	0.438	NonSig
15q11.2dup	-0.250	0.074	-3.380	0.001	lh_rostralanteriorcingulate_thickness	217	1081	0.035	Sig
15q11.2dup	-0.250	0.074	-3.375	0.001	lh_rostralmiddlefrontal_thickness	217	1081	0.035	Sig
15q11.2dup	-0.106	0.074	-1.430	0.153	lh_superiorfrontal_thickness	217	1081	0.390	NonSig
15q11.2dup	-0.062	0.074	-0.828	0.408	lh_superiorparietal_thickness	217	1081	0.564	NonSig

15q11.2dup	-0.146	0.074	-1.962	0.050	lh_superiortemporal_thickness	217	1081	0.233	NonSig
15q11.2dup	-0.029	0.074	-0.387	0.699	lh_supramarginal_thickness	217	1081	0.754	NonSig
15q11.2dup	-0.133	0.074	-1.789	0.074	lh_frontalpole_thickness	217	1081	0.258	NonSig
15q11.2dup	-0.080	0.074	-1.069	0.285	lh_temporalpole_thickness	217	1081	0.477	NonSig
15q11.2dup	-0.153	0.074	-2.054	0.040	lh_transversetemporal_thickness	217	1081	0.233	NonSig
15q11.2dup	-0.223	0.074	-3.014	0.003	lh_insula_thickness	217	1081	0.039	Sig
15q11.2dup	-0.112	0.074	-1.507	0.132	rh_bankssts_thickness	217	1081	0.377	NonSig
15q11.2dup	-0.062	0.074	-0.836	0.403	rh_caudalanteriorcingulate_thickness	217	1081	0.564	NonSig
15q11.2dup	-0.220	0.074	-2.965	0.003	rh_caudalmiddlefrontal_thickness	217	1081	0.039	Sig
15q11.2dup	-0.105	0.074	-1.407	0.160	rh_cuneus_thickness	217	1081	0.390	NonSig
15q11.2dup	-0.179	0.074	-2.409	0.016	rh_entorhinal_thickness	217	1081	0.121	NonSig
15q11.2dup	-0.140	0.074	-1.881	0.060	rh_fusiform_thickness	217	1081	0.233	NonSig
15q11.2dup	-0.112	0.074	-1.503	0.133	rh_inferiorparietal_thickness	217	1081	0.377	NonSig
15q11.2dup	-0.086	0.074	-1.161	0.246	rh_inferiortemporal_thickness	217	1081	0.444	NonSig
15q11.2dup	-0.120	0.074	-1.608	0.108	rh_isthmuscingulate_thickness	217	1081	0.337	NonSig
15q11.2dup	-0.104	0.074	-1.396	0.163	rh_lateraloccipital_thickness	217	1081	0.390	NonSig
15q11.2dup	-0.143	0.074	-1.918	0.055	rh_lateralorbitofrontal_thickness	217	1081	0.233	NonSig
15q11.2dup	-0.052	0.074	-0.704	0.481	rh_lingual_thickness	217	1081	0.611	NonSig
15q11.2dup	-0.236	0.074	-3.184	0.001	rh_medialorbitofrontal_thickness	217	1081	0.037	Sig
15q11.2dup	-0.146	0.074	-1.970	0.049	rh_middletemporal_thickness	217	1081	0.233	NonSig
15q11.2dup	-0.221	0.074	-2.976	0.003	rh parahippocampal_thickness	217	1081	0.039	Sig
15q11.2dup	-0.080	0.074	-1.077	0.282	rh_paracentral_thickness	217	1081	0.477	NonSig
15q11.2dup	-0.151	0.074	-2.032	0.042	rh_parsopercularis_thickness	217	1081	0.233	NonSig
15q11.2dup	-0.141	0.074	-1.902	0.057	rh_parsorbitalis_thickness	217	1081	0.233	NonSig
15q11.2dup	-0.207	0.074	-2.793	0.005	rh_parstriangularis_thickness	217	1081	0.061	NonSig
15q11.2dup	-0.108	0.074	-1.446	0.148	rh_pericalcarine_thickness	217	1081	0.390	NonSig
15q11.2dup	-0.233	0.074	-3.136	0.002	rh_postcentral_thickness	217	1081	0.037	Sig
15q11.2dup	-0.160	0.074	-2.157	0.031	rh_posteriorcingulate_thickness	217	1081	0.199	NonSig
15q11.2dup	-0.195	0.074	-2.624	0.009	rh_precentral_thickness	217	1081	0.082	NonSig
15q11.2dup	-0.112	0.074	-1.511	0.131	rh_precuneus_thickness	217	1081	0.377	NonSig
15q11.2dup	-0.089	0.074	-1.193	0.233	rh_rostralanteriorcingulate_thickness	217	1081	0.438	NonSig
15q11.2dup	-0.160	0.074	-2.149	0.032	rh_rostralmiddlefrontal_thickness	217	1081	0.199	NonSig

15q11.2dup	-0.109	0.074	-1.471	0.141	rh_superiorfrontal_thickness	217	1081	0.390	NonSig
15q11.2dup	-0.034	0.074	-0.458	0.647	rh_superiorparietal_thickness	217	1081	0.727	NonSig
15q11.2dup	-0.249	0.074	-3.357	0.001	rh_superiortemporal_thickness	217	1081	0.035	Sig
15q11.2dup	-0.088	0.074	-1.185	0.236	rh_supramarginal_thickness	217	1081	0.438	NonSig
15q11.2dup	-0.140	0.074	-1.882	0.060	rh_frontalpole_thickness	217	1081	0.233	NonSig
15q11.2dup	-0.102	0.074	-1.369	0.171	rh_temporalpole_thickness	217	1081	0.400	NonSig
15q11.2dup	-0.039	0.074	-0.526	0.599	rh_transversetemporal_thickness	217	1081	0.708	NonSig
15q11.2dup	-0.246	0.074	-3.315	0.001	rh_insula_thickness	217	1081	0.035	Sig
15q11.2dup	-0.049	0.075	-0.660	0.509	lh_bankssts_area	215	1066	0.626	NonSig
15q11.2dup	-0.036	0.075	-0.485	0.628	lh_caudalanteriorcingulate_area	215	1066	0.719	NonSig
15q11.2dup	-0.064	0.075	-0.862	0.389	lh_caudalmiddlefrontal_area	215	1066	0.550	NonSig
15q11.2dup	-0.099	0.075	-1.325	0.185	lh_cuneus_area	215	1066	0.409	NonSig
15q11.2dup	0.065	0.075	0.876	0.381	lh_entorhinal_area	215	1066	0.545	NonSig
15q11.2dup	-0.057	0.075	-0.769	0.442	lh_fusiform_area	215	1066	0.592	NonSig
15q11.2dup	-0.088	0.075	-1.177	0.239	lh_inferiorparietal_area	215	1066	0.438	NonSig
15q11.2dup	-0.092	0.075	-1.233	0.218	lh_inferiortemporal_area	215	1066	0.438	NonSig
15q11.2dup	-0.149	0.075	-1.994	0.046	lh_isthmuscingulate_area	215	1066	0.233	NonSig
15q11.2dup	-0.085	0.075	-1.133	0.258	lh_lateraloccipital_area	215	1066	0.457	NonSig
15q11.2dup	0.060	0.075	0.800	0.424	lh_lateralorbitofrontal_area	215	1066	0.573	NonSig
15q11.2dup	-0.071	0.075	-0.956	0.339	lh_lingual_area	215	1066	0.525	NonSig
15q11.2dup	0.062	0.075	0.824	0.410	lh_medialorbitofrontal_area	215	1066	0.564	NonSig
15q11.2dup	-0.146	0.075	-1.958	0.050	lh_middletemporal_area	215	1066	0.233	NonSig
15q11.2dup	0.056	0.075	0.747	0.455	lh parahippocampal_area	215	1066	0.594	NonSig
15q11.2dup	0.068	0.075	0.908	0.364	lh_paracentral_area	215	1066	0.531	NonSig
15q11.2dup	0.084	0.075	1.129	0.259	lh_parsopercularis_area	215	1066	0.457	NonSig
15q11.2dup	0.092	0.075	1.225	0.221	lh_parsorbitalis_area	215	1066	0.438	NonSig
15q11.2dup	0.030	0.075	0.408	0.684	lh_parstriangularis_area	215	1066	0.754	NonSig
15q11.2dup	-0.037	0.075	-0.495	0.620	lh_pericalcarine_area	215	1066	0.719	NonSig
15q11.2dup	-0.071	0.075	-0.949	0.343	lh_postcentral_area	215	1066	0.525	NonSig
15q11.2dup	-0.104	0.075	-1.393	0.164	lh_posteriorcingulate_area	215	1066	0.390	NonSig
15q11.2dup	-0.200	0.075	-2.684	0.007	lh_precentral_area	215	1066	0.079	NonSig
15q11.2dup	-0.068	0.075	-0.914	0.361	lh_precuneus_area	215	1066	0.531	NonSig

15q11.2dup	-0.100	0.075	-1.333	0.183	lh_rostralanteriorcingulate_area	215	1066	0.409	NonSig
15q11.2dup	0.002	0.075	0.026	0.979	lh_rostralmiddlefrontal_area	215	1066	0.986	NonSig
15q11.2dup	-0.096	0.075	-1.289	0.198	lh_superiorfrontal_area	215	1066	0.417	NonSig
15q11.2dup	-0.049	0.075	-0.653	0.514	lh_superiorparietal_area	215	1066	0.626	NonSig
15q11.2dup	-0.138	0.075	-1.843	0.066	lh_superior temporal_area	215	1066	0.234	NonSig
15q11.2dup	-0.067	0.075	-0.900	0.368	lh_supramarginal_area	215	1066	0.531	NonSig
15q11.2dup	-0.035	0.075	-0.463	0.644	lh_frontalpole_area	215	1066	0.727	NonSig
15q11.2dup	0.029	0.075	0.393	0.694	lh_temporalpole_area	215	1066	0.754	NonSig
15q11.2dup	-0.080	0.075	-1.069	0.285	lh_transversetemporal_area	215	1066	0.477	NonSig
15q11.2dup	-0.142	0.075	-1.896	0.058	lh_insula_area	215	1066	0.233	NonSig
15q11.2dup	-0.048	0.075	-0.648	0.517	rh_bankssts_area	215	1066	0.626	NonSig
15q11.2dup	0.069	0.075	0.927	0.354	rh_caudalanteriorcingulate_area	215	1066	0.531	NonSig
15q11.2dup	0.108	0.075	1.451	0.147	rh_caudalmiddlefrontal_area	215	1066	0.390	NonSig
15q11.2dup	-0.079	0.075	-1.056	0.291	rh_cuneus_area	215	1066	0.480	NonSig
15q11.2dup	-0.034	0.075	-0.454	0.650	rh_entorhinal_area	215	1066	0.727	NonSig
15q11.2dup	-0.107	0.075	-1.431	0.153	rh_fusiform_area	215	1066	0.390	NonSig
15q11.2dup	-0.122	0.075	-1.637	0.102	rh_inferiorparietal_area	215	1066	0.325	NonSig
15q11.2dup	-0.093	0.075	-1.249	0.212	rh_inferiortemporal_area	215	1066	0.438	NonSig
15q11.2dup	-0.115	0.075	-1.543	0.123	rh_isthmuscingulate_area	215	1066	0.369	NonSig
15q11.2dup	-0.089	0.075	-1.186	0.236	rh_lateraloccipital_area	215	1066	0.438	NonSig
15q11.2dup	0.080	0.075	1.071	0.285	rh_lateralorbitofrontal_area	215	1066	0.477	NonSig
15q11.2dup	-0.139	0.075	-1.855	0.064	rh_lingual_area	215	1066	0.234	NonSig
15q11.2dup	-0.073	0.075	-0.975	0.330	rh_medialorbitofrontal_area	215	1066	0.525	NonSig
15q11.2dup	-0.072	0.075	-0.959	0.338	rh_middletemporal_area	215	1066	0.525	NonSig
15q11.2dup	-0.026	0.075	-0.346	0.729	rh parahippocampal_area	215	1066	0.776	NonSig
15q11.2dup	0.052	0.075	0.699	0.484	rh_paracentral_area	215	1066	0.611	NonSig
15q11.2dup	-0.119	0.075	-1.599	0.110	rh_parsopercularis_area	215	1066	0.337	NonSig
15q11.2dup	0.106	0.075	1.423	0.155	rh_parsorbitalis_area	215	1066	0.390	NonSig
15q11.2dup	-0.033	0.075	-0.445	0.656	rh_parstriangularis_area	215	1066	0.729	NonSig
15q11.2dup	-0.017	0.075	-0.226	0.821	rh_pericalcarine_area	215	1066	0.849	NonSig
15q11.2dup	-0.056	0.075	-0.753	0.452	rh_postcentral_area	215	1066	0.594	NonSig
15q11.2dup	-0.043	0.075	-0.577	0.564	rh_posteriorcingulate_area	215	1066	0.671	NonSig

15q11.2dup	-0.036	0.075	-0.488	0.626	rh_precentral_area	215	1066	0.719	NonSig
15q11.2dup	-0.131	0.075	-1.751	0.080	rh_precuneus_area	215	1066	0.273	NonSig
15q11.2dup	-0.008	0.075	-0.102	0.919	rh_rostralanteriorcingulate_area	215	1066	0.932	NonSig
15q11.2dup	-0.010	0.075	-0.140	0.889	rh_rostralmiddlefrontal_area	215	1066	0.913	NonSig
15q11.2dup	-0.224	0.075	-3.000	0.003	rh_superiorfrontal_area	215	1066	0.039	Sig
15q11.2dup	-0.071	0.075	-0.955	0.340	rh_superiorparietal_area	215	1066	0.525	NonSig
15q11.2dup	-0.052	0.075	-0.699	0.484	rh_superiortemporal_area	215	1066	0.611	NonSig
15q11.2dup	-0.127	0.075	-1.703	0.089	rh_supramarginal_area	215	1066	0.295	NonSig
15q11.2dup	-0.102	0.075	-1.362	0.173	rh_frontalpole_area	215	1066	0.400	NonSig
15q11.2dup	0.036	0.075	0.486	0.627	rh_temporalpole_area	215	1066	0.719	NonSig
15q11.2dup	-0.051	0.075	-0.680	0.496	rh_transversetemporal_area	215	1066	0.620	NonSig
15q11.2dup	-0.072	0.075	-0.960	0.337	rh_insula_area	215	1066	0.525	NonSig
15q11.2dup	-0.017	0.072	-0.229	0.819	Left-Thalamus-Proper	230	1140	0.849	NonSig
15q11.2dup	0.049	0.072	0.674	0.500	Right-Thalamus-Proper	230	1140	0.620	NonSig
15q11.2dup	-0.058	0.072	-0.806	0.421	Left-Caudate	230	1140	0.573	NonSig
15q11.2dup	-0.086	0.072	-1.187	0.235	Right-Caudate	230	1140	0.438	NonSig
15q11.2dup	-0.043	0.072	-0.595	0.552	Left-Putamen	230	1140	0.663	NonSig
15q11.2dup	-0.065	0.072	-0.901	0.368	Right-Putamen	230	1140	0.531	NonSig
15q11.2dup	0.022	0.072	0.305	0.760	Left-Pallidum	230	1140	0.803	NonSig
15q11.2dup	-0.029	0.072	-0.396	0.692	Right-Pallidum	230	1140	0.754	NonSig
15q11.2dup	0.009	0.072	0.122	0.903	Left-Hippocampus	230	1140	0.921	NonSig
15q11.2dup	0.086	0.072	1.190	0.234	Right-Hippocampus	230	1140	0.438	NonSig
15q11.2dup	0.137	0.072	1.896	0.058	Left-Amygdala	230	1140	0.233	NonSig
15q11.2dup	0.095	0.072	1.312	0.190	Right-Amygdala	230	1140	0.413	NonSig
15q11.2dup	-0.020	0.072	-0.281	0.779	Left-Accumbens-area	230	1140	0.817	NonSig
15q11.2dup	0.071	0.072	0.986	0.324	Right-Accumbens-area	230	1140	0.525	NonSig

**Table S16.**

Group differences in RID-scores for 15q11.2 BP1-BP2 duplication carriers.

<b>CNV</b>	<b>Estimate</b>	<b>S.E.</b>	<b>T-value</b>	<b>P-value</b>	<b>Region of Interest</b>	<b>Cases</b>	<b>Controls</b>	<b>PFDR</b>	<b>Pcorrected</b>	<b>dic</b>
15q11.2dup	-0.091	0.074	-1.221	0.222	lh_bankssts_thickness	217	1081	0.748	0.748	NonSig
15q11.2dup	-0.064	0.074	-0.855	0.393	lh_caudalanteriorcingulate_thickness	217	1081	0.831	0.831	NonSig
15q11.2dup	0.074	0.074	0.993	0.321	lh_caudalmiddlefrontal_thickness	217	1081	0.807	0.807	NonSig
15q11.2dup	0.013	0.074	0.178	0.859	lh_cuneus_thickness	217	1081	0.961	0.961	NonSig
15q11.2dup	0.082	0.074	1.107	0.268	lh_entorhinal_thickness	217	1081	0.787	0.787	NonSig
15q11.2dup	-0.006	0.074	-0.078	0.938	lh_fusiform_thickness	217	1081	0.970	0.970	NonSig
15q11.2dup	0.219	0.074	2.950	0.003	lh_inferiorparietal_thickness	217	1081	0.242	0.242	NonSig
15q11.2dup	0.064	0.074	0.854	0.393	lh_inferiortemporal_thickness	217	1081	0.831	0.831	NonSig
15q11.2dup	0.047	0.074	0.627	0.531	lh_isthmuscingulate_thickness	217	1081	0.942	0.942	NonSig
15q11.2dup	0.180	0.074	2.423	0.016	lh_lateraloccipital_thickness	217	1081	0.488	0.488	NonSig
15q11.2dup	-0.070	0.074	-0.936	0.350	lh_lateralorbitofrontal_thickness	217	1081	0.807	0.807	NonSig
15q11.2dup	0.028	0.074	0.374	0.709	lh_lingual_thickness	217	1081	0.952	0.952	NonSig
15q11.2dup	0.097	0.074	1.308	0.191	lh_medialorbitofrontal_thickness	217	1081	0.748	0.748	NonSig
15q11.2dup	-0.049	0.074	-0.653	0.514	lh_middletemporal_thickness	217	1081	0.942	0.942	NonSig
15q11.2dup	-0.019	0.074	-0.253	0.800	lh_parahippocampal_thickness	217	1081	0.952	0.952	NonSig
15q11.2dup	-0.036	0.074	-0.484	0.628	lh_paracentral_thickness	217	1081	0.952	0.952	NonSig
15q11.2dup	-0.093	0.074	-1.247	0.213	lh_parsopercularis_thickness	217	1081	0.748	0.748	NonSig
15q11.2dup	0.015	0.074	0.206	0.837	lh_parsorbitalis_thickness	217	1081	0.952	0.952	NonSig
15q11.2dup	-0.030	0.074	-0.397	0.691	lh_parstriangularis_thickness	217	1081	0.952	0.952	NonSig
15q11.2dup	0.080	0.074	1.069	0.285	lh_pericalcarine_thickness	217	1081	0.787	0.787	NonSig
15q11.2dup	-0.149	0.074	-2.005	0.045	lh_postcentral_thickness	217	1081	0.521	0.521	NonSig
15q11.2dup	-0.007	0.074	-0.100	0.920	lh_posteriorcingulate_thickness	217	1081	0.965	0.965	NonSig
15q11.2dup	0.031	0.074	0.421	0.674	lh_precentral_thickness	217	1081	0.952	0.952	NonSig
15q11.2dup	0.043	0.074	0.577	0.564	lh_precuneus_thickness	217	1081	0.942	0.942	NonSig
15q11.2dup	-0.135	0.074	-1.811	0.070	lh_rostralanteriorcingulate_thickness	217	1081	0.556	0.556	NonSig
15q11.2dup	-0.157	0.074	-2.114	0.035	lh_rostralmiddlefrontal_thickness	217	1081	0.521	0.521	NonSig
15q11.2dup	0.045	0.074	0.602	0.547	lh_superiorfrontal_thickness	217	1081	0.942	0.942	NonSig
15q11.2dup	0.079	0.074	1.066	0.287	lh_superiorparietal_thickness	217	1081	0.787	0.787	NonSig

15q11.2dup	-0.022	0.074	-0.291	0.771	lh_superiortemporal_thickness	217	1081	0.952	NonSig
15q11.2dup	0.159	0.074	2.135	0.033	lh_supramarginal_thickness	217	1081	0.521	NonSig
15q11.2dup	0.001	0.074	0.008	0.993	lh_frontalpole_thickness	217	1081	0.993	NonSig
15q11.2dup	0.079	0.074	1.062	0.289	lh_temporalpole_thickness	217	1081	0.787	NonSig
15q11.2dup	-0.053	0.074	-0.712	0.477	lh_transversetemporal_thickness	217	1081	0.932	NonSig
15q11.2dup	-0.114	0.074	-1.533	0.126	lh_insula_thickness	217	1081	0.604	NonSig
15q11.2dup	0.023	0.074	0.313	0.754	rh_bankssts_thickness	217	1081	0.952	NonSig
15q11.2dup	0.080	0.074	1.081	0.280	rh_caudalanteriorcingulate_thickness	217	1081	0.787	NonSig
15q11.2dup	-0.116	0.074	-1.556	0.120	rh_caudalmiddlefrontal_thickness	217	1081	0.604	NonSig
15q11.2dup	0.007	0.074	0.092	0.926	rh_cuneus_thickness	217	1081	0.965	NonSig
15q11.2dup	-0.029	0.074	-0.385	0.700	rh_entorhinal_thickness	217	1081	0.952	NonSig
15q11.2dup	0.008	0.074	0.101	0.920	rh_fusiform_thickness	217	1081	0.965	NonSig
15q11.2dup	0.027	0.074	0.363	0.717	rh_inferioparietal_thickness	217	1081	0.952	NonSig
15q11.2dup	0.068	0.074	0.920	0.358	rh_inferiortemporal_thickness	217	1081	0.807	NonSig
15q11.2dup	0.015	0.074	0.196	0.844	rh_isthmuscingulate_thickness	217	1081	0.952	NonSig
15q11.2dup	0.044	0.074	0.598	0.550	rh_lateraloccipital_thickness	217	1081	0.942	NonSig
15q11.2dup	-0.003	0.074	-0.045	0.964	rh_lateralorbitofrontal_thickness	217	1081	0.983	NonSig
15q11.2dup	0.104	0.074	1.398	0.162	rh_lingual_thickness	217	1081	0.717	NonSig
15q11.2dup	-0.100	0.074	-1.339	0.181	rh_medialorbitofrontal_thickness	217	1081	0.733	NonSig
15q11.2dup	-0.017	0.074	-0.226	0.821	rh_middletemporal_thickness	217	1081	0.952	NonSig
15q11.2dup	-0.089	0.074	-1.203	0.229	rh parahippocampal_thickness	217	1081	0.748	NonSig
15q11.2dup	0.053	0.074	0.709	0.478	rh_paracentral_thickness	217	1081	0.932	NonSig
15q11.2dup	-0.016	0.074	-0.213	0.832	rh_parsopercularis_thickness	217	1081	0.952	NonSig
15q11.2dup	-0.017	0.074	-0.235	0.814	rh_parsorbitalis_thickness	217	1081	0.952	NonSig
15q11.2dup	-0.094	0.074	-1.261	0.207	rh_parstriangularis_thickness	217	1081	0.748	NonSig
15q11.2dup	0.031	0.074	0.410	0.682	rh_pericalcarine_thickness	217	1081	0.952	NonSig
15q11.2dup	-0.156	0.074	-2.099	0.036	rh_postcentral_thickness	217	1081	0.521	NonSig
15q11.2dup	-0.035	0.074	-0.474	0.635	rh_posteriorcingulate_thickness	217	1081	0.952	NonSig
15q11.2dup	-0.075	0.074	-1.009	0.313	rh_precentral_thickness	217	1081	0.807	NonSig
15q11.2dup	0.021	0.074	0.288	0.773	rh_precuneus_thickness	217	1081	0.952	NonSig
15q11.2dup	0.038	0.074	0.505	0.614	rh_rostralanteriorcingulate_thickness	217	1081	0.952	NonSig
15q11.2dup	-0.018	0.074	-0.242	0.809	rh_rostralmiddlefrontal_thickness	217	1081	0.952	NonSig



15q11.2dup	0.044	0.074	0.597	0.551	rh_superiorfrontal_thickness	217	1081	0.942	NonSig
15q11.2dup	0.120	0.074	1.609	0.108	rh_superiorparietal_thickness	217	1081	0.600	NonSig
15q11.2dup	-0.165	0.074	-2.226	0.026	rh_superiortemporal_thickness	217	1081	0.521	NonSig
15q11.2dup	0.026	0.074	0.345	0.730	rh_supramarginal_thickness	217	1081	0.952	NonSig
15q11.2dup	-0.008	0.074	-0.101	0.920	rh_frontalpole_thickness	217	1081	0.965	NonSig
15q11.2dup	0.053	0.074	0.711	0.477	rh_temporalpole_thickness	217	1081	0.932	NonSig
15q11.2dup	0.091	0.074	1.227	0.220	rh_transversetemporal_thickness	217	1081	0.748	NonSig
15q11.2dup	-0.139	0.074	-1.873	0.061	rh_insula_thickness	217	1081	0.544	NonSig
15q11.2dup	-0.022	0.075	-0.299	0.765	lh_bankssts_area	215	1066	0.952	NonSig
15q11.2dup	0.015	0.075	0.198	0.843	lh_caudalanteriorcingulate_area	215	1066	0.952	NonSig
15q11.2dup	-0.016	0.075	-0.215	0.830	lh_caudalmiddlefrontal_area	215	1066	0.952	NonSig
15q11.2dup	-0.048	0.075	-0.641	0.522	lh_cuneus_area	215	1066	0.942	NonSig
15q11.2dup	0.140	0.075	1.871	0.062	lh_entorhinal_area	215	1066	0.544	NonSig
15q11.2dup	-0.001	0.075	-0.014	0.989	lh_fusiform_area	215	1066	0.993	NonSig
15q11.2dup	-0.036	0.075	-0.482	0.630	lh_inferiorparietal_area	215	1066	0.952	NonSig
15q11.2dup	-0.064	0.075	-0.855	0.393	lh_inferiortemporal_area	215	1066	0.831	NonSig
15q11.2dup	-0.113	0.075	-1.508	0.132	lh_isthmusingulate_area	215	1066	0.604	NonSig
15q11.2dup	-0.020	0.075	-0.269	0.788	lh_lateraloccipital_area	215	1066	0.952	NonSig
15q11.2dup	0.129	0.075	1.722	0.085	lh_lateralorbitofrontal_area	215	1066	0.579	NonSig
15q11.2dup	-0.009	0.075	-0.119	0.905	lh_lingual_area	215	1066	0.965	NonSig
15q11.2dup	0.125	0.075	1.672	0.095	lh_medialorbitofrontal_area	215	1066	0.592	NonSig
15q11.2dup	-0.114	0.075	-1.529	0.126	lh_middletemporal_area	215	1066	0.604	NonSig
15q11.2dup	0.122	0.075	1.628	0.104	lh parahippocampal_area	215	1066	0.599	NonSig
15q11.2dup	0.151	0.075	2.023	0.043	lh_paracentral_area	215	1066	0.521	NonSig
15q11.2dup	0.128	0.075	1.713	0.087	lh_parsopercularis_area	215	1066	0.579	NonSig
15q11.2dup	0.142	0.075	1.901	0.058	lh_parsorbitalis_area	215	1066	0.544	NonSig
15q11.2dup	0.086	0.075	1.144	0.253	lh_parsstriangularis_area	215	1066	0.787	NonSig
15q11.2dup	0.034	0.075	0.461	0.645	lh_pericalcarine_area	215	1066	0.952	NonSig
15q11.2dup	-0.021	0.075	-0.281	0.778	lh_postcentral_area	215	1066	0.952	NonSig
15q11.2dup	-0.057	0.075	-0.762	0.446	lh_posteriorcingulate_area	215	1066	0.917	NonSig
15q11.2dup	-0.180	0.075	-2.406	0.016	lh_precentral_area	215	1066	0.488	NonSig
15q11.2dup	-0.011	0.075	-0.143	0.886	lh_precuneus_area	215	1066	0.965	NonSig

15q11.2dup	-0.076	0.075	-1.017	0.309	lh_rostralanteriorcingulate_area	215	1066	0.807	NonSig
15q11.2dup	0.069	0.075	0.927	0.354	lh_rostralmiddlefrontal_area	215	1066	0.807	NonSig
15q11.2dup	-0.069	0.075	-0.916	0.360	lh_superiorfrontal_area	215	1066	0.807	NonSig
15q11.2dup	-0.009	0.075	-0.118	0.906	lh_superiorparietal_area	215	1066	0.965	NonSig
15q11.2dup	-0.137	0.075	-1.838	0.066	lh_superiortemporal_area	215	1066	0.553	NonSig
15q11.2dup	-0.032	0.075	-0.434	0.665	lh_supramarginal_area	215	1066	0.952	NonSig
15q11.2dup	0.011	0.075	0.150	0.881	lh_frontalpole_area	215	1066	0.965	NonSig
15q11.2dup	0.068	0.075	0.908	0.364	lh_temporalpole_area	215	1066	0.807	NonSig
15q11.2dup	-0.048	0.075	-0.643	0.521	lh_transversetemporal_area	215	1066	0.942	NonSig
15q11.2dup	-0.117	0.075	-1.568	0.117	lh_insula_area	215	1066	0.604	NonSig
15q11.2dup	-0.002	0.075	-0.027	0.978	rh_bankssts_area	215	1066	0.992	NonSig
15q11.2dup	0.127	0.075	1.703	0.089	rh_caudalanteriorcingulate_area	215	1066	0.579	NonSig
15q11.2dup	0.160	0.075	2.147	0.032	rh_caudalmiddlefrontal_area	215	1066	0.521	NonSig
15q11.2dup	-0.025	0.075	-0.336	0.737	rh_cuneus_area	215	1066	0.952	NonSig
15q11.2dup	0.015	0.075	0.199	0.842	rh_entorhinal_area	215	1066	0.952	NonSig
15q11.2dup	-0.078	0.075	-1.042	0.297	rh_fusiform_area	215	1066	0.797	NonSig
15q11.2dup	-0.095	0.075	-1.277	0.202	rh_inferioparietal_area	215	1066	0.748	NonSig
15q11.2dup	-0.052	0.075	-0.694	0.488	rh_inferiortemporal_area	215	1066	0.938	NonSig
15q11.2dup	-0.070	0.075	-0.931	0.352	rh_isthmuscingulate_area	215	1066	0.807	NonSig
15q11.2dup	-0.034	0.075	-0.459	0.646	rh_lateraloccipital_area	215	1066	0.952	NonSig
15q11.2dup	0.150	0.075	2.007	0.045	rh_lateralorbitofrontal_area	215	1066	0.521	NonSig
15q11.2dup	-0.080	0.075	-1.065	0.287	rh_lingual_area	215	1066	0.787	NonSig
15q11.2dup	-0.042	0.075	-0.568	0.570	rh_medialorbitofrontal_area	215	1066	0.942	NonSig
15q11.2dup	-0.042	0.075	-0.566	0.572	rh_middletemporal_area	215	1066	0.942	NonSig
15q11.2dup	0.039	0.075	0.521	0.603	rh parahippocampal_area	215	1066	0.952	NonSig
15q11.2dup	0.112	0.075	1.504	0.133	rh_paracentral_area	215	1066	0.604	NonSig
15q11.2dup	-0.085	0.075	-1.132	0.258	rh_parsopercularis_area	215	1066	0.787	NonSig
15q11.2dup	0.193	0.075	2.587	0.010	rh_parsorbitalis_area	215	1066	0.488	NonSig
15q11.2dup	0.016	0.075	0.216	0.829	rh_parstriangularis_area	215	1066	0.952	NonSig
15q11.2dup	0.060	0.075	0.801	0.423	rh_pericalcarine_area	215	1066	0.881	NonSig
15q11.2dup	-0.010	0.075	-0.134	0.893	rh_postcentral_area	215	1066	0.965	NonSig
15q11.2dup	0.016	0.075	0.213	0.831	rh_posteriorcingulate_area	215	1066	0.952	NonSig

15q11.2dup	-0.009	0.075	-0.124	0.901	rh_precentral_area	215	1066	0.965	NonSig
15q11.2dup	-0.090	0.075	-1.204	0.229	rh_precuneus_area	215	1066	0.748	NonSig
15q11.2dup	0.049	0.075	0.662	0.508	rh_rostralanteriorcingulate_area	215	1066	0.942	NonSig
15q11.2dup	0.037	0.075	0.496	0.620	rh_rostralmiddlefrontal_area	215	1066	0.952	NonSig
15q11.2dup	-0.247	0.074	-3.312	0.001	rh_superiorfrontal_area	215	1066	0.143	NonSig
15q11.2dup	-0.026	0.075	-0.350	0.726	rh_superiorparietal_area	215	1066	0.952	NonSig
15q11.2dup	-0.044	0.075	-0.592	0.554	rh_superiortemporal_area	215	1066	0.942	NonSig
15q11.2dup	-0.081	0.075	-1.086	0.278	rh_supramarginal_area	215	1066	0.787	NonSig
15q11.2dup	-0.055	0.075	-0.734	0.463	rh_frontalpole_area	215	1066	0.932	NonSig
15q11.2dup	0.070	0.075	0.943	0.346	rh_temporalpole_area	215	1066	0.807	NonSig
15q11.2dup	-0.025	0.075	-0.332	0.740	rh_transversetemporal_area	215	1066	0.952	NonSig
15q11.2dup	-0.042	0.075	-0.556	0.578	rh_insula_area	215	1066	0.943	NonSig
15q11.2dup	-0.033	0.072	-0.461	0.645	Left-Thalamus-Proper	230	1140	0.952	NonSig
15q11.2dup	0.027	0.072	0.375	0.708	Right-Thalamus-Proper	230	1140	0.952	NonSig
15q11.2dup	-0.093	0.072	-1.286	0.199	Left-Caudate	230	1140	0.748	NonSig
15q11.2dup	-0.140	0.072	-1.940	0.053	Right-Caudate	230	1140	0.544	NonSig
15q11.2dup	-0.071	0.072	-0.983	0.326	Left-Putamen	230	1140	0.807	NonSig
15q11.2dup	-0.118	0.072	-1.639	0.101	Right-Putamen	230	1140	0.599	NonSig
15q11.2dup	0.048	0.072	0.670	0.503	Left-Pallidum	230	1140	0.942	NonSig
15q11.2dup	-0.018	0.072	-0.248	0.804	Right-Pallidum	230	1140	0.952	NonSig
15q11.2dup	0.004	0.072	0.052	0.959	Left-Hippocampus	230	1140	0.983	NonSig
15q11.2dup	0.126	0.072	1.747	0.081	Right-Hippocampus	230	1140	0.579	NonSig
15q11.2dup	0.097	0.072	1.349	0.178	Left-Amygdala	230	1140	0.733	NonSig
15q11.2dup	0.065	0.072	0.904	0.366	Right-Amygdala	230	1140	0.807	NonSig
15q11.2dup	-0.022	0.072	-0.307	0.759	Left-Accumbens-area	230	1140	0.952	NonSig
15q11.2dup	0.099	0.072	1.367	0.172	Right-Accumbens-area	230	1140	0.733	NonSig





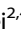






II

II

## ARTICLE OPEN



# No signs of neurodegenerative effects in 15q11.2 BP1-BP2 copy number variant carriers in the UK Biobank

Rune Boen<sup>1,2</sup>, Tobias Kaufmann<sup>2,3</sup>, Oleksandr Frei<sup>2,4</sup>, Dennis van der Meer<sup>2,5</sup>, Srdjan Djurovic<sup>1,6,7</sup>, Ole A. Andreassen<sup>1,2,7</sup>, Kaja K. Selmer<sup>8</sup>, Dag Alnæs<sup>2,9</sup> and Ida E. Sønderby<sup>1,2,7</sup>

© The Author(s) 2023

The 15q11.2 BP1-BP2 copy number variant (CNV) is associated with altered brain morphology and risk for atypical development, including increased risk for schizophrenia and learning difficulties for the deletion. However, it is still unclear whether differences in brain morphology are associated with neurodevelopmental or neurodegenerative processes. This study derived morphological brain MRI measures in 15q11.2 BP1-BP2 deletion ( $n = 124$ ) and duplication carriers ( $n = 142$ ), and matched deletion-controls ( $n = 496$ ) and duplication-controls ( $n = 568$ ) from the UK Biobank study to investigate the association with brain morphology and estimates of brain ageing. Further, we examined the ageing trajectory of age-affected measures (i.e., cortical thickness, surface area, subcortical volume, reaction time, hand grip strength, lung function, and blood pressure) in 15q11.2 BP1-BP2 CNV carriers compared to non-carriers. In this ageing population, the results from the machine learning models showed that the estimated brain age gaps did not differ between the 15q11.2 BP1-BP2 CNV carriers and non-carriers, despite deletion carriers displaying thicker cortex and lower subcortical volume compared to the deletion-controls and duplication carriers, and lower surface area compared to the deletion-controls. Likewise, the 15q11.2 BP1-BP2 CNV carriers did not deviate from the ageing trajectory on any of the age-affected measures examined compared to non-carriers. Despite altered brain morphology in 15q11.2 BP1-BP2 CNV carriers, the results did not show any clear signs of apparent altered ageing in brain structure, nor in motor, lung or heart function. The results do not indicate neurodegenerative effects in 15q11.2 BP1-BP2 CNV carriers.

*Translational Psychiatry* (2023)13:61; <https://doi.org/10.1038/s41398-023-02358-w>

## INTRODUCTION

The human brain undergoes structural changes as people age, including cortical thinning and volume loss [1–4]. Such age-related changes in brain morphology have been linked to cognitive decline [5, 6] and physical deterioration [7], and are presumably the results of a complex interplay between many neurobiological processes, including links to genetic factors [8–10]. Ageing affects individuals differently as reflected in increased heterogeneity in brain structure and cognition in mid to late adulthood [11]. In the last couple of decades, several potential age biomarkers have been investigated, e.g., through the use of measures of telomere length, DNA methylation [12–14] and brain structure.

Studies have used machine learning (ML) techniques to predict chronological age by using structural MRI measures as input features [15–17]. The estimations provide a measure of an individual's brain age gap, i.e., the difference between the predicted age and chronological age. Higher brain age gap has been suggested to reflect either (i) an accelerated ageing rate throughout life, (ii) an accentuated, but stable ageing, or (iii) an accentuated and accelerated ageing [12]. Higher predicted brain

age has been associated with other indicators of older age—e.g. accelerated body age, older physical appearance, lower cognitive functioning [15], weaker grip strength, poorer lung function, slower walking speed, and increased mortality risk [18]. Brain age gap has been found to be heritable and increased in several neurological and psychiatric conditions [17, 19], linking brain age to brain disorders and genetics. However, studies investigating brain age in individuals carrying rare genetic variants and displaying alterations in brain structure are scarce.

Some rare recurrent copy number variants (CNVs), i.e., regions of the genome that are either deleted or duplicated, are associated with alterations in brain structure [20–23]. Individuals carrying recurrent microdeletions or duplications at the 15q11.2 BP1-BP2 genomic locus display differences in brain morphology through altered cortical thickness, surface area, and white matter fiber tracts [24, 25]. The 15q11.2 BP1-BP2 genomic region contains four evolutionary highly conserved genes: *CYFIP1*, *TUBGCP5*, *NIPA1*, and *NIPA2* [26], which have been reported to be critical for typical neurodevelopment [27]. Indeed, both the *CYFIP1* and the *NIPA1* are highly expressed in the developing mouse brain [28].

<sup>1</sup>Department of Medical Genetics, Oslo University Hospital, Oslo, Norway. <sup>2</sup>NORMENT, Division of Mental Health and Addiction, Oslo University Hospital and Institute of Clinical Medicine, University of Oslo, Oslo, Norway. <sup>3</sup>Department of Psychiatry and Psychotherapy, Tübingen Center for Mental Health, University of Tübingen, Tübingen, Germany. <sup>4</sup>Centre for Bioinformatics, Department of Informatics, University of Oslo, Oslo, Norway. <sup>5</sup>School of Mental Health and Neuroscience, Faculty of Health, Medicine and Life Sciences, Maastricht University, Maastricht, The Netherlands. <sup>6</sup>NORMENT, Department of Clinical Science, University of Bergen, Bergen, Norway. <sup>7</sup>KG Jebsen Centre for Neurodevelopmental Disorders, University of Oslo, Oslo, Norway. <sup>8</sup>Department of Research and Innovation, Division of Clinical Neuroscience, Oslo University Hospital and the University of Oslo, Oslo, Norway. <sup>9</sup>Kristiania University College, Oslo, Norway. ✉email: boenrune@gmail.com

Received: 21 December 2021 Revised: 30 January 2023 Accepted: 6 February 2023

Published online: 18 February 2023

Further, the *CYFIP1* has been suggested to important for dendritic spine morphology [29, 30] and myelination [31]. The *NIPA1* and the *NIPA2* encode for magnesium transporters [32], whereas the *TUBGCP5* is important for microtubule nucleation [33]. At the phenotypic level, 15q11.2 BP1-BP2 deletion carriers have an increased risk for schizophrenia [34] and learning difficulties, such as dyslexia and dyscalculia [35], as well as lower cognitive functioning [24, 25]. Duplication carriers, on the other hand, have not been convincingly associated with any neurodevelopmental or psychiatric disease and perform similarly to non-carriers on cognitive tests [35–37]. Cortical thickness displays a dose response of the 15q11.2 BP1-BP2 CNVs (i.e., decreased cortical thickness with increasing copy number) with deletion carriers having significantly thicker cortices, lower surface area and smaller nucleus accumbens compared to non-carriers. Cortical thickness, surface area, and subcortical volume are structural brain measures that exhibit clear age-related changes during typical aging, including cortical thinning [9, 38, 39], reductions in surface area [40] and lower subcortical volume [41]. However, it is unclear whether the group differences in brain structure among 15q11.2 BP1-BP2 CNV carriers are reflected by altered ageing as indicated by estimations of brain age gap. There are also other factors that may indicate accentuated ageing among 15q11.2 BP1-BP2 CNV carriers. For instance, the 15q11.2 BP1-BP2 CNV is also associated with several physical traits that typically deteriorate in older ages, including reaction time, hand grip strength, lung function and blood pressure [25, 42]. All of these measures are important features for an age biomarker that is associated with mortality and hospital admissions in older individuals [43], emphasizing their clinical significance. In sum, the differences in brain morphology and performance in physical traits that declines with age may indicate altered ageing among 15q11.2 BP1-BP2 CNV carriers.

In the current study, we investigated apparent brain ageing in 15q11.2 BP1-BP2 CNV carriers. Due to alterations in brain morphology and in physical traits among 15q11.2 BP1-BP2 CNV carriers [25, 42], i.e., where the majority of these traits indicate accentuated ageing, we predicted that the 15q11.2 BP1-BP2 CNV carriers would also exhibit group differences in brain age gap. To test for accelerated or decelerating ageing in other age-affected measures, we follow-up brain age gap estimations with testing for a cross-sectional interaction effect between 15q11.2 BP1-BP2 copy number and age on brain measures and an effect on the longitudinal ageing trajectory in reaction time, grip strength, lung function and blood pressure.

## METHODS

### Participants

The present study includes 124 15q11.2 BP1-BP2 deletion and 142 duplication carriers, 496 non-carrier deletion controls and 568 non-carrier duplication controls from the UK biobank study—all with neuroimaging data. Four non-carrier controls were matched to each CNV carrier based on age, sex, scanner site, affection status (diagnosis of a neurological or mental/behavioral disorder) and estimated intracranial volume (ICV). The CNVs were identified as described previously [25]. We also extracted a sample of individuals diagnosed with multiple sclerosis ( $n = 60$ ) to validate the brain age prediction models against the unaffected participants from the deletion-control and duplication-control groups ( $n = 1210$ ). A training group consisting of non-carrier individuals ( $n = 36,013$  individuals) with no reported neurological or mental/behavioral diagnoses was used as a training set for brain age prediction (see supplementary note 1 and supplementary table 1 for details and descriptive statistics for the full data set). The estimated effect sizes for group differences that could be reliably detected using the current test sample ranged from Cohen's  $d = 0.26$  to  $0.36$  (see supplementary note 2 for power sensitivity analysis).

### MRI acquisition

All MRI data were acquired on a 3T Siemens Skyra scanner from three scanner sites. Detailed information about the image processing and quality control for the UK biobank is reported elsewhere [44]. Briefly, the

TI-weighted images were acquired with a sagittal orientation at 1.0 mm isotropic resolution,  $TI = 880$  ms,  $TE = 2.01$  ms,  $TR = 2000$  ms.

### Structural brain/morphology measures

The MR images were preprocessed in Freesurfer version 5.3.0 [45] and provided estimates of cortical thickness, surface area, volume across 180 regions per hemisphere, in addition to subcortical and cortical summary measures using the Human Connectome Project (HCP) parcellation atlas [46]. These HCP features were used to create models for brain age prediction in a training set and used to predict brain age in an independent test sample (see below). Participants were excluded if they had a Euler number that was missing or exceeded three standard deviations from the sample mean, or if they had mean values that exceeded four standard deviations from the sample mean on cortical thickness, surface area or subcortical volume adjusted for covariates (see supplementary notes 1 for details). Here, we focus on the mean cortical thickness, total cortical surface area, and total subcortical volume to increase statistical power. Regional group differences between 15q11.2 BP1-BP2 CNV carriers and non-carriers have been reported elsewhere for 34 regions of interest [25]. However, to fully exploit the complex relationship between brain structures, we used all of the values from the parcellated brain regions to get a single estimated score for each participant (i.e., predicted age).

### Motor, lung, and heart function

Reaction time, grip strength, forced expiratory volume (lung function), systolic and diastolic blood pressure (incl. body mass index (BMI) as covariate for measures of blood pressure) were extracted from the UK biobank. These measures are available from up to three timepoints, resulting in a mix of cross sectional and longitudinal data. We used mixed effects models in these analyses to cope with the dependency in the data.

### Brain age gap estimations

We used the XGBoost package in R [47, 48] to build a ML model to predict age from a set of cortical thickness, cortical surface area, cortical volume, subcortical volume (i.e., 180/180/180/8 regions of interest for each hemisphere) and cortical summary measures from the training group, in total 1145 measures (similar to; [17, 49, 50] henceforth termed the 'full ML model'). In addition, we trained three separate ML models that included either measures of (i) cortical thickness (360 measures), (ii) surface area (360 measures) or (iii) subcortical volume measures (16 measures) only to predict age. These three models will be referred to as 'cortical thickness ML model', 'surface area ML model' and 'subcortical volume ML model', respectively. The XGBoost package was used as it is resource efficient and flexible, including implementation of machine learning algorithms using gradient boosting, parallel computation, and flexible parameter settings. It has also been shown to be superior to other machine learning models as demonstrated in machine learning competitions [47]. Parameters for the brain age ML models were tuned individually for each model following an optimization procedure (see supplementary note 3 for details). An overestimation and underestimation of the predicted ages at the tails of the chronological age distribution is commonly observed in brain age prediction models [49, 51, 52]. Thus, we corrected for this bias using a recent correction method for predicted brain age [53] (see supplementary note 4 for details). Next, we subtracted each individual's chronological age from the corrected predicted brain age to get an estimate of brain age gap. That is, if an individual is 50 years of age, while the predicted brain age is 52, the 2-year brain age gap will indicate that the individual has an older looking brain than what is expected based on the individual's chronological age.

### Statistical analysis

All analyses were carried out in R version 4.0.0. The brain measures (i.e. mean cortical thickness, total cortical surface area, total subcortical volume, brain age gap) were pre-residualized for age,  $age^2$ , sex, scanner site, affection status, ICV and Euler number using linear regression. First, for group comparisons, deletion and duplication carriers were compared to their respective non-carrier matched control group, and deletion carriers were compared to duplication carriers. The dependent variables were brain morphological measures (mean cortical thickness, total cortical surface area, total subcortical volume) and brain age gap (i.e., derived from the 'cortical thickness ML model', 'surface area ML model', 'subcortical volume ML model', and the 'full ML model'). These were tested using a



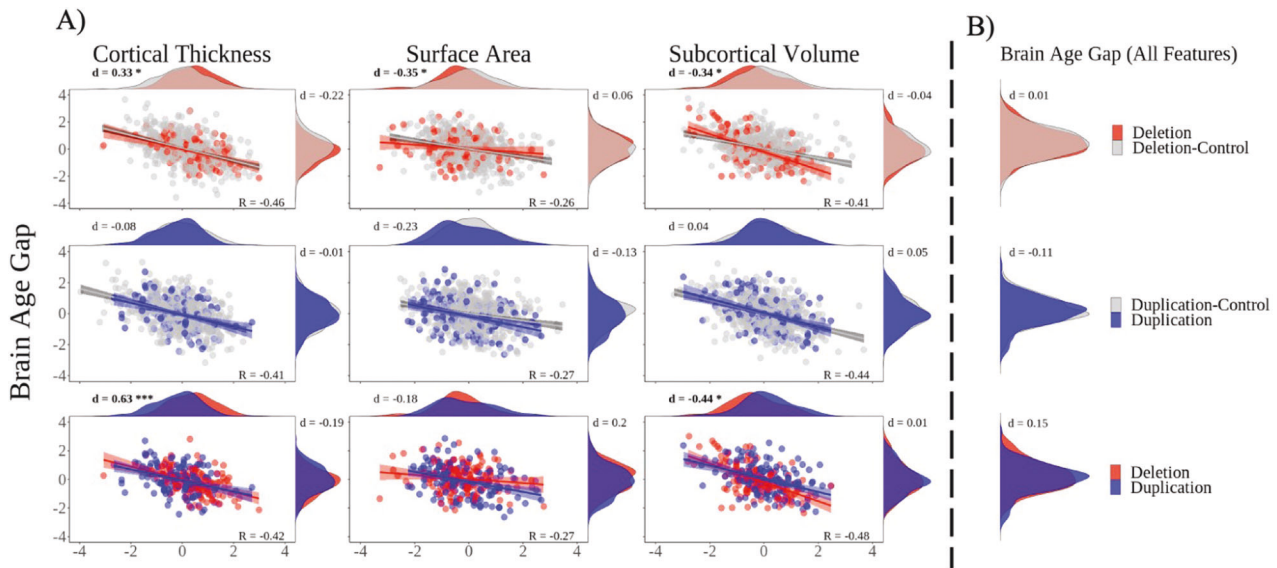


**Fig. 1 Brain morphology and brain age in 15q11.2 BP1-BP2 carriers.** **A** Scatterplots: Residualized brain measures vs brain age gap. Density plots; Horizontal: Brain measures, Vertical: Brain age gaps from the 'cortical thickness machine learning model', 'surface area machine learning model', and 'subcortical volume machine learning model'. Columns: Mean cortical thickness (left), total surface area (middle), and total subcortical volume (right). Rows: Comparisons between: Deletion carriers versus deletion-controls, duplication carriers versus duplication-controls and deletion carriers versus duplication carriers. **B** Brain age gap group differences obtained from the 'full machine learning model'. All values were adjusted for age, age<sup>2</sup>, sex, scanner site, affection status (having either a F or G-ICD10 diagnosis), ICV and Euler number. All values were scaled for visualization purposes. Raw residuals, confidence intervals, and *p*-values can be found in Supplementary Figs. 1–3 (for measures of brain morphology) and Supplementary Figs. 6–9 (for measures of brain age gap). Red = deletion, carriers, gray = non-carriers, blue = duplication-carriers. *R* = correlation value across the two included groups. *d* = Cohens *d*. Group differences that survive the multiple comparison threshold are marked in bold. \**p* < 0.0014, \*\*\**p* < 0.000014.

two-sided *t*-test. Cohen's *d* was calculated as measure of effect size for the group comparisons.

Second, we investigated an interaction effect between age and carrier status using the following linear model:  $Y \sim \text{age} + \text{age}^2 + \text{carrier status} + \text{age} \times \text{carrier status}$  after regressing out the effect of scanner site, affection status, ICV and Euler number from the dependent variables. Carrier status was coded as "yes" and "no" (i.e., "yes" for deletion and duplication carriers, and "no" for deletion-control and duplication-control). The interaction effect was tested separately between the 15q11.2 BP1-BP2 CNV groups, such that deletion carriers and deletion-control were tested against each other, and duplication-carriers and duplication control were tested against each other. Dependent variables were mean cortical thickness, total cortical surface area and total subcortical volume.

Third, we examined the age-related trajectory of reaction time, grip strength, lung function, systolic and diastolic blood pressure. We used cross sectional and longitudinal data (First visit:  $n = 1330$ , Mean age = 55.3, SD = 7.53, age range = 40.5–70.6, Second visit:  $n = 224$ , Mean age = 60.8, SD = 7.07, age range = 45.4–73.8, Third visit:  $n = 1330$ , Mean age = 64.2, SD = 7.62, age range = 46.8–81.3) and mixed effects models. The models were fitted with a random effect of participant on intercepts and with sex and affection status included as covariates (+BMI for the blood pressure measures). To obtain the best ageing model, we compared models with either: (a) only covariates, (b) age and covariates, or (c) age, age<sup>2</sup> and covariates. The models were tested stepwise to get the age model that best fitted the data. Then, we tested this model against the same model but including carrier status as either (d) main effect or (e) interaction effect. We used the Akaike information criterion (AIC) as model criterion, where the more complex model was chosen if the AIC dropped by 2 with a *p*-value < 0.05 (see supplementary note 5 for details). Finally, we examined the correlation between brain age gap and age-affected physical measures (reaction time, grip strength, lung function, systolic and diastolic blood pressure). Here, we pre-residualized the measures for the variables included in the model that best fit the data as described above, before running the correlations. Bonferroni corrections were conducted across all comparisons. The significance threshold for group comparisons on measures of brain structure and brain age gap (21 comparisons), interaction effect between age and measures of brain structure (6 comparisons), and brain age gap correlations with measures of motor, lung, and heart function (10 correlations), resulted in alpha set to 0.05/(21 + 6 + 10) = 0.0014. For the models of motor, lung, and heart function,

the predictors were considered significant if the *p* < 0.05 in the model that best fitted the data according to the selection criteria stated above. The uncorrected *p*-value is presented across all analyses.

## RESULTS

### 15q11.2 copy number variants and brain morphology

In the current study, 15q11.2 BP1-BP2 deletion carriers had significantly thicker cortex ( $d = 0.33$ , CI = 0.13, 0.53;  $d = 0.63$ , CI = 0.38, 0.87, both  $p < 0.001$ ), and lower subcortical volume ( $d = -0.34$ , CI = -0.54, -0.14;  $d = -0.44$ , CI = -0.68, -0.20, both  $p < 0.001$ ) compared to deletion-controls and duplication carriers, respectively, and lower total surface area ( $d = -0.35$ , CI = -0.55, -0.15,  $p < 0.001$ ) in comparison to deletion-controls (Fig. 1; Supplementary Figs. 1–3). The results did not reveal any significant difference for duplication-carriers compared to duplication-controls, nor any interaction effects of age and carrier status on any of the brain measures (see Supplementary Tables 3–4; Supplementary Fig. 4). Part of the sample has previously shown higher mean cortical thickness and lower total cortical surface area in deletion carriers compared to non-carriers, and lower mean cortical thickness in duplication carriers compared to non-carriers [25].

### Brain age gap in 15q11.2 BP1-BP2 copy number variant carriers

The 'full ML model' yielded the highest correlation between predicted age and chronological age ( $r = .80$ ) outperforming the three simpler/narrower models—the 'cortical thickness ML model' ( $r = .71$ ), the 'surface area ML model' ( $r = 0.63$ ), and the 'subcortical volume ML model' ( $r = 0.64$ ; Supplementary Fig. 5). None of the four ML models for brain age gap estimations showed any significant differences between 15q11.2 BP1-BP2 deletion and duplication carriers and non-carriers, nor between deletion and duplication carriers (Fig. 1A, B; Supplementary Figs. 6–9). Overall, brain age gap from the cortical thickness, surface area or subcortical volume ML models correlated negatively with

the mean cortical thickness, total surface area and total subcortical volume, respectively ( $r$  ranging from  $-0.26$  to  $-0.48$ ; Fig. 1A). To ensure that the lack of identified brain age gap was not a result of poor brain age models, we briefly validated our brain age models in a sample of individuals diagnosed with multiple sclerosis. In support of the validity of our models, the results showed strong group differences in brain age gap between the multiple sclerosis group and a healthy control group Cohens  $d = 0.49$  to  $1.11$ ; see Supplementary Table 6), which is in line with the previous literature [17, 54]. Thus, this leads us to the conclusion that the 15q11.2 BP1-BP2 CNV is not associated with a clear altered brain age gap.

#### Age-related decline in motor, lung, and heart function

None of the mixed models that included an interaction term between age and carrier status yielded a better model fit compared to the other age models without the inclusion of the interaction term. Thus, generally the 15q11.2 BP1-BP2 deletion and duplication carriers do not deviate strongly from non-carriers on the expected age-related reductions in reaction time, grip strength, lung function, and diastolic and systolic blood pressure based on mixed cross-sectional and longitudinal data (Supplementary Fig. 10; Supplementary Tables 6–7). However, there were some main effects of carrier status, as the deletion carriers had slower reaction time compared to deletion-controls (Supplementary Table 6), whereas duplication carriers exhibited higher diastolic and systolic blood pressure compared to duplication-controls (Supplementary Table 7). In general, there were no significant associations between brain age gap derived from the ‘full ML model’ and the selected age-affected physical measures among the deletion-carriers and deletion-controls or duplication-carriers and duplication-controls. The exception was for the duplication-carriers and duplication-controls, that displayed a significant negative correlation between higher brain age gap and lower lung function ( $r = -0.17$ ,  $p < 0.001$ ; Supplementary note 6).

#### DISCUSSION

Focusing exclusively on an ageing population (47–81 years of age), we showed that the 15q11.2 BP1-BP2 deletion carriers did not display a significant difference in brain age gap in comparison to non-carriers. In concordance with this pattern, the cross-sectional age effect on cortical thickness, surface area and subcortical volume did not significantly interact with 15q11.2 BP1-BP2 copy number, indicating comparable ageing trajectory in brain structure. Likewise, the mixed cross-sectional and longitudinal analysis indicate that both deletion and duplication-carriers had age-related deterioration at a comparable rate to non-carriers in selected age-affected measures—reaction time, grip strength, lung function and blood pressure. Further, we expanded on previous results to show that 15q11.2 BP1-BP2 deletion carriers exhibited a lower total subcortical volume overall compared to deletion-control and duplication-carriers and confirmed results on cortical thickness and surface area (i.e., thicker cortex and lower surface area in deletion carriers compared to non-carriers). Thus, the data did not show evidence for accelerated ageing among 15q11.2 BP1-BP2 CNV carriers compared to non-carriers but rather a stable ageing trajectory. Brain age gap—the difference between the predicted age and chronological age—has been suggested to reflect brain ageing, where higher brain age gap may reflect accelerated ageing, or accentuated, but stable ageing, or accentuated and accelerated ageing [12]. In contrast to our hypothesis, the current study shows that group differences in brain structure among 15q11.2 deletion carriers did not coincide with group differences in brain age gap estimations, neither when using a ML model with many (i.e., ‘the full ML model’) or fewer features (i.e., ‘cortical thickness ML model’, ‘surface area ML

model’, or ‘subcortical volume ML model’). The results indicate stable adult group-level differences in brain structure between the 15q11.2 BP1-BP2 deletion carriers and non-carriers. This seems to indicate that the observed group differences in brain phenotypes have been established before the individuals reached their current age range. This would indicate that the structural differences are due to other factors unrelated to ageing. Whilst caution is warranted given the lack of data to test this more directly, this may suggest that the brain alterations identified in 15q11.2 BP1-BP2 CNV carriers are more likely explained by an early offset in brain structure caused by early atypical neurodevelopment rather than neurodegeneration.

This study has strengths and limitations. The cross-sectional nature of the MR data limits our interpretation of the brain ageing trajectory. For instance, it is crucial to follow individuals over time to gain information on the slope of brain atrophy, ideally through multiple time points across the lifespan. As always, caution should be made when interpreting the results of cross-sectional data. Future studies using longitudinal brain imaging data are needed to fully characterize the age-related changes in brain structure. However, our mixed cross-sectional and longitudinal data on other age-affected measures (i.e., motor, lung and heart function) do seem to indicate a similar ageing trajectory between 15q11.2 BP1-BP2 CNV carriers and non-carriers.

The interpretation of the brain age gap estimations from the brain age models are relying on the assumption that the models are reliable and valid. Indeed, the brain age gap is simply the difference between the predicted chronological age and the chronological age, which means that the brain age gap is the error term from the brain age model. In the current study, however, brain age gap was associated with lung function among a sample of 15q11.2 BP1-BP2 duplication carriers and duplication-controls. This indicates that the brain age gap also carries useful biological information beyond measurement error. In addition, the current study showed that our brain age model yielded strong group differences between a multiple sclerosis group and a healthy control group, replicating previously identified brain age gap differences [17, 54]. Furthermore, brain age estimations are based on models that are informed by the strong associations between MRI features and age. Thus, deviation from a healthy brain age trajectory might reflect alterations in brain structure unrelated to ageing. It has also been suggested that brain age might reflect variations in the brain from early life [15]. Indeed, if the brain age models were simply reflecting variations in the brain, we would expect the 15q11.2 BP1-BP2 CNV carriers to exhibit alterations in brain age as they exhibit group-level differences in cortical thickness, surface area, and subcortical volume. However, we did not find any significant group differences in brain age gap among 15q11.2 BP1-BP2 CNV carriers. The low prevalence of carriers with the 15q11.2 BP1-BP2 CNV hinders the detection of small effects. Thus, the lack of significant statistical group differences does not imply that there is no neurodegenerative effect at all. However, the results do not support strong neurodegenerative effects that would have been of potential clinical relevance.

The 15q11.2 BP1-BP2 CNV carriers show phenotypic heterogeneity [25, 28, 35, 55]. This is important to note as the sample is drawn from the UK Biobank, which has a healthy volunteer bias at baseline [56], as well as a bias in the follow-up components [57]. For instance, the participants in the UK Biobank have been found to be healthier (e.g., lower rate of cancer, lower levels of smoking and daily alcohol consumption, lower likelihood of obesity) [56]. In addition, the follow-up components in the UK Biobank have been shown to be influenced by sample characteristics, including cognitive ability, adiposity, and liability to certain neurodevelopmental disorders [57]. This could potentially underestimate differences between 15q11.2 BP1-BP2 carriers and non-carriers.

Despite the overall biases in the UK Biobank, we still identify group-level differences in brain structure but not in their brain age gap. Thus, these results do not support clear neurodegenerative effects among the 15q11.2 BP1-BP2 CNV. However, more research is needed in an unbiased population and caution is urged if extrapolating the current result to the full population of 15q11.2 BP1-BP2 carriers.

## CONCLUSION

To conclude, the 15q11.2 BP1-BP2 deletion carriers exhibit altered cortical thickness, surface area and subcortical volume compared to non-carriers. We did not find support for the hypothesis that the differences in brain structure among 15q11.2 BP1-BP2 CNV carriers are due to accentuated ageing neither in cross-sectional MR data, brain age gap, or age-affected physical measures. Thus, despite altered brain morphology and worse performance in physical traits, these deviations do not seem to have significant clinical implications for neurodegeneration or physical deterioration in an ageing sample. The altered brain morphology in 15q11.2 BP1-BP2 CNV carriers could reflect other factors unrelated to ageing, possibly atypical neurodevelopment. Future studies should investigate early developmental trajectories of 15q11.2 BP1-BP2 CNV carriers on brain structure and other physical measures to clarify the life-span trajectory of the altered brain morphology. Finally, the “healthy volunteer” bias in the UK Biobank warrants caution when interpreting the results, and studies examining age-related changes in a more population-representative sample are needed.

## REFERENCES

- Fjell AM, McEvoy L, Holland D, Dale AM, Walhovd KB. What is normal in normal aging? Effects of aging, amyloid and Alzheimer's disease on the cerebral cortex and the hippocampus. *Prog Neurobiol*. 2014;117:20–40.
- Fjell AM, Westlye LT, Amlien I, Espeseth T, Reinvang I, Raz N, et al. High consistency of regional cortical thinning in aging across multiple samples. *Cereb Cortex*. 2009;19:2001–12.
- Fjell AM, Walhovd KB. Structural brain changes in aging: courses, causes and cognitive consequences. *Rev Neurosci*. 2010;21:187–221.
- Frangou S, Modabbernia A, Williams SCR, Papachristou E, Doucet GE, Agartz I, et al. Cortical thickness across the lifespan: Data from 17,075 healthy individuals aged 3–90 years. *Hum Brain Mapp*. 2021. [cited 2021 Oct 25] Available from: <https://onlinelibrary.wiley.com/doi/abs/10.1002/hbm.25364>.
- Persson J, Pudas S, Lind J, Kauppi K, Nilsson LG, Nyberg L. Longitudinal structure-function correlates in elderly reveal MTL dysfunction with cognitive decline. *Cereb Cortex*. 2012;22:2297–304.
- Fjell AM, Westlye LT, Grydeland H, Amlien I, Espeseth T, Reinvang I, et al. Accelerating cortical thinning: unique to dementia or universal in aging? *Cereb Cortex*. 2014;24:919–34.
- Erickson KI, Gildengers AG, Butters MA. Physical activity and brain plasticity in late adulthood. *Dialogues Clin Neurosci*. 2013;15:99–108.
- Batouli SAH, Trollor JN, Wen W, Sachdev PS. The heritability of volumes of brain structures and its relationship to age: A review of twin and family studies. *Ageing Res Rev*. 2014;13:1–9.
- Fjell AM, Grydeland H, Krogstad SK, Amlien I, Rohani DA, Ferschmann L, et al. Development and aging of cortical thickness correspond to genetic organization patterns. *Proc Natl Acad Sci USA*. 2015;112:15462–7.
- Brouwer RM, Panizzon MS, Glahn DC, Hibar DP, Hua X, Jahanshad N, et al. Genetic influences on individual differences in longitudinal changes in global and subcortical brain volumes: Results of the ENIGMA plasticity working group. *Hum Brain Mapp*. 2017;38:4444–58.
- Nyberg L, Boraxbekk CJ, Sörman DE, Hansson P, Herlitz A, Kauppi K, et al. Biological and environmental predictors of heterogeneity in neurocognitive ageing: evidence from Betula and other longitudinal studies. *Ageing Res Rev*. 2020;64:101184.
- Cole JH, Marioni RE, Harris SE, Deary IJ. Brain age and other bodily ‘ages’: implications for neuropsychiatry. *Mol Psychiatry*. 2019;24:266–81.
- Mather KA, Jorm AF, Parslow RA, Christensen H. Is telomere length a biomarker of aging? A review. *J Gerontol Ser A*. 2011;66A:202–13.
- Horvath S, Raj K. DNA methylation-based biomarkers and the epigenetic clock theory of ageing. *Nat Rev Genet*. 2018;19:371–84.
- Elliott ML, Belsky DW, Knodt AR, Ireland D, Melzer TR, Poulton R, et al. Brain-age in midlife is associated with accelerated biological aging and cognitive decline in a longitudinal birth cohort. *Mol Psychiatry*. 2021;26:3829–38.
- Cole JH, Franke K. Predicting age using neuroimaging: innovative brain ageing biomarkers. *Trends Neurosci*. 2017;40:681–90.
- Kaufmann T, van der Meer D, Doan NT, Schwarz E, Lund MJ, Agartz I, et al. Common brain disorders are associated with heritable patterns of apparent aging of the brain. *Nat Neurosci*. 2019;22:1617–23.
- Cole JH, Ritchie SJ, Bastin ME, Valdés Hernández MC, Muñoz Maniega S, Royle N, et al. Brain age predicts mortality. *Mol Psychiatry*. 2018;23:1385–92.
- Cole JH, Poudel RPK, Tsagkrasoulis D, Caan MWA, Steves C, Spector TD, et al. Predicting brain age with deep learning from raw imaging data results in a reliable and heritable biomarker. *NeuroImage*. 2017;163:115–24.
- Fan CC, Brown TT, Bartsch H, Kuperman JM, Hagler DJ, Schork A, et al. Williams syndrome-specific neuroanatomical profile and its associations with behavioral features. *NeuroImage Clin*. 2017;15:343–7.
- Sun D, Ching CRK, Lin A, Forsyth JK, Kushan L, Vajdi A, et al. Large-scale mapping of cortical alterations in 22q11.2 deletion syndrome: Convergence with idiopathic psychosis and effects of deletion size. *Mol Psychiatry*. 2020;25:1822–34.
- Sønderby IE, van der Meer D, Moreau C, Kaufmann T, Walters GB, Ellegaard M, et al. 1q21.1 distal copy number variants are associated with cerebral and cognitive alterations in humans. *Transl Psychiatry*. 2021;11:1–16.
- Sønderby IE, Gústafsson Ó, Doan NT, Hibar DP, Martin-Brevet S, Abdellaoui A, et al. Dose response of the 16p11.2 distal copy number variant on intracranial volume and basal ganglia. *Mol Psychiatry*. 2020;25:584–602.
- Silva AI, Ulfarsson MO, Stefansson H, Gustafsson O, Walters GB, Linden DEJ, et al. Reciprocal white matter changes associated with copy number variation at 15q11.2 BP1-BP2: a diffusion tensor imaging study. *Biol Psychiatry*. 2019;85:563–72.
- Writing Committee for the ENIGMA-CNV Working Group, van der Meer D, Sønderby IE, Kaufmann T, Walters GB, Abdellaoui A, et al. Association of copy number variation of the 15q11.2 BP1-BP2 region with cortical and subcortical morphology and cognition. *JAMA Psychiatry*. 2020;77:420–30.
- Chai JH, Locke DP, Greally JM, Knoll JHM, Ohta T, Dunai J, et al. Identification of four highly conserved genes between breakpoint hotspots BP1 and BP2 of the Prader-Willi/Angelman Syndromes deletion region that have undergone evolutionary transposition mediated by flanking duplicons. *Am J Hum Genet*. 2003;73:898–925.
- Rafi SK, Butler MG. The 15q11.2 BP1-BP2 microdeletion (Burnside–Butler) syndrome: in silico analyses of the four coding genes reveal functional associations with neurodevelopmental disorders. *Int J Mol Sci*. 2020;21:3296.
- Zwaag B, van der, Staal WG, Hochstenbach R, Poot M, Spierenburg HA, Jonge MVDE, et al. A co-segregating microduplication of chromosome 15q11.2 pinpoints two risk genes for autism spectrum disorder. *Am J Med Genet B Neuropsychiatr Genet*. 2010;153B:960–6.
- De Rubeis S, Pasciuto E, Li KW, Fernández E, Di Marino D, Buzzi A, et al. CYFIP1 coordinates mRNA translation and cytoskeleton remodeling to ensure proper dendritic spine formation. *Neuron*. 2013;79:1169–82.
- Oguro-Ando A, Rosensweig C, Herman E, Nishimura Y, Werling D, Bill BR, et al. Increased CYFIP1 dosage alters cellular and dendritic morphology and dysregulates mTOR. *Mol Psychiatry*. 2015;20:1069–78.
- Silva AI, Haddon JE, Ahmed Syed Y, Trent S, Lin TCE, Patel Y, et al. Cyfip1 haploinsufficient rats show white matter changes, myelin thinning, abnormal oligodendrocytes and behavioural inflexibility. *Nat Commun*. 2019;10:3455.
- Quamme GA. Molecular identification of ancient and modern mammalian magnesium transporters. *Am J Physiol-Cell Physiol*. 2010;298:C407–29.
- Murphy SM, Preble AM, Patel UK, O’Connell KL, Dias DP, Moritz M, et al. GCP5 and GCP6: two new members of the human  $\gamma$ -tubulin complex. *Mol Biol Cell*. 2001;12:3340–52.
- Stefansson H, Rujescu D, Cichon S, Pietiläinen OPH, Ingason A, Steinberg S, et al. Large recurrent microdeletions associated with schizophrenia. *Nature*. 2008;455:232–6.
- Stefansson H, Meyer-Lindenberg A, Steinberg S, Magnusdottir B, Morgen K, Arnarsdottir S, et al. CNVs conferring risk of autism or schizophrenia affect cognition in controls. *Nature*. 2014;505:361–6.
- Kendall KM, Rees E, Escott-Price V, Eimon M, Thomas R, Hewitt J, et al. Cognitive performance among carriers of pathogenic copy number variants: analysis of 152,000 UK Biobank subjects. *Biol Psychiatry*. 2017;82:103–10.
- Kendall KM, Bracher-Smith M, Fitzpatrick H, Lynham A, Rees E, Escott-Price V, et al. Cognitive performance and functional outcomes of carriers of pathogenic copy number variants: analysis of the UK Biobank. *Br J Psychiatry*. 2019;214:297–304.
- Salat DH, Buckner RL, Snyder AZ, Greve DN, Desikan RSR, Busa E, et al. Thinning of the cerebral cortex in aging. *Cereb Cortex*. 2004;14:721–30.



39. Thambisetty M, Wan J, Carass A, An Y, Prince JL, Resnick SM. Longitudinal changes in cortical thickness associated with normal aging. *NeuroImage*. 2010;52:1215–23.
40. Hogstrom LJ, Westlye LT, Walhovd KB, Fjell AM. The structure of the cerebral cortex across adult life: age-related patterns of surface area, thickness, and gyrification. *Cereb Cortex*. 2013;23:2521–30.
41. Fjell AM, Westlye LT, Grydeland H, Amlien I, Espeseth T, Reinvang I, et al. Critical ages in the life course of the adult brain: nonlinear subcortical aging. *Neurobiol Aging*. 2013;34:2239–47.
42. Owen D, Bracher-Smith M, Kendall KM, Rees E, Einon M, Escott-Price V, et al. Effects of pathogenic CNVs on physical traits in participants of the UK Biobank. *BMC Genomics*. 2018;19. [cited 2021 Jun 21] Available from: <https://www.ncbi.nlm.nih.gov/pmc/articles/PMC6278042/>.
43. Chan MS, Arnold M, Offer A, Hammami I, Mafham M, Armitage J, et al. A biomarker-based biological age in UK Biobank: composition and prediction of mortality and hospital admissions. *J Gerontol Ser A*. 2021;76:1295–302.
44. Alfaro-Almagro F, Jenkinson M, Bangerter NK, Andersson JLR, Griffanti L, Douaud G, et al. Image processing and Quality Control for the first 10,000 brain imaging datasets from UK Biobank. *NeuroImage*. 2018;166:400–24.
45. Fischl B. FreeSurfer. *NeuroImage*. 2012;62:774–81.
46. Glasser MF, Coalson TS, Robinson EC, Hacker CD, Harwell J, Yacoub E, et al. A multi-modal parcellation of human cerebral cortex. *Nature*. 2016;536:171–8.
47. Chen T, Guestrin C. XGBoost: A Scalable Tree Boosting System. In: *Proceedings of the 22nd ACM SIGKDD International Conference on Knowledge Discovery and Data Mining [Internet]*. New York, NY, USA: Association for Computing Machinery; 2016. [cited 2022 Oct 3] p. 785–94. (KDD '16). Available from: <https://doi.org/10.1145/2939672.2939785>.
48. Chen T, He T, Benesty M, Khotilovich V, Tang Y, Cho H, et al. xgboost: Extreme Gradient Boosting. 2022. [cited 2022 Oct 4] Available from: <https://CRAN.R-project.org/package=xgboost>.
49. Lange AMG, de, Kaufmann T, Meer D, van der, Maglanoc LA, Alnæs D, Moberget T, et al. Population-based neuroimaging reveals traces of childbirth in the maternal brain. *Proc Natl Acad Sci USA*. 2019;116:22341–6.
50. de Lange AMG, Anatóürk M, Suri S, Kaufmann T, Cole JH, Griffanti L, et al. Multi-modal brain-age prediction and cardiovascular risk: the Whitehall II MRI sub-study. *NeuroImage*. 2020;222:117292.
51. Le TT, Kuplicki RT, McKinney BA, Yeh HW, Thompson WK, Paulus MP, et al. A nonlinear simulation framework supports adjusting for age when analyzing brainAGE. *Front Aging Neurosci*. 2018;10:317.
52. Smith SM, Vidaurre D, Alfaro-Almagro F, Nichols TE, Miller KL. Estimation of brain age delta from brain imaging. *NeuroImage*. 2019;200:528–39.
53. de Lange AMG, Cole JH. Commentary: Correction procedures in brain-age prediction. *NeuroImage Clin*. 2020 [cited 2021 Jan 28];26. Available from: <https://www.ncbi.nlm.nih.gov/pmc/articles/PMC7049655/>.
54. Høgestøl EA, Kaufmann T, Nygaard GO, Beyer MK, Sowa P, Nordvik JE, et al. Cross-sectional and longitudinal MRI brain scans reveal accelerated brain aging in multiple sclerosis. *Front Neurol*. 2019 [cited 2021 Jun 22];10. Available from: <https://doi.org/10.3389/fneur.2019.00450/full>.
55. Burnside RD, Pasion R, Mikhail FM, Carroll AJ, Robin NH, Youngs EL, et al. Microdeletion/microduplication of proximal 15q11.2 between BP1 and BP2: a susceptibility region for neurological dysfunction including developmental and language delay. *Hum Genet*. 2011;130:517–28.
56. Fry A, Littlejohns TJ, Sudlow C, Doherty N, Adamska L, Sprosen T, et al. Comparison of sociodemographic and health-related characteristics of UK Biobank participants with those of the general population. *Am J Epidemiol*. 2017;186:1026–34.
57. Tyrrell J, Zheng J, Beaumont R, Hinton K, Richardson TG, Wood AR, et al. Genetic predictors of participation in optional components of UK Biobank. *Nat Commun*. 2021;12:886.

## ACKNOWLEDGEMENTS

This research has been conducted using the UK Biobank Resource under Application Number 27412. We acknowledge the support from the Research Council of Norway #223273 (NORMENT) and #276082 (TK). IES is supported by South-Eastern Norway Regional Health Authority (#2020060) and Kristian Gerhard Jebsen Stiftelsen (SKGJ-MED-021). RB is supported by South-Eastern Norway Regional Health Authority (#2020060). This work has received funding from the European Union's Horizon 2020 Research and Innovation Programme under Grant agreement No 847776. This work was performed on Services for sensitive data (TSD), the University of Oslo, Norway, with resources provided by UNINETT Sigma2 - the National Infrastructure for High Performance Computing and Data Storage in Norway.

## AUTHOR CONTRIBUTIONS

RB: Conceptualization, Methodology, software, formal analysis, data curation, writing—original draft, writing—review and editing, visualization. TK: conceptualization, methodology, writing—review and editing. OF: Data curation, resources, software. DVM: Data curation, resources, software, writing—review and editing. SD: Writing—review and editing. OAA: Resources, writing—review and editing, project administration, funding acquisition. KKS: Conceptualization, writing—review and editing, supervision. DA: Conceptualization, Writing—review and editing, supervision. IES: Conceptualization, Writing—review and editing, supervision, project administration, funding acquisition.

## COMPETING INTERESTS

OAA is a consultant for HealthLytix. The other authors declare no competing interests.

## ADDITIONAL INFORMATION

**Supplementary information** The online version contains supplementary material available at <https://doi.org/10.1038/s41398-023-02358-w>.

**Correspondence** and requests for materials should be addressed to Rune Boen.

**Reprints and permission information** is available at <http://www.nature.com/reprints>

**Publisher's note** Springer Nature remains neutral with regard to jurisdictional claims in published maps and institutional affiliations.



**Open Access** This article is licensed under a Creative Commons Attribution 4.0 International License, which permits use, sharing, adaptation, distribution and reproduction in any medium or format, as long as you give appropriate credit to the original author(s) and the source, provide a link to the Creative Commons license, and indicate if changes were made. The images or other third party material in this article are included in the article's Creative Commons license, unless indicated otherwise in a credit line to the material. If material is not included in the article's Creative Commons license and your intended use is not permitted by statutory regulation or exceeds the permitted use, you will need to obtain permission directly from the copyright holder. To view a copy of this license, visit <http://creativecommons.org/licenses/by/4.0/>.

© The Author(s) 2023

## Supplementary information

### Overview:

**Supplementary note 1:** Participants

**Supplementary note 2:** Statistical power: sensitivity analysis

**Supplementary note 3:** Brain age prediction model using machine learning

**Supplementary note 4:** Correction method for the brain age models

**Supplementary note 5:** Model selection of age-related changes in motor, lung and heart function

**Supplementary note 6:** Motor, lung, and heart function and brain age

**Supplementary Table 1.** Descriptive statistics for deletion-carriers, deletion-controls, duplication-controls, duplication-carriers and the training sample.

**Supplementary Table 2.** Descriptive statistics for the control and multiple sclerosis groups

**Supplementary Table 3.** Deletion-carriers vs deletion control: Age-related changes in cortical thickness, surface area and subcortical volume

**Supplementary Table 4.** Duplication-carriers vs duplication control: Age-related changes in cortical thickness, surface area and subcortical volume

**Supplementary Table 5.** Brain age prediction in a sample of patients with multiple sclerosis

**Supplementary Table 6.** Final motor, lung, and heart function models from the model selection procedure: Deletion-carriers and deletion-controls

**Supplementary Table 7.** Final motor, lung, and heart function models from the model selection procedure: Duplication-carriers and duplication-controls.

**Supplementary Figures 1-3:** Group differences between deletion-carriers, deletion-controls, duplication-controls, and duplication carriers on measures of brain morphology

**Supplementary Figure 4:** Age-related changes between deletion-carriers and deletion-control and duplication and duplication-control in cortical thickness, surface area and subcortical volume.

**Supplementary Figure 5.** Correlations between chronological age and predicted age based on machine learning algorithm (both corrected and uncorrected).

**Supplementary Figures 6-9:** Group differences between deletion-carriers, deletion-controls, duplication-controls, and duplication carriers on measures of brain age gap

**Supplementary Figure 10.** Age-related changes in reaction time, grip strength, lung function, diastolic and systolic blood pressure in 15q11.2 BP1-BP2 CNV carriers versus matched controls.

## Supplementary Note 1: Participants

In total, 41,959 individuals with a set of T1-weighted MR images from the UK biobank and genetics were available to the study. Participants were excluded in quality control based on a Euler number exceeding 3 standard deviations ( $n = 717$ ), missing Euler number ( $n = 3$ ) or having cortical thickness, surface area or subcortical volume exceeding 4 SD after regressing out age, age<sup>2</sup>, sex, scanner site, affection status (i.e., diagnosed with a neurological disorder or mental/behavioral disorder), estimated intracranial volume (ICV) and Euler number ( $n = 88$ ), leaving a total of 41,151 participants. CNV carriers were identified as previously described<sup>1</sup>. The final quality controlled imaging subset contained 124 15p11.2 BP1-BP2 deletion and 142 duplication carriers and 39,886 non-carriers (i.e. not carrying other pathogenic CNVs as per<sup>1</sup>). We extracted two controls groups for the deletion carriers and duplication carriers separately by matching each carrier on age, sex, scanner site, affection status (absence or presence of a reported psychiatric or neurological diagnosis as defined by a F or G-ICD10 diagnosis) and ICV using propensity scores with the “MatchIt” package in R<sup>2</sup>. The remaining non-carrier sample was used as a training set for the machine learning (ML), following the removal of individuals with a reported psychiatric or neurological diagnosis as defined by a F or G-ICD10 diagnosis, leaving a total of 36,013 individuals ( $M_{\text{age}} = 64.4$ ,  $SD_{\text{age}} = 7.56$ , 52.4% females). Descriptive statistics for the deletion-carriers, deletion-controls, duplication-controls, duplication-carriers and the training sample are presented in Supplementary Table 1.

As part of the validation of the brain age model prediction, we also extracted out individuals diagnosed with multiple sclerosis (ICD10-code: G35,  $n = 60$ ) to compare against a healthy control group. Here, the deletion-control and duplication-control groups (excluding individuals with a F or G-ICD10 diagnosis) were used as the control group ( $n = 1210$ ).

Descriptive statistics for multiple sclerosis and control group are presented in Supplementary Table 2.

### **Supplementary Note 2: Statistical Power: Sensitivity analysis**

We performed a power sensitivity analysis in G\*power 3.1 to obtain the estimated effect size that can be reliably detected using an independent t-test given alpha level = .05 and power = .8. The estimated effect size was  $d = .28$  for deletion carriers ( $n = 124$ ) compared to deletion-control ( $n = 496$ ),  $d = .26$  for duplication ( $n = 142$ ) to duplication-control ( $n = 568$ ) and  $d = .35$  for deletion carriers to duplication carriers. The reports from a previous study indicated thicker cortex ( $d = .36$ ), lower surface area ( $d = -.41$ ) and smaller nucleus accumbens ( $d = -.27$ ) in deletion carriers compared to non-carriers<sup>1</sup>, which indicate that the current study has sufficient power to reliably detect differences in cortical thickness and surface area. We also expected that the smaller effects on subcortical volumes to accumulate for deletion carriers, yielding a larger effect size when using the total subcortical volume as dependent variable compared to the effect size estimated with nucleus accumbens alone. Thus, the current sample size should be sufficient to reliably detect differences in total subcortical volume as well.

### **Supplementary note 3: Brain age prediction model using machine learning**

To tune the models, we ran a grid search on the parameters learning rate (i.e., 0.01, 0.05, 0.1) and maximum depth (i.e., 3,4, 5 6) with 50 iterations, ten-fold cross-validation and early stopping after 10 rounds (i.e., training stopped if the model did not improve within 10 rounds). Root mean squared error (RMSE) for the test set was used for early stopping. The

initial prediction of the model was set to the mean age of the training group. Next, we used the parameters obtained from the models with the lowest RMSE value to train the ML model for the brain age prediction models with 5000 iterations as maximum and early stopping after 10 rounds.

#### **Supplementary note 4: Correction method for the brain age models**

The corrected brain age models were based on the following corrected method where step 1 is conducted on the training group to obtain the slope and the intercept (where  $\alpha$  is the slope,  $\Omega$  represent the chronological age, and  $\beta$  is the intercept) <sup>3</sup>:

1. Predicted age =  $\alpha \times \Omega + \beta$

Thus, the  $\alpha$  and  $\beta$  are fixed numbers obtained from the training group and further used to correct for brain age bias in the test set:

2. Corrected predicted age = Predicted age +  $[\Omega - (\alpha \times \Omega + \beta)]$

Finally, the corrected predicted age is subtracted from the chronological age to obtain an estimate of the brain age gap.

3. Corrected brain age gap = Corrected predicted age -  $\Omega$



## **Supplementary note 5: Model selection of age-related changes in motor, lung, and heart function**

We selected one cognitive measure and four biomedical measures that are associated with ageing<sup>4</sup> and that have been associated with carrying a 15q11.2 BP1-BP2 CNV<sup>1,5</sup>. These measures included reaction time (Data-Field 20023), averaged hand grip strength for left and right hand (Data field 46 and 47), forced expiratory volume in 1-second (Data-Field 3063), systolic and diastolic blood pressure (Data filed 4079 and 4080) and body mass index (Data-Field 21001). Participants included in the analyses had measures from either one, two or three time points, thus analyses were conducted with mixed cross sectional and longitudinal data. To cope with the dependency in the data, we used a mixed effect model with a random effect of participant on intercepts with maximum likelihood as the estimator. To test the age-related changes in the abovementioned measures, we first tested three different models to capture the age model that best fitted the data with sex and affection status as covariates (including BMI for the blood pressure variables).

The models were as follows:

- 1)  $Y = \text{Sex} + \text{Affection status} + \text{random}(1 \mid \text{participant ID}) + \text{error}$
- 2)  $Y = \text{Age} + \text{Sex} + \text{Affection status} + \text{random}(1 \mid \text{participant ID}) + \text{error}$
- 3)  $Y = \text{Age} + \text{Age}^2 + \text{Sex} + \text{Affection status} + \text{random}(1 \mid \text{participant ID}) + \text{error}$

Secondly, to test whether 15q11.2 BP1-BP2 carriers deviated from their respective control group, two models were created with 1) an inclusion of a main term of carrier status and 2) an interaction term between age and carrier status to the age-model that best fitted the data (e.g., for a linear model):

- 4)  $Y = \text{Age} + \text{Sex} + \text{Affection status} + \text{Carrier status} + \text{random}(1 \mid \text{participant ID}) + \text{error}$

5)  $Y = \text{Age} + \text{Sex} + \text{Affection status} + \text{Carrier status} + \text{Age} * \text{Carrier status} + \text{random (1 | participant ID)} + \text{error}$

The models were tested step-wise using the Akaike Information Criterion (AIC), where the more complex model was selected if the AIC dropped with at least 2 and with a p-value < .05

### **Supplementary note 6: Motor, heart and lung function and brain age**

Among the deletion-carriers and deletion-control group, there were no significant associations between brain age gap and reaction time ( $r(571) = .07, p = .092$ ), grip strength ( $r(604) = -.08, p = 0.056$ ), lung function ( $r(556) = -.07, p = .108$ ) systolic ( $r(501) = .01, p = .906$ ) and diastolic blood pressure ( $r(501) = .06, p = .215$ ). Among the duplication-carriers and deletion-control group, there was a significant negative correlation between brain age gap and lung function ( $r(630) = -.17, p < .001$ ), whereas there were no associations between brain age gap and reaction time ( $r(653) = .10, p = .012$ ), grip strength ( $r(682) = -.08, p = .029$ ), systolic ( $r(563) = .10, p = .0167$ ) and diastolic blood pressure ( $r(563) = .09, p = .034$ ).

## References

1. Writing Committee for the ENIGMA-CNV Working Group *et al.* Association of Copy Number Variation of the 15q11.2 BP1-BP2 Region With Cortical and Subcortical Morphology and Cognition. *JAMA Psychiatry* **77**, 420–430 (2020).
2. Ho, D., Imai, K., King, G. & Stuart, E. A. MatchIt: Nonparametric Preprocessing for Parametric Causal Inference. *J. Stat. Softw.* **42**, 1–28 (2011).
3. de Lange, A.-M. G. & Cole, J. H. Commentary: Correction procedures in brain-age prediction. *NeuroImage Clin.* **26**, (2020).
4. Chan, M. S. *et al.* A Biomarker-based Biological Age in UK Biobank: Composition and Prediction of Mortality and Hospital Admissions. *J. Gerontol. Ser. A* **76**, 1295–1302 (2021).
5. Owen, D. *et al.* Effects of pathogenic CNVs on physical traits in participants of the UK Biobank. *BMC Genomics* **19**, (2018).

**Supplementary Table 1.** Descriptive statistics for deletion-carriers, deletion-controls, duplication-controls, duplication-carriers and the training sample.

	Deletion (n = 124)	Deletion- control (n = 496)	Duplication (n = 142)	Duplication- control (n = 568)	Training set (n = 36,013)
<b>Age</b>					
Mean (SD)	64.7 (7.5)	64.9 (7.4)	63.9 (7.5)	63.6 (7.82)	64.4 (7.6)
Median [Min, Max]	65.5 [49.3, 77.5]	65.5 [47.2, 80.5]	64.2 [46.7, 81.3]	64.2 [48.3, 80.2]	64.9 [44.9, 82.8]
<b>Sex</b>					
Female	62.0 (50.0%)	248.0 (50.0%)	75.0 (52.8%)	300.0 (52.8%)	18,880 (52.4%)
<b>Reported Diagnosis</b>					
CNS/mental/behavioral	9.0 (7.3%)	36.0 (7.3%)	15.0 (10.6%)	60.0 (10.6%)	0.0 (0%)
F-diagnosis	4.0 (3.2%)	17.0 (3.4%)	6.0 (4.2%)	28.0 (4.9%)	
G-diagnosis	5.0 (4.0%)	18.0 (3.6%)	9.0 (6.3%)	32.0 (5.6%)	
None	115 (92.7%)	460 (92.7%)	127 (89.4%)	508 (89.4%)	36, 013 (100%)
<b>Estimated ICV</b>					
Mean (SD)	1500000 (150000)	1500000 (154000)	1460000 (149000)	1460000 (149000)	14900000 (148000)
Median [Min, Max]	1500000 [1190000, 1900000]	1490000 [1120000, 1960000]	1430000 [1150000, 1890000]	1440000 [1110000, 1910000]	1480000 [722000, 2270000]

Note. CNS/mental/behavioral = Central nervous system disease or mental/behavioral disorders. ICV = intracranial volume

**Supplementary Table 2.** Descriptive statistics for the control and multiple sclerosis groups

	Multiple Sclerosis (n = 60)	Control-group (n = 1210)
<b>Age</b>		
Mean (SD)	61.2 (7.86)	64.2 (7.59)
Median [Min, Max]	60.8 [47.9, 78.5]	64.7 [47.2, 81.3]
<b>Sex</b>		
Female	43.0 (71.7%)	650.0 (53.7%)
<b>Reported Diagnosis</b>		
CNS/mental/behavioral	60.0 (100%)	0.0 (0%)
None	0.0 (0%)	1210 (100%)
<b>Estimated ICV</b>		
Mean (SD)	1450000 (135000)	1470000 (150000)
Median [Min, Max]	1430000 [1170000,	

1730000]

1460000 [1110000,  
1960000]

Note. CNS/mental/behavioral = Central nervous system disease or mental/behavioral disorders. ICV = intracranial volume

**Supplementary Table 3.** Deletion-carriers vs deletion-control: Age-related changes in cortical thickness, surface area and subcortical volume

	<b>Estimates</b>	<b>Std. Error</b>	<b>CI [95%]</b>	<b>Statistic</b>	<b>P-value</b>
<b>Cortical Thickness</b>					
Intercept	-0.06	0.24	-0.53, 0.40	-0.27	0.789
Age	0.01	0.01	-0.01, 0.02	0.89	0.372
Age <sup>2</sup>	-0.00	0.00	-0.00, 0.00	-1.49	0.136
Deletion-carrier	0.11	0.07	-0.03, 0.25	1.53	0.126
Age*Deletion-carrier	-0.00	0.00	-0.00, 0.00	-1.17	0.244
<b>Surface Area</b>					
Intercept	-29928.48	10684.15	-50910.33, -8946.62	-2.80	0.005
Age	1065.69	334.46	408.87, 1722.50	3.19	0.002
Age <sup>2</sup>	-9.20	2.60	-14.30, -4.10	-3.54	<0.001
Deletion-carrier	-3690.93	3299.86	-10171.29, 2789.43	-1.12	0.264
Age*Deletion-carrier	36.86	50.66	-62.62, 136.34	0.73	0.467
<b>Subcortical Volume</b>					
Intercept	-7609.92	8536.68	-24374.50, 9154.66	-0.89	0.373
Age	415.96	267.23	-108.84, 940.75	1.56	0.120
Age <sup>2</sup>	-4.58	2.07	-8.65, -0.50	-2.21	0.028
Deletion-carrier	3498.01	2636.60	-1679.82, 8675.85	1.33	0.185
Age*Deletion-carrier	-69.97	40.48	-149.45, 9.52	-1.73	0.084

Note. Observations = 620, R<sup>2</sup> = 0.165 (Cortical Thickness), 0.080 (Surface Area), 0.195 (Subcortical Volume)

**Supplementary Table 4.** Duplication-carriers vs duplication-control: Age-related changes in cortical thickness, surface area and subcortical volume

	<b>Estimates</b>	<b>Std. Error</b>	<b>CI [95%]</b>	<b>Statistic</b>	<b>P-value</b>
<b>Cortical thickness</b>					
Intercept	0.04	0.20	-0.36, 0.43	0.18	0.589
Age	0.00	0.01	-0.01, 0.02	0.60	0.548
Age <sup>2</sup>	-0.00	0.00	-0.00, 0.00	-1.37	0.170
Duplication-carrier	0.01	0.07	-0.12, 0.15	0.21	0.833
Age*Duplication-carrier	-0.00	0.00	-0.00, 0.00	-0.32	0.752
<b>Surface Area</b>					
Intercept	-8145.15	9253.82	-26313.50, 10023.20	-0.88	0.379
Age	370.27	294.15	-207.24, 947.78	1.26	0.209
Age <sup>2</sup>	-3.65	2.31	-8.19, 0.89	-1.58	0.115
Duplication-carrier	7146.67	3053.81	1151.01, 13142.32	2.34	0.020
Age*Duplication-carrier	-125.45	47.52	-218.74, - 32.26	-2.64	0.008
<b>Subcortical Volume</b>					
Intercept	-3304.56	7223.85	-17487.40, 10878.28	-0.46	0.647
Age	307.88	229.62	-142.94, 758.71	1.34	0.180
Age <sup>2</sup>	-3.90	1.81	-7.44, -0.35	-2.16	0.031
Duplication-carrier	3811.92	2383.91	-868.50, 8492.34	1.60	0.110
Age*Duplication-carrier	-58.03	37.09	-130.86, 14.80	-1.56	0.118

Note. Observations = 710, R<sup>2</sup> = 0.181(Cortical Thickness), 0.067 (Surface Area), 0.215 (Subcortical Volume)

**Supplementary Table 6.** Brain age prediction in a sample of patients with multiple sclerosis

Brain age model	Multiple Sclerosis	Healthy Controls	t-statistic (df)	p-value	Cohens d (CI)
Mean Brain Age (SD)					
Cortical thickness ML model	2.55 (4.43)	-.13 (3.63)	5.51 (1268)	< .001	.73 (.47, .99)
Surface area ML model	1.69 (4.10)	-.08 (3.60)	3.69 (1268)	<.001	.49 (.23, .75)
Subcortical volume ML model	2.99 (4.47)	-.15 (3.81)	6.16 (1268)	<.001	.81 (.55, 1.08)
Full ML model	3.75 (3.99)	-.19 (3.53)	8.37 (1268)	<.001	1.11 (.84, 1.37)

*Note.* SD = standard deviation, df = degrees of freedom, CI = 95% confidence interval. Mean brain age is adjusted for age, age<sup>2</sup>, sex, scanner site, intracranial volume, and Euler number. ML = machine learning

**Supplementary Tables 7.** Final motor, heart and lung function models from the model selection procedure: Deletion-carriers and deletion-controls

	Estimates	Std.Error	CI (95%)	Statistic	P-value
<b>Reaction Time</b>					
Intercept	5.78	0.04	5.70, 5.86	147.48	<0.001
Age	0.01	0.00	0.01, 0.01	17.26	<0.001
Sex [Male]	-0.03	0.01	-0.06, -0.01	-2.89	0.004
Affection status [None]	-0.02	0.02	-0.07, 0.02	-1.04	0.298
Deletion-carrier	0.04	0.01	0.01, 0.07	2.85	0.004
<b>Grip Strength</b>					
Intercept	38.47	1.65	35.24, 41.70	23.34	<0.001
Age	-0.27	0.02	-0.31, -0.23	-11.92	<0.001
Sex [Male]	15.56	0.51	14.56, 16.57	30.42	<0.001
Affection status [None]	1.65	0.99	-0.28, 3.59	1.67	0.095
<b>Lung Function</b>					
Intercept	4.41	0.13	4.16, 4.67	33.62	<0.001
Age	-0.04	0.00	-0.04, -0.03	-21.12	<0.001
Sex [Male]	1.02	0.04	0.93, 1.10	23.27	<0.001
Affection Status [None]	0.18	0.08	0.02, 0.35	2.21	0.028
<b>Blood Pressure, Diastolic</b>					
Intercept	66.48	3.08	60.44, 72.52	21.58	<0.001

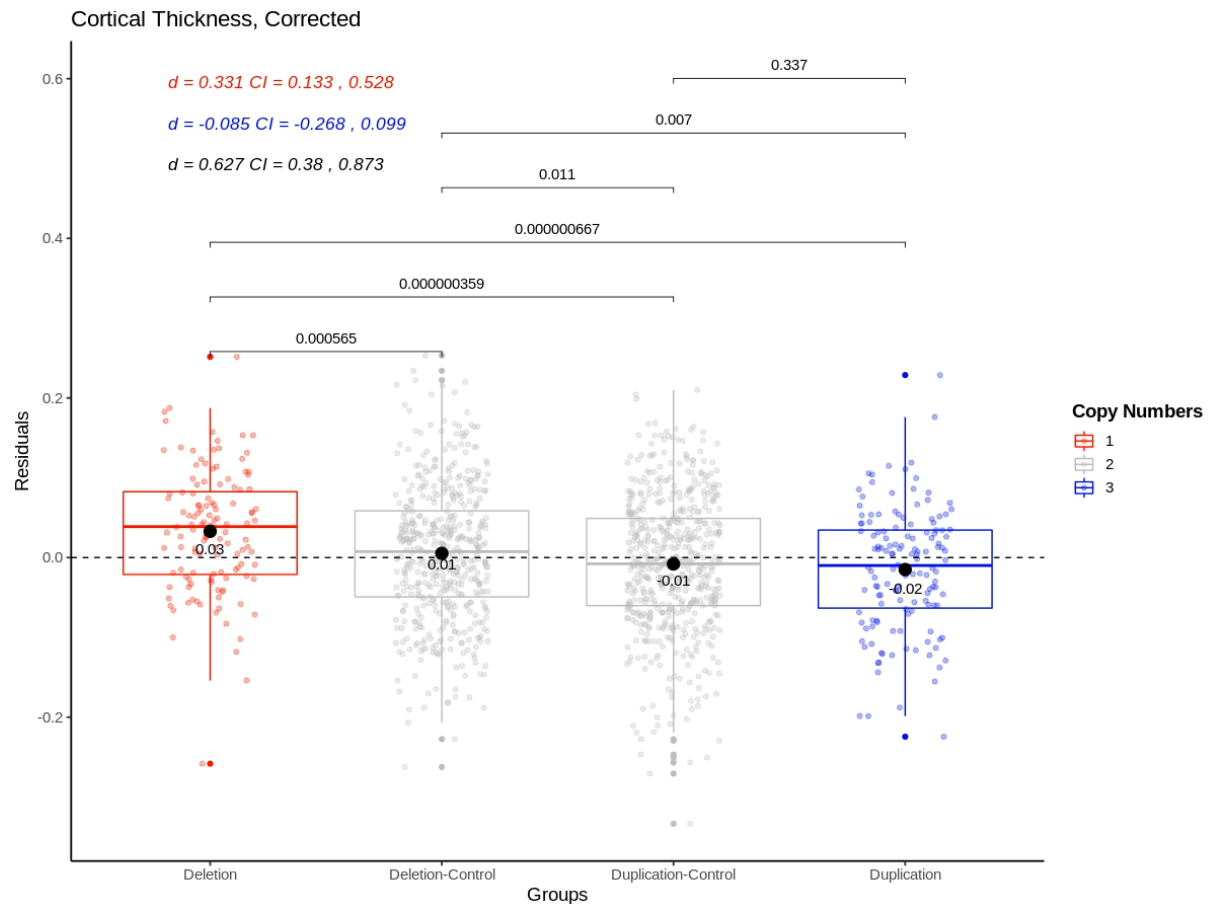
Age	-0.09	0.03	-0.16, -0.03	-2.87	0.004
Sex [Male]	3.57	0.68	2.23, 4.90	5.23	<0.001
Affection Status [None]	-0.27	1.31	-2.83, 2.29	-0.21	0.837
BMI	0.65	0.07	0.50, 0.79	8.76	<0.001
<b>Blood Pressure, Systolic</b>					
Intercept	76.15	5.80	64.77, 87.52	13.12	<0.001
Age	0.63	0.06	0.51, 0.75	10.18	<0.001
Sex [Male]	3.90	1.28	1.38, 6.41	3.04	0.002
Affection Status [None]	1.44	2.46	-3.39, 6.26	0.58	0.560
BMI	0.78	0.14	0.51, 1.05	5.60	<0.001

**Supplementary Tables 8.** Final motor, heart and lung function models from the model selection procedure: Duplication-carriers and duplication-control.

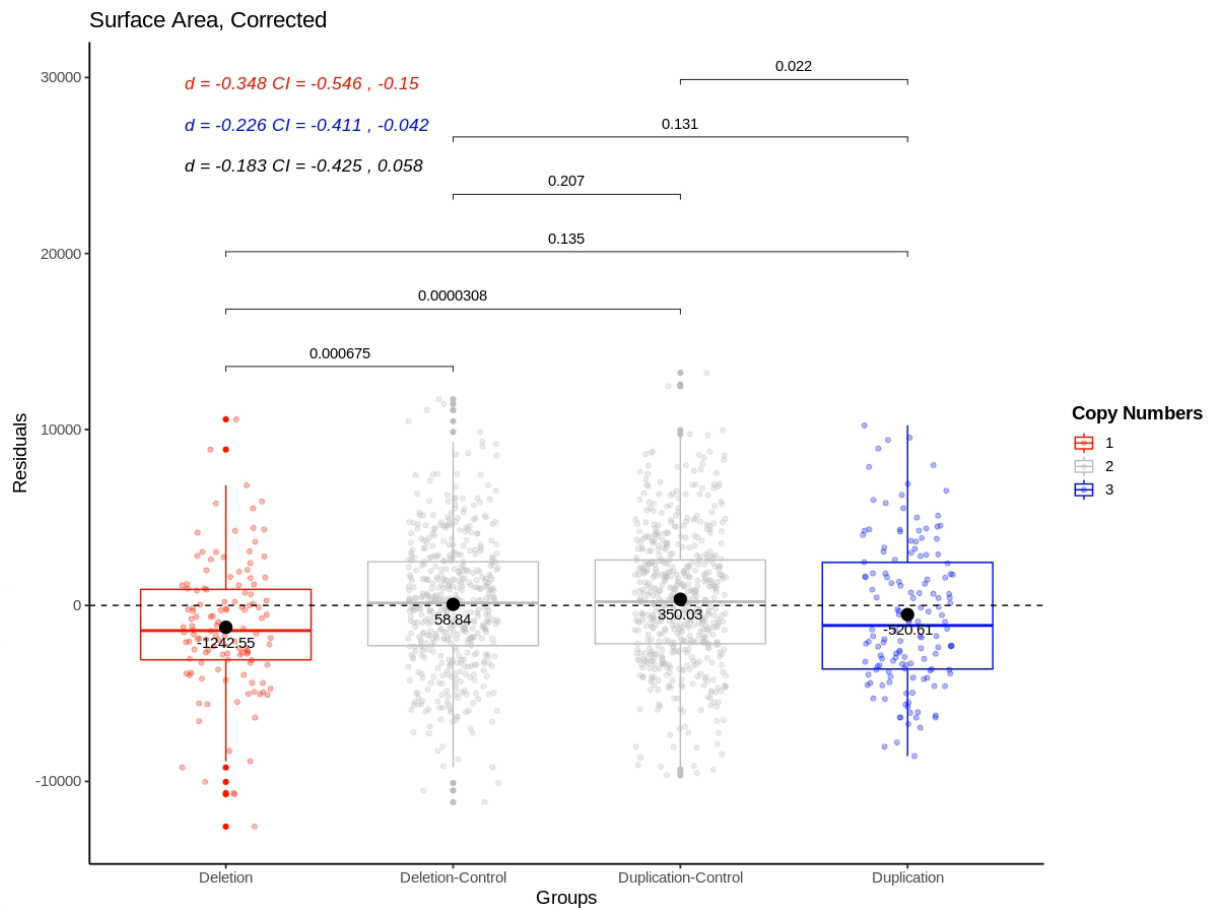
	Estimates	Std.Error	CI (95%)	Statistic	P-value
<b>Reaction Time</b>					
Intercept	5.76	0.03	5.70, 5.83	172.20	<0.001
Age	0.01	0.00	0.01,0.01	19.21	<0.001
Sex [Male]	-0.04	0.01	-0.06, -0.02	-3.89	<0.001
Affection status [None]	0.01	0.02	-0.02, 0.05	0.84	0.402
<b>Grip Strength</b>					
Intercept	42.15	1.37	39.47, 44.84	30.81	<0.001
Age	-0.32	0.02	-0.35, -0.28	-16.48	<0.001
Sex [Male]	15.30	0.46	14.39, 16.20	33.04	<0.001
Affection status [None]	0.68	0.75	-0.80,2.16	0.90	0.367
<b>Lung Function</b>					
Intercept	4.41	0.11	4.19, 4.63	39.08	<0.001
Age	-0.03	0.00	-0.04, -0.03	-21.88	<0.001
Sex [Male]	0.95	0.04	0.88, 1.03	24.09	<0.001
Affection Status [None]	-0.01	0.06	-0.14, 0.11	-0.23	0.815
<b>Blood Pressure, Diastolic</b>					
Intercept	66.35	2.93	60.61, 72.08	22.67	<0.001
Age	-0.08	0.03	-0.15, -0.02	-2.65	0.008
Sex [Male]	4.08	0.67	2.77, 5.39	6.10	<0.001
Affection Status [None]	-0.04	1.09	-2.18, 2.09	-0.04	0.968
BMI	0.63	0.07	0.50,0.77	9.11	<0.001
Duplication-carrier	1.84	0.81	0.26, 3.41	2.28	0.023
<b>Blood Pressure, Systolic</b>					
Intercept	105.69	16.03	74.30, 137.08	6.59	<0.001
Age	-0.44	0.54	-1.50, 0.62	-0.82	0.413
Age <sup>2</sup>	0.01	0.00	0.00, 0.02	2.05	0.041



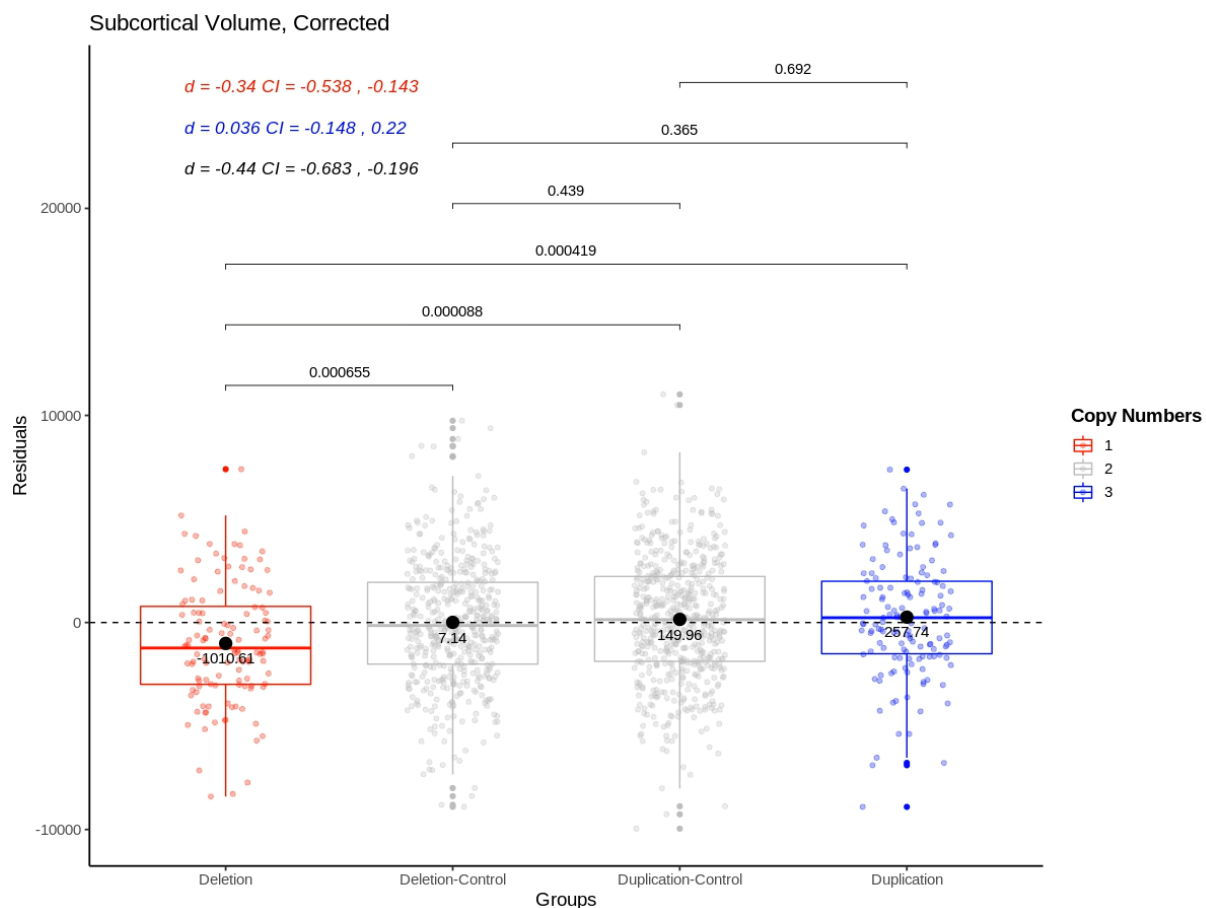
Sex [Male]	6.73	1.21	4.35,9.10	5.55	<0.001
Affection Status [None]	0.80	1.97	-3.06,4.66	0.40	0.686
BMI	0.80	0.12	0.55,1.04	6.40	<0.001
Duplication-carrier	2.94	1.46	0.08,5.80	2.01	0.045



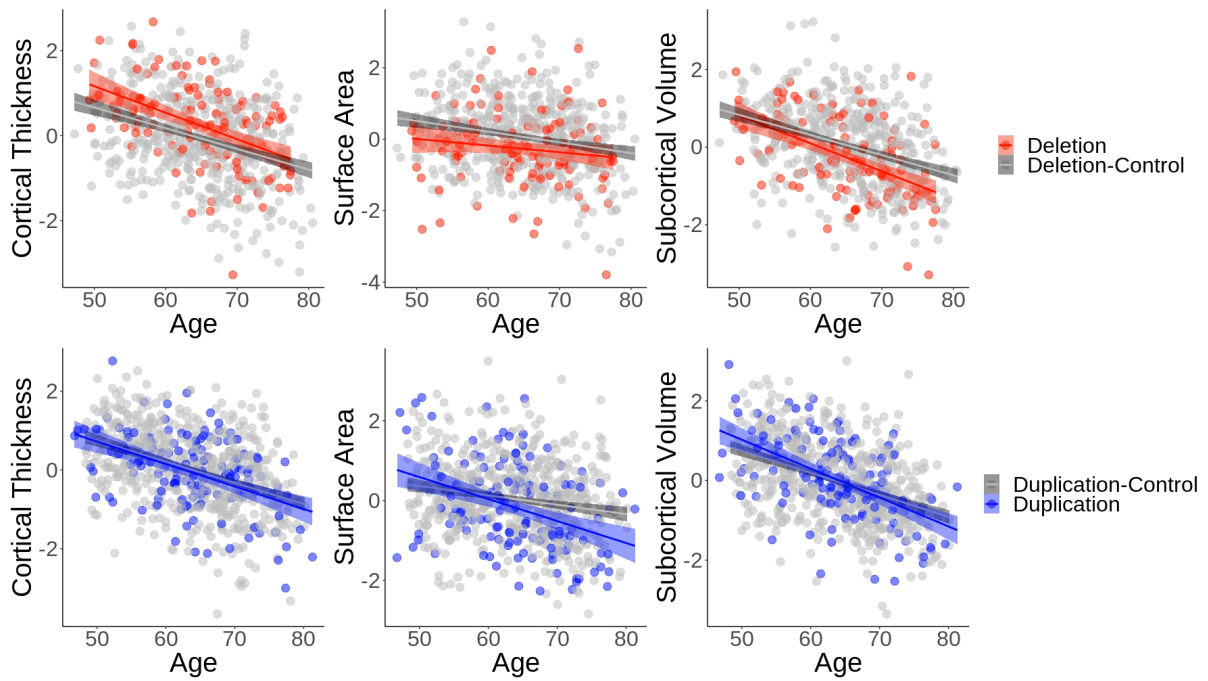
**Supplementary Figure 1.** Group differences in cortical thickness adjusted for age, age<sup>2</sup>, sex, scanner site, affection status, intracranial volume and Euler number. P-values are uncorrected and are based on two-sided independent t-tests. Cohens d are presented in the top left corner where the coloring of the effect sizes correspond to the following comparisons: Red = Deletion vs Deletion-Control, Blue = Duplication vs Duplication-Control, Black = Deletion vs Duplication. d = Cohens d, CI = 95% confidence interval.



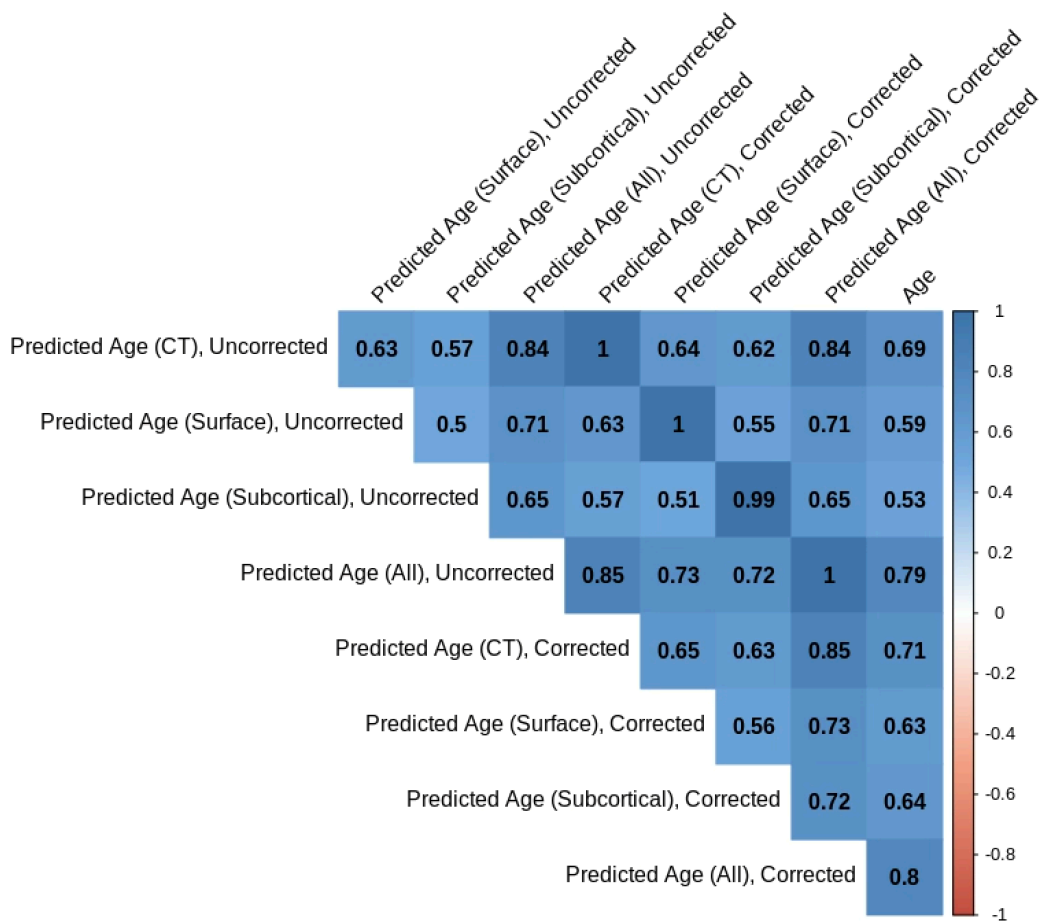
**Supplementary Figure 2.** Group differences in surface area adjusted for age, age<sup>2</sup>, sex, scanner site, affection status, scanner site, intracranial volume and Euler number. P-values are uncorrected and are based on two-sided independent t-tests. Cohens d are presented in the top left corner where the coloring of the effect sizes correspond to the following comparisons: Red = Deletion vs Deletion-Control, Blue = Duplication vs Duplication-Control, Black = Deletion vs Duplication. d = Cohens d, CI = 95% confidence interval.



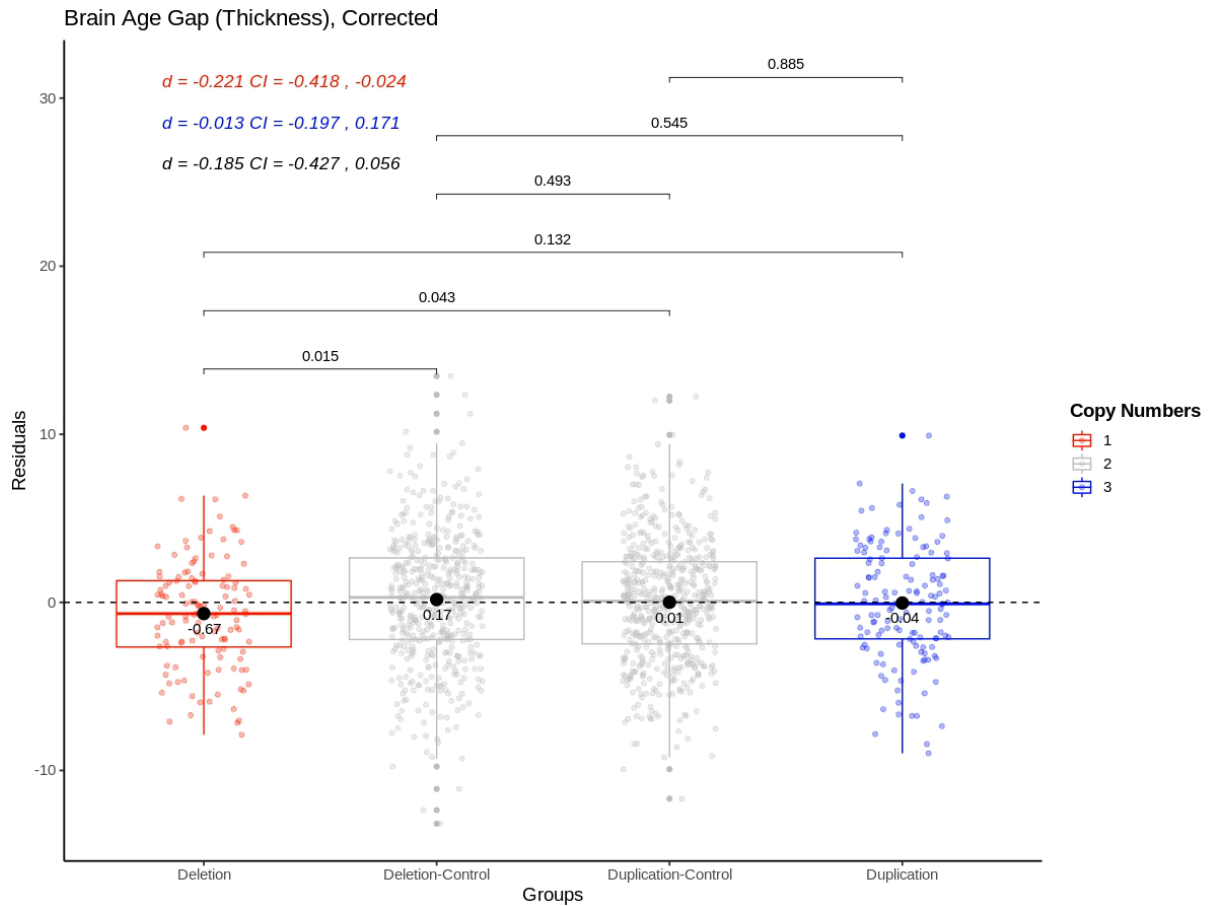
**Supplementary Figure 3.** Group differences in subcortical volume adjusted for age, age<sup>2</sup>, sex, scanner site, affection status, scanner site, intracranial volume and Euler number. P-values are uncorrected and are based on two-sided independent t-tests. Cohens d are presented in the top left corner where the coloring of the effect sizes correspond to the following comparisons: Red = Deletion vs Deletion-Control, Blue = Duplication vs Duplication-Control, Black = Deletion vs Duplication. d = Cohens d, CI = 95% confidence interval.



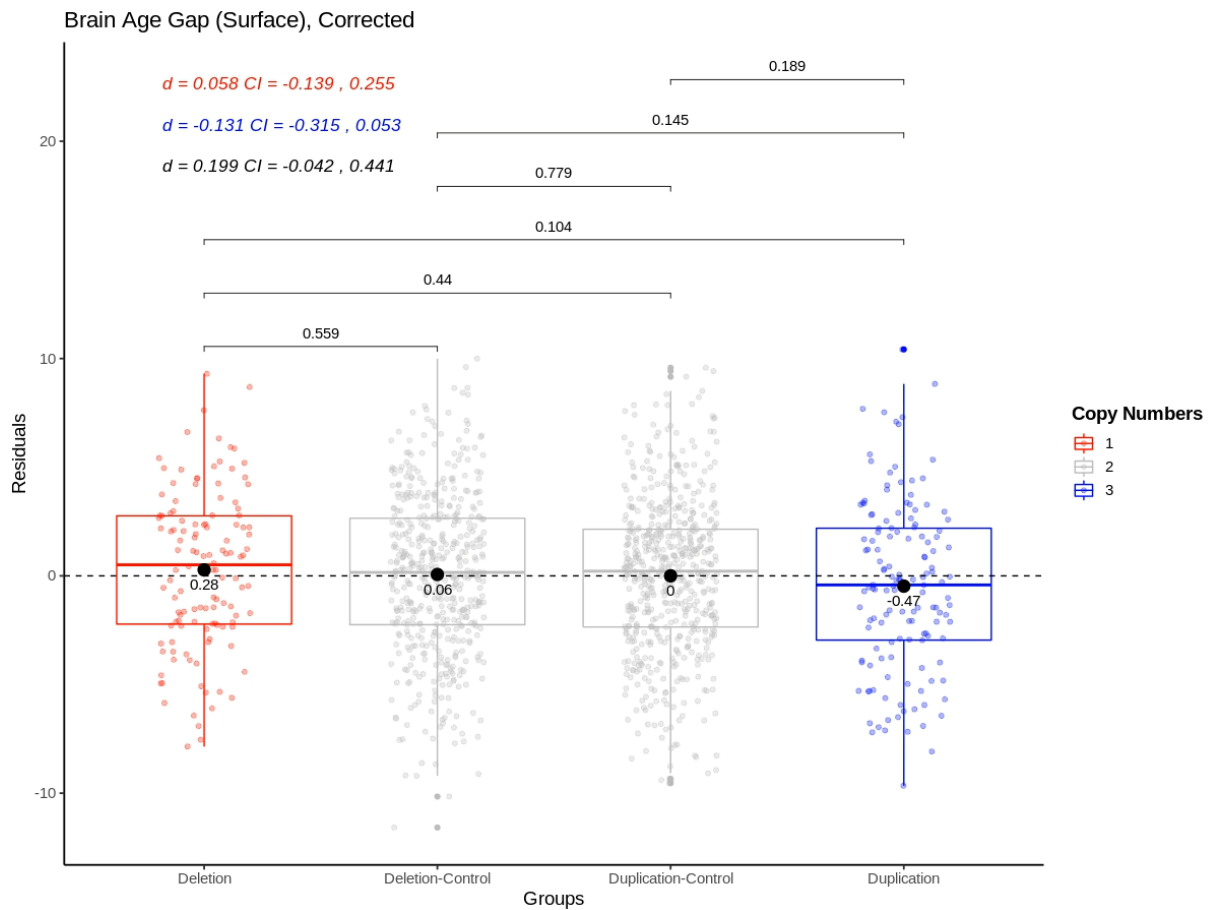
**Supplementary Figure 4.** Age-related changes between deletion-carriers and deletion-controls (upper) and duplication-carriers and duplication-controls (lower) in cortical thickness, surface area and subcortical volume. Regression lines were fitted using linear regression, adjusting for sex, scanner site, affection status, intracranial volume and Euler number. The dependent variables were standardized for visualization purposes.



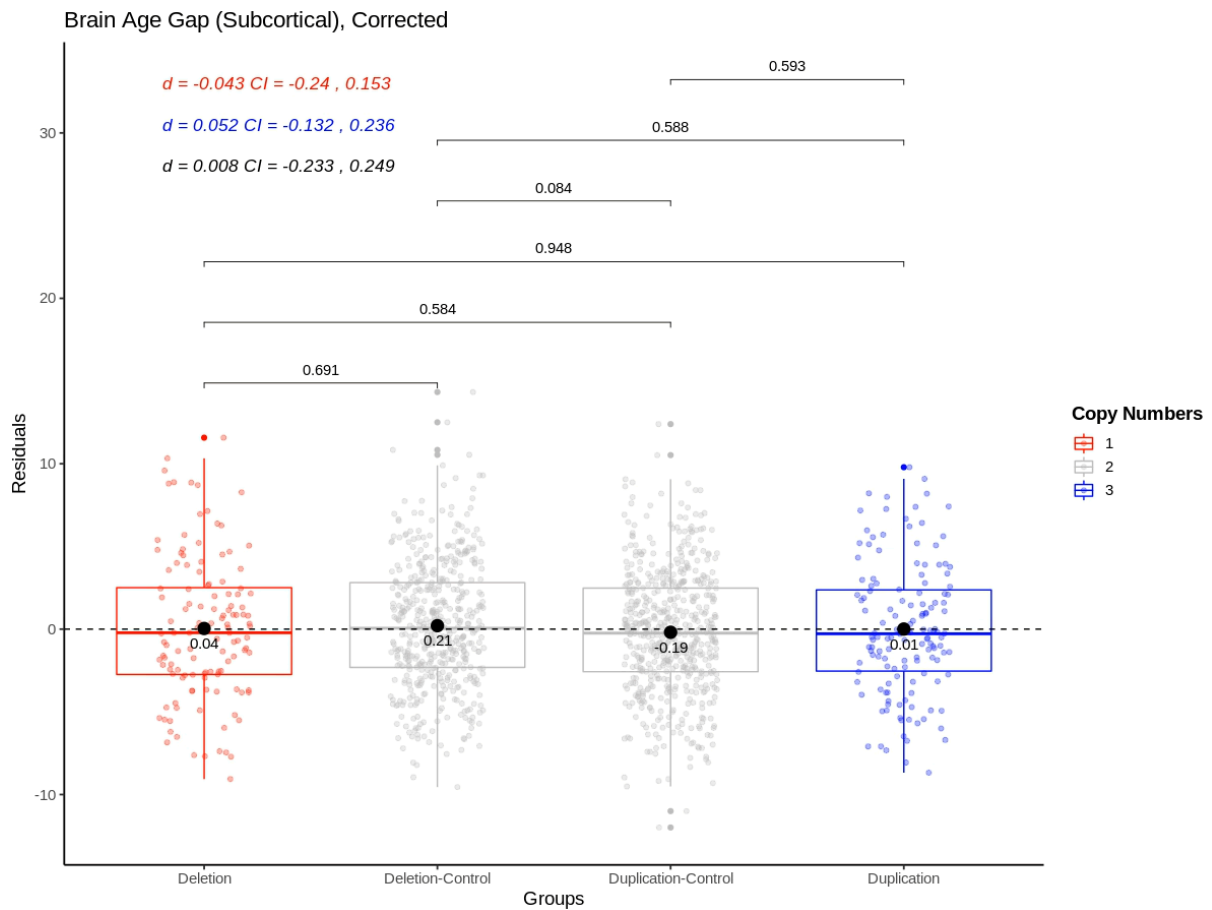
**Supplementary Figure 5.** Correlations between chronological age and predicted age based on machine learning algorithm (both corrected and uncorrected). CT = Cortical thickness only model, Surface = surface area only model, Subcortical = subcortical volume only model, All = full model.



**Supplementary Figure 6.** Group differences in brain age gap, estimated through the cortical thickness only model, adjusted for age, age<sup>2</sup>, sex, scanner site, affection status, intracranial volume and Euler number. P-values are uncorrected and are based on two-sided independent t-tests. Cohens d are presented in the top left corner where the coloring of the effect sizes correspond to the following comparisons: Red = Deletion vs Deletion-Control, Blue = Duplication vs Duplication-Control, Black = Deletion vs Duplication. d = Cohens d, CI = 95% confidence interval.

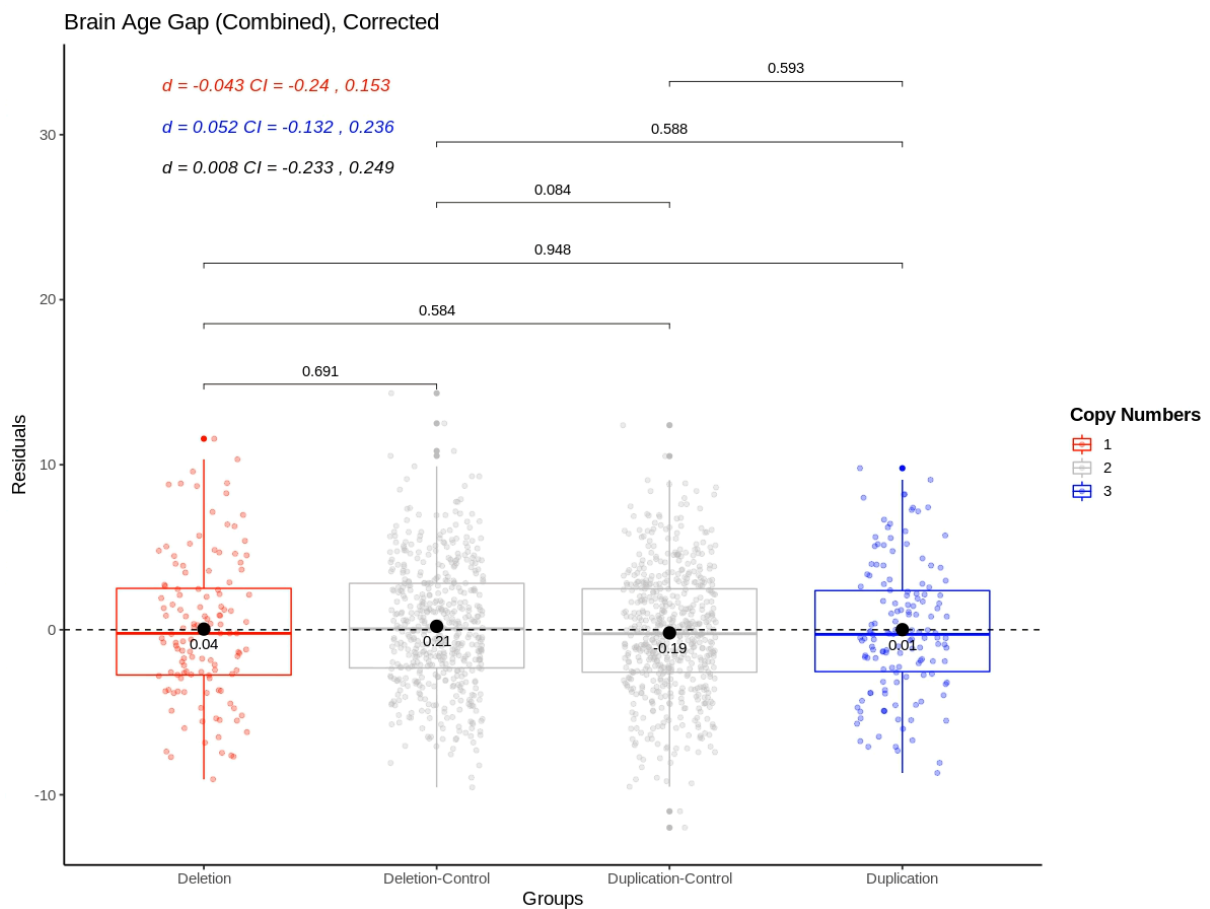


**Supplementary Figure 7.** Group differences in brain age gap, estimated through the surface area only model, adjusted for age, age<sup>2</sup>, sex, scanner site, affection status, intracranial volume and Euler number. P-values are uncorrected and are based on two-sided independent t-tests. Cohens d are presented in the top left corner where the coloring of the effect sizes correspond to the following comparisons: Red = Deletion vs Deletion-Control, Blue = Duplication vs Duplication-Control, Black = Deletion vs Duplication. d = Cohens d, CI = 95% confidence interval.

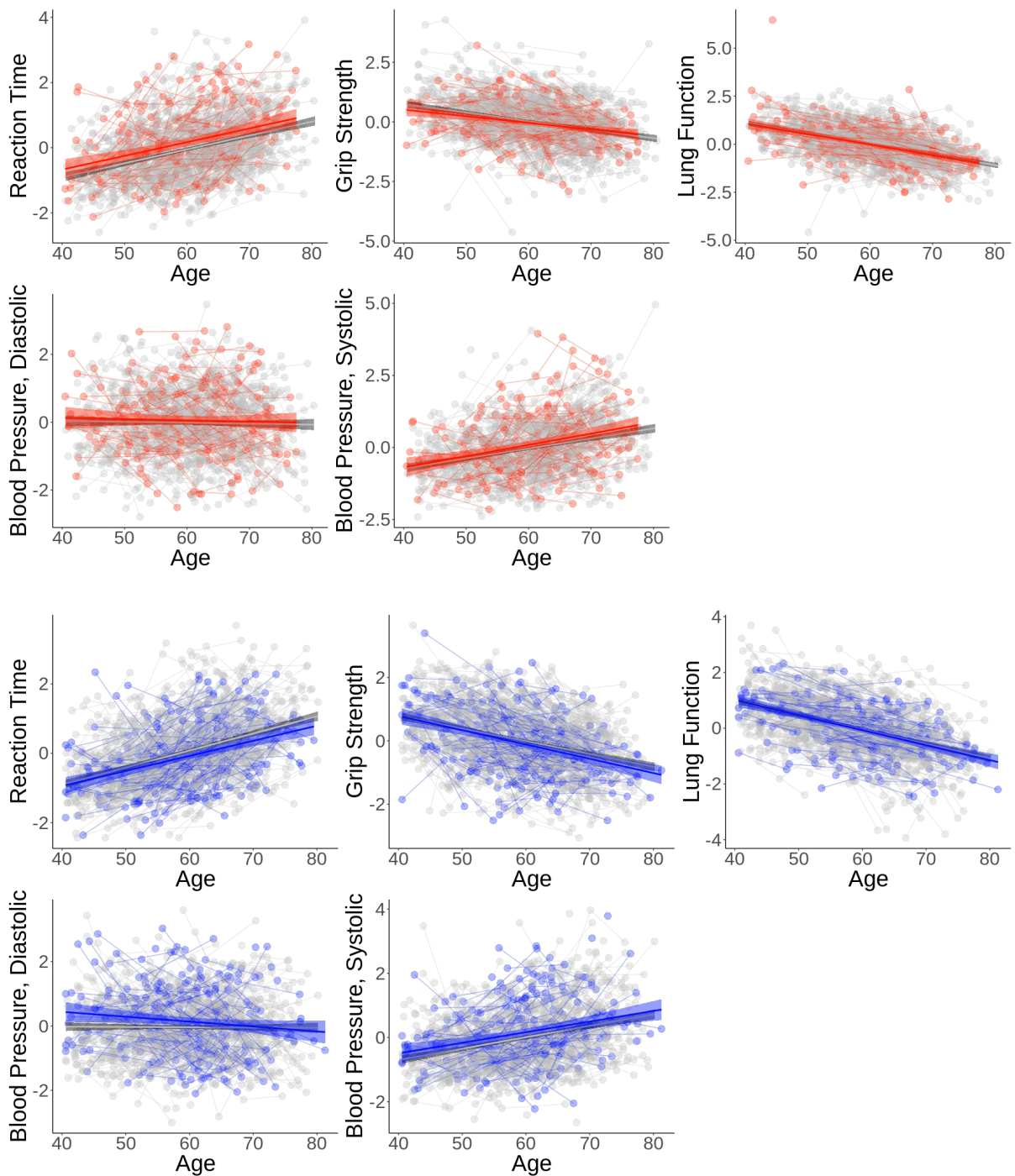


**Supplementary Figure 8.** Group differences in brain age gap, estimated through the subcortical volume only model, adjusted for age, age<sup>2</sup>, sex, scanner site, affection status, intracranial volume and Euler number. P-values are uncorrected and are based on two-sided independent t-tests. Cohens d are presented in the top left corner where the coloring of the effect sizes correspond to the following comparisons: Red = Deletion vs Deletion-Control, Blue = Duplication vs Duplication-Control, Black = Deletion vs Duplication. d = Cohens d, CI = 95% confidence interval.





**Supplementary Figure 9.** Group differences in brain age gap, estimated through the full model, age, age<sup>2</sup>, sex, scanner site, affection status, intracranial volume and Euler number. P-values are uncorrected and are based on two-sided independent t-tests. Cohens d are presented in the top left corner where the coloring of the effect sizes correspond to the following comparisons: Red = Deletion vs Deletion-Control, Blue = Duplication vs Duplication-Control, Black = Deletion vs Duplication. d = Cohens d, CI = 95% confidence interval.



**Supplementary Figure 10.** Age-related changes in reaction time, grip strength, lung function, diastolic and systolic blood pressure in 15q11.2 BP1-BP2 CNV carriers versus matched controls. Red = deletion carriers, grey = non-carriers, blue = duplication carriers. All values were residualized for sex and affection status (incl. BMI for blood pressure) using linear regression and standardized for visualization purposes only. The results from the mixed effects models are shown in Supplementary Tables 7 (Deletion-carriers and deletion-controls) and Supplementary Tables 8 (Duplication-carriers and duplication-controls).



III

